
MODELLING THE GIANT SANDWAVES OF SAN FRANCISCO BAY

*A study on process based sandwave
modelling, with an exploration on the
mechanisms that result in the formation
of these bedforms*

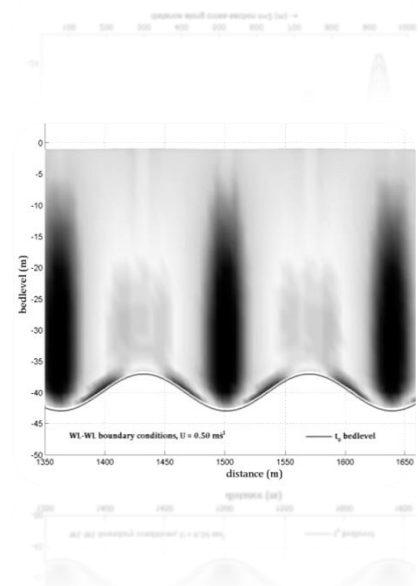
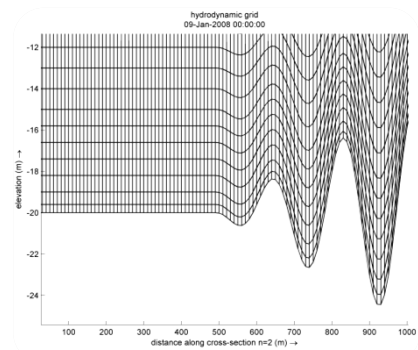
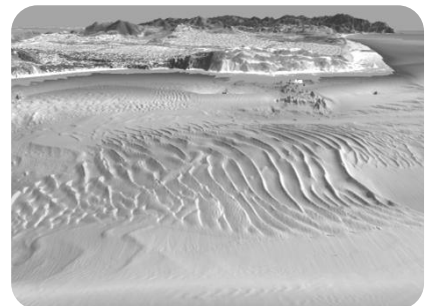
MSc Thesis

June 9, 2009


TU Delft
Delft University of Technology


USGS
science for a changing world

Deltares
Enabling Delta Life 



Prepared for:
USGS

Modelling the Giant Sandwaves of San Francisco Bay

A study on process based sandwave
modelling, with an exploration on the
mechanisms that lead to formation of these
bedforms

Author:
J. Kooistra
Student number:
1225138

Supervising Committee:
Prof. dr. ir. M.J.F. Stive
dr. ir. E.P.L. Elias
dr. D.M. Hanes
dr. ir. J.E.A. Storms
ir. D.J. Walstra

Main Report

June 9, 2009

PREFACE

This M.Sc. thesis is written to complete my master in Coastal Engineering at the faculty of Civil Engineering and Geosciences of Delft University of Technology.

The thesis describes the development of a 2Dv-model of the San Francisco Bay sandwaves using DELFT3D to study the capability of a process based model to capture the formation mechanisms. The thesis is part of the cooperation between Deltares (former WL|Delft Hydraulics) and United States Geological Survey (USGS), within the framework of numerous studies USGS is performing in the San Francisco Bay region.

Many people have contributed in even more different ways to the realization of this thesis. First of all I would like to thank my graduation committee, prof. dr. ir. Marcel J. F. Stive (Delft University of Technology), dr. Daniel M. Hanes (USGS), dr. ir. Edwin P.L. Elias (Deltares & USGS), ir. Dirk Jan Walstra (Deltares & USGS) and dr. ir. Joep E.A. Storms (Delft University of Technology) for the interesting discussions we had, taking this thesis to a much higher level. I also thank Gerben de Boer for his help using DELFT3D. Furthermore I would like to thank Deltares for the facilities they offered in the Netherlands and USGS for the facilities in Santa Cruz, USA.

Then I would like to thank my fellow graduates at Het afstudeerhok for the many discussions, support, coffee and many laughs. I want to express warm words of gratitude towards Li, Patrick, Larissa, Kate and Elizabeth for making my stay in Santa Cruz very pleasant.

Finally without my roommates, friends, my parents and brother and sister this work would have been a lot more difficult. So a very big thank you to them as well.

I hope you will enjoy reading this report.

Jeroen Kooistra



Amsterdam, June 2009

SUMMARY

The more than 2,000 km long West Coast of California was recently mapped in high resolution by a multibeam sonar survey, performed by the U.S. Geological Survey (USGS) and California State University, Monterey Bay. Connected to the Pacific Ocean by the Golden Gate channel, the San Francisco Bay accommodates a widely spread field of sandwaves that show large spatial variations which are not yet fully understood. Insight into the formation of sandwaves is necessary to understand and predict the processes that control sand transport and sedimentation patterns in San Francisco Bay. The aim of this research is to study the capability of DELFT3D to model the sandwaves using a 2Dv-model, with emphasis on assessing the formation mechanisms. The morphological development of multiple sandwave configurations under various flow conditions is compared to gain insight in the differences between the modelled sandwaves and the sandwaves found in the inlet mouth of San Francisco Bay. Residual vector plots displaying magnitude and residual flow direction are used to quantify the difference in residual velocity profiles, for different sandwave configurations. In extend, the effect of alternating physical parameters and flow configurations is analyzed to gain insight in the sensitivity of the 2Dv-model.

The numerical model is built using a sinusoidal shaped bed level and flow velocities with large temporal variations. Input is taken from two project sites referred to as Baker Beach and Mouth Center, that contain a large set of sandwaves of which wave height and length are most important for setting up the bathymetry of the 2Dv-model. Peak tidal velocities vary greatly and measure up to 1.50 ms^{-1} . Physically stable channel flow is therefore schematized by prescribing water levels on the boundaries of a 3000 m long channel, simulating a passing tidal wave by applying a small phase difference between both boundaries. The forcing type for both boundaries is set on harmonic, using a radial frequency of 30 degrees per hour and water level amplitude of 1.00 m. The sandwave configurations are represented by a lengths varying from 75 m to 175 m and heights varying from 2 m to 10 m.

Model results show that equilibrium in sandwave height is found for relatively large scale lengths and that modelled sandwaves show different growth and decay rates for steeper slopes and higher velocities. Stability in sandwave development is contributed mainly to a term which hinders the formation of steep slopes resulting in a so called equilibrium slope angle, and a growing term based on the residual near-bed current velocity. For the studied range of sandwave lengths, heights were found to be independent of the local water depth and increasing flow velocities only allow the largest dimensions to reach equilibrium. Growth in height is found to be mainly caused by the hindering crest velocity term, being not large enough to compensate for the high near-bed upslope velocities. Decay in height is mainly attributed to asymmetric residual current flow, due to an initial bed level steepness that is too gentle. Although not all length scales have been successfully described using the 2Dv-model, the results give a valuable indicative idea of how sandwaves develop in the inlet mouth of San Francisco Bay.

TABLE OF CONTENTS

| | |
|---|-----------|
| PREFACE | 1 |
| SUMMARY | 2 |
| TABLE OF CONTENTS | 3 |
| LIST OF FIGURES | 7 |
| LIST OF TABLES | 12 |
| 1. INTRODUCTION | 13 |
| 1.1 PROJECT DESCRIPTION | 13 |
| 1.2 OBJECTIVE | 16 |
| 1.3 OUTLINE | 17 |
| 1.4 ACKNOWLEDGEMENTS | 17 |
| 2. SAN FRANCISCO BAY | 18 |
| 2.1 PROJECT AREA | 18 |
| 2.2 HYDRODYNAMIC CONDITIONS | 20 |
| 2.2.1 TIDE | 20 |
| 2.2.2 CURRENTS | 23 |
| 2.3 MORPHODYNAMIC CONDITIONS | 26 |
| 2.3.1 SEDIMENT TRANSPORT | 26 |
| 2.3.2 SEDIMENT CHARACTERISTICS | 28 |
| 2.3.3 SANDWAVES | 29 |
| 3. THEORY ON SANDWAVES | 31 |
| 3.1 CHARACTERISTICS | 31 |
| 3.2 SANDWAVE FORMATION | 33 |
| 3.2.1 VERTICAL RESIDUAL CIRCULATION CELLS | 33 |
| 3.2.2 FLOW SEPARATION | 35 |
| 3.3 SANDWAVE MIGRATION | 36 |

| | |
|--|-----------|
| 4. RESEARCH APPROACH | 38 |
| 4.1 MODEL CONSTRUCTION | 38 |
| 4.2 ASSUMPTIONS | 39 |
| 4.2.1 PROJECT AREA PARTITION | 39 |
| 4.2.2 BATHYMETRY REPRESENTATION | 39 |
| 4.2.3 EQUILIBRIUM | 39 |
| 4.2.4 CALIBRATION AND VALIDATION | 40 |
| 4.3 MODEL SIMULATIONS | 40 |
| 4.3.1 MORPHODYNAMIC SIMULATIONS | 41 |
| 4.3.2 HYDRODYNAMIC SIMULATIONS | 41 |
| 4.3.3 SENSITIVITY ANALYSIS | 41 |
| 4.4 ANALYZING RESULTS | 41 |
| 5. DATA ANALYSIS | 42 |
| 5.1 BACKGROUND INFORMATION | 42 |
| 5.2 FIELD DATA INTERPRETATION | 44 |
| 5.2.1 SANDWAVE CHARACTERISTICS | 44 |
| 5.2.2 SEDIMENT GRAIN-SIZE | 45 |
| 5.3 2DH-MODEL INTERPRETATION | 46 |
| 5.3.1 PEAK TIDAL FLOW VELOCITIES | 46 |
| 5.3.2 RESIDUAL TIDAL FLOW VELOCITIES | 47 |
| 5.4 PARAMETER RELATIONS | 48 |
| 5.4.1 COMPARING FIELD DATA | 48 |
| 5.4.2 COMPARING FIELD AND 2DH-MODEL DATA | 49 |
| 5.4.3 IMPLEMENTING THE DATA IN THE PROFILE MODEL | 50 |
| 6. SANDWAVE MODEL SETUP (2DV) | 51 |
| 6.1 INTRODUCTION IN DELFT3D | 51 |
| 6.2 BATHYMETRIC SCHEMATIZATION | 53 |
| 6.2.1 COMPUTATIONAL GRID | 53 |
| 6.2.2 BATHYMETRY | 54 |
| 6.2.3 OBSERVATION POINTS | 54 |
| 6.3 FLOW BOUNDARY CONDITIONS | 55 |
| 6.3.1 BOUNDARY TYPES | 55 |
| 6.3.2 SELECTING BOUNDARY CONDITIONS | 55 |
| 6.3.3 FLOW VELOCITY ANALYSIS | 57 |
| 6.4 PARAMETER SETTINGS | 59 |
| 6.4.1 HYDRODYNAMIC PARAMETERS | 59 |
| 6.4.2 MORPHODYNAMIC PARAMETERS | 60 |

| | |
|--|------------|
| 7. SANDWAVE MODEL RESULTS | 64 |
| 7.1 MORPHODYNAMIC EQUILIBRIUM | 64 |
| 7.1.1 GROWTH RATES FOR BAKER BEACH DEPTH | 64 |
| 7.1.2 GROWTH RATES FOR MOUTH CENTER DEPTH | 66 |
| 7.1.3 STATE OF EQUILIBRIUM | 68 |
| 7.2 HYDRODYNAMIC EQUILIBRIUM | 70 |
| 7.2.1 RESIDUAL FLOW PATTERN FOR BAKER BEACH DEPTH | 70 |
| 7.2.2 RESIDUAL FLOW PATTERN FOR MOUTH CENTER DEPTH | 73 |
| 7.2.3 STATE OF EQUILIBRIUM | 76 |
| 7.3 SENSITIVITY ANALYSIS RESULTS | 81 |
| 7.3.1 EFFECT OF FLOW SEPARATION | 81 |
| 7.3.2 EFFECT OF BED-SLOPE FACTOR (ALFABS) | 83 |
| 7.3.3 EFFECT OF MEDIAN GRAIN-SIZE DIAMETER | 84 |
| 8. ANALYSIS AND DISCUSSION | 85 |
| 8.1 FORMATION MECHANISMS | 85 |
| 8.1.1 CONTRIBUTION OF HYDRODYNAMIC CONFIGURATION | 85 |
| 8.1.2 CONTRIBUTION OF BED LEVEL CONFIGURATION | 89 |
| 8.1.3 DEVELOPMENT CONDITIONS | 91 |
| 8.2 2DV-MODEL RESULTS VS FIELD DATA RESULTS | 95 |
| 8.2.1 COMPARING DATA | 95 |
| 8.2.2 BAKER BEACH COMPARISON | 95 |
| 8.2.3 MOUTH CENTER COMPARISON | 97 |
| 8.3 SENSITIVITY OF MODEL PARAMETERS | 99 |
| 9. CONCLUSIONS AND RECOMMENDATIONS | 100 |
| 9.1 DELFT3D SANDWAVE MODEL | 100 |
| 9.1.1 THE 2DV-MODEL | 100 |
| 9.1.2 REPRESENTING SAN FRANCISCO BAY SANDWAVES | 100 |
| 9.1.3 RECOMMENDATIONS FOR FURTHER IMPROVEMENT | 101 |
| 9.2 RESEARCH OBJECTIVE | 103 |
| 9.2.1 MAIN QUESTIONS | 103 |
| 9.2.2 SUB QUESTIONS | 104 |
| REFERENCES | 105 |

| | |
|--|------------|
| APPENDICES | 108 |
| A. SAN FRANCISCO BAY | 109 |
| B. GRAIN SIZE CLASS | 110 |
| C. STEEPNESS INDEX | 111 |
| D. DEPTH OVER HEIGHT RATIO | 112 |
| E. LINEAR THREE-DIMENSIONAL STABILITY MODEL | 113 |
| F. WATER DEPTH DISTRIBUTION PROJECT SITES | 115 |
| G. LONG TERM BOUNDARY DISTURBANCES | 116 |
| H. SANDWAVE GRAIN-SIZE SAMPLE LOCATIONS | 117 |
| I. PROJECT AREA FIELD AND 2DH-MODEL DATA | 118 |
| J. FIELD AND 2DH-MODEL DATA SCATTERPLOTS | 123 |
| K. GRAIN-SIZE RELATIONSHIP WITH SANDWAVES | 132 |
| L. 2DV-MODEL MONITORING POINTS | 133 |
| M. SIMULATION SETTINGS | 134 |
| N. BED LEVEL RESPONSE FOR GROWTH AND DECAY | 136 |
| O. BAKER BEACH – HYDRODYNAMIC TIME SERIES | 138 |
| P. MOUTH CENTER – HYDRODYNAMIC TIME SERIES | 142 |
| Q. TIME SERIES DATA OVERVIEW | 146 |

LIST OF FIGURES

- Figure 1-1 From small to large map; United States of America and San Francisco Bay area (copyright © 2005-2008 [United-States-Maps.com](#) and Google Earth™, 2008)
- Figure 1-2 Perspective view southwest over the Golden Gate Bridge toward the Pacific Ocean at the entrance of San Francisco Bay. The features on the sea floor in the center of the inlet mouth are sandwaves. The distance across the bottom of the image is about 3 km (by Barnard *et al.*, courtesy of USGS, 2006)
- Figure 1-3 Perspective view northeast over the entrance to San Francisco Bay. The water depth over the sandwaves within this field ranges from 30 to 100 m. The distance of the image is about 2.4 km (by Barnard *et al.*, courtesy of USGS, 2006)
- Figure 2-1 High resolution image of the entire San Francisco Bay inlet mouth, entitled as the project area of this study (by Barnard *et al.*, 2006, USGS)
- Figure 2-2 High resolution image showing the San Francisco Bay inlet mouth from the north (by Barnard *et al.*, 2006, USGS)
- Figure 2-3 Predicted and observed tidal elevation for January 1, 2007 to January 1, 2008 (ID 9414290, San Francisco Bay, CA, [Tidesandcurrents.NOAA.gov](#), 2008)
- Figure 2-4 Predicted and observed tidal elevation for October 27, 2007 to December 5, 2007 (ID 9414290, San Francisco Bay, CA, [Tidesandcurrents.NOAA.gov](#), 2008)
- Figure 2-5 Peak-flood current velocities retrieved from the San Francisco 2Dh-model on Feb 20, 2004 at 06:00:00, when discharge through Golden Gate was maximal; $1.65 \cdot 10^5 \text{ m}^3\text{s}^{-1}$
- Figure 2-6 Peak-ebb current velocities retrieved from the San Francisco 2Dh-model on Feb 19, 2004 at 22:00:00, when discharge through Golden Gate was minimal; $-1.85 \cdot 10^5 \text{ m}^3\text{s}^{-1}$
- Figure 2-7 Water circulation pattern in the inlet mouth of San Francisco Bay, A) Circulation pattern in the Golden Gate area during maximum flood. Water enters the Bay in a jet current. B) During ebb circulation west of the Golden Gate water exits the Bay as a jet with adjacent counter-rotating eddies. C) Flow directions of the strongest currents beneath the jets are flood oriented in the Bay and ebb oriented west of the Golden Gate. Strongest currents adjacent to the jets are ebb oriented in the Bay and flood oriented west of the Golden Gate (by Rubin & McCulloch, 1979)
- Figure 2-8 Residual current velocity pattern retrieved from the San Francisco 2Dh-model

- Figure 2-9 Tidal currents from DELFT3D superimposed over the bathymetry, illustrating good agreement between peak flow vectors during ebbing tide and bedform morphology (by Barnard *et al.*, 2006, courtesy of USGS)
- Figure 2-10 Ebb tidal delta change between 1956 and 2005 (by Barnard *et al.*, courtesy of USGS)
- Figure 2-11 Central San Francisco Bay sediment size (by Rubin & McCulloch, 1980)
- Figure 2-12 San Francisco Bay inlet mouth cross sections A-B and C-D (by Barnard *et al.*, 2005, USGS). The shaded relief bathymetry was created with a 2-m grid and a 4x vertical exaggeration
- Figure 2-13 Cross section A-B and C-D of 8 adjacent sandwaves in San Francisco inlet mouth (by Barnard *et al.*, 2005, USGS). Note that the vertical scale is exaggerated by a factor 4
- Figure 3-1 Digital rendering of sandwaves in San Francisco Bay (courtesy of USGS)
- Figure 3-2 Schematization of sandwave height and length (by Buijsman, 2007)
- Figure 3-3 Stoss and lee slopes of sandwaves (by Whitmeyer and FitzGerald, 2006)
- Figure 3-4 Residual circulation cells believed to support sandwave formation (by Hulscher, 1996)
- Figure 3-5 Flow separation over river dunes (by Hulscher & Dohmen-Janssen, 2005)
- Figure 4-1 Schematic diagram of converting data into setup for the DELFT3D 2Dv-model
- Figure 5-1 Curvilinear DELFT3D-FLOW grid and boundaries. Inset shows locations of current measurement sites (by Barnard *et al.*, 2007)
- Figure 5-2 Distribution of the area specific sandwave height
- Figure 5-3 Distribution of the area specific sandwave length
- Figure 5-4 Distribution of the area specific median grain-size
- Figure 5-5 Distribution of the area specific peak ebb current velocity
- Figure 5-6 Distribution of the area specific peak flood current velocity
- Figure 5-7 Distribution of the area specific residual current velocity
- Figure 5-8 Scatterplot of sandwave height versus length
- Figure 5-9 Scatterplot of median grain-size versus maximum current velocity

- Figure 6-1 Detailed presentation of the vertical σ -grid in combination with the sandwave bed level
- Figure 6-2 Computational grid of a sandwave field, represented by a symmetrical sinusoidal wave-train with its largest wave in the center of the field
- Figure 6-3 Erroneous bed level response when combining velocity and water level boundaries, with $U_1 = 1.00 \text{ ms}^{-1}$ placed on the right side and $\zeta_1 = 1.00 \text{ m}$ placed on the left side. After 1 hydrodynamic day the disturbance is excessively high and starts to affect the morphodynamic development
- Figure 6-4 Velocity time series for $U = 0.50 \text{ ms}^{-1}$, 1.00 ms^{-1} and 1.50 ms^{-1} , measured at the top of the center sandwave monitoring point. The Baker Beach and Mouth Center velocities were created on a fixed sandwave bed, using a sandwave length of 100 m and a height of 7.8 m and 9 m, respectively. The horizontal velocities are taken in the water surface layer.
- Figure 6-5 Computational time step comparison for $U_{\text{hor}} = 0.50 \text{ ms}^{-1}$ and $U_{\text{hor}} = 1.50 \text{ ms}^{-1}$
- Figure 6-6 Stability of a symmetrical equilibrium sandwave. A) Flow components and thresholds acting at a point P where the sandwave has a maximum slope α . B) Equilibrium of a spherical grain beneath a current on a bed of similar grains (by Allen, 1980).
- Figure 7-1 Baker Beach sandwave configurations ($U_1 = 0.50 \text{ ms}^{-1}$)
- Figure 7-2 Baker Beach sandwave configurations ($U_1 = 1.00 \text{ ms}^{-1}$)
- Figure 7-3 Baker Beach sandwave configurations ($U_1 = 1.50 \text{ ms}^{-1}$)
- Figure 7-4 Mouth Center sandwave configurations ($U_1 = 0.50 \text{ ms}^{-1}$)
- Figure 7-5 Mouth Center sandwave configurations ($U_1 = 1.00 \text{ ms}^{-1}$)
- Figure 7-6 Mouth Center sandwave configurations ($U_1 = 1.50 \text{ ms}^{-1}$)
- Figure 7-7 Bed level change of the equilibrium sandwave configuration in 20 m water depth, for a current velocity of 1.00 ms^{-1}
- Figure 7-8 Bed level change of the equilibrium sandwave configuration in 40 m water depth, for a current velocity of 1.00 ms^{-1}
- Figure 7-9 Residual flow velocity field in 20 m depth that belongs to a sandwave height of 9.8 m and a length of 125 m. The displayed flow pattern and magnitude is the result of running the model on a fixed sandwave bed and results in an equilibrium sandwave height.
- Figure 7-10 Residual flow velocity field in 20 m depth that belongs to a sandwave height of 5.0 m and a length of 125 m. The displayed flow pattern and magnitude is the result of running the model on a fixed sandwave bed and results in growth of sandwave height.

- Figure 7-11 Residual flow velocity field in 20 m depth that belongs to a sandwave height of 5.9 m and a length of 75 m. The displayed flow pattern and magnitude is the result of running the model on a fixed sandwave bed and results in decay of sandwave height. Note that the scaling is similar to Figure 7-9 and 7-10, only the sandwave length is smaller therefore grid size appears larger.
- Figure 7-12 Residual flow velocity field in 40 m depth that belongs to a sandwave height of 13.5 m and a length of 150 m. The displayed flow pattern and magnitude is the result of running the model on a fixed sandwave bed and results in an equilibrium sandwave height.
- Figure 7-13 Residual flow velocity field in 40 m depth that belongs to a sandwave height of 5.0 m and a length of 150 m. The displayed flow pattern and magnitude is the result of running the model on a fixed sandwave bed and results in growth of sandwave height.
- Figure 7-14 Residual flow velocity field in 40 m depth that belongs to a sandwave height of 6.8 m and a length of 75 m. The displayed flow pattern and magnitude is the result of running the model on a fixed sandwave bed and results in decay of sandwave height. Note that the scaling is similar to Figure 7-12 and 7-14, only the sandwave length is smaller therefore grid size appears larger.
- Figure 7-15 Baker Beach equilibrium configuration time series for velocities and shear stresses at the Crest monitoring point, using a sandwave height of 9.8 m with a length of 125 m.
- Figure 7-16 Baker Beach equilibrium configuration time series for velocities and shear stresses at the Slope1 monitoring point, using a sandwave height of 9.8 m with a length of 125 m.
- Figure 7-17 Baker Beach equilibrium configuration time series for velocities and shear stresses at the Trough monitoring point, using a sandwave height of 9.8 m with a length of 125 m.
- Figure 7-18 Mouth Center equilibrium configuration time series for velocities and shear stresses at the Crest monitoring point, using a sandwave height of 13.5 m with a length of 150 m.
- Figure 7-19 Mouth Center equilibrium configuration time series for velocities and shear stresses at the Slope1 monitoring point, using a sandwave height of 13.5 m with a length of 150 m.
- Figure 7-20 Mouth Center equilibrium configuration time series for velocities and shear stresses at the Trough monitoring point, using a sandwave height of 13.5 m with a length of 150 m.

- Figure 7-21 Instantaneous velocity pattern over steep profile using the hydrostatic (σ -layer) approach [$U_0 = 0.35 \text{ ms}^{-1}$]. On the right hand side of the crest flow increases to $U = 1.00 \text{ ms}^{-1}$ and velocity vectors are pointed straight down followed by upward pointed vectors.
- Figure 7-22 Influence of bed-slope factor on sandwave growth rate.
- Figure 7-23 Influence of median grain-size on sandwave growth rate.
- Figure 8-1 Instantaneous sediment transport rates and bed shear stress time series, for the equilibrium sandwave configurations at 20m and 40m water depth, respectively.
- Figure 8-2 Equilibrium sandwave heights for different lengths using the median water depths of Baker Beach and Mouth Center for the flow velocities $U_1 = 0.50, 1.00$ and 1.50 ms^{-1} . Blue markers correspond to equilibrium heights of Baker Beach median depth, green markers correspond to Mouth Center.
- Figure 8-3a Residual flow pattern of Baker Beach decaying sandwave configuration. Showing a net current directed towards the eastern boundary. Note the scale on y-axis.
- Figure 8-3b Residual flow pattern of Mouth Center decaying sandwave configuration. Showing a net current directed towards the western boundary. Note the scale on y-axis.
- Figure 8-4 2Dv-model data overlay on top of the collection of field data points. Baker Beach markers are colored blue, Mouth Center markers are green. The 2Dv-model data points drawn are the equilibrium heights applying $U = 1.00 \text{ ms}^{-1}$, with a linear trend line showing an R^2 value of 0.99 for both project areas.

LIST OF TABLES

| | |
|-----------|--|
| Table 2-1 | Tide levels in meters and feet (ID9414290, San Francisco Bay, CA, 1983-2001) |
| Table 2-2 | Main harmonic constituents of San Francisco Bay (ID 9414290, San Francisco Bay, CA, Tidesandcurrents.NOAA.gov , 2008) |
| Table 2-3 | Main harmonic constituents with their description (ID 9414290, San Francisco Bay, CA, Tidesandcurrents.NOAA.gov , 2008) |
| Table 3-1 | Bedform classification and characteristics |
| Table 6-1 | Phase differences between East and West boundary forcings, corresponding to maximum center crest flow velocities on fixed bed levels at depths of 20 and 40 m |
| Table 7-1 | Length over height ratios that belong to the equilibrium sandwave configurations, presented for both study areas |
| Table 7-2 | Growth rates for determined equilibrium sandwave heights, depicted for both study areas and for different velocity amplitudes |
| Table 8-1 | DELFT3D 2Dv-model restrictions upon achieving equilibrium in sandwave height and length development |
| Table 8-2 | DELFT3D 2Dv-model restrictions upon achieving growth in sandwave height and length development |
| Table 8-3 | DELFT3D 2Dv-model restrictions upon achieving decay in sandwave height and length development. |
| Table 8-4 | Field data results versus DELFT3D model results. Median values of sandwave field data are compared with the range of values found using the 2Dv-model. Peak current velocities calculated with the 2Dv-model are the largest velocities of all performed runs, using the velocity magnitude of 1.50 ms^{-1} . These peak velocities are found on top of the (largest) center sandwave. |

1. INTRODUCTION

1.1 Project description

The more than 2,000 km long West Coast of California was recently mapped in high resolution by a multibeam sonar survey, performed by the U.S. Geological Survey (USGS) and California State University, Monterey Bay. Connected to the Pacific Ocean by the Golden Gate Channel on the 37° latitude, the San Francisco Bay (Figure 1-1) accommodates a widely spread field of underwater bedforms. The highly detailed maps illustrated in Figure 1-2 and Figure 1-3, are based on data collected in 2004 and 2005, and show large fields of sandwaves that cover an area of roughly four square kilometers and reside just west of the Golden Gate Bridge.

The existence of sandwaves in the San Francisco Bay area is long known, however their features were not. The bathymetric survey revealed a depth range of 30 to 106 m, sandwave lengths and -heights that measured up to 317 m and 10 m respectively, a modest tidal range of 2.65 m and strong bidirectional tidal flow with peak currents of more than 2.50 ms⁻¹. The scale of the San Francisco sandwaves is not unique. Examples of comparable sandwave dimensions have also been discovered in the Cook Inlet, Alaska (Bouma et al., 1980), the Bay of Fundy (Dalrymple et al., 1978), the Japanese Sea (Knaapen et al., 2002) and Messina Strait, Italy (Santoro et al., 2002).

Studying the behavior and development of sandwaves is part of a project that analyzes the processes that control sand transport and sedimentation patterns of Ocean Beach (upper left of Figure 1-2). This area encompasses a complex coastal setting that bears the tidal influence of San Francisco Bay, as well as the south- and northwest Pacific swell. The goal of this project is to assess the cause of the erosion hot spot at the south end of Ocean Beach by quantifying the physical processes, determining the dominant sediment transport pathways, identifying seasonal trends and evaluating the efficiency of potential coastal management solutions. Eventually sediment dynamics of the San Francisco tidal inlet might benefit by an improved understanding of sandwave behavior.



Figure 1-1: From small to large map; United States of America and San Francisco Bay area (copyright © 2005-2008 United-States-Maps.com and Google Earth™, 2008).

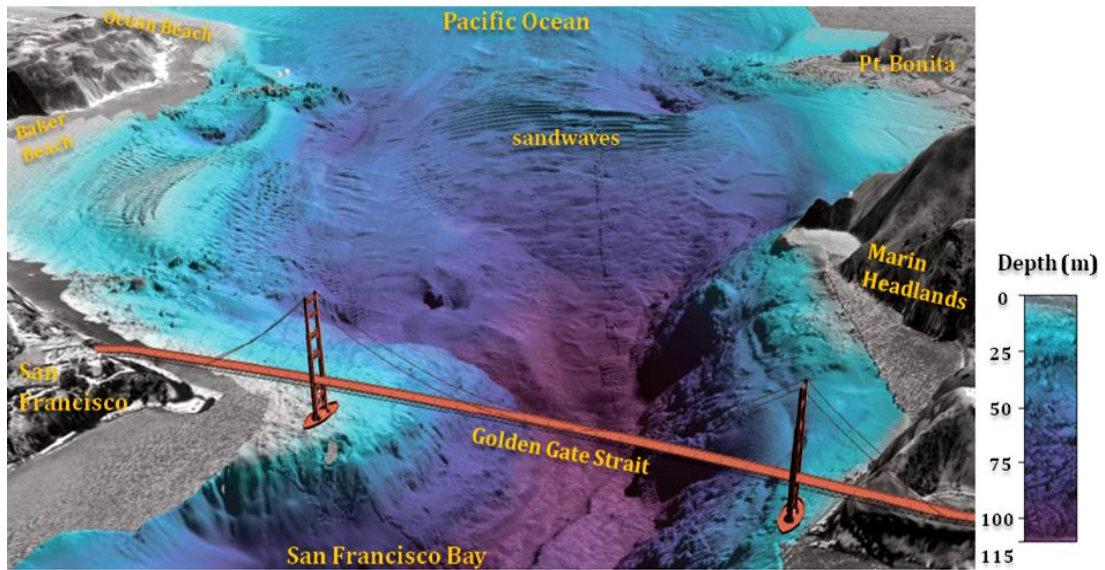


Figure 1-2: Perspective view southwest over the Golden Gate Bridge toward the Pacific Ocean at the entrance of San Francisco Bay. The features on the sea floor in the center of the inlet mouth are sandwaves. The distance across the bottom of the image is about 3 km (by Barnard et al., courtesy of USGS, 2006).

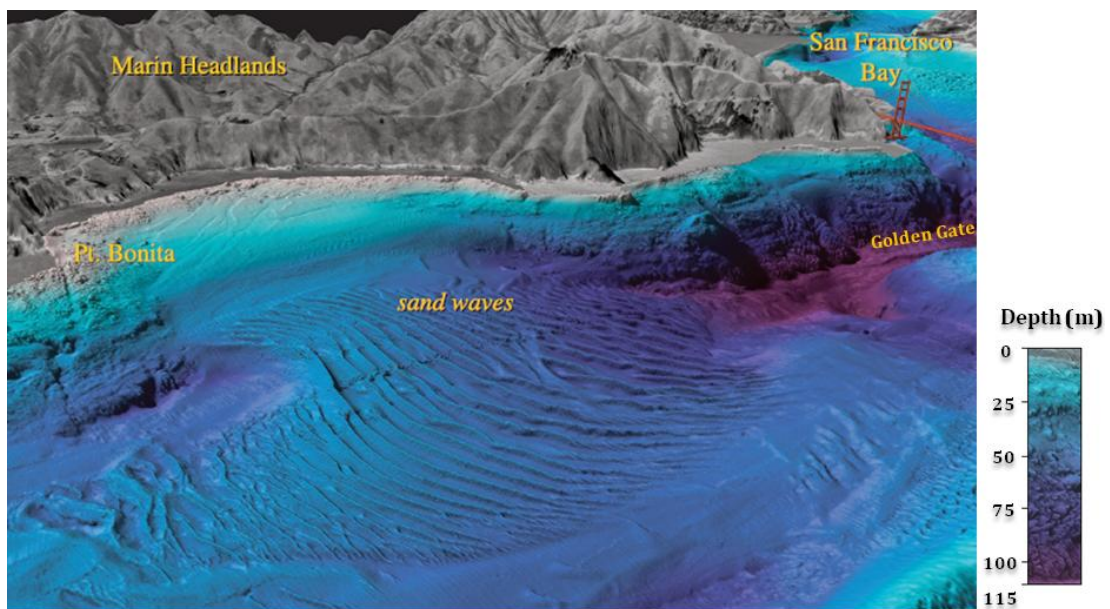


Figure 1-3: Perspective view northeast over the entrance to San Francisco Bay. The water depth over the sandwaves within this field ranges from 30 to 100 m. The distance across the bottom of the image is about 2.4 km (by Barnard et al., courtesy of USGS, 2006).

1.2 Objective

The San Francisco sandwaves show large temporal and spatial variations which are not yet fully understood. Various studies have been performed to model bedforms classified as sandwaves¹, (e.g. Hulscher, 1996; Németh *et al.*, 2002; Morelissen *et al.*, 2003; Besio, 2004; Tonnon *et al.* 2007) however none of these studies elaborated on the ability of numerical process-based models to capture the sandwave formation mechanisms. Two generally accepted mechanisms are vertical residual circulation cells and flow separation induced eddies.

The main objective of this MSc project is to study the capability of DELFT3D to model the San Francisco sandwaves using a 2Dv-model, with emphasis on assessing the formation mechanisms. The objective is translated into the following research questions.

Main questions:

- I. What are the main mechanisms that control the development of sandwaves?
- II. Which requirements are necessary for the 2Dv-model to reach a state of equilibrium?

Sub questions:

- III. Under what conditions is DELFT3D capable of describing the hypothesized formation mechanisms?
- IV. What is the influence of the residual current on the morphologic behavior of the sandwaves?

To properly answer the stated research questions, the output and analysis of the 2Dv-model will focus on three key aspects. First, the morphological development of all sandwave configurations is compared to gain insight in the differences between the modelled sandwaves and the sandwaves found in the inlet mouth of San Francisco Bay. This is done by a stability analysis of the monitoring points in the final bathymetry output. Second, the residual flow patterns and near bed velocities are compared for each simulation, to provide insight in the formation mechanisms. Residual vector plots displaying magnitude and residual flow direction are used to quantify the difference in residual velocity profiles, using different sandwave configurations. Finally, in extend of the previous two aspects; the effect of alternating physical parameters and flow configurations is analyzed to acquire insight in the sensitivity of the numerical model.

¹ See Table 3-1 for bedform classifications and characteristics

1.3 Outline

Chapter 2 elaborates on the project location of San Francisco Bay. In chapter 3 theory regarding sandwave characteristics and formation mechanisms is presented. Chapter 4 explains the approach of this research, followed by chapter 5 which describes the data analysis necessary to represent the San Francisco sandwaves in the 2Dv-model. Chapter 6 elaborates on 2Dv-model setup and in chapter 7 the results of the morphodynamic and hydrodynamic simulations are presented. These simulations are analyzed and discussed in chapter 8. Chapter 9 is the final chapter with conclusions and recommendations.

Along with this printed version of the report a DVD is provided. This DVD contains the majority of the appendices, the MATLAB script files and the most important simulations.

1.4 Acknowledgements

The presented thesis is the result of a project partly executed at the Pacific Science Center of the U.S. Geological Survey (USGS) in Santa Cruz, California and at Delft University of Technology. Participation of both USGS and Deltares is gratefully acknowledged as they both contributed with help and information to great extent. In addition, the author would like to thank the following people for their supervision and helpful advice:

- Prof. dr. ir. M.J.F. Stive (Delft University of Technology)
- dr. ir. E.P.L. Elias (Deltares)
- dr. D.M. Hanes (US Geological Survey)
- dr. ir. J.E.A. Storms (Delft University of Technology)
- dr. L. Erikson (U.S. Geological Survey)
- dr. P.L. Barnard (U.S. Geological Survey)
- ir. D.J. Walstra (Deltares)
- ir. G. de Boer (Deltares)
- ir. F. van der Meer (Twente University of Technology)

2. SAN FRANCISCO BAY

The following section covers the background of San Francisco Bay. An overview of the project area topography and history is described based on recent and past studies. Subsequently, the sections hydrodynamic and morphodynamic conditions cover the physical aspects of the Bay, including a description of the tide, sediment and sandwave characteristics.

2.1 Project area

San Francisco Bay is a large urbanized estuary encompassing an area of roughly 4,100 km². The inlet mouth of the estuary is the main area of interest in this study and borders to the Golden Gate on the east side, the ebb-tidal delta on the west side, the Marin Headlands on the north side and finally Baker Beach on the south side (Figure 2-1). The project area, or west-central San Francisco Bay, is the deepest part of the estuary containing the coarsest sediment and the strongest currents. Bedrock pinnacles and sandy shoals focus tidal currents and produce a wide range of bedform morphologies that were first mapped by Rubin and McCulloch (1979) and later in high resolution multibeam by Chin et al. (1997b; 2004) and Kvitek (2007). Appendix A illustrates a historic map of the Bay area back in 1850 before developments, encompassing all three subembayments.

The mouth of San Francisco Bay is morphologically dominated by the San Francisco Bar, a massive ebb tidal delta that covers a region of approximately 175 km² with an average depth of 17 m. This region is exposed to highly energetic waves and swell directed from the Pacific Ocean. In general there is a strong dominance of waves coming from the northwest direction. The average annual maximum offshore significant wave height is 8.0 meters, and the annual average offshore significant wave height is 2.5 meters. The average annual maximum offshore peak wave period measures 16.6 s.

The project area varies greatly in depth. At approximately 2.5 km distance from the Golden Gate Strait, just offshore of Baker Beach, the water depth varies from a 20 m average up to a maximum of 65 m. In the center of the inlet mouth the average water depth measures 41 m, while the maximum depth here is 74 m. And just offshore of Point Lobos the depth range varies from an average of 27 m to a maximum of 42 m.

Through the Golden Gate, the channel has scoured down into bedrock at a maximum depth of 115 m. Several of the submerged rock knobs that are found above the central San Francisco Bay floor, posed a serious hazard to navigation and have been lowered by blasting in the past. West-central San Francisco Bay in particular has several of such rock knobs, and all of these are believed to be part of the same geological formation, the Franciscan Complex. This heterogeneous rock assemblage of Jurassic-Cretaceous age (190 to 65 million years old) is the bedrock beneath much of the San Francisco Bay area (Konigsmark, 1998). Franciscan rocks form Angel and Alcatraz Islands, as well as the hills of San Francisco and the Marin Headlands adjacent to the Golden Gate.

Tidal currents accelerate through the erosion resistant rocky strait of the Golden Gate. As these currents decelerate, large bedforms are created on either side of the Golden Gate including the large field of sandwaves just seaward of the strait (Barnard *et al.*, 2007). The orientation of the large scale bedforms throughout the project area is believed to be controlled by the dominant tidal current directions in and out of San Francisco Bay. The only exception is an area of divergence along the southern lobe of the ebb tidal delta, where the bar intersects central Ocean Beach. The largest bedforms are found in the inlet throat (Figure 2-2), near the Golden Gate, where tidal currents can be more than 2.5 ms^{-1} during peak ebb and peak flood tide.

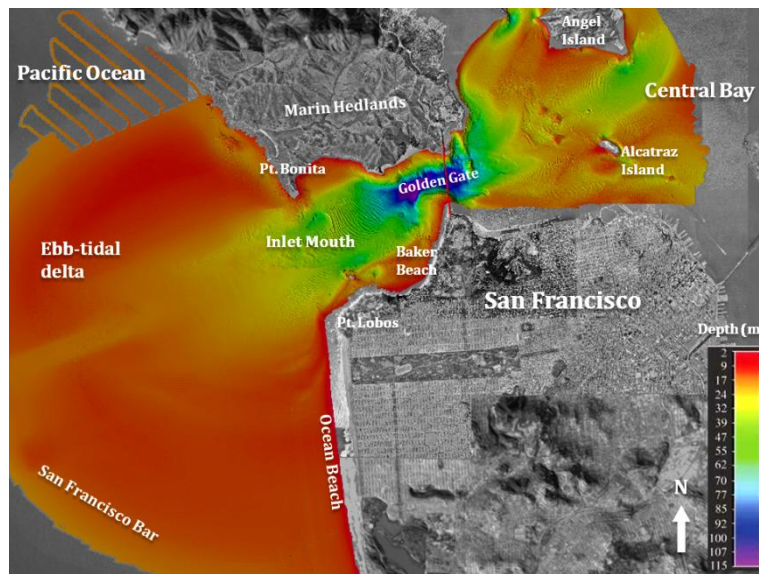


Figure 2-1: High resolution image of the entire San Francisco Bay inlet mouth, entitled as the project area of this study (by Barnard *et al.*, 2006, USGS).

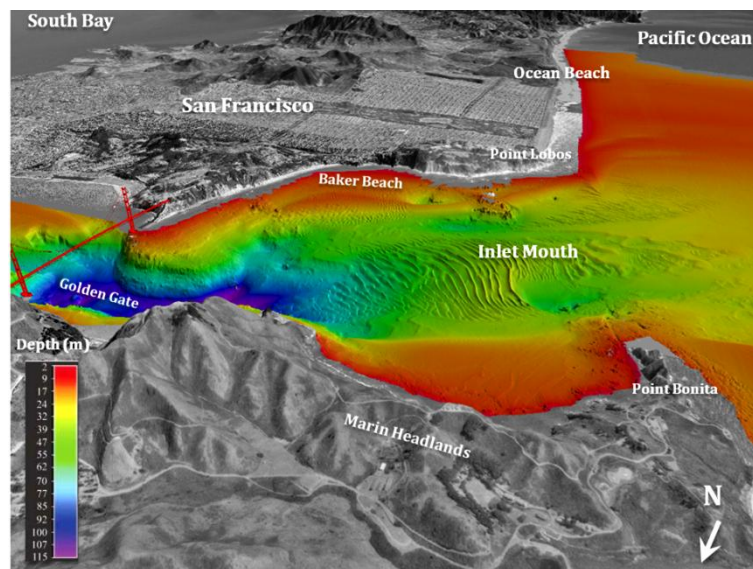


Figure 2-2: High resolution image showing the San Francisco Bay inlet mouth from the north (by Barnard *et al.*, 2006, USGS).

2.2 Hydrodynamic conditions

2.2.1 Tide

The National Ocean and Atmospheric Administration (NOAA) provides tidal records with great detail of San Francisco Bay. A time series analysis of water level data (1983 to 2001) results in the list of chart data presented in Table 2-1. All data is referenced to MLLW. One year of water level data (2007) is plotted in Figure 2-3 to show an average water level of 1.00 m above MLLW. Another plot of measured water levels is shown in Figure 2-4 which displays a representative image of the tidal elevation without presence of storm activities from October 27, 2007 to December 5, 2007.

The tidal prism² that enters the San Francisco Bay through a narrow opening at the Golden Gate is $2 \cdot 10^9$ m³, has a range of nearly 2 meters and is composed primarily of the M2 and K1 constituents. A complete list of the ten most important tidal constituents with their definitions is presented in Table 2-2 and Table 2-3. Both tables display the amplitudes and the phase lags of the observed tidal constituents, (phase relative to the theoretical equilibrium tide) and the rate of change in the phase of a constituent (speed). Only constituents with the largest amplitude are displayed.

| Chart datum | Water level (m) compared to MLLW | Water level (ft) compared to MLLW |
|--------------------|-------------------------------------|--------------------------------------|
| MHHW | 1.78 | 5.84 |
| MHW | 1.60 | 5.23 |
| MSL | 0.95 | 3.12 |
| MLW | 0.35 | 1.13 |
| MLLW | 0.00 | 0.00 |
| Station Max (1983) | 2.64 | 8.66 |
| Station Min (1933) | -0.88 | -2.88 |

Table 2-1: Tide levels in meters and feet (ID 9414290, San Francisco Bay, CA, 1983-2001).

² The tidal prism is equal to the volume of tidal flow. For San Francisco Bay the tidal prism is in the order of 2 billion m³

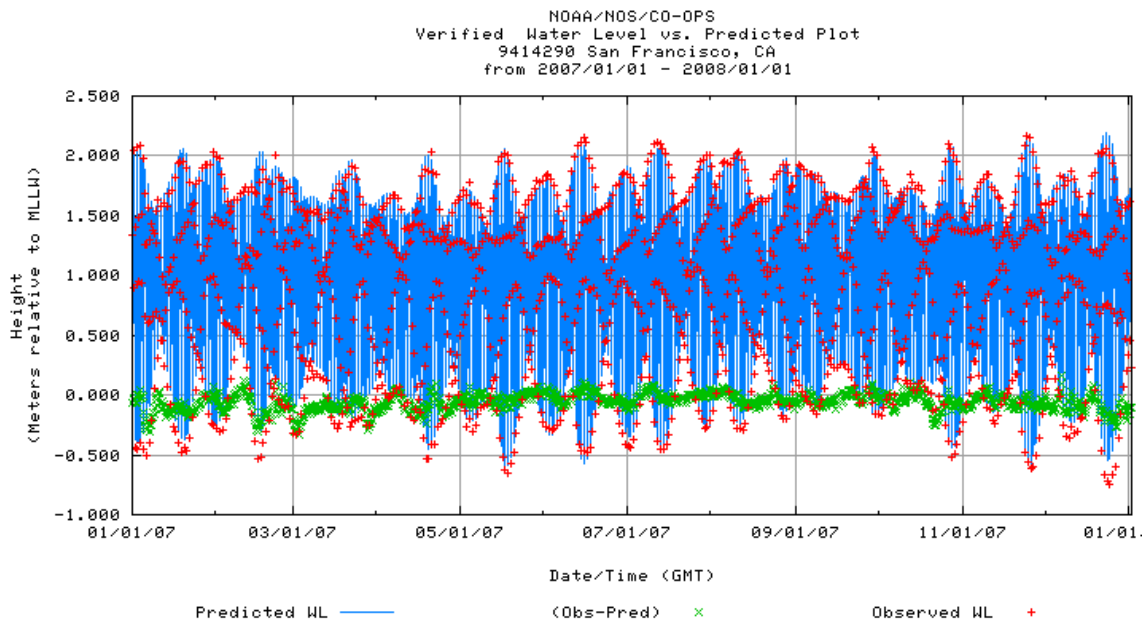


Figure 2-3: Predicted and observed tidal elevation for January 1, 2007 to January 1, 2008 (ID 9414290, San Francisco Bay, CA, Tidesandcurrents.NOAA.gov, 2008).

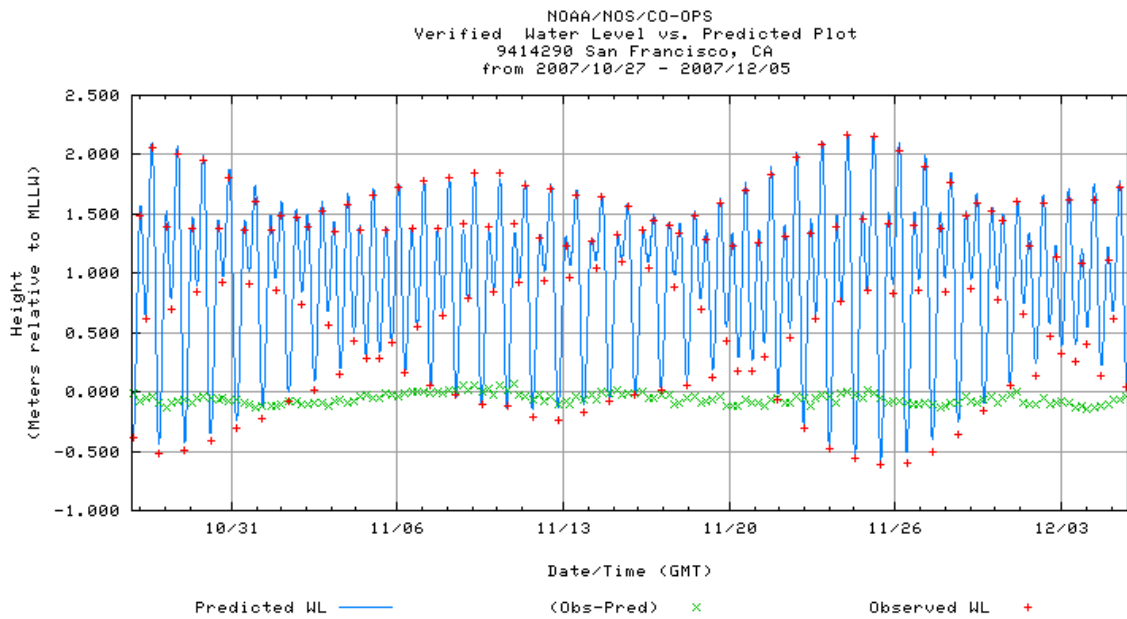


Figure 2-4: Predicted and observed tidal elevation for October 27, 2007 to December 5, 2007 (ID 9414290, San Francisco Bay, CA, Tidesandcurrents.NOAA.gov, 2008).

| Name | Amplitude (m) | Phase (deg) | Speed (deg/hour) |
|------|---------------|-------------|------------------|
| M2 | 0.580 | 210.6 | 28.98 |
| K1 | 0.368 | 226.5 | 15.04 |
| O1 | 0.230 | 210.1 | 13.94 |
| S2 | 0.137 | 218.4 | 30.00 |
| N2 | 0.123 | 184.9 | 28.44 |
| NU2 | 0.026 | 188.3 | 28.51 |
| M4 | 0.023 | 142.0 | 57.97 |
| MK3 | 0.019 | 129.0 | 44.03 |
| J1 | 0.019 | 243.8 | 15.59 |
| 2N2 | 0.014 | 158.4 | 27.90 |

Table 2-2: Main harmonic constituents of San Francisco Bay
(ID 9414290, San Francisco Bay, CA, Tidesandcurrents.NOAA.gov, 2008).

| Name | Definition |
|------|--|
| M2 | Principal lunar semidiurnal constituent |
| K1 | Lunar diurnal constituent |
| O1 | Lunar diurnal constituent |
| S2 | Principal solar semidiurnal constituent |
| N2 | Larger lunar elliptic semidiurnal constituent |
| NU2 | Larger lunar evectional constituent |
| M4 | Shallow water overtides of principal lunar constituent |
| MK3 | Shallow water diurnal |
| J1 | Smaller lunar elliptic diurnal constituent |
| 2N2 | Lunar elliptical semidiurnal second-order constituent |

Table 2-3: Main harmonic constituents with their description
(ID 9414290, San Francisco Bay, CA, Tidesandcurrents.NOAA.gov, 2008).

2.2.2 Currents

The following section is based on parts by Rubin & McCulloch (1979), Barnard *et al.*, 2007 and the hydrodynamic model results retrieved from the 2Dh-model of San Francisco Bay³, calibrated and validated using tidal constituent data measured in the tidal inlet (Barnard *et al.*, 2007). From the calibrated model, a suite of data was obtained spanning 36 days starting at the end of January 2004 and encompassing a spring tide cycle.

Peak flood and ebb flow

The access channel to San Francisco Bay is dominated by high velocity flows generated by jet currents that are formed by peak ebb and flood tides as they flow through the Golden Gate. These powerful and spatially variable currents result in an incredibly diverse array of bedform sizes and shapes both inside and outside the Golden Gate. During flood flow, ocean water enters the Gate and accelerates because the channel decreases in cross-sectional area. The jet current enters the Bay with depth-averaged velocities of more than 1.50 ms^{-1} (Figure 2-5), and is maintained for some distance by its momentum. During ebb flow, Bay water converges radially towards the Golden Gate due to the constriction of the inlet throat, with peak velocities at over 2.00 ms^{-1} (Figure 2-6). East of the Gate, where the jet current flows, flood velocities slightly exceed ebb velocities, however in adjacent areas north, south and west of the jet, ebb velocities exceed flood velocities. Flood and ebb velocities north and south of the tidal jet quickly decrease in strength to the range of 0.50 to 1.00 ms^{-1} . South of the estuary's inlet near Baker Beach, velocities during peak flood and peak ebb⁴ are found to be in the order of 0.50 ms^{-1} , much smaller than the peak ebb peak velocity of approximately 1.50 ms^{-1} in the center of the inlet mouth. At 10 km distance from the inlet throat near the edge of the ebb tidal delta, peak ebb currents are found to exceed 1.00 ms^{-1} illustrating the great extent of the tidal jet.

Residual flow

Figure 2-7 pictures an impression of the spatial current pattern in San Francisco Bay, based on several measurements carried out by Rubin & McCulloch (1979). Tidal residuals found using the 2Dh-model are depicted in Figure 2-8 and show the residual velocity pattern in the entire inlet mouth, ranging all the way to the ebb-tidal delta rim. The inlet mouth residuals range from zero to 0.25 ms^{-1} , and display a large circulating pattern in the center rotating counterclockwise. A much smaller circulating pattern is found just offshore of Baker Beach, which rotates clockwise. The dominant ebb-tidal jet flow through the Golden Gate can be seen to be reasonably in line with the westerly direction of residual flow. According to the two dimensional model, residual velocities just offshore of Baker Beach and in the center of the inlet mouth are relatively small, with values varying between 0.05 and 0.15 ms^{-1} .

³ For a more detailed explanation of the 2Dh-model see section 5.3.

⁴ Peak flood and ebb flow is measured at the point when discharge through the Golden Gate Strait is maximal and minimal, respectively.

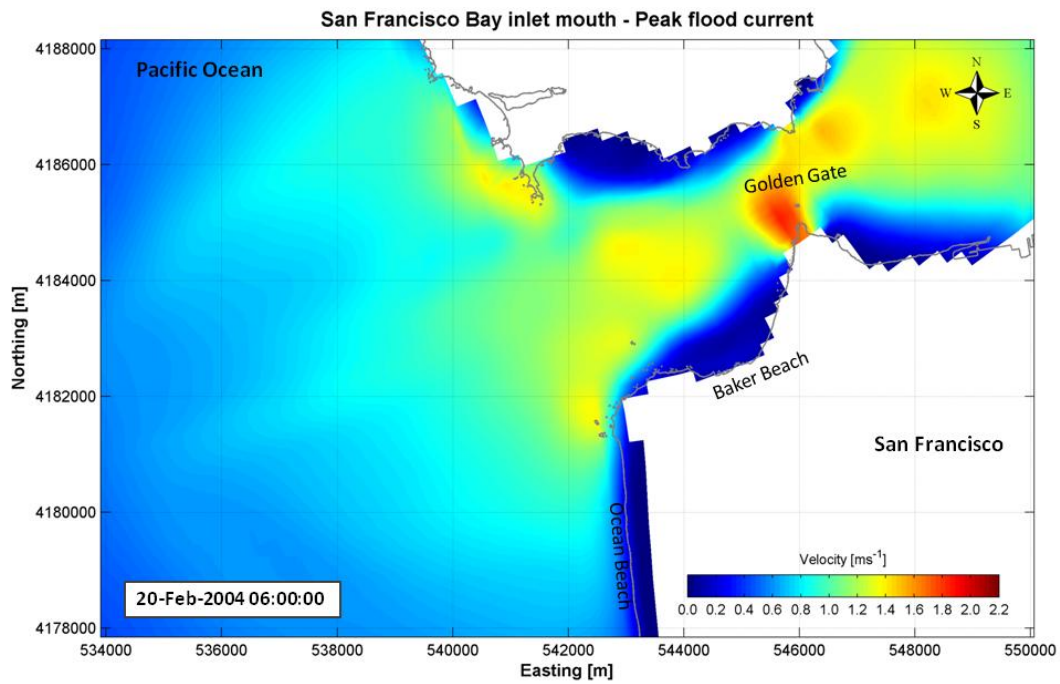


Figure 2-5: Peak-flood current velocities retrieved from the San Francisco 2Dh-model on Feb 20, 2004 at 06:00:00, when discharge through Golden Gate was maximal; $1.65 \cdot 10^5 \text{ m}^3 \text{ s}^{-1}$.

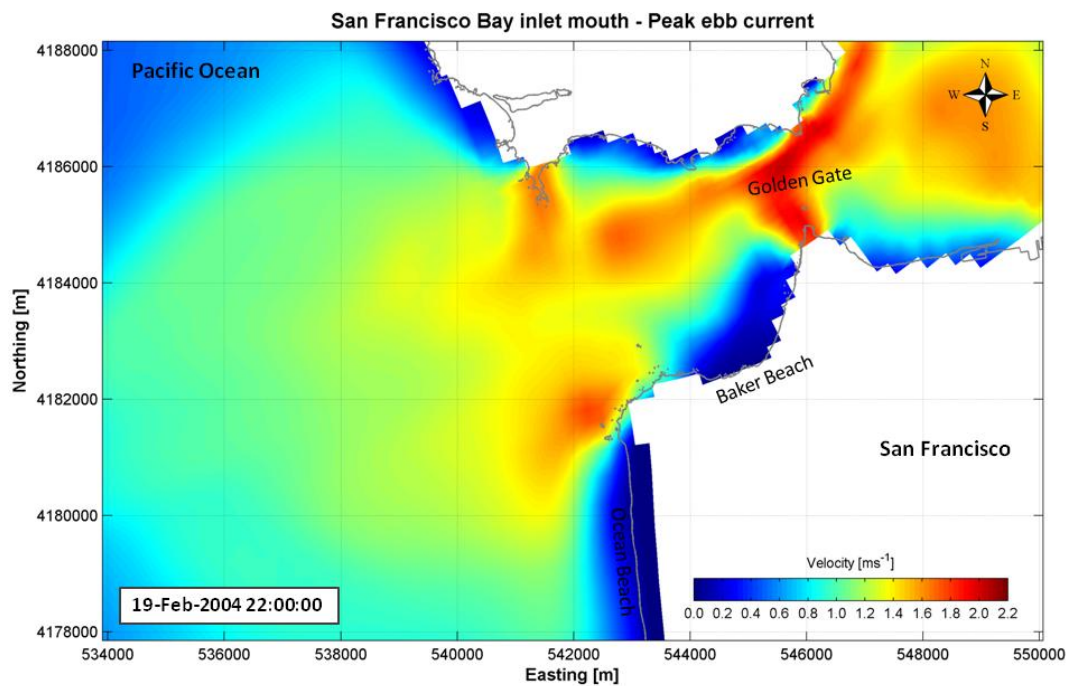


Figure 2-6: Peak-ebb current velocities retrieved from the San Francisco 2Dh-model on Feb 19, 2004 at 22:00:00, when discharge through Golden Gate was minimal; $-1.85 \cdot 10^5 \text{ m}^3 \text{ s}^{-1}$.

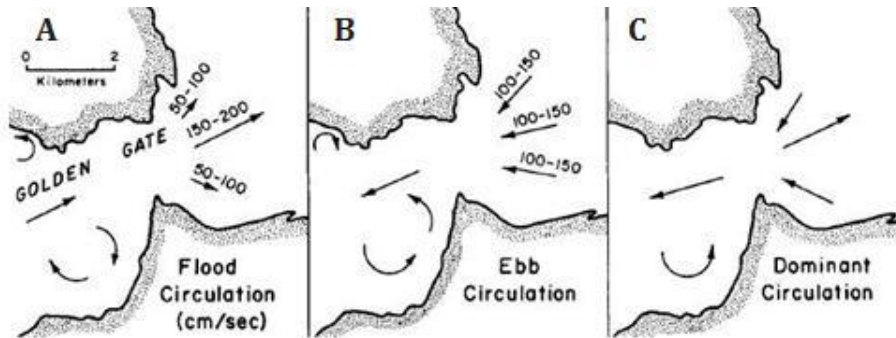


Figure 2-7: Water circulation pattern in the inlet mouth of San Francisco Bay, A) Circulation pattern in the Golden Gate area during maximum flood. Water enters the Bay in a jet current. B) During ebb circulation west of the Golden Gate water exits the Bay as a jet with adjacent counter-rotating eddies. C) Flow directions of the strongest currents beneath the jets are flood oriented in the Bay and ebb oriented west of the Golden Gate. Strongest currents adjacent to the jets are ebb oriented in the Bay and flood oriented west of the Golden Gate (by Rubin & McCulloch, 1979).

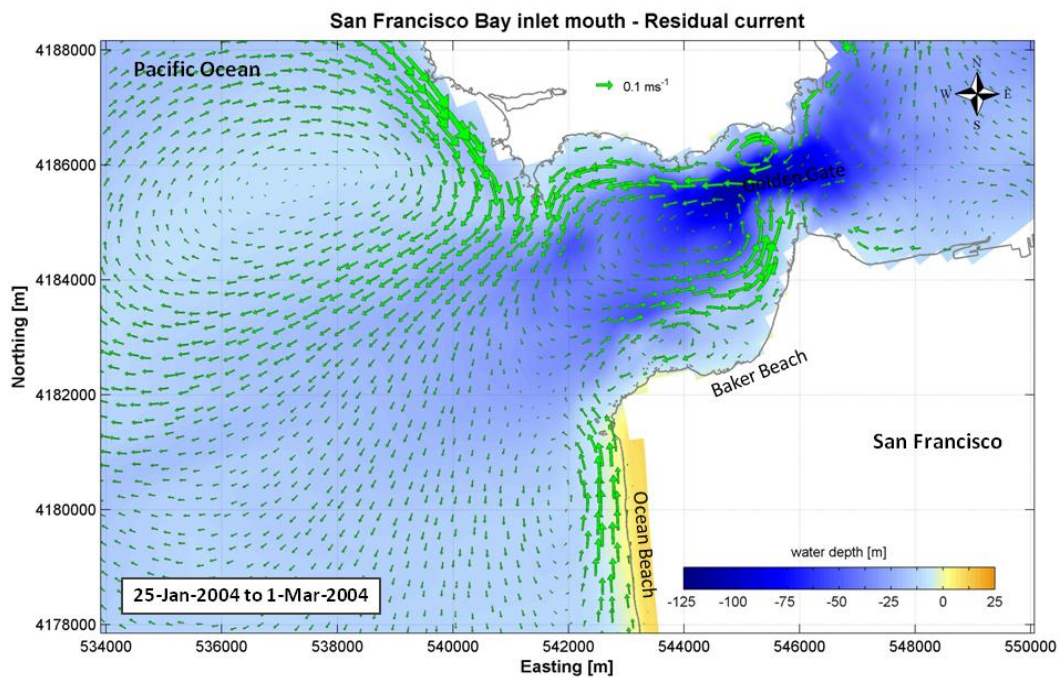


Figure 2-8: Residual current velocity pattern retrieved from the San Francisco 2Dh-model.

2.3 Morphodynamic conditions

2.3.1 Sediment transport

Throughout the last century the impact of anthropogenic activities such as channel dredging and sand mining, has had a significant impact on the coastal system of San Francisco Bay (Chin *et al.*, 2004). Recently, Barnard *et al.* (2007) determined that the estuary's inlet mouth has lost over 90 million m³ of sand-sized sediment during the last 50 years. This loss of sediment is the result of a net transport of sediment, directed from the Golden Gate Strait towards the Pacific Ocean. In reverse direction, e.g. towards the Central Bay, a net transport is observed along the side of the center sandwave field. This transport is caused by the presence of flood-dominated residual eddies which, according to Rubin & McCulloch (1979), are present along the south side of the sandwave field (Figure 2-9). The net seaward transport of sediment through the center of the inlet and toward the Bay has been categorized as mostly bedload sediment transport.

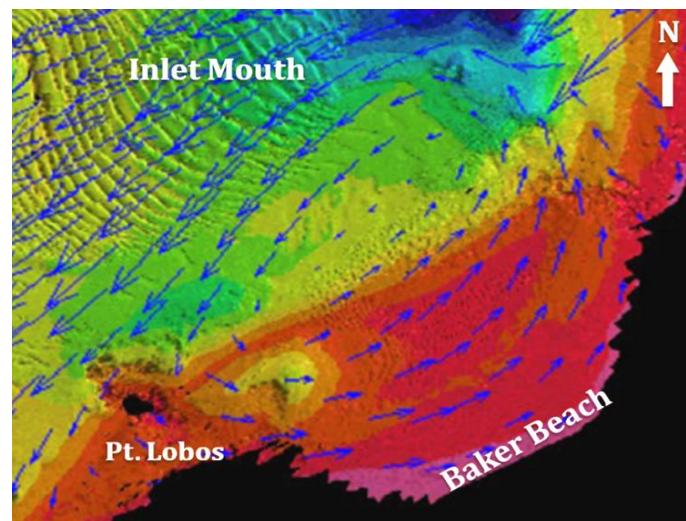


Figure 2-9: Tidal currents from DELFT3D superimposed over the bathymetry, illustrating good agreement between peak flow vectors during ebbing tide and bedform morphology (by Barnard *et al.*, 2006, courtesy of USGS).

Figure 2-10 displays the outer lobe of the ebb-tidal delta where structural erosion has led to an average eroded bed of -60 cm. Signs of accretion are observed along the north end of Ocean Beach (rates of over 5 m per year) and just south of the main shipping channel. The rate of accretion at the north end suggest that a significant amount of sediment must be transported from offshore or from the north, potentially from the strong tidal currents carrying sediment around Point Lobos from the Golden Gate. Recent studies by Barnard *et al.* (2006) hypothesize the accretion as a result of onshore sediment transport from the existing dredge disposal site (i.e. SF-8), where in 1971 the United States Army Corps of Engineers (USACE) began disposing of ship channel dredge material south of the main shipping channel on the ebb tidal delta.

The dominant sediment transport patterns outside the surf zone are believed to be controlled by tidal forcing, evident by the presence of alongshore migrating bedforms (Barnard *et al.*, 2006). According to Rubin & McCulloch (1980), the sandwaves present in the Bay area indicate the local hydraulic environment that prevailed when the sandwaves were formed, and can be used to estimate sediment transport rates to a certain degree. Directions of the bed load transport can be estimated by assuming the sediment is transported normal to the sandwave crest. And although the current reverses during each tidal cycle, the net transport occurs down the steeper slope of the sandwaves. Rubin & McCulloch (1980) continue by stating that since sediment transport rates increase as a high power of the flow velocity, the transport is strongly biased in the direction of the peak tidal current velocity. The steep and rocky geometry of the Golden Gate leads to the formation of jet flow and together with the most rapid changes in sea level in downward direction, this leads to a dominating ebb flow, and the directions of sediment transport closely resemble the direction of ebb circulation.

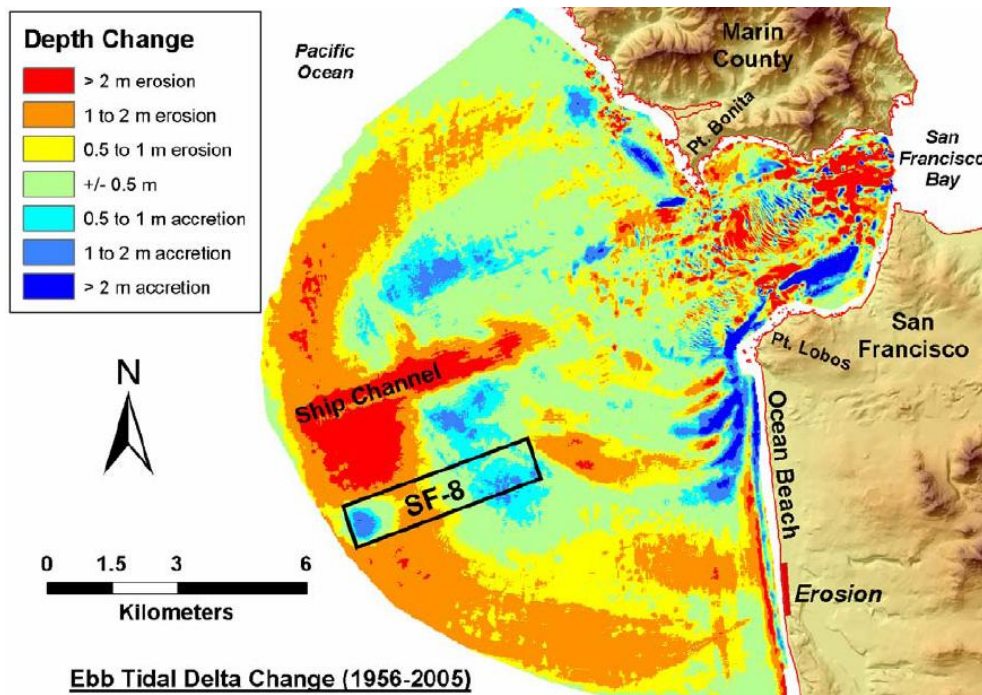


Figure 2-10: Ebb tidal delta change between 1956 and 2005 (by Barnard *et al.*, 2007, courtesy of USGS).

2.3.2 Sediment characteristics

Oscillating tidal flows, estuarine circulation and wind-generated waves are the main mechanisms that are responsible for hydraulic sorting of the bed load, which largely determines the composition, pattern, rate, and total flux of sediment in the estuary (Rubin & McCulloch, 1980). The eastern and northern margins of West-Central Bay are lined with broad muddy flats in shallow water. Between these flats and the of bare bedrock composed Golden gate, the Bay is floored with sand. Figure 2-11 demonstrates that grain-sizes peak in the inlet throat on the large sandwave field, and steadily decreases with increasing distance from the center of the inlet.

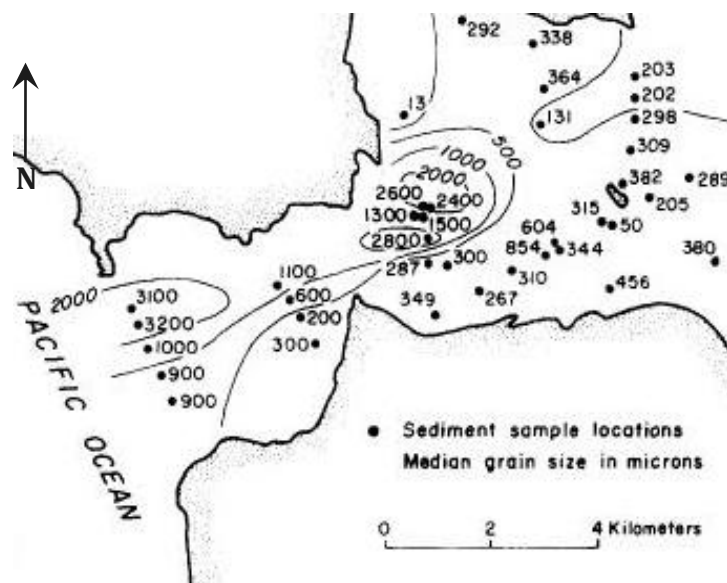


Figure 2-11: Central San Francisco Bay sediment size (by Rubin & McCulloch, 1980).

Sediment at the mouth of San Francisco Bay is highly variable, ranging from very fine sand on the outer reaches of the ebb tidal delta, to coarse sand and gravel in the inlet throat, in the heart of the sandwave field (Appendix B). The distribution of sediment grain size is linked to tidal current strength, with the coarsest sediment associated with the strongest currents, as in the inlet throat. Sediment sampling at the near shore disposal site after the June 2005 disposal indicates a median grain size of 0.18 mm in that location (Barnard et al., 2007).

2.3.3 Sandwaves

Recently, Barnard *et al.* (2006) analyzed more than 3,000 bedforms of the San Francisco Bay derived from a series of multibeam surveys, measuring a total of 1,598 individual bedforms along 262 transects. The survey focussed on nineteen adjoining sandwaves along the centerline axis in a water depth ranging up to 80 m. It showed that sandwaves in the center of the inlet mouth have an average of 82 m, much larger than the median length of the entire Bay which varies between 10 and 20 m. Sandwaves larger than 5 m in height were found in the inlet throat just seaward of the Golden Gate Strait. In the immediate vicinity of the inlet mouth and in the confined channels inside the Bay, all sandwave heights were found to be larger than 2 m. Sandwaves were found not to exist in the narrowest portions of the inlet throat, near the Golden Gate Bridge, where flow velocities can exceed 2.5 ms^{-1} hence having swept all sediment out of this region, leaving only exposed bedrock.

The transect lines A-B and C-D, depicted in Figure 2-12, were mapped four times in 2004 and three times in 2005. Figures 2-13a and 2-13b display both cross sections A-B and C-D, taken in the center and south of the inlet mouth respectively. Section A-B clearly demonstrates a significant underlying slope with a sandwave shape asymmetry⁵ directed towards the Pacific Ocean. Section C-D depicts a similar underlying slope with sandwaves that are shaped more symmetrically.

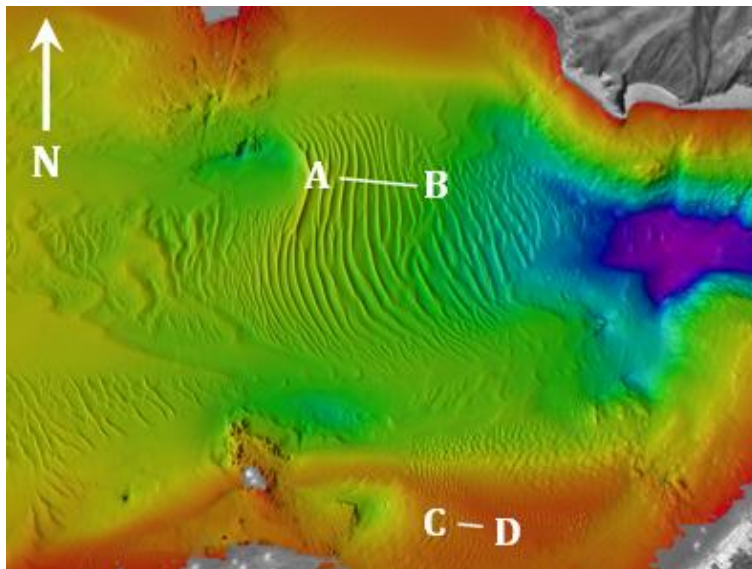


Figure 2-12: San Francisco Bay inlet mouth cross sections A-B and C-D (by Barnard *et al.*, 2005, USGS). The shaded relief bathymetry was created with a 2-m grid and a 4x vertical exaggeration.

⁵ Here, the ebb-direction asymmetry ($A < 0$) is equivalent to the orientation of the sandwave (steepest) lee slope facing the Pacific Ocean. Flood-directed asymmetry ($A > 0$) indicates the lee slope facing the San Francisco Bay.

The steepest sandwaves (i.e. low steepness index⁶) are found in the center of the inlet mouth, with steepness values smaller than 20 (Appendix C). The most gently sloping sandwaves are located in the south of the inlet mouth along Ocean Beach, where steepness values are larger than 200. Depths versus height ratios (Appendix D) were found to be lowest in the inlet throat and in the confined channels inside the San Francisco Bay. For a more elaborate exploration of the inlet mouth sandwave characteristics, see section 5.2.1 for the field data analysis.

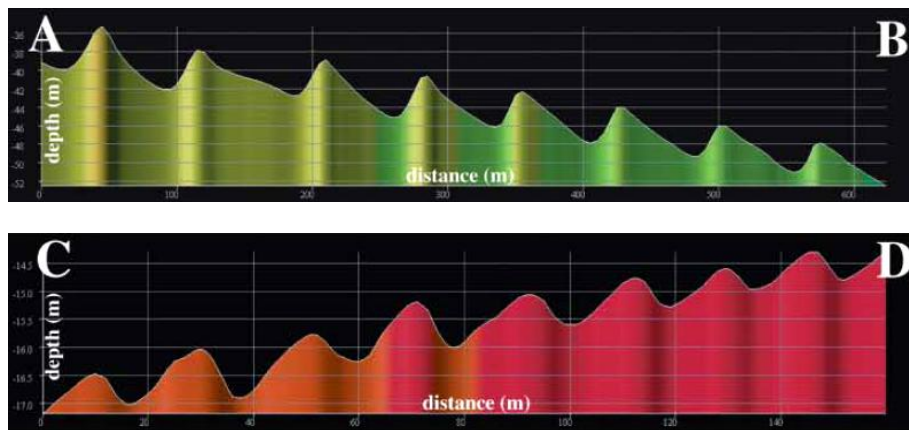


Figure 2-13 a,b: Cross section A-B and C-D of 8 adjacent sandwaves in San Francisco inlet mouth (by Barnard et al., 2005, USGS). Note that the vertical scale is exaggerated by a factor 4.

A spatial lag correlation analysis along the central axis of the inlet mouth sandwave field indicates there is a net offshore migration of 7 m in one year. A number of crests positions however, were seen alternating up to 3 m a day, depending on the daily tidal current. The net migration suggests a significant flux of sand out of the Bay, indicating the importance of the sandwaves on local and regional sediment management problems. Based on theories regarding sandwave migration (e.g. Knaapen, 2005 and Németh et al., 2002) it was concluded that the sandwaves were migrating seaward in the center of the Inlet Mouth, implying an uphill migration.

⁶ The steepness index is described as the Length over Height ratio

3. THEORY ON SANDWAVES

The following chapter presents theories that bear reference to sandwaves and is used to obtain better understanding of sandwaves in general. The goal is to gain insight into processes which play a prominent role in the development of sandwaves. Most important and recent theories regarding the characteristics, formation and migration will be treated consecutively in this section.

3.1 Characteristics

Sandwaves can be described as large-scale patterns formed on the interface of sandy marine bottoms and turbulent flow caused by strong tidal currents. They cover the shallow parts of tidal inlets and ebb-tidal deltas (Figure 3-1) and are characterized by a length of a few hundred meters, a height of several meters and an orientation almost perpendicular to the main tidal current direction (Terwindt, 1971 and Hulscher, 1996).



Figure 3-1: Digital rendering of sandwaves in San Francisco Bay (courtesy of USGS).

In general, sandwaves are observed at a water depth in the order of 30 m (Németh et al., 2002) with crests growing up to approximately one third of the water depth (McCave, 1971). Table 3-1 presents a range of bedforms with their spatial and temporal scales, as described by Dalrymple et al. (1978), Ashley (1990) and Morelissen et al. (2003).

| Bedform ⁷ | Height | Length | Migration rate | Times scale |
|----------------------|----------------|------------|----------------|-------------|
| Sandwaves | 0.75 - 20 m | 10 - 500 m | ~ 10 m/year | years |
| Megaripples | 0.075 - 0.75 m | 0.6 - 10 m | ~ 100 m/year | days |
| Ripples | < 0.075 m | < 0.6 m | ~ 1 m/day | hours |

Table 3-1: Bedform classification and characteristics.

⁷ Megaripples and sandwaves are frequently designated as *sand dunes* in literature. The distinction is made because megaripples are frequently found superimposed upon sandwaves (McCave, 1971)

Shape characteristics are obtained from the sandwave crest and trough positions collected in a bathymetric survey. The data is filtered using a low-pass filter, which removes all noise related to very small bedforms (i.e. bedforms smaller than ripples). Crests and troughs are then identified as respectively the local maxima and minima of bed levels in the direction of the main tidal current. The exact levels of crests and troughs are retrieved from the raw, unfiltered data set. This avoids underprediction of the sandwave heights due to the filtering procedure (Knaapen, 2005).

In theory the sandwave length is defined as the horizontal distance between the centers of two consecutive troughs on opposite sides of the crest. Sandwave height is defined as the vertical distance between the top of the crest and the baseline of the two consecutive trough levels, z_1 and z_2 respectively (Figure 3-2).

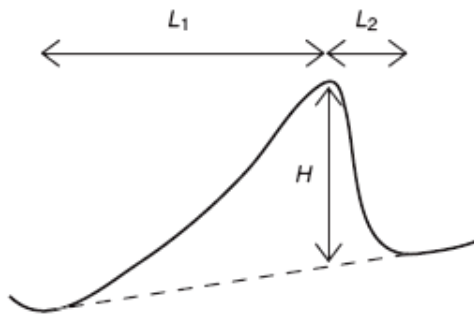


Figure 3-2: Schematization of sandwave height and length (by Buijsman, 2007).

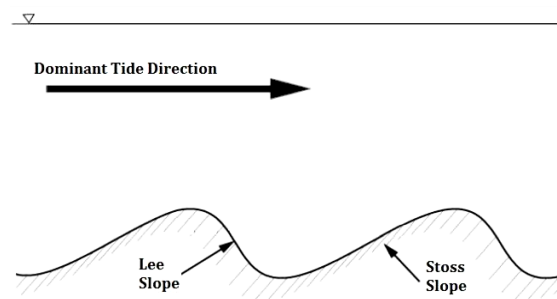


Figure 3-3: Stoss and lee slopes of sandwaves (by Whitmeyer and FitzGerald, 2006).

$$L = L_1 + L_2 \quad [3.1]$$

$$H = z_{crest} - \frac{z_1 L_2 + z_2 L_1}{L} \quad [3.2]$$

Figure 3-3 illustrates the orientation of stoss and lee slopes exposed to the dominant tide direction, useful to describe the shape of bedforms. Sandwave asymmetry is defined as the distance between crest and trough at the stoss slope side (L_1) minus the lee slope distance between crest and the trough (L_2), divided by the total sandwave length (Knaapen, 2005):

$$A = \frac{L_1 - L_2}{L_1 + L_2} \quad [3.3]$$

Asymmetry values range between -1 and 1, with symmetrical sandwaves when A equals zero. A positive asymmetry indicates that the steepest slope of a sandwave faces the positive x or y direction. In general slope angles of stoss and lee sides range between 10° and 20° (Dalrymple et al., 1978), therefore not resembling slip faces.

3.2 Sandwave formation

3.2.1 Vertical residual circulation cells

Recent theoretical studies on sandwaves in a three-dimensional shallow water model⁸ describe tide and topography as a coupled system in which sandwaves can occur as free instabilities, see Huthnance (1982) and Hulscher (1996a,b). It is believed that sandwaves are the long term result of an interaction between topography and hydrodynamics, and that the combination of sandwaves and residual currents causes the formation of vertical circulation cells (Figure 3-4). These residual cells turn out to be necessary to describe the formation of large scale bottom features like sandwaves.

The theory that relates sandwaves to residual circulation cells is illustrated by a linear three-dimensional stability model which consists of two coupled parts; a flow model and a sediment-transport model. This model contains boundaries in horizontal direction which are placed infinitely far away, and at the bottom a partial slip condition is used to model the shear stress without including explicitly the complicated processes in the thin bottom boundary layer. The sediment transport model includes only bed load transport⁹ and is presented as a function of the bottom shear stress. For a more extensive elaboration of the stability-based model see Appendix E.

In great sense this stability model is comparable to the approach of a morphodynamic numerical model such as DELFT3D. A morphodynamic numerical model calculates non-steady flow and transport phenomena, resulting from tidal and/or meteorological forcing acting on a curvilinear, boundary fitted grid. Similar to the stability model it is based on the numerical solution of the three-dimensional shallow water equations, however this time in combination with a surface wave propagation model and the advection-diffusion equation for sediment particles with online bed updating after each time step.

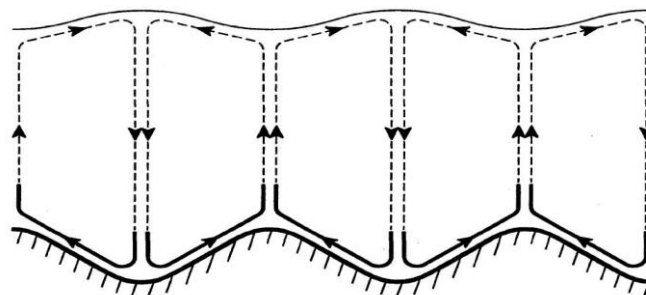


Figure 3-4: Residual circulation cells believed to support sandwave formation (by Hulscher, 1996).

⁸ The models are based on the three-dimensional shallow water equations since in coastal seas a tidal wave is long compared to the depth. Therefore hydrostatic pressure can be assumed.

⁹ Bed load transport is assumed to be dominant for offshore tidal regimes (Hulscher, 1996)

To investigate whether the presence of sandwaves can be associated with free instabilities in the morphological system modelled with DELFT3D, a basic state is to be defined which describes a tidal current over an undulating initial bottom that represents a field of sandwaves. The final long-term shape of the sandwave will be a result of the interaction between the periodic perturbations and tidal currents. In theory, small perturbations of the bottom will cause small perturbations in the flow field and vice versa. This allows the bed to respond in two ways; either remain stable, which means that all sandwaves will retain the initial height and length scales; or unstable, meaning that the bed will change resulting in growth or decay.

The linear stability model results revealed that the vertical component of the residual velocity was one order less of magnitude than the horizontal component and that the direction was upward above the crests and downward in the troughs. Both residual flow components cause a residual circulation which favors the growth of the sandwave, as shown in Figure 3-4. During ebb and flood, the tidal current moving upslope was found larger than the current moving downslope as flow accelerates when depth decreases. Consecutively the sediment transport increases with increasing bed shear stress, meaning that due to the oscillating character of the flow, convergence of sediment transport at the crests will take place, resulting in sandwave growth. Depending on the circumstances such as flow velocity and water depth, sandwaves with different lengths will show different growth and decay rates. Results of the stability model also showed that growth of sandwaves is determined by a growing term based on residual bottom shear stresses and a term which hinders the formation of steep slopes. The latter causes damping of sandwaves with small wavelengths.

According to Tonnon *et al.* (2007) numerical morphodynamic models such as DELFT3D, are highly capable to simulate the temporary behavior of sandwaves on a time scale of ten to twenty years, contrary to stability-based models which are more focussed on long-term behavior of idealized wave shapes for strongly schematized forcing conditions. Tonnon *et al.* (2007) recently studied the morphodynamic modelling of tidal sandwaves on the shoreface of the Dutch coast using a longshore DELFT3D model. The model was setup to gain insight in the physical processes of an idealized sandwave and to study the effect of tides, waves and basic model settings on the morphological development over five years. Conclusions regarding the formation processes attributed to the deformation of the velocity profiles along the sandwave to be the main cause of sandwave growth, resulting in a vertical circulation cell with net time-averaged velocities toward the sandwave crest in the near-bed region. Tonnon *et al.* (2007) also concluded that the effect of sandwave growth could only be studied using a 3D-model resolving the vertical structure of the flow.

3.2.2 Flow separation

An elaborate study on the sandwave field in the Bahia Blanca estuary in Argentina by Aliotta & Perillo (1987), lead to the conclusion that the presence of large lee slopes and so called mega-ripples, are indicative features for flow separation; a concept seldom mentioned with subtidal sandwaves. The study area revealed sandwaves with lee slopes up to 28° and 30° , being very close to the underwater angle of repose of the sediment¹⁰ and separation of the boundary layer flow was stated to be very likely. Under conditions of flow separation, maximum shear stress is found normally at the crest and sediment entrained as bed load is consecutively further moved by avalanching down the lee slope. The lee eddy and consequent lee counter current will steepen the angle of the downstream slope until it finds the angle of repose.

Usually this mechanism is observed in rivers, where subaqueous dunes are characterized by a mild and slightly curved upstream surface and a downstream slope approximately equal to the angle of repose. Right behind the crest of the dune, flow changes from accelerating flow in a very strong adverse pressure gradient, to decelerating flow in a slightly favorable pressure gradient along the mildly positive slope of the dune. Visualized in Figure 3-5, flow separation occurs at the top of the dune, reattaching again in the trough. Bottom rollers are formed at the lee side, completing a zone of turbulence where large quantities of turbulent energy is produced and dissipated. On the upstream side of the dune the shear stress moves sediment particles uphill until they pass the crest and eventually become buried in the bed for a period of time. Erosion of the crests increases due to peak currents as low tide approaches, resulting in a decrease of dune height. Concentrations of sand in suspension also increase with increasing current velocities, leading to deposition in troughs and a further reduction in dune height and leeside slope angle. As sediment is moved from the upstream side and deposited on the lee side of the dune, the result is a slow and continuous downstream migration of the dune pattern (Engelund & Fredsøe, 1982).

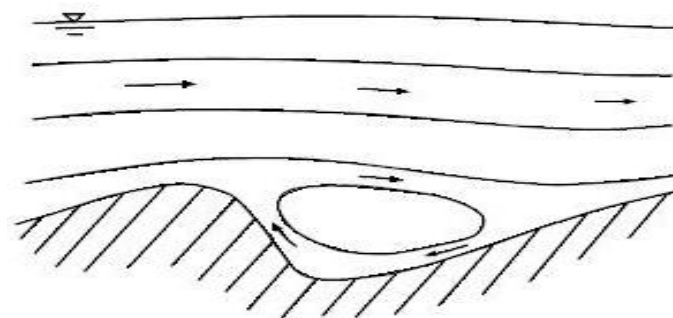


Figure 3-5: Flow separation over river dunes (by Hulscher & Dohmen-Janssen, 2005).

¹⁰ The underwater angle of repose is $32-35^\circ$ according to Miller & Byrne (1966).

When an idealized sinusoidal sandwave is created, slopes are generally too mild for flow separation. According to Santoro *et al.* (2002) and Van Dijk & Kleinhans (2005) the steepness of sandwaves is considered not to be large enough to introduce the effect of flow separation on sandwave morphodynamics. The linear stability analysis performed by Hulscher (1996) was restricted to the height of small and formally infinitesimal sinusoidal-shaped sandwaves. As such topography corresponds to small-slope features; flow separation does not take place. This however, is inconsistent with the finite amplitude sandwaves for which the possibility of flow separation has to be investigated in further detail. Also, the second order effect of superimposed higher frequency modulations is believed to initiate flow separation if their slopes grow very steep. Small scale ripples on top of sandwaves that are able to induce flow separation, can play an important role in the formation processes of the primary sandwave. This second order effect makes it worthwhile to investigate the role of flow separation with sandwaves.

3.3 Sandwave migration

As a result of their migration speed and significant spatial dimensions, sandwaves can interfere with manmade structures such as navigation channels, pipelines and cables. For this reason many engineering and navigational projects have required increasingly precise information about the shape and stability of the sea bed. These requirements are often particularly important in sandwave fields, where it is considered that the sea bed sediments are especially mobile (Langhorne, 1982). As already pointed out in the first section of this chapter, one of the sandwave characteristics is that their crests are practically orthogonal to the direction of the tidal mean current. According to Allen (1980), sandwaves start moving when the peak dominant flow velocity exceeds $0.50 - 0.60 \text{ ms}^{-1}$ and appreciable changes in shape occur at $0.75 - 0.80 \text{ ms}^{-1}$. Complete reversal the sandwave shape is accomplished if both dominant and subordinate peak depth-averaged current velocities exceed 0.85 ms^{-1} ; see Terwindt *et al.*, 1986. The rate of migration strongly depends on the tide characteristics, but migration velocities can be up to several tens of meters per year (Terwindt, 1971; Buijsman, 2007). Long-term upstream or downstream migration is believed to be controlled by local residual currents (Németh *et al.*, 2002) or tidal asymmetry due to higher components (Besio, 2004).

Residual current and tide asymmetry

Knaapen (2005) states there is a strong correlation between sandwave shape and migration rate, presuming that longer sandwaves travel faster and higher waves travel slower. This relation, which assumes that the sandwaves migrate in the direction of the steepest slope, can be translated into a migration predictor following a quadratic relation with the sandwave asymmetry. Németh *et al.* (2002) supports this idea by confirming that tidal asymmetry not only results in migration of sandwaves, but also in lee-stoss asymmetry, indicating that migration is indeed in the direction of the steepest slope.

According to Besio (2004), the presence of a residual current induces a distortion of the spatial pattern of the recirculation cells which will then no longer be symmetric with respect to the crests and troughs of the sandwave, therefore causing sandwaves to migrate. Studying the North Sea sandwaves, Besio (2004) succeeded in modelling sandwave migration in upstream migration with an additional steady current to the oscillating tidal flow. He showed that upstream and downstream migration is mainly controlled by the relative strength of the residual current with respect to the amplitude of the quarter-diurnal tide constituent (M4) and by the phase shift between the semi-diurnal tide constituent (M2) and quarter-diurnal tide constituent¹¹. Therefore in order to accurately predict field observation migration, a detailed knowledge of the direction, strength and phase difference of the tidal constituents is required. Further contribution to the study of sandwaves is that of Németh *et al.* (2002), who introduces the effect of the residual current and tide asymmetry by including an asymmetric basic flow on a horizontally averaged symmetrical tidal motion. The study shows that the steady current inducing an asymmetry in the basic state, can cause migration of sandwaves in the direction of the steady current. The above implies that in order to model sandwaves correctly, both residual and tidal currents should be included.

Extreme weather conditions

An exploratory study on sandwaves impeding coastal inlet navigation channels by Whitmeyer & FitzGerald (2006) revealed that the presence and significance of sandwaves can change seasonally with changing water level. This idea is supported by Buijsman (2007) who claims that sandwaves in the Marsdiep Inlet (the Netherlands) have significant seasonal and inter-annual variability. While the volume of sediment in the Marsdiep Inlet was conserved, sandwaves showed significant seasonal variations in height, length and asymmetry. Buijsman (2007) also describes that as sandwaves migrate faster, their height decreases, wave length increases and asymmetry decreases. Suggesting that sandwave migration rate is directly coupled to shape characteristics. Although the cause of this variability is still unknown, Terwindt (1971) and Langhorne (1982) attribute this variation to stronger currents and orbital velocities that occur during storms. Consequently, an increase of net sediment transport might serve as a good indication of sandwave migration.

¹¹ M2 is the principal lunar semi-diurnal tide with a frequency of 12 hours and 25 min; M4 is the lunar quarter-diurnal tide and has a frequency of 6 hours and 12.5 min.

4. RESEARCH APPROACH

This chapter explains what approach is used to answer the research questions stated in the introduction chapter. The first section briefly explains why the DELFT3D model is constructed. Section two discusses the assumptions which were made for this study. The third section elaborates on the different simulations used to assess the research questions. The final section briefly explains what is analyzed when model results are obtained.

4.1 Model construction

Numerous studies have been performed to simulate sandwave morphology with stability models and numerical process-based models (e.g. Hulscher, 1996; Németh *et al.*, 2002; Morelissen *et al.*, 2003; Besio, 2004; Tonnon *et al.* 2007), however none of these approaches elaborate on the ability of numerical process-based models to capture the sandwave formation mechanisms. Therefore in order to assess the capability of DELFT3D to model the San Francisco sandwave morphodynamics and their formation mechanisms, a two-dimensional numerical model of a sandwave field is created with DELFT3D.

Developing a model with DELFT3D gives the opportunity to study the morphodynamic behavior of sandwaves and allows for quantification of the hydrodynamic processes that play a role in forming the sandwaves. The model is kept relatively simple, involving grid schematization, determination of boundary conditions as well as the physical and numerical parameters. To setup representative sandwave bottoms and comparable flow conditions, the model is provided with existing field and 2Dh-model data which is carefully analyzed in Chapter 5. The validity of these datasets is not questioned in this research. The process of converting the collected field and 2Dh-model data into settings and parameters for the sandwave model is visualized in Figure 4-1.

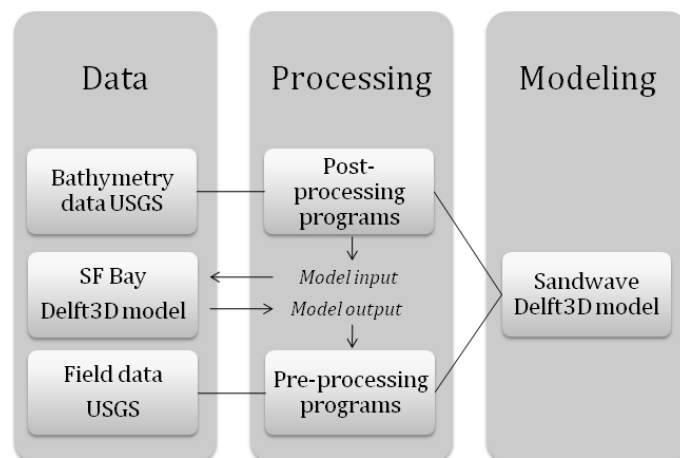


Figure 4-1: Schematic diagram of converting data into setup for the DELFT3D 2Dv-model.

4.2 Assumptions

4.2.1 Project area partition

The more than three thousand individual bedforms measured by Barnard *et al.* (2006) brought about a large set of data, of which only a small part is used for this study. For reasons of simplicity the area of interest is focused on the tidal inlet mouth only. This area displays sandwaves with a large diversity in size and shape, in relatively shallow water depths. A distinctive difference in depth (see Appendix F) and similar fields of sandwaves with comparable scale is the main reason why the area of interest is divided in two sites. The sites are located in the center and southeast of the inlet mouth respectively and are referred to as Mouth Center and Baker Beach. The centrally located Mouth Center has a median depth of 40 m and portrays the largest and most progressive sandwaves of the estuary's inlet mouth. The area just offshore of Baker Beach has a median depth of 20 m and displays linguoid-shaped sandwaves that are less great in size.

4.2.2 Bathymetry representation

The 2Dv-model is kept relatively simple, assuming the field of sandwaves as a repetitive chain of sinusoidal shapes along a straight line. The grid follows the sandwaves placed centrally in a domain bounded by a flat horizontal bed on both sides. Smaller scale features like megaripples are not taken into account. In this research it is assumed that those aspects are of little or no influence to the large scale processes. The initial bathymetry setup is based on median values of sandwave lengths, -heights and corresponding water depths. It is assumed that this unrefined approximation of reality is sufficient for further model setup, since the intent is to start out with a very basic schematization that allows for elemental studies on the morphodynamic response of sandwaves.

4.2.3 Equilibrium

To determine whether the bed evolution of sandwaves is in equilibrium, a growth factor parameter ω is introduced. The growth factor is calculated by dividing the final sandwave height on the initial sandwave height, averaged over the total number of time steps. The center crest and trough height changes will be used as the representative sandwave height for the entire field. The development of sandwave is in equilibrium when the growth factor ω , averaged over the first 250 morphological days, fulfills the definition of equilibrium. Large initial gradients in height development for a certain sandwave height indicate that the bedlevel configuration is far from equilibrium.

The definition of equilibrium for this study states that growth or decay cannot be more than 1% of the initial sandwave height over a period of 250 morphological days ($\omega < 0.01$). In other words, when for instance a sandwave with an initial height of 2 m is forced with a flow velocity of 0.50 ms^{-1} over a period of 250 morphological days, the maximum allowed growth rate of 0.01 is equivalent to a maximum of 2 cm growth in sandwave height over a period of 250 days. This is convincingly close to no change in height and therefore stated as acceptable.

Theoretically, exact equilibrium is reached when the growth factor ω equals zero, whereas a negative and positive value for ω corresponds to decay and growth. These definitions of growth factor and equilibrium allow for proper review of the morphological and hydrodynamic model results, which are discussed in the next section. The simulation time of 250 morphological days only revealed significant changes in the height of sandwaves. Apparently a change in sandwave length can only be observed for a simulation time much greater than 250 days, however due to the limited amount of time and erroneous sandwave development due to boundary influences (Appendix G) this study only focuses on the development in height rather than length.

4.2.4 Calibration and validation

The profile model is preliminary setup as a 2-dimensional horizontally averaged model. It is calibrated representing the fluctuations in water level found in San Francisco Bay. Since the model is built to allow for a quantification of the hydrodynamic processes on top of sandwaves, initiated flow velocities are equal to current velocities found near the fields of sandwaves in the inlet mouth. It is presumed that the magnitudes of currents are representing the range of tidal currents in the project area.

4.3 Model simulations

When the profile model is validated, a conceptual analysis is performed to evaluate the sensitivity of morphodynamic equilibrium. For several simulations with varying flow conditions, different configurations of sandwave length and height are used to determine the stages of morphological development. The performed simulations to assess the research questions consist of two different analyses of the formation mechanism;

- I. Morphodynamic stability analysis of different sandwave configurations and increasing flow velocities.
- II. Hydrodynamic analysis of the residual flow field that belongs to different sandwave configurations and increasing flow velocities.

The first analysis is to gain insight into the conditions in which equilibrium and non-equilibrium will occur. The second will give qualitative answers to the importance of residual circulation to the formation of sandwaves.

4.3.1 Morphodynamic simulations

Since the primary goal of the study is to assess the formation mechanisms that enable sandwaves to develop, a series of morphodynamic simulations is performed containing a narrower range of sandwave configurations. This will allow for a quantification of the different stages of development, necessary to answer assess the importance of bed configuration to the formation of sandwaves. The morphological development of the investigated sandwave configurations will be compared to the sandwaves found in the inlet mouth of San Francisco Bay, to investigate the capability of Delft3D to model the sandwaves.

4.3.2 Hydrodynamic simulations

For different flow velocities, the residual flow patterns and near bed velocities are compared for each simulation, to provide insight in the formation mechanisms. Residual vector plots displaying magnitude and residual flow direction are used to quantify the difference in residual velocity profiles, using different sandwave configurations. Residual vector plots displaying magnitude and residual flow direction are used to quantify the difference in residual velocity profiles, using different sandwave configurations. Finally, in extend of the previous two aspects; the effect of alternating physical parameters and flow configurations is analyzed to acquire insight in the sensitivity of the numerical model.

4.3.3 Sensitivity analysis

Different model parameters within Delft3D-FLOW allow for calibration of the model for cases in which no equilibrium is found in the development of sandwaves. In particular the effects of bedslope parameter α_{BS} , the grain-size diameter σ_S and the configuration of flow are interesting when studying the model sensitivity. Insight into these parameters and hydrodynamic configurations will result in an improved interpretation of the model results.

4.4 Analyzing results

The analysis of the 2Dv-model results will focus on three key aspects. First, the morphological development of all sandwave configurations is compared to gain insight in the differences between the modelled sandwaves and the sandwaves found in the inlet mouth of San Francisco Bay. This is done by a stability analysis of the monitoring points in the final bathymetry output. Second, the residual flow patterns and near bed velocities are compared for each simulation, to provide insight in the formation mechanisms. Residual vector plots displaying magnitude and residual flow direction are used to quantify the difference in residual velocity profiles, using different sandwave configurations. Finally, in extend of the previous two aspects; the effect of alternating physical parameters and flow configuration is analyzed to acquire insight in the sensitivity of the 2Dv-model.

5. DATA ANALYSIS

This chapter describes how the field and DELFT3D (2Dh-model) data are used to setup the profile model. The first section contains background information on the available data used for this study. Section two discusses the analysis of sandwave characteristics necessary to setup a representative bathymetry and grain-size. The third section covers the analysis on the available 2Dh-model results. Finally section four compares the different parameters and discusses how this data will be used to construct the profile model.

5.1 Background information

In this study bed level, sediment grain-size and hydrodynamic data are required to setup, calibrate and validate the sandwave model. U.S. Geological Survey provided three sets of data which are briefly described in this section.

Multibeam mapping

Forty-four days of multibeam mapping were conducted at the mouth of San Francisco Bay during the fall of 2004 and 2005 through a USGS-USACE California State University, Monterey Bay Seafloor Mapping Lab collaboration (Barnard et al., 2006a & 2006c). The primary goals of this survey were to evaluate bathymetric change at the mouth of San Francisco Bay since the last comprehensive bathymetric survey was completed in 1956, to document dominant sediment transport pathways and to estimate bedload transport via multiple surveys of a transect through the active sandwave field.

Grain-size mapping

The 2004 and 2005 bathymetry surveys included a regional sediment sampling survey of the inlet mouth of San Francisco Bay. Large-scale grain size patterns, sediment and sources were documented. The locations of these samples are depicted in Appendix H. The samples were taken along different transects located on the crests, slopes and troughs of the sandwave. This way characteristics such as wave length and height were determined for all individual bedforms, including those located in the two project sites referred to as Mouth Center and Baker Beach. For the area Mouth Center this results in a group of data containing 176 sample points, whilst for the site of Baker Beach this amounts to 56 sample points.

San Francisco Bay DELFT3D model

This section is completely taken from Barnard et al. (2006). In order to understand and predict the hydro- and morphodynamics in San Francisco Bay, offshore regions and near Ocean beach, it was desirable to employ a process-based numerical model to set up a process-based numerical model using DELFT3D. Once validated, the model would serve as a predictive tool for coastal change.

The model domain of the two-dimensional (2Dh) model includes the entire San Francisco Bay and extended approximately 50 km offshore. The offshore open boundary was extended to minimize boundary effects along the near shore region immediately south of the inlet; the main focus of an adjacent project. A flexible curvi-linear grid, depicted in Figure 5-1, was employed to allow for higher spatial resolution through the Golden Gate where detecting strong gradients in tidal energy was most crucial. Grid cell resolution ranged from approximately 2 km near the western open boundary to as fine as approximately 200 m through the Golden Gate.

Measured wave conditions at offshore buoys were used to force the model at the open boundaries. The measured wave conditions were collected primarily by the CDIP Point Reyes buoy 029 (SCRIPPS Institution of Oceanography, 2006) and secondarily by the NDBC Monterey buoy (NOAA, 2006a). Bulk wave statistics were used to force the wave model. These statistics included significant wave height, peak period and mean wave direction. Conditions observed at these buoys were applied to all open boundaries, including lateral boundaries, of the model.

Calibration and validation tidal constituents was done via harmonic analysis (Pawlocicz *et al.*, 2002) and several model iterations, employing only the FLOW module, until the amplitude ratios and phase differences were less than 0.5% between predicted and observed water levels. The simulation time covered 36 days starting at the end of January 2004, encompassing a complete spring tide cycle. Tidal currents and residuals were retrieved from the Fourier analysis of the 2Dh-model.

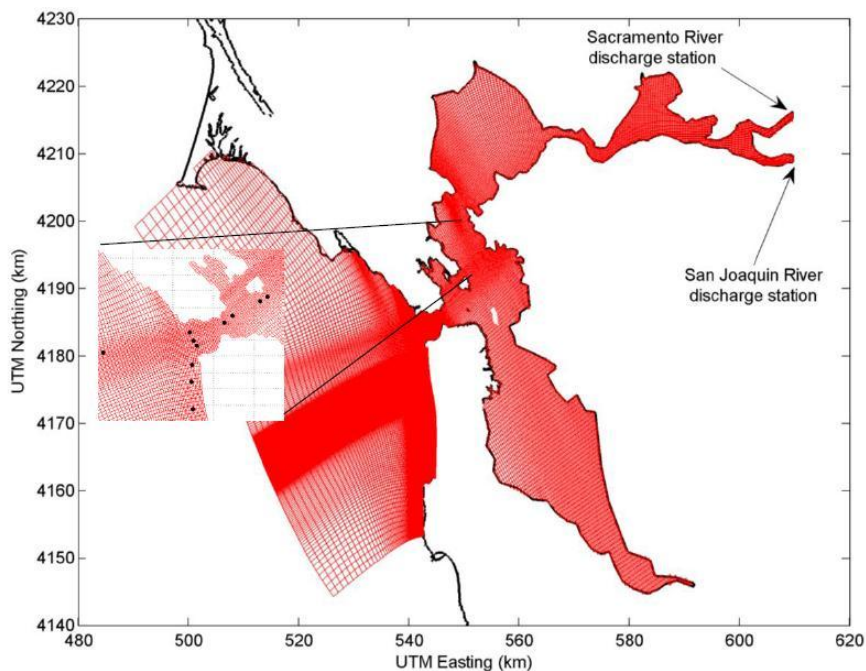


Figure 5-1: Curvilinear DELFT3D-FLOW grid and boundaries. Inset shows locations of current measurement sites (by Barnard *et al.*, 2007).

5.2 Field data interpretation

Both project sites Baker Beach and Mouth Center contain a large set of sandwave data, of which wave height and length are most important for setting up the bathymetry of the profile model. Since grain-size is an important parameter in representing the sandwaves correctly, this physical parameter is included in the analysis as well. A complete list of project area field data is found in Appendix I, displaying not only length and height but also characteristics such as shape asymmetry.

5.2.1 Sandwave characteristics

Figures 5-2 and 5-3 display the distribution of sandwave length and -height by means of histograms, included with the median and maximum values found for both project sites. The histograms are colored blue for the median depth of 20 m (Baker Beach) and green for the median depth of 40 m (Mouth Center). According to the definition of wave length and height this means length is measured from trough to trough, while height is measured from the top of the crest to the baseline of the two consecutive trough levels.

Using a bin width of 0.5 m, the median wave height found for Mouth Center equals 2.9 m, with a maximum of 10.1 m. The standard deviation for this distribution is 2.0 m. The area of Baker Beach contains a median wave height of 1.2 m, with a maximum of 3.0 m. For this distribution the standard deviation equals 0.5 m. For a bin width of 20 m, the median wave length found for Mouth Center equals 57.7 m, with a maximum of 167.4 m. The standard deviation for this distribution is 28.6 m. The area of Baker Beach contains a median wave length of 30.0 m, with a maximum of 124.6 m. For this distribution the standard deviation equals 18.6 m.

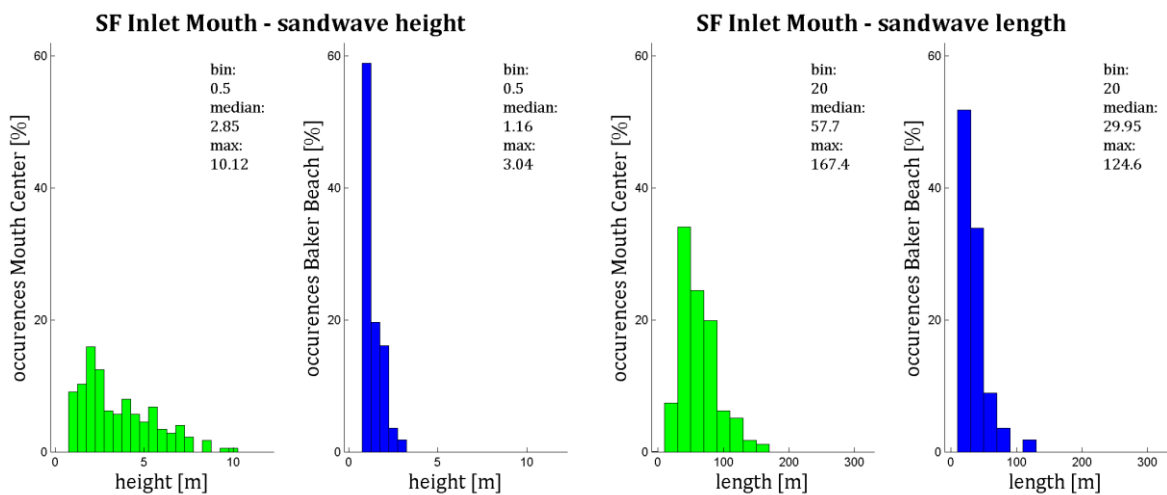


Figure 5-2: Distribution of the area specific sandwave height.

Figure 5-3: Distribution of the area specific sandwave length.

Concerning the initial bathymetry of the 2Dv-model, a choice must be made what dimensions of sandwaves can represent those observed in San Francisco Bay. The field data shows an overall maximum wave height of approximately 10 m and an overall maximum wave length of approximately 170 m. However the difference in maximum height and length between both locations is rather large. For that reason the range will vary in wave height from 2 m to 10 m using an interval of 2 m, and in length from 25 m to 200 m using an interval of 25 m. By using identical combinations of wave height and length for both project sites, the effect of water depth on sandwave development and hydrodynamic flow patterns can be investigated properly.

5.2.2 Sediment grain-size

Figure 5-4 displays the distribution of median grain-sizes for both project sites, again using the similar colors to identify the differences in median water depth. For a bin width of 0.05 mm, the median of the median grain-size (or D_{50}) found for Mouth Center equals 0.77 mm, with a maximum of 0.97 mm. The standard deviation for this distribution is 0.17 mm. The sediment of Baker Beach has a median grain-size diameter of 0.23 mm, with a maximum of 0.37 mm. For this distribution the standard deviation equals 0.05 m.

The 2Dv-model requires a realistic value for the sediment diameter as this will determine the stability of the sandwave configuration and consequently the outcome of model results. For reasons of comparison and simplicity, the mean of both median grain-size diameters will serve as the representative median grain-size for both sites. This results in a value of 0.50 mm, which will be set as the default grain-size in the 2Dv-model. A sensitivity analysis in section 7.3.3 discusses the influence of a finer and coarser grain-size on the development of sandwaves.

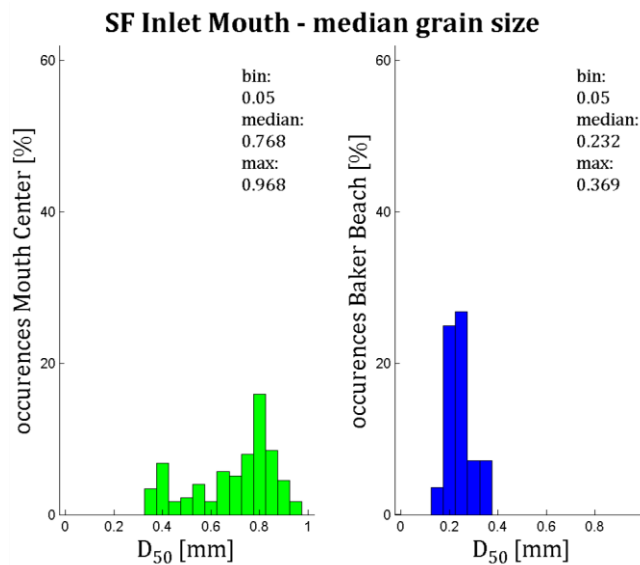


Figure 5-4: Distribution of the area specific median grain-size.

5.3 2Dh-model interpretation

Due to the inter-related nature of sandwaves versus the hydrodynamic processes, it is essential to include the 2Dh-model data in order to understand and predict the hydro- and morphodynamics of the San Francisco Bay sandwaves. First the peak tidal velocities are discussed, followed by the tidal residual velocities. A complete list of project area 2Dh-model data is found in Appendix I, displaying not only maximum tidal current velocities but also residual current magnitudes.

5.3.1 Peak tidal flow velocities

Of particular interest for the study on sandwave formation mechanisms are the peak tidal flow velocities. To simulate the tidal flow currents found near the observed sandwaves of Mouth Center and Baker Beach, an analysis of the 2Dh-model velocities is performed. The ranges of velocities found from this data are translated into different boundary conditions necessary to force current flow and consequently morphodynamic change in the profile model.

Figure 5-5 depicts the distribution of peak ebb flow velocity found on both project locations, with green bars representing Mouth Center and blue bars representing Baker Beach. Near Mouth Center the median peak ebb velocity measures 1.58 ms^{-1} with a maximum peak ebb velocity of 1.82 ms^{-1} . Baker Beach measures a median peak ebb velocity of 1.13 ms^{-1} with a maximum peak ebb velocity of 1.31 ms^{-1} . Similarly, Figure 5-6 depicts the histograms of the peak flood flow velocity on both project locations. Near Mouth Center the median peak flood velocity measures 1.34 ms^{-1} with a maximum peak flood velocity of 1.46 ms^{-1} . Baker Beach shows a median peak flood velocity of 1.04 ms^{-1} with a maximum peak flood velocity of 1.38 ms^{-1} .

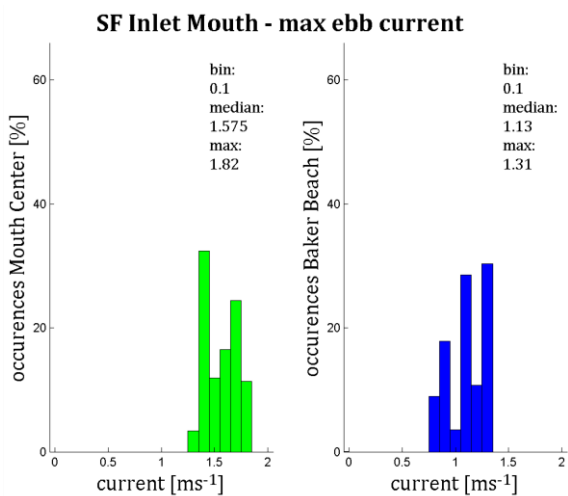


Figure 5-5: Distribution of the area specific peak ebb current velocity.

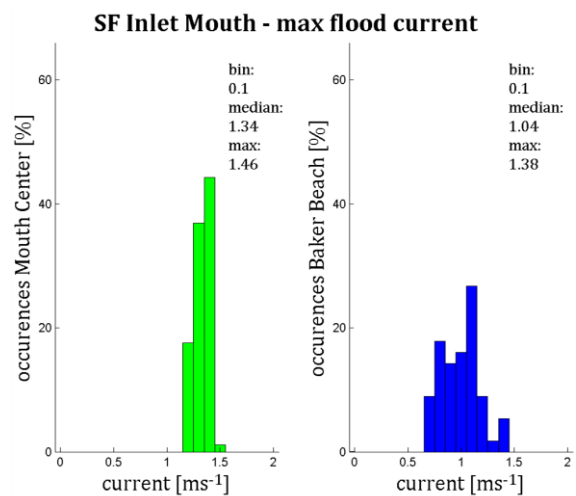


Figure 5-6: Distribution of the area specific peak flood current velocity.

Based on the histograms, median and maximum velocities appear to be higher when water depth is larger; suggesting that the difference in water depth between both project sites is related to the observed velocities. For the profile model the average maximum peak tidal velocity is used as the maximum forced flow velocity across the domain. This velocity is equal to 1.49 ms^{-1} and will be rounded up to 1.50 ms^{-1} . To study the effect of different flow stages on the development of sandwaves, this maximum velocity will be divided into three ranges of flow magnitude being 0.50 , 1.00 and 1.50 ms^{-1} .

5.3.2 Residual tidal flow velocities

Of comparable interest for the study on sandwave formation mechanisms are the residual tidal flow velocities. Based on theories regarding sandwave formation found in section 3.2.1, these velocities are believed to explain the presence of sandwaves. For that reason generated 2Dh-model residuals will be used to compare the residual current velocities of the profile model in order to explain the necessity of residuals on the presence of the San Francisco Bay sandwaves.

Figure 5-7 depicts the histograms of the residual current magnitude on both project locations, again with green bars representing Mouth Center and blue bars representing Baker Beach. Near Mouth Center the median residual velocity measures 0.06 ms^{-1} with a maximum residual velocity of 0.13 ms^{-1} . Baker Beach measures a median residual velocity of 0.13 ms^{-1} with a maximum residual velocity of 0.16 ms^{-1} .

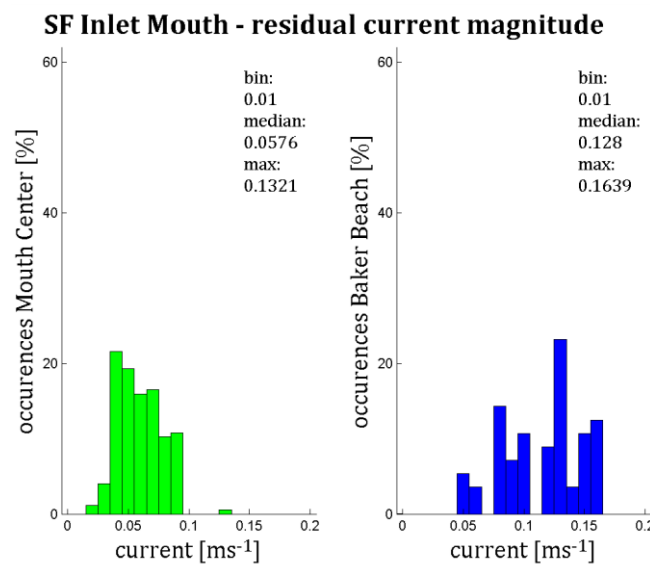


Figure 5-7: Distribution of the area specific residual current velocity.

5.4 Parameter relations

When considering whether two parameters relate with each other, one has to consider the coefficient of determination (i.e. R^2) to be a good indication of the relation between two different sets of data. This parameter analysis reduces the number of data points to those belonging to the areas Mouth Center and Baker Beach, consequently showing a much more area dependent relation of sandwave features and local hydrodynamics. The relation between sandwave characteristics and hydrodynamics can best be studied by producing scatterplots of the field and 2Dh-model data. A complete overview of scatterplots is presented in Appendix J, containing relations of field and 2Dh-model data separately and combined. The scatterplots are depicted with the coefficients of determination, which indicate a medium correlation when the R^2 value lies between 0.30 and 0.49, and a high correlation when R^2 is larger than 0.50.

5.4.1 Comparing field data

The comparison depicted in Figure 5-8 is made between sandwave height and length. Both characteristics show reasonably good correlation with Mouth Center data ($R^2 = 0.58$), while a poor relation is found with the data of Baker Beach ($R^2 = 0.33$). Height and length versus water depth are uncorrelated with R^2 values smaller than 0.20. Comparing grain-size with sandwave length, height and water depth does not give any correlation (R^2 values smaller than 0.14). When comparing the length over height ratio versus the median grain-size no correlation is found either (R^2 smaller than 0.09).

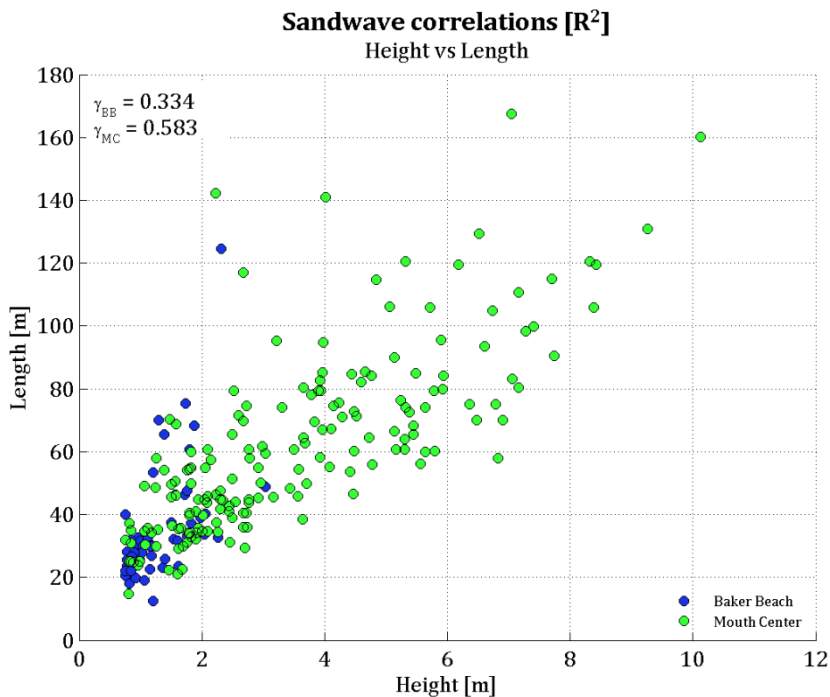


Figure 5-8: Scatterplot of sandwave height versus length.

5.4.2 Comparing field and 2Dh-model data

When comparing the sandwave height with the maximum ebb velocity, a relatively poor correlation is found for the Baker Beach data ($R^2 = 0.29$), while no correlation at all is found for Mouth Center ($R^2 = 0.06$). When comparing sandwave height with the maximum flood velocity similar values are found; $R^2 = 0.33$ and $R^2 = 0.06$ respectively. For sandwave length versus maximum ebb and flood velocities there is no correlation at all (R^2 values smaller than 0.10).

Figure 5-9 illustrates the relatively high correlation between the median grain-size diameter and the maximum current velocity (i.e. maximum ebb velocity) when comparing the Mouth Center data (R^2 value of 0.84). For the data of Baker Beach the correlation is less strong, resulting in a R^2 value of 0.41.

A very poor correlation is found when comparing the tidal residuals with sandwave length and height (R^2 values smaller than 0.20). Even so, both ratio of length over height and water depth versus the residual velocity do not show any correlation (R^2 values smaller than 0.04). When taking the residual velocity to the third power¹² the residual sediment transport rate can be estimated roughly. Comparing this value with the grain-size diameter, a relatively good correlation for the Baker Beach data is found (R^2 equals 0.51) and a very poor relation is found for the Mouth Center data ($R^2 = 0.10$).

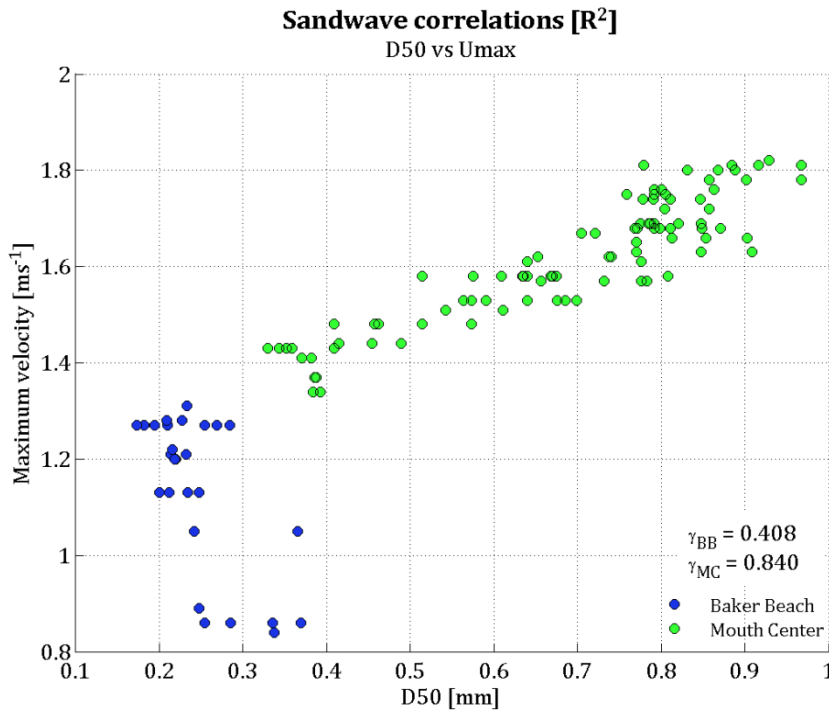


Figure 5-9: Scatterplot of median grain-size versus maximum current velocity.

¹² Thus taking $u^3 \sim s$

5.4.3 Implementing the data in the profile model

The data of Baker Beach and Mouth Center shows no correlation whatsoever between the local sandwave heights and the median grain size, illustrated by the coefficient of determination that equals 0.02 for Baker Beach and 0.12 for Mouth Center. This contradicts with the results found when relating all field data in the entire inlet mouth. Apparently, the results obtained by Barnard et al. (2006) which state that the best predictor for sandwave scale and flow conditions is surficial grain-size (R^2 equals 0.50, see Appendix K), do not entirely match with the relations found when focusing on the areas of Mouth Center and Baker Beach.

Similar to previous results, best correlations are found when comparing sandwave length versus height and median grain-size versus maximum current velocity. All other relations show little to no correlation at all, implying that it is difficult to directly relate the presence of sandwaves to local hydrodynamics. A direct relation is important when setting up the bathymetry of the model as this would save time in terms of different combinations of sandwave height versus length. Clearly the correlation between length and height shows that in general larger sandwave lengths also need larger heights to remain stable. The other strong relation between grain-size and maximum current suggests that using a higher flow velocity through the model, inevitably leads to the requirement of coarser grain-sizes.

6. SANDWAVE MODEL SETUP (2DV)

This chapter describes the construction of the numerical model. In the first section a basic introduction of DELFT3D is given. Section two describes the grid and bathymetry used in for modelling the sandwaves. In section three the boundary conditions are discussed. Section four elaborates on the time step, followed by a description of the physical and numerical parameters in section five. The chapter concludes with a description of the monitoring points.

6.1 Introduction in DELFT3D

The DELFT3D package is developed by WL|Delft Hydraulics (nowadays Deltares) in close cooperation with Delft University, and consists of a number of integrated modules which together allow the simulation of two- or three-dimensional hydrodynamic flow (under shallow-water assumption), computation of the transport of water-borne constituents (e.g. salinity and heat), short wave generation and propagation, sediment transport and morphological changes, and the modelling of ecological processes and water quality parameters. One of the modules is the FLOW module which is able to provide wave, current and sediment transport estimates on varying spatial- and time-scales, describing the physical processes in terms of differential equations. DELFT3D offers four options to do the schematization of a body of water. The 1D-schematization is the least accurate, where both vertical and horizontal directions are averaged. The 2D-schematization either averages the width or depth. And the 3D-schematization is the most accurate with no averaging in any direction. A considerable disadvantage of increasing accuracy is that the computational time needed also increases.

Taking into account the morphodynamic procedure, the model has to consist of a set of flow equations, a sediment transport model and a sediment balance equation. In addition, input in the form of bathymetric data, tidal data and granulometric data is required as well. Output is provided as bedlevel response, flow fields and sediment fluxes over the domain of interest. In order to solve the equations, modification is necessary for numerical approximation. Since vertical accelerations are assumed to be very small compared to the gravitational acceleration, this term is not taken into account. This leads to the following set of shallow water equations for a vertical σ -grid¹³:

$$\frac{\partial u}{\partial t} + u \frac{\partial u}{\partial x} + v \frac{\partial u}{\partial y} + \frac{w}{H} \frac{\partial u}{\partial \sigma} = -g \frac{\partial \zeta}{\partial x} + fv + v_t^v \left(\frac{\partial^2 u}{\partial x^2} + \frac{\partial^2 u}{\partial y^2} \right) + \frac{1}{H^2} \frac{\partial}{\partial \sigma} \left(v_t^v \frac{\partial u}{\partial \sigma} \right) \quad [6.1]$$

$$\frac{\partial v}{\partial t} + u \frac{\partial v}{\partial x} + v \frac{\partial v}{\partial y} + \frac{w}{H} \frac{\partial v}{\partial \sigma} = -g \frac{\partial \zeta}{\partial y} + fu + v_t^H \left(\frac{\partial^2 v}{\partial x^2} + \frac{\partial^2 v}{\partial y^2} \right) + \frac{1}{H^2} \frac{\partial}{\partial \sigma} \left(v_t^v \frac{\partial v}{\partial \sigma} \right) \quad [6.2]$$

I II III IV V VI

¹³ See section 6.2.1 for a brief explanation of the σ -grid

$$\frac{\partial \zeta}{\partial t} + \frac{\partial HU}{\partial x} + \frac{\partial HV}{\partial y} = 0 \quad [6.3]$$

I *II*

With the roman symbols representing the terms:

- I.* Velocity gradient
- II.* Advective terms
- III.* Barotropic pressure gradient
- IV.* Coriolis force
- V.* Horizontal eddy viscosity
- VI.* Vertical eddy viscosity

And the continuity equation:

$$\frac{\partial \zeta}{\partial t} = \frac{\partial Hu}{\partial x} + \frac{\partial Hv}{\partial y} + \frac{\partial \omega}{\partial \sigma} = 0 \quad [6.4]$$

In which:

| | | |
|------------------|---|-----------------------------------|
| u, v | Velocity | [ms ⁻¹] |
| x, y | Distance | [m] |
| ω, σ | Velocity and distance relative to the σ -plane | [-] |
| ζ | Free surface elevation above reference plane | [m] |
| H | Total water depth ($d + \zeta$) | [m] |
| f | Coriolis parameter | [s ⁻¹] |
| ν^H, ν^V | Horizontal and vertical eddy viscosity | [m ² s ⁻¹] |
| U, V | Depth averaged velocities | [ms ⁻¹] |

In order to solve the numerical approximation of these equations a finite difference scheme on a staggered grid is chosen. This type of grid is characterized by arranging the velocity and water level variables on a certain way. This means that for each single grid cell DELFT3D calculates velocities and water levels based on the water level and velocities of previous grid cells. To solve the numerical scheme DELFT3D uses the Alternating Direction Implicit (ADI) method. Basically the ADI-method splits one time step into two stages with each stage consisting of half a time step. In both stages all terms of the model equations are solved in a consistent way with at least second order accuracy in space. This way the method is able to solve large matrix equations in a very fast way.

For a more extensive elaboration of DELFT3D and the FLOW module, see Lesser et al. (2000) and WL|Delft Hydraulics (2006).

6.2 Bathymetric schematization

6.2.1 Computational grid

Model computations are made with a two-dimensional vertical grid (i.e. averaged in horizontal direction or 2Dv). A small number of grid cells are favored with a grid size as large as possible to reduce the calculation time. However, in order to describe all sandwave configurations with sufficient accuracy the grid size has to be fine enough. For that reason a grid cell size of 5 x 10 m is chosen, maintaining the shape of the sinusoidal bed elevation and allowing for a detailed description of hydrodynamic processes (e.g. the formation of eddies).

In the vertical direction DELFT3D-FLOW offers two different vertical grid systems: the σ -coordinate system (σ -grid) and the Cartesian Z-coordinate system (Z-grid). The first type of vertical grid is chosen and consists of layers bounded by two sigma planes, following the bottom topography and the free surface as seen in Figure 6-1. Because the σ -grid is boundary fitted to both the bottom and the moving free surface, a smooth representation of the sandwaves is obtained. The σ -grid is refined close to the bottom in order to describe the bed flow velocity in greater detail. In total 22 layers are made to describe hydrodynamics properly. The σ -coordinate system is defined as:

$$\sigma = \frac{z - \zeta}{d + \zeta} = \frac{z - \zeta}{H} \tag{6.5}$$

In which:

| | | |
|-----|---|-----|
| z | Vertical co-ordinate in physical space | [m] |
| d | Depth below reference plane (at $z = 0$) | [m] |

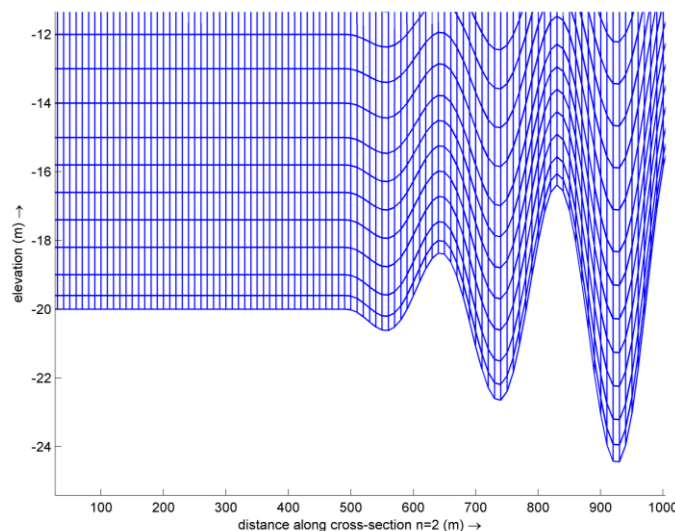


Figure 6-1: Detailed presentation of the vertical σ -grid in combination with the sandwave bed level.

6.2.2 Bathymetry

The initial bed level of the 2Dv-model is a sinusoidal wave-train over a domain length of 2000 m. This length is approximately 10 times the maximum sandwave length found in the tidal inlet mouth (see section 5.2.1), which is considered to be sufficient. The wavy bottom is made symmetrical to allow for fully symmetrical sandwave development in theory. An additional 500 m is added on both sides of the domain to minimize boundary disturbances that can enter the domain, therefore completing the total domain to a length of 3000 m (see Figure 6-2).

In order to analyze the morphodynamic evolution of the sandwave bed level, only the center sandwave is evaluated for its height and length development. The scale of the simulated height versus length ratios corresponds with the range of dimensions found in the project areas; however the length scale is limited to the number of grid cells available. In order to describe a sinusoidal sandwave properly there are at least 10 grid points necessary to draw a smooth line. Therefore with the purpose to describe the wave-train properly¹⁴ and to save calculation time (i.e. largest grid size possible), initial simulations are performed with sandwave lengths ranging from 50 to 200 m with an interval of 50 m.

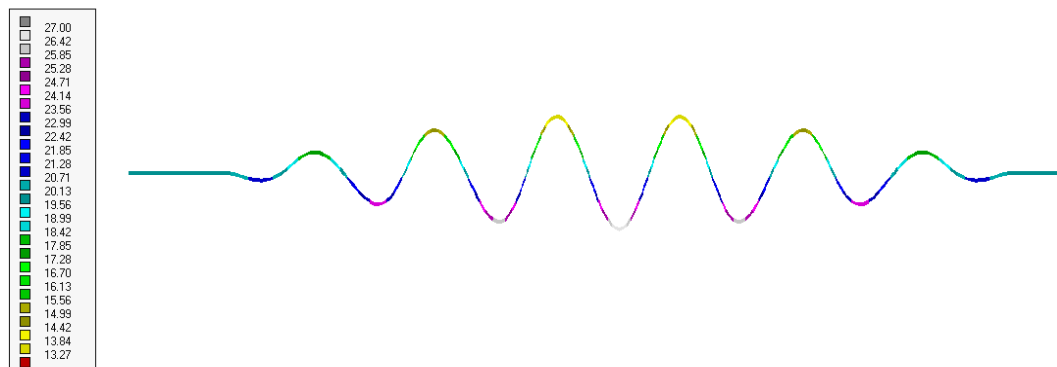


Figure 6-2: Computational grid of a sandwave field, represented by a symmetric sinusoidal wave-train with its largest wave in the center of the field.

6.2.3 Observation points

The model contains observation points that are created in the center of the sandwave field. The monitoring points are located on the *Crest*, *Slope1*, *Trough* and *Slope2* to describe the processes that are of interest regarding the development of sandwaves (e.g. near bed flow velocity, bed shear stress, bed load transport rates). The stations ID's are illustrated in Appendix L for a random sandwave configuration.

¹⁴ Based on a first series of runs, it turned out that relatively small wave lengths (e.g. 50 m) demand correspondingly small grid cells sizes 10 times smaller in size (5 m) in order to describe the sinusoidal wave properly.

6.3 Flow boundary conditions

6.3.1 Boundary types

The 2Dv-model boundary conditions have to be specified for flow and sediment transport passing through the open boundaries. There are different types of flow and transport boundary conditions that can be prescribed. With respect to flow, the following types are available in DELFT3D-FLOW:

- Water level
- Current
- Discharge or flux (total or per grid cell)
- Neumann (water level gradient)
- Riemann or weakly reflective boundaries

Concerning what type of boundary condition is most suitable for the 2Dv-model, the purpose is to generate symmetric flow through the domain in order to identify the mechanism attributed to sandwave development. One of the theories on sandwaves regards residual circulation cells to be mainly responsible for the growth and stability of sandwaves. Consequently, this demands symmetric flow (i.e. no residual current) since this could emphasize the importance of an additional residual current to the development of sandwaves. Therefore, in the perfect scenario where equilibrium in sandwave configuration is found using a symmetric bed level pattern forced with symmetric flow, the profile model should show the presence of circulating residual cells believed to generate and maintain sandwaves. With symmetric flow through the domain this would result in symmetrical recirculation cells on both sides of the sandwave crest, showing uphill transport of sediment.

6.3.2 Selecting boundary conditions

Generally there are two ways to describe physically stable channel flow when there is more than one open boundary in the model area. The first method is to describe the normal velocity component at one end of the channel and the water level at the other. For this method one has to be very precise in matching the outgoing velocity components to the forced water level boundary, since velocities are only weakly coupled to water levels due to the non-linear relation. The other way is to prescribe water levels on both sides of the channel, simulating a passing tidal wave when applying a small phase difference between both boundaries. The discharge, Neumann and Riemann type boundaries are not considered in this study.

The forcing type for both boundaries is set on harmonic, using a radial frequency of 30 degrees per hour and water level amplitude of 1.00 m. The radial frequency of the S2 tide is chosen for reasons of simplicity. Boundary conditions are placed on the *East* and *West* boundaries of the 2Dv-model, leaving the other two boundaries as closed boundaries for which the free-slip condition holds.

The harmonic boundary signal $F(t)$ is constructed by super-imposing the following individual components:

$$F(t) = A_0 + \sum_{i=1}^n A_i \cos(2\pi f_i t - \varphi_i) \quad [6.6]$$

With:

| | | |
|-------------|--|----------------------------|
| t | Time | [s] |
| A_0 | Mean water level or velocity over a certain period | [m] or [ms ⁻¹] |
| A_i | Local tidal amplitude of harmonic component i | [m] or [ms ⁻¹] |
| f_i | Frequency of harmonic component | [rads ⁻¹] |
| φ_i | Phase of harmonic component | [°] |
| N | Number of frequency components | [-] |

The unit of the amplitudes depends on the quantity prescribed, they are respectively [m] for water elevations and [ms⁻¹] for velocities. In this equation each harmonic component (i) is defined by a characteristic frequency (f_i) and amplitude (A_i). These are the same for all wave conditions.

Velocity vs water level boundaries

When selecting a velocity boundary on one side and a water level boundary on the opposite side, initial model runs reveal a considerably growing disturbance on the velocity boundary side developing more extremely for higher flow velocities. Although this combination of boundary types can successfully lead to the generation of physically stable and symmetric tidal flow, this disturbance affects the development of the sandwave field which in the end results in erroneous morphological development as can be seen in Figure 6-3.

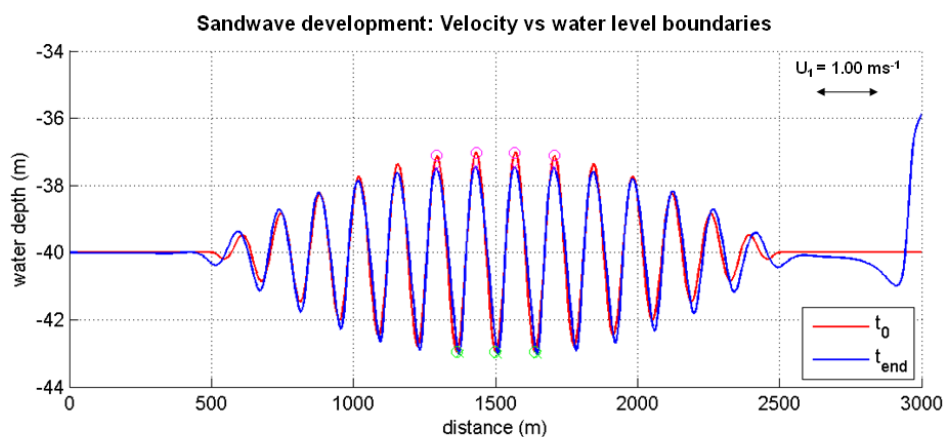


Figure 6-3: Erroneous bed level response when combining velocity and water level boundaries, with $U_1 = 1.00 \text{ ms}^{-1}$ placed on the right side and $\zeta_1 = 1.00 \text{ m}$ placed on the left side. After 1 hydrodynamic day the disturbance is excessively high and starts to affect the morphodynamic development.

The disturbance at the left boundary is most likely the result of a disparity between the applied water level fluctuation and the corresponding flow velocity. A non-linear relation between these boundary types demands a consistent update of the water level versus flow velocity relation after each time step. This computational effort complicates the simplicity of this basic profile model in such a way that a different combination of boundary types is preferred.

Water level vs water level boundaries

Two water level boundaries are even so able to generate physically stable and symmetric tidal flow, except without the formation of disturbances at the boundaries. The phase of the harmonic component, which has to be specified for the *East* and *West* boundaries of the domain, will be determined for all three flow conditions¹⁵. Table 6-1 displays the phase differences that correspond to results in the generated sandwave model velocities, with the magnitude quantified at the *West* boundary of the 2Dv-model. The runs were carried out on fixed bottoms for depths of 20 m and 40 m with a range of reference velocities equivalent to the three representative current velocities obtained with the 2Dh-model. The forced water level amplitude ζ represents the long term average tidal wave height and is set on 1.00 m.

| Water level amplitude [m] | Water depth [m] | Phase difference in forcing [°] | Sandwave model velocity [ms ⁻¹] | Reference velocity [ms ⁻¹] |
|---------------------------|-----------------|---------------------------------|---|--|
| Model type | | 2Dv | 2Dv | 2Dh |
| 1.00 | 20 | 1.19 | 0.56 – 0.64 | 0.50 |
| | | 2.23 | 1.01 – 1.15 | 1.00 |
| | | 4.70 | 1.59 – 1.78 | 1.50 |
| | 40 | 1.19 | 0.57 – 0.72 | 0.50 |
| | | 2.25 | 0.99 – 1.17 | 1.00 |
| | | 3.38 | 1.61 – 1.89 | 1.50 |

Table 6-1: Phase differences between East and West boundary forcings, corresponding to maximum center crest flow velocities on fixed bed levels at depths of 20 and 40 m.

6.3.3 Flow velocity analysis

Now that all ranges of flow velocities can be generated within reasonable margins of the reference velocities, the sandwave model can be forced using the determined phase differences. The depicted maximum center crest flow velocities in Table 6-1 illustrate the maximum flow velocity present in the 2Dv-model. This is the case when taking a 10 m high sandwave in a water depth of 20 or 40 m, achieving the (minimum) depths of 15 and 35 m, respectively.

¹⁵ Flow conditions are $U = 0.50, 1.00$ and 1.50 ms^{-1} ; representing average tidal flow velocity, median peak tidal velocity and maximum peak tidal velocity in the inlet mouth of San Francisco Bay, respectively (see 5.3.1).

The velocity time series depicted in Figure 6-4 show very little spin-up time for the 2Dv-model to reach the steady state solution. Initial runs reveal that a spin-up time of 1 hydrodynamic day is sufficient to reach physically stable flow for all studied velocities.

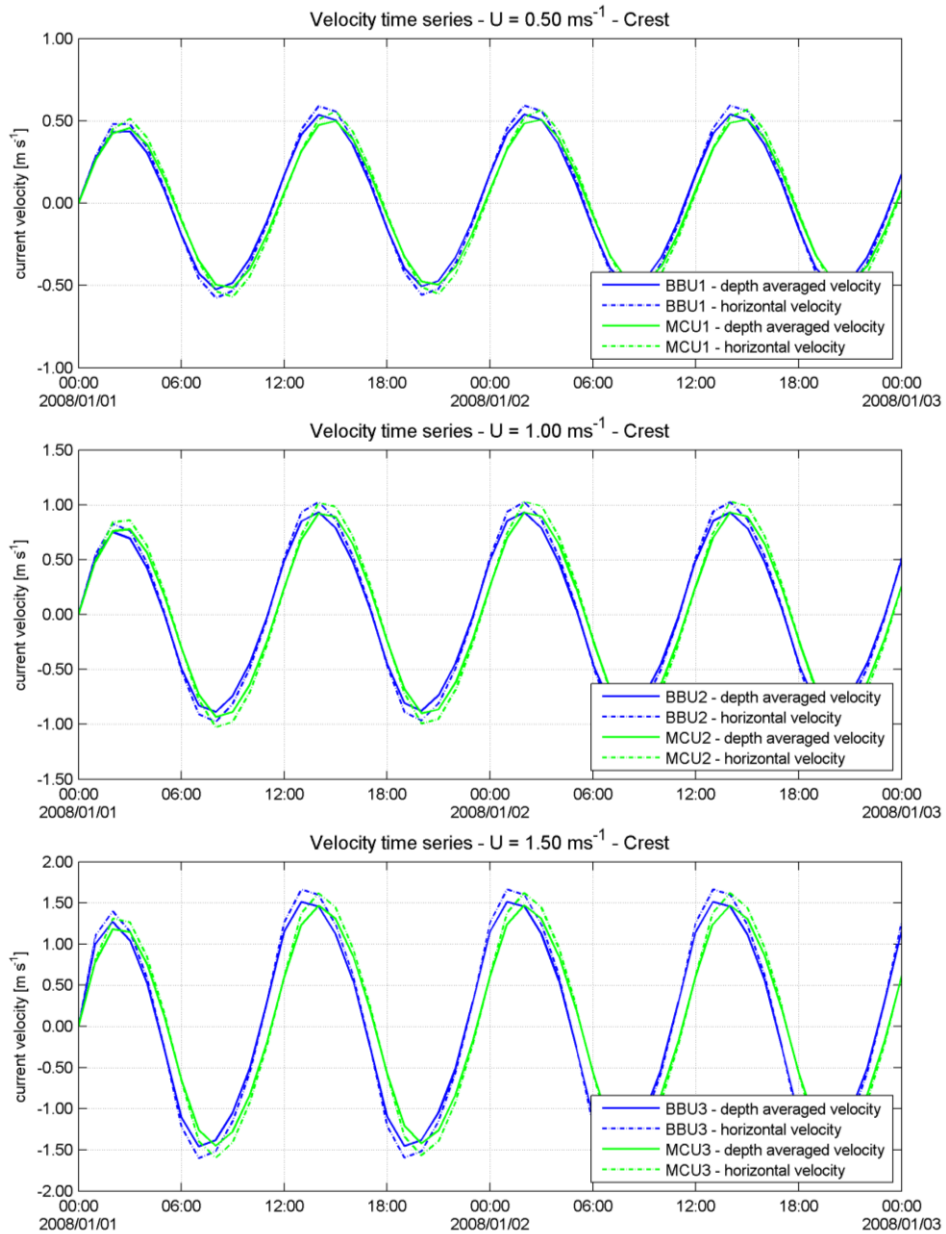


Figure 6-4: Velocity time series for $U = 0.50, 1.00$ and 1.50 ms^{-1} , measured at the top of the center sandwave monitoring point. The Baker Beach and Mouth Center velocities were created on a fixed sandwave bed, using a sandwave length of 100 m and a height of 7.8 and 9 m, respectively. The horizontal velocities are taken in the water surface layer.

The difference between mean ebb water depth and mean flood water depth explains the slightly higher flood velocity. This holds for a symmetric tidal flow, where the tidal wave travels faster during flood since the direction of propagation is in the direction from *West* to *East* (defined by boundary conditions). Since ebb and flood velocities are not exactly equal, this mismatches with the forced harmonic frequency component and slight deformation of current velocities is the result. For larger phase differences between water level boundaries this deformation of velocities becomes larger, as the frequency component is diverging.

6.4 Parameter settings

The parameter settings for the initial runs are listed in the tables of Appendix M. The most important parameter settings are however discussed in this section.

6.4.1 Hydrodynamic parameters

FLOW time step

To allow the simulation to undergo spin-up time, one hydrodynamic day is simulated before morphodynamic change is allowed. This permits the model to complete two tidal cycles, sufficient to cancel out numerical errors and irregularities travelling through the domain. The hydrodynamic time step mainly depends on the desired level of accuracy and numerical stability, which can be calculated with the Courant number. Given that the Courant number in DELFT3D-FLOW generally should not exceed the value 10 (WL|Delft Hydraulics, 2006), the maximum tolerable time step is 2.4 s, using the grid cell size of 5 m and a maximum local water depth of 40 m. To compare the influence of larger time steps on model accuracy, the analysis of different horizontal velocity vector errors over one tidal sequence is presented in Figure 6-5.

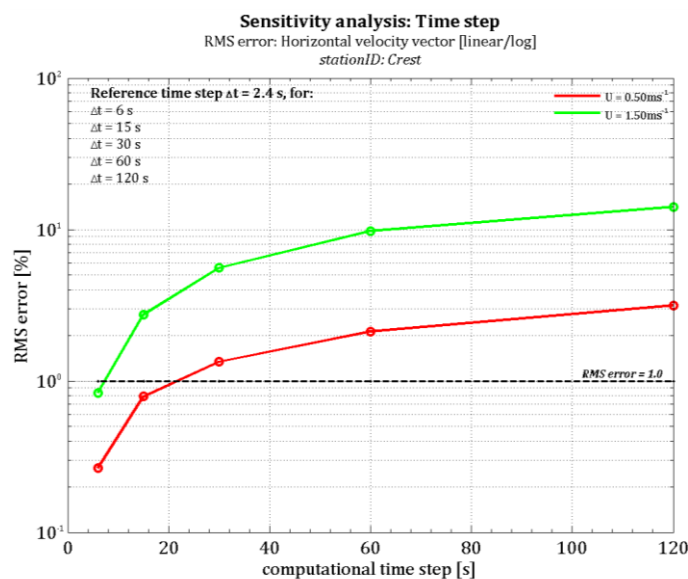


Figure 6-5: Computational time step comparison for $U_{hor} = 0.50 \text{ ms}^{-1}$ and $U_{hor} = 1.50 \text{ ms}^{-1}$.

For this study it is assumed that the largest time step possible has to fulfill the condition of a Root Mean Square (RMS) error smaller than 1%. The RMS condition implies that the difference in the flow velocity vectors calculated with a different computational time step, cannot be greater than 1% in size compared to the same velocity vectors generated with the reference timestep of 2.4 s. Flow simulations with different time steps (i.e. 6, 15, 30, 60 and 120 s) have shown that for time steps up to $\Delta t = 6$ s the velocity fields are identical for the range of flow velocities used in the sandwave model. Considering the lengthy duration time of simulation this results in the previously mentioned one hydrodynamic day of runtime.

Grain size diameter

The median grain size of sand is set to 0.50 mm, and represents the average of the median field data values described in section 5.2.2. The median grain size is important for the sandwave morphodynamics, since the settling velocity of sand in suspension is determined by this parameter. A sensitivity analysis of the median grain size will clarify how important this parameter actually is in the development of sandwaves.

6.4.2 Morphodynamic parameters

Morphological scale factor

To simulate sandwave morphology correctly, the model runtime must be set in such a way that the time scale of morphological change (order of years) is converted into a simulation runtime that is relatively short (order of hours). One way to achieve this is to introduce the use of the morphological factor or MORFAC, through which the bed evolution is upscaled (accelerated) after each hydrodynamic time step. The morphological upscaling factor depends on the dynamic response of the area of interest, meaning that dynamic areas require a lower MORFAC value whereas for more stable environments the MORFAC can be increased (typical range is between 10 and 1000 for dynamic and stable areas respectively). For example, when using a MORFAC that equals 100, a morphological prediction based on a tidal cycle of 12.5 hours would represent 52 days.

Initial runs show that for flow velocities smaller than 1.00 ms^{-1} the application of a MORFAC of 250 still gives accurate results compared to a morphological factor of 10. For flow velocities larger than 1.00 ms^{-1} , the maximum allowed morphological factor is restricted to 50 compared to a morphological factor of 10. A complete list of the morphological and transport parameters is specified in the morphology input file of Appendix M.

Transport formula

The instantaneous total transport equation by Engelund-Hansen (1967) was chosen for reasons of a straightforward description of the total load of sediments. The Engelund-Hansen transport formula allows for a straightforward analysis of sandwave evolution, without being sensitive for calibration factors usually associated with the description of suspended sediment transport. The formula relates velocity directly and locally to sediment transport rates:

$$S = S_b + S_{s,eq} = \frac{0.05 \alpha q^5}{\sqrt{g} C^3 \Delta^2 D_{50}} \quad [6.7]$$

In which:

- S Sediment transport
- q Magnitude of flow velocity
- Δ Relative density
- C Chézy friction coefficient
- q Magnitude of flow velocity
- α Calibration coefficient

The bed-slope effect is taken into account by adjusting the magnitude of the transport based on the slope along the sediment transport vector, calculated based on the velocity field. Also, the direction of the transport is adjusted based on the slope perpendicular to the sediment transport vector calculated based on the velocity field.

Threshold of motion

To determine the threshold of particle motion the relation in equation 6.9 by Allen (1980) is used, taking the moments of lift, drag and gravity forces (equations 6.8 a-c) about the pivotal point P as illustrated in Figure 6-6. The derivation of this relation will not be questioned and is assumed to be correct.

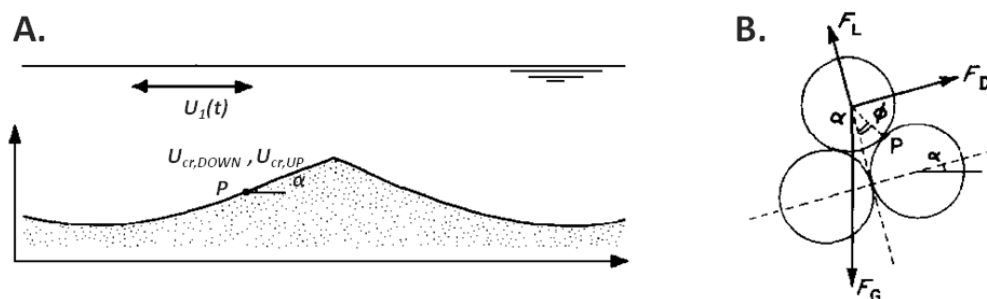


Figure 6-6: Stability of a symmetrical equilibrium sandwave. A) Flow components and thresholds acting at a point P where the sandwave has a maximum slope α . B) Equilibrium of a spherical grain beneath a current on a bed of similar grains (by Allen, 1980).

The nominal drag force on a particle of diameter D and density σ , the lift force acting on the grain and the gravity force holding the particle in place, read:

$$F_D = \frac{\pi}{4} \tau_{cr} D^2$$

$$F_L = k \cdot F_D \quad [6.8 \text{ a-c}]$$

$$F_G = \frac{\pi}{6} (\sigma - \rho) g D^3$$

In which:

- $\tau_{b,cr}$ critical bed shear stress
- k numerical coefficient, found for $\alpha = 0$
- ρ fluid density
- g acceleration due to gravity

Combining the equations in 6.8 results in the critical bed shear stress relation:

$$\tau_{b,cr} = \frac{2}{3} (\sigma - \rho) g D \frac{\sin(\phi \pm \alpha)}{(\cos \phi + k \sin \phi)} \quad [6.9]$$

In which:

- α bed slope angle relative to the horizontal
- ϕ angle between a normal to the bed and the line joining the pivotal point P with the particle centre, through which the forces are assumed to act

Now the critical bed shear stress can be expressed kinematically using the following well-known definition:

$$\tau_{b,cr} = \frac{f}{8} \rho_w u_{b,cr}^2 \quad [6.10]$$

In which:

- f Darcy-Weisbach bed friction coefficient, ranging from 0.02 for a flat bed to 0.10 for a dune covered bed (Bridge, 2003) therefore the commonly used value 0.06 is applied for the sandwave covered bed
- ρ_w density of water
- $u_{b,cr}$ critical (threshold) near-bed fluid velocity

Page left blank on purpose.

7. SANDWAVE MODEL RESULTS

This chapter contains a series of model runs with varying bed level and hydrodynamic configurations to identify the most essential parameters influencing sandwave morphodynamics and relating hydrodynamics. In the first section the morphodynamic equilibrium is investigated by presenting growth rates for different flow velocities. Section two presents the results of the investigated hydrodynamic equilibrium flow patterns. The final section three presents the results of the sensitivity analysis.

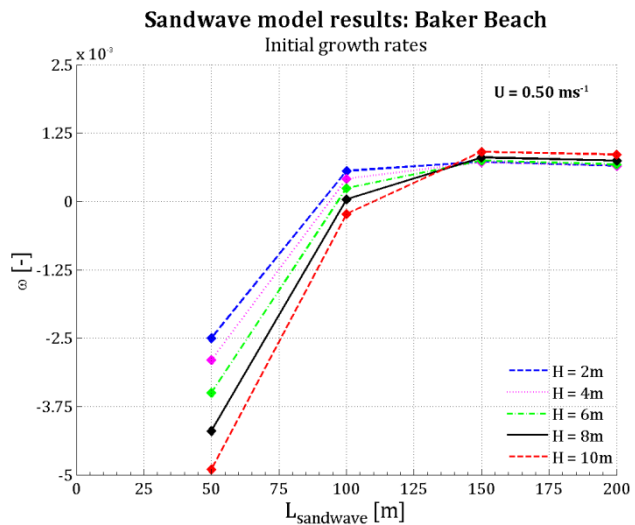
7.1 Morphodynamic equilibrium

7.1.1 Growth rates for Baker Beach depth

Figures 7-1 through 7-3 display the sandwave height growth rates for twenty different configurations of sandwave length and height, using a water depth of 20 m and velocity amplitudes ranging from mean tidal flow to peak tidal flow (i.e. 0.50 ms^{-1} to 1.50 ms^{-1} velocity categories¹⁶). All plots are provided with a table listing the exact growth rates for all combinations.

| Growth rates: ω | | Length [m] | | | |
|------------------------|----|------------|---------|--------|--------|
| | | 50 | 100 | 150 | 200 |
| Height [m] | 2 | -0.0025 | 0.0006 | 0.0007 | 0.0006 |
| | 4 | -0.0029 | 0.0004 | 0.0007 | 0.0007 |
| | 6 | -0.0035 | 0.0002 | 0.0007 | 0.0007 |
| | 8 | -0.0042 | 0.0000 | 0.0008 | 0.0007 |
| | 10 | -0.0049 | -0.0002 | 0.0009 | 0.0009 |

Figure 7-1: Baker Beach sandwave configurations ($U = 0.50 \text{ ms}^{-1}$).

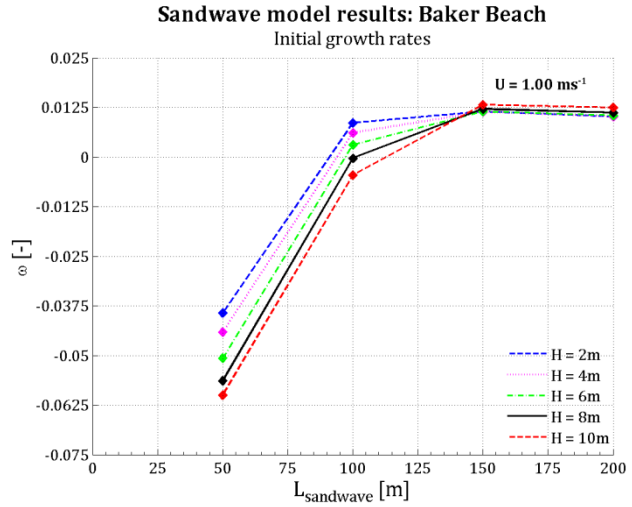


The linear interpolated growth rate lines in Figure 7-1 show that the model is capable of reaching equilibrium in sandwave height using a velocity of 0.50 ms^{-1} at a depth of 20 m. All growth rates suffice the equilibrium condition found in section 4.2.3. Through linear extrapolation the combination of an 8.3 m high sandwave with a length of 100 m results in a zero growth rate or exact equilibrium.

¹⁶ These velocities represent different stages of tidal flow similar to those observed in San Francisco Bay inlet mouth (see section 5.3.1 for a quantification of these magnitudes)

| Growth rates: ω | | Length [m] | | | |
|------------------------|----|------------|---------|--------|--------|
| | | 50 | 100 | 150 | 200 |
| Height [m] | 2 | -0.0393 | 0.0086 | 0.0115 | 0.0102 |
| | 4 | -0.0441 | 0.0061 | 0.0114 | 0.0102 |
| | 6 | -0.0507 | 0.0031 | 0.0115 | 0.0105 |
| | 8 | -0.0564 | -0.0003 | 0.0121 | 0.0112 |
| | 10 | -0.0600 | -0.0045 | 0.0132 | 0.0125 |

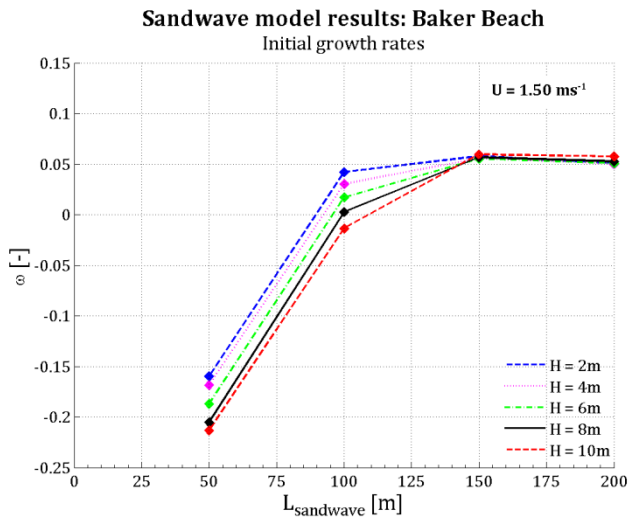
Figure 7-2: Baker Beach sandwave configurations ($U = 1.00 \text{ ms}^{-1}$).



The growth rates depicted in Figure 7-2 show that the model is capable of reaching equilibrium in sandwave height using a velocity of 1.00 ms^{-1} at a water depth of 20 m. The combinations of 2 m to 10 m high sandwaves with a length of 100 m meet the requirements of equilibrium. Exact equilibrium is reached for the combination of 7.9 m in height and 100 m in length using linear extrapolation.

| Growth rates: ω | | Length [m] | | | |
|------------------------|----|------------|---------|--------|--------|
| | | 50 | 100 | 150 | 200 |
| Height [m] | 2 | -0.1598 | 0.0422 | 0.0579 | 0.0508 |
| | 4 | -0.1685 | 0.0305 | 0.0558 | 0.0500 |
| | 6 | -0.1870 | 0.0173 | 0.0554 | 0.0507 |
| | 8 | -0.2052 | 0.0026 | 0.0566 | 0.0527 |
| | 10 | -0.2133 | -0.0135 | 0.0597 | 0.0575 |

Figure 7-3: Baker Beach sandwave configurations ($U = 1.50 \text{ ms}^{-1}$).



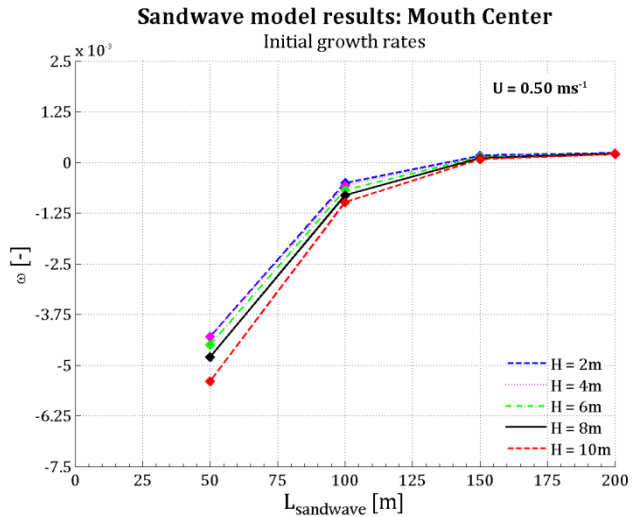
The growth rates in Figure 7-3 show that the model is capable of reaching equilibrium in sandwave height with velocities of 1.50 ms^{-1} at a depth of 20 m. Through linear extrapolation of the growth rate points, the combination of 8.3 m in height and 100 m length shows a growth rate that suffices the exact equilibrium condition.

7.1.2 Growth rates for Mouth Center depth

Figures 7-4 through 7-6 display the sandwave height growth rates for twenty different configurations of sandwave length and heights, using a water depth of 40 m and velocity amplitudes ranging from mean tidal flow to peak tidal flow (i.e. 0.50 ms^{-1} to 1.50 ms^{-1} velocity categories). All plots are provided with a table listing the exact growth rates for all combinations.

| Growth rates: ω | | Length [m] | | | |
|------------------------|----|------------|---------|--------|--------|
| | | 50 | 100 | 150 | 200 |
| Height [m] | 2 | -0.0043 | -0.0005 | 0.0002 | 0.0002 |
| | 4 | -0.0043 | -0.0006 | 0.0001 | 0.0002 |
| | 6 | -0.0045 | -0.0007 | 0.0001 | 0.0002 |
| | 8 | -0.0048 | -0.0008 | 0.0001 | 0.0002 |
| | 10 | -0.0054 | -0.0010 | 0.0001 | 0.0002 |

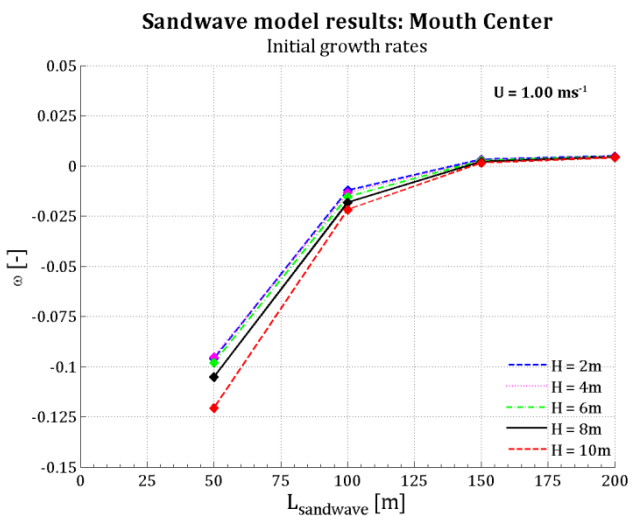
Figure 7-4: Mouth Center sandwave configurations ($U = 0.50 \text{ ms}^{-1}$).



The linear interpolated growth rate lines in Figure 7-4 show that the model is capable of reaching equilibrium in sandwave height using a velocity of 0.50 ms^{-1} at a depth of 40 m. All growth rates depicted suffice the equilibrium condition found in section 4.2.3. Through linear extrapolation, the combination of a 14.5 m high sandwave with a length of 150 m results in a growth rate closest to zero or exact equilibrium.

| Growth rates: ω | | Length [m] | | | |
|------------------------|----|------------|---------|--------|--------|
| | | 50 | 100 | 150 | 200 |
| Height [m] | 2 | -0.0960 | -0.0121 | 0.0032 | 0.0048 |
| | 4 | -0.0954 | -0.0134 | 0.0029 | 0.0046 |
| | 6 | -0.0981 | -0.0154 | 0.0026 | 0.0045 |
| | 8 | -0.1052 | -0.0182 | 0.0021 | 0.0043 |
| | 10 | -0.1207 | -0.0218 | 0.0015 | 0.0042 |

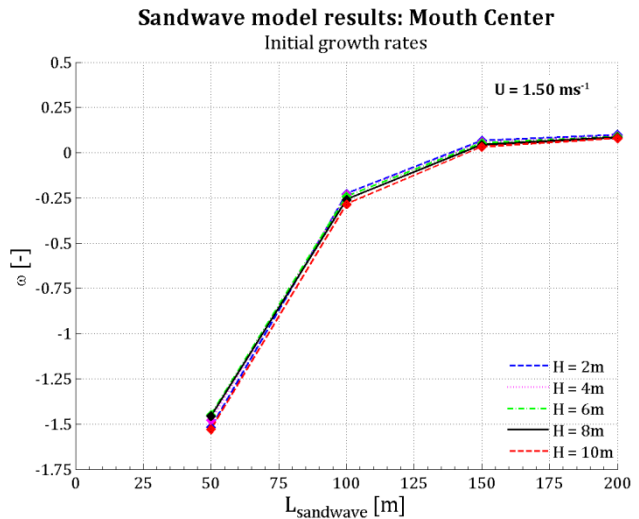
Figure 7-5: Mouth Center sandwave configurations ($U = 1.00 \text{ ms}^{-1}$).



The growth rates depicted in Figure 7-5 show that the model is capable of reaching equilibrium in sandwave height using a velocity of 1.00 ms^{-1} at a depth of 40 m. All combinations of 2 m to 10 m high sandwaves with a length of 150 m or 200 m suffice the equilibrium condition. Through linear extrapolation the configuration closest to exact equilibrium is found for a 13.5 m high sandwave with a length of 150 m.

| Growth rates: ω | Length [m] | | | | |
|------------------------|------------|---------|---------|--------|--------|
| | 50 | 100 | 150 | 200 | |
| Height [m] | 2 | -1.5184 | -0.2270 | 0.0674 | 0.0984 |
| | 4 | -1.4789 | -0.2310 | 0.0611 | 0.0937 |
| | 6 | -1.4502 | -0.2412 | 0.0533 | 0.0892 |
| | 8 | -1.4570 | -0.2589 | 0.0435 | 0.0841 |
| | 10 | -1.5292 | -0.2846 | 0.0325 | 0.0795 |

Figure 7-6: Mouth Center sandwave configurations ($U = 1.50 \text{ ms}^{-1}$).



The growth rates depicted in Figure 7-6 show that the model is capable of reaching equilibrium in sandwave height using a velocity of 1.00 ms^{-1} at a depth of 40 m. Although none of the listed height and length combinations fulfills the equilibrium condition, a linear extrapolation of the listed growth rate points suggests that the height of 14.7 m in combination with a length of 150 m fulfills condition of exact equilibrium.

7.1.3 State of equilibrium

In this section the range of equilibrium height configurations are determined based on the length over height ratio found for the zero growth rate runs. This way an estimate of the equilibrium heights for a broader set of sandwave lengths can be found. Table 7-1 displays the zero growth rate slope ratios for the six investigated morphodynamic equilibrium scenarios in section 7.1.1 and 7.1.2.

Baker Beach median depth

| Equilibrium configuration | Velocity amplitude | Length / height ratio |
|---------------------------|---------------------------|-----------------------|
| L = 100 m; H = 8.3 m | U = 0.50 ms ⁻¹ | 12.0 |
| L = 100 m; H = 7.9 m | U = 1.00 ms ⁻¹ | 12.7 |
| L = 100 m; H = 8.3 m | U = 1.50 ms ⁻¹ | 12.0 |

Mouth Center median depth

| Equilibrium configuration | Velocity amplitude | Length / height ratio |
|---------------------------|---------------------------|-----------------------|
| L = 150 m; H = 14.5 m | U = 0.50 ms ⁻¹ | 10.3 |
| L = 150 m; H = 13.5 m | U = 1.00 ms ⁻¹ | 11.1 |
| L = 150 m; H = 14.7 m | U = 1.50 ms ⁻¹ | 10.2 |

Table 7-1: Length over height ratios that belong to the equilibrium sandwave configurations, presented for both study areas.

The length over height ratios that belong to $U = 1.00 \text{ ms}^{-1}$ are used to calculate the equilibrium heights for lengths found in Table 7-2. The length range of 75 to 175 m covers the largest sandwave lengths found in both project areas according to the field data in section 5.2.1. The model runs are repeated under exact same depth and flow configurations, using the length over height ratio that belongs to $U = 1.00 \text{ ms}^{-1}$ to estimate the expected equilibrium height. The resulting growth rates are listed for all three velocity amplitudes.

| Baker Beach <i>growth rates ω for different velocities</i> | | | | | Mouth Center <i>growth rates ω for different velocities</i> | | | |
|---|---------------------|--------------------------|--------------------------|--------------------------|--|--------------------------|--------------------------|--------------------------|
| L [m] | H _{EQ} [m] | 0.50 [ms ⁻¹] | 1.00 [ms ⁻¹] | 1.50 [ms ⁻¹] | H _{EQ} [m] | 0.50 [ms ⁻¹] | 1.00 [ms ⁻¹] | 1.50 [ms ⁻¹] |
| 75 | 5.9 | 0.00120 | -0.02530 | -0.27270 | 6.8 | -0.00630 | -0.06920 | -0.40560 |
| 100 | 7.8 | -0.00110 | -0.00530 | -0.17140 | 9.0 | -0.00330 | -0.04400 | -0.33640 |
| 125 | 9.8 | 0.00330 | 0.00180 | -0.11030 | 11.3 | -0.00150 | -0.01780 | -0.21460 |
| 150 | 11.7 | 0.00520 | 0.00750 | -0.04470 | 13.5 | 0.00021 | 0.00100 | -0.04000 |
| 175 | 13.7 | 0.00630 | 0.00220 | 0.00019 | 15.8 | 0.00098 | 0.00520 | 0.01340 |

Table 7-2: Growth rates for determined equilibrium sandwave heights, depicted for both study areas and for different velocity amplitudes.

Figures 7-7 and 7-8, display two of the seventeen equilibrium configurations listed in Table 7-2. Both figures display the morphodynamic evolution of the Baker Beach (BB) and Mouth Center (MC) median water depths, for the velocity amplitude of 1.00 ms^{-1} . The blue dotted line represents the bed level after 125 days. The red dotted line displays the bed level after 250 days. In both cases the equilibrium configurations show very little decay in both length and height, and are well within margin of the equilibrium growth rate found in section 4.2.3. Appendix N displays the bed level responses of two of the growth configurations and two of the decay configurations.

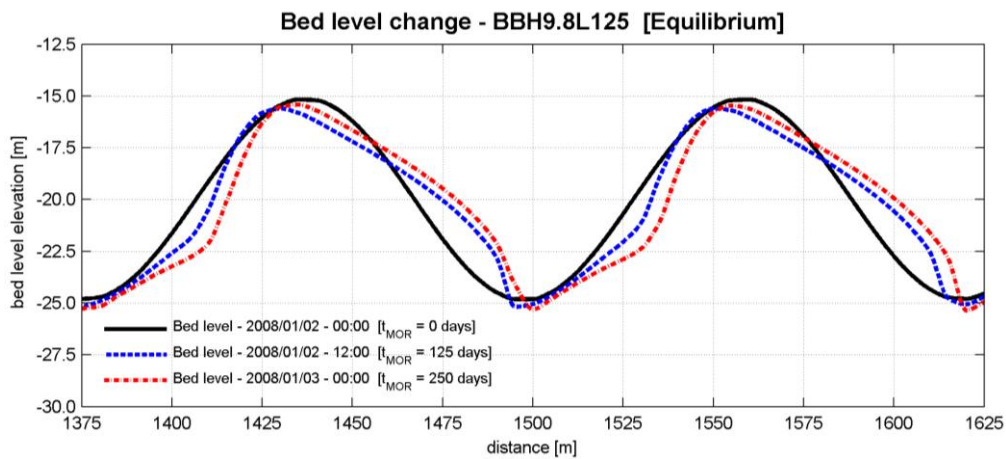


Figure 7-7: Bed level change of the equilibrium sandwave configuration in 20 m water depth, for a current velocity of 1.00 ms^{-1} .

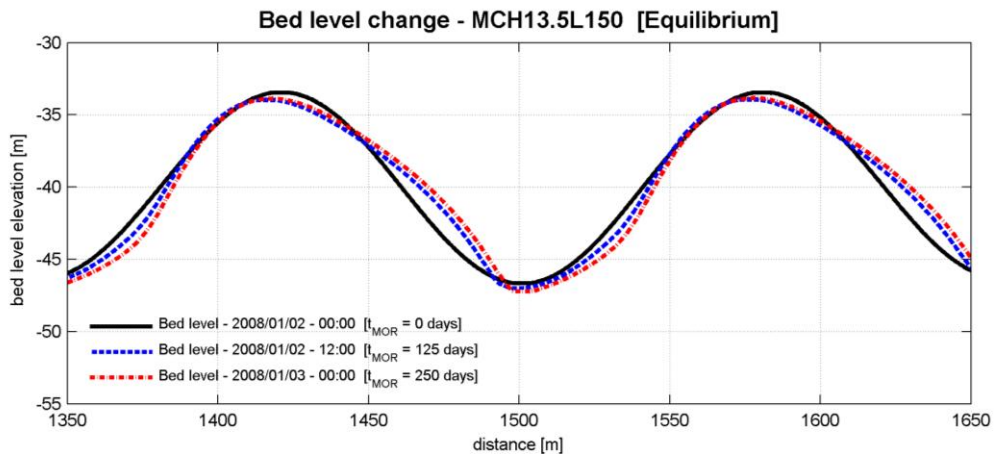


Figure 7-8: Bed level change of the equilibrium sandwave configuration in 40 m water depth, for a current velocity of 1.00 ms^{-1} .

7.2 Hydrodynamic equilibrium

7.2.1 Residual flow pattern for Baker Beach depth

Figures 7-9 through 7-11 display the residual current flow pattern observed for the three stages of sandwave development; equilibrium, growth and decay. All simulations in this section were carried out at a depth of 20 m, using a fixed bed level and the velocity amplitude of 1.00 ms⁻¹.

Residual flow pattern for sandwave equilibrium:

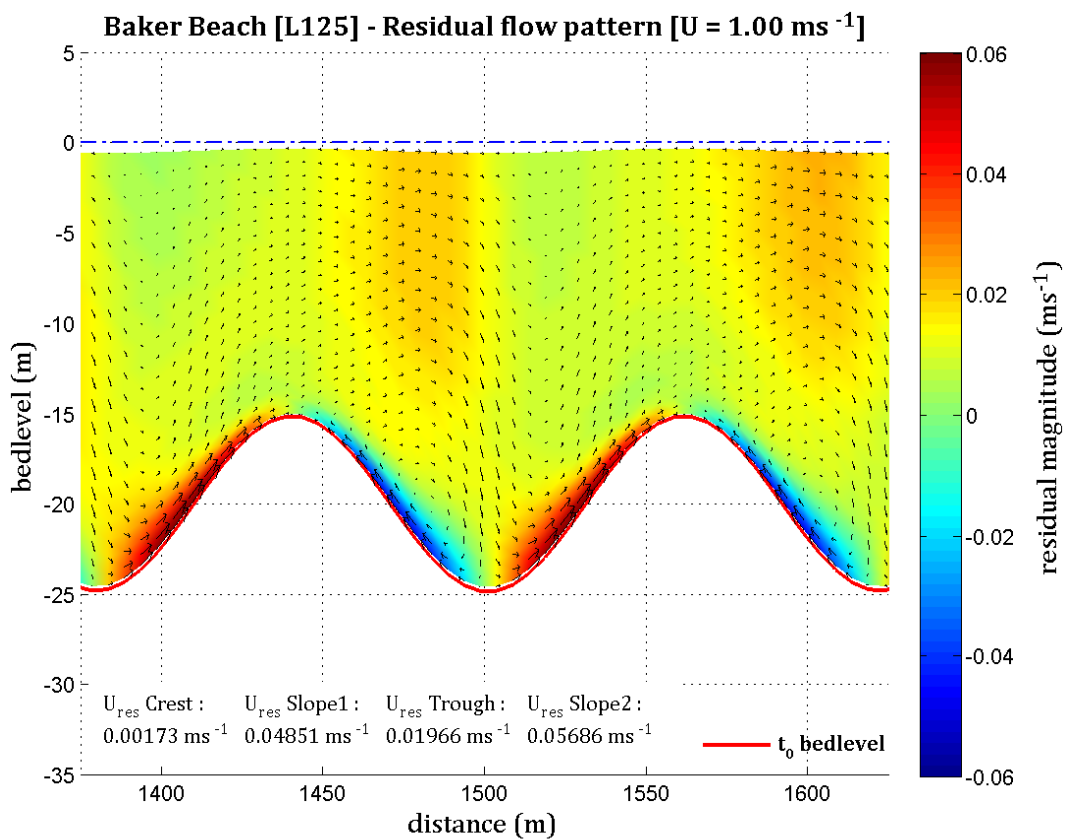


Figure 7-9: Residual flow velocity field in 20 m depth that belongs to a sandwave height of 9.8 m and a length of 125 m. The displayed flow pattern and magnitude is the result of running the model on a fixed sandwave bed and results in an equilibrium sandwave height.

Figure 7-9 displays the residual current flow pattern on a sandwave bed with a height of 9.8 m and a length of 125 m. The near bed residuals on both sides of the sandwave crest show a magnitude difference of a factor 1.2. The smallest near bed residual flow velocity is observed at the crest, being almost 33 times smaller than those observed on the left side slope of the crest. The near bed velocities show upward directed flow vectors, displaying a circular motion on both sides of the crest.

Residual flow pattern for sandwave growth:

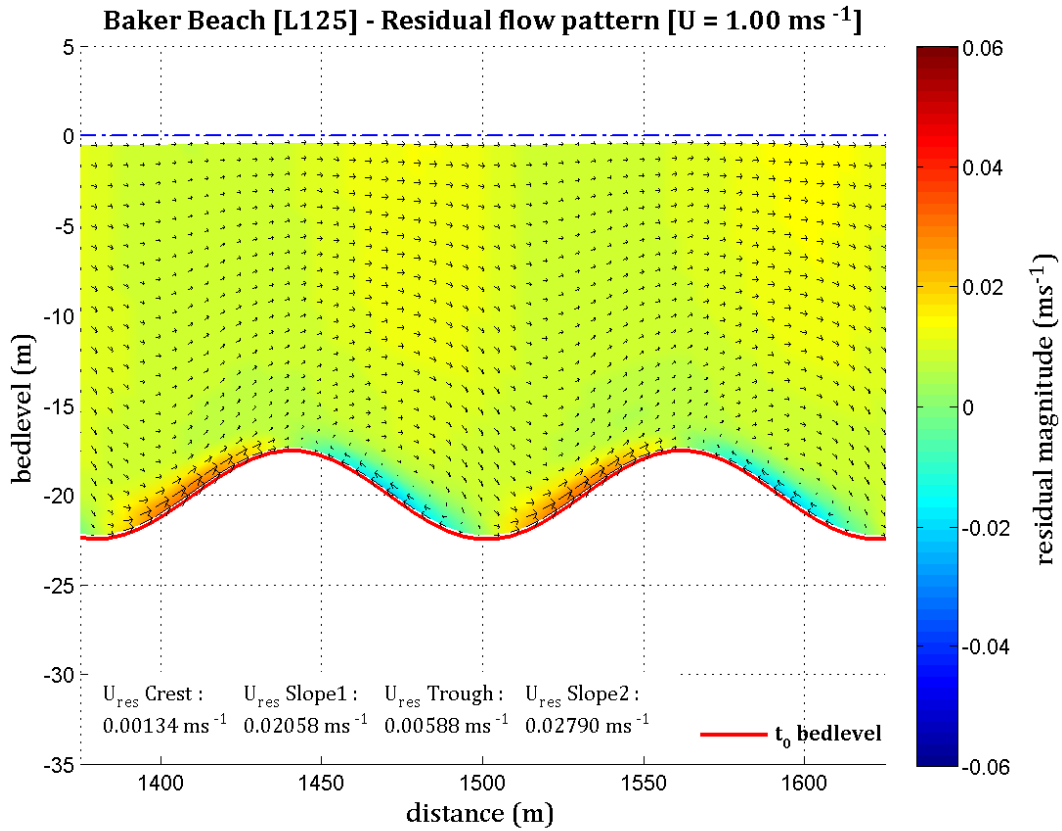


Figure 7-10: Residual flow velocity field in 20 m depth that belongs to a sandwave height of 5.0 m and a length of 125 m. The displayed flow pattern and magnitude is the result of running the model on a fixed sandwave bed and results in growth of sandwave height.

Figure 7-10 displays the residual velocity pattern as a result of forcing tidal flow on a sandwave bed with a height of 5.0 m and a length of 125 m. The near bed residuals show a difference in magnitude of a factor 1.4 with the largest residuals on the left side of the crest. The smallest near bed residual velocity is observed at the crest of the sandwave, and similar residuals are found in the trough. The near bed residuals at the crest show up- and eastward directed flow vectors. In between the right hand side of the crest and the trough a small eddy shaped net circular motion is observed in the first four layers, with residual vectors in the trough pointed towards the crest. The flow field is not symmetrical because almost all vertical layers show velocity vectors pointed east, indicating a small net residual current.

Residual flow pattern for sandwave decay:

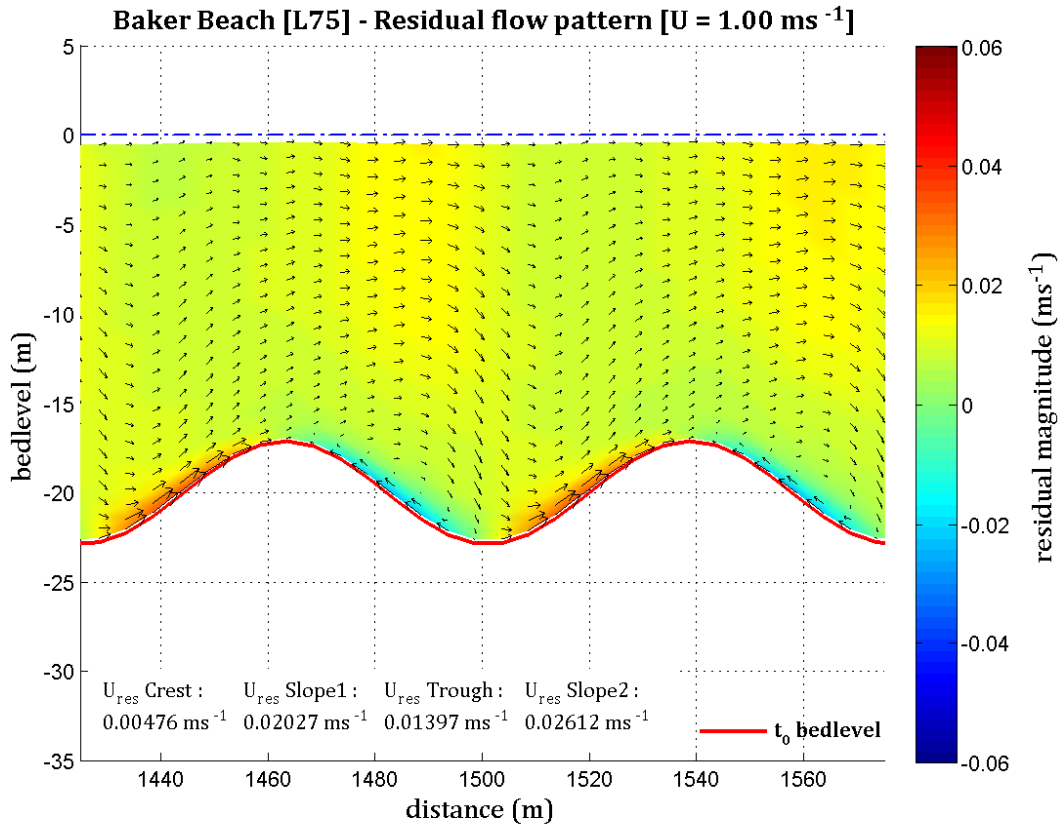


Figure 7-11: Residual flow velocity field in 20 m depth that belongs to a sandwave height of 5.9 m and a length of 75 m. The displayed flow pattern and magnitude is the result of running the model on a fixed sandwave bed and results in decay of sandwave height. Note that the scaling is similar to Figure 7-9 and 7-10, only the sandwave length is smaller therefore grid size appears larger.

Figure 7-11 displays the residual velocity pattern as a result of forcing tidal flow on a sandwave bed with a height of 5.9 m and a length of 75 m. The near bed residuals on the left side of the crest are a factor 1.3 stronger to those observed at the right side. Residual flow on the top and left hand slope of the crest illustrate a dominating easterly directed net current. The residual magnitude at the crest is about five times less strong than those observed at the left side slope. On the right side of the crest the near bed residuals show upward directed flow, displaying a small net circular motion between the trough and the right side slope.

7.2.2 Residual flow pattern for Mouth Center depth

Figures 7-12 through 7-14 display the hydrodynamic flow pattern that is observed for three stages of sandwave development: equilibrium, growth and decay. All simulations in this section were carried out at a depth of 40 m, using a fixed bed level and the velocity amplitude of 1.00 ms⁻¹.

Residual flow pattern for sandwave equilibrium:

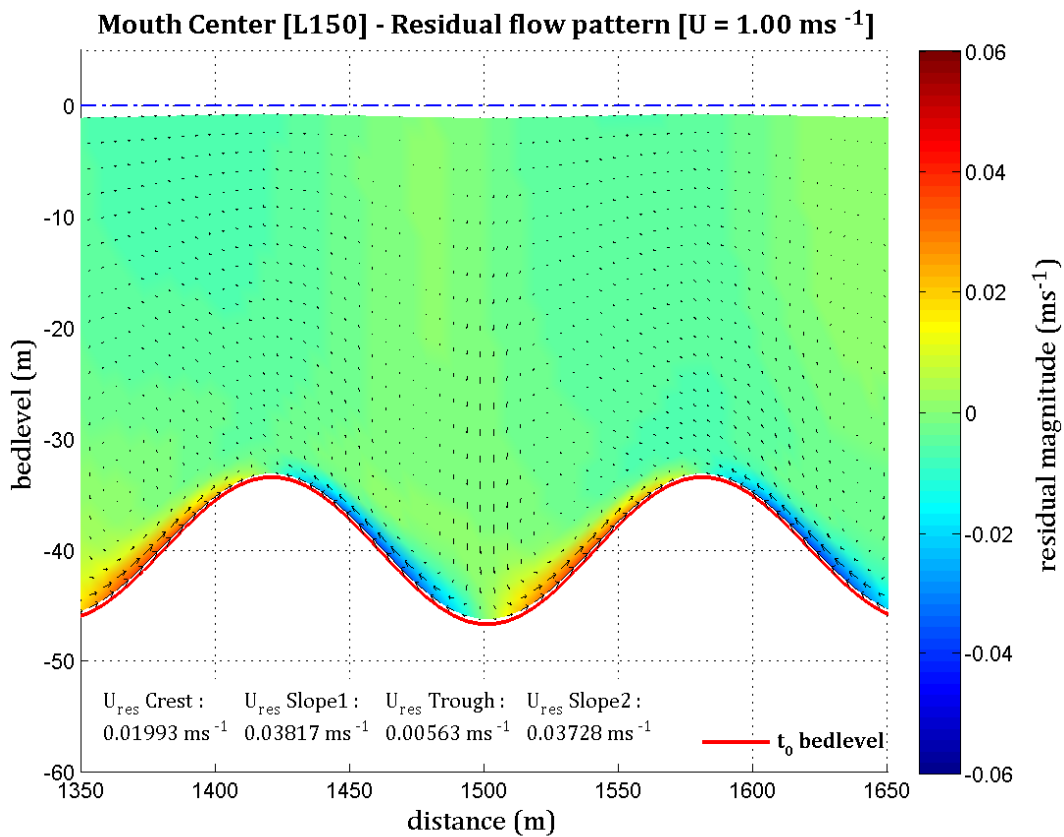


Figure 7-12: Residual flow velocity field in 40 m depth that belongs to a sandwave height of 13.5 m and a length of 150 m. The displayed flow pattern and magnitude is the result of running the model on a fixed sandwave bed and results in an equilibrium sandwave height.

Figure 7-12 displays the residual velocity vector field as a result of forcing tidal flow on a sandwave bed with a height of 13.5 m and a length of 150 m. The near bed residuals on both sides of the sandwave crest are almost identical in size, showing a residual of 0.0382 ms⁻¹ on the right side slope and a residual of 0.0373 ms⁻¹ on the left side slope. The smallest near bed residual flow velocity is observed in the trough, being almost 7 times smaller in magnitude than those on the right side slope. The resulting pattern displays a close to exact symmetric flow since the residual vectors in the upper layers are close to negligible.

Residual flow pattern for sandwave growth:

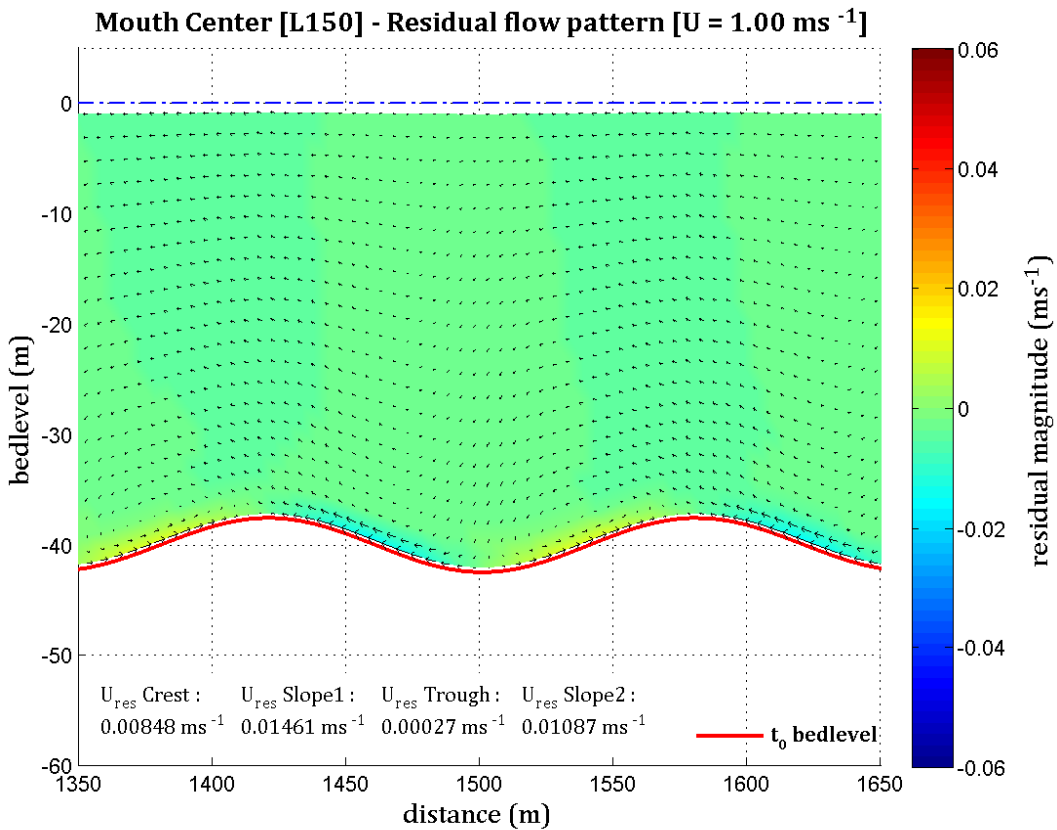


Figure 7-13: Residual flow velocity field in 40 m depth that belongs to a sandwave height of 5.0 m and a length of 150 m. The displayed flow pattern and magnitude is the result of running the model on a fixed sandwave bed and results in growth of sandwave height.

Figure 7-13 displays the residual velocity pattern as a result of forcing tidal flow on a sandwave bed with a height of 5.0 m and a length of 150 m. The near bed residuals show a difference in magnitude of a factor 1.3 with the largest residuals on the right side of the sandwave crest. The smallest near bed residual velocity is observed at the crest of the sandwave, and similar residuals are found in the trough. The near bed residuals at the crest show up- and slightly westward directed flow vectors. In between the right hand side of the crest and the trough near bed residuals are pointing towards the crest. The flow field is close to symmetrical since the upper layer velocity vectors show an almost negligible small net current directed to the west.

Residual flow pattern for sandwave decay:

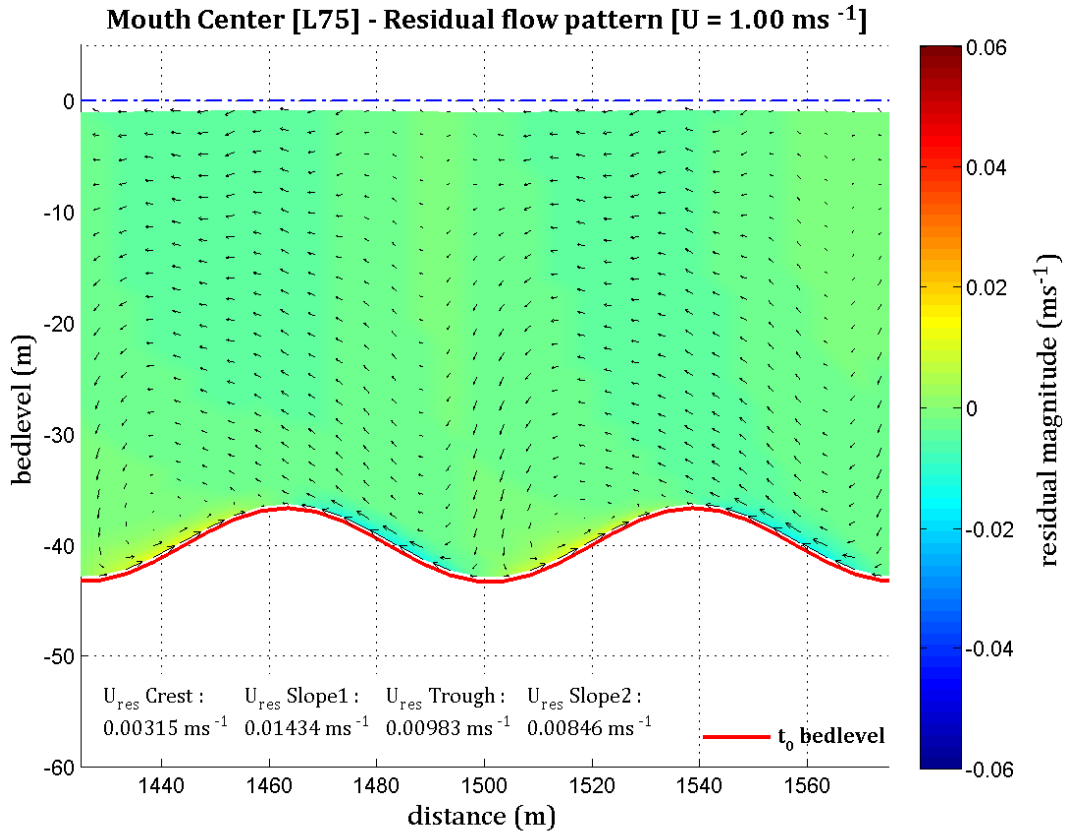


Figure 7-14: Residual flow velocity field in 40 m depth that belongs to a sandwave height of 6.8 m and a length of 75 m. The displayed flow pattern and magnitude is the result of running the model on a fixed sandwave bed and results in decay of sandwave height. Note that the scaling is similar to Figure 7-12 and 7-14, only the sandwave length is smaller therefore grid size appears larger.

Figure 7-14 displays the residual velocity pattern as a result of forcing tidal flow on a sandwave bed with a height of 6.8 m and a length of 75 m. The near bed residuals show magnitudes that are in favor of the right hand side of the sandwave crests, as they are 1.7 times larger than those at the left hand side. The near bed velocities show upward directed flow vectors on both sides of the crest, displaying a small circular motion in the first few layers of the left side slope. On top of the crests a net current pointed westward is visible throughout the entire water column.

7.2.3 State of equilibrium

In this section the near-bed current velocity and bed shear stress time series, found for the monitoring points *Crest*, *Slope1* and *Trough*, are presented for the equilibrium configurations of Baker Beach and Mouth Center. Time series for the Baker Beach and Mouth Center configurations that result in growth and decay of sandwave height, are presented in Appendices O and P. Results are presented for both project sites considering only the velocity amplitude of 1.00 ms^{-1} . Reason for this is the exceedence of critical near-bed flow velocity magnitude, which is not exceeded when applying 0.50 ms^{-1} but which is exceeded for $U = 1.00 \text{ ms}^{-1}$. The critical values for near-bed velocities $u_{b,cr}$ and bed shear stress $\tau_{b,cr}$ have been determined using the equations found in section 6.4.2.

Baker Beach equilibrium H 9.8m L 125m – time series

Figures 7-15 through 7-17 display the time series at Baker Beach for both near-bed flow velocities (blue lines) versus the critical near-bed flow velocity (dotted lines) and the time series for bed shear stress (red lines) versus the critical bed shear stress (dotted lines), that results in equilibrium. Time series are shown for two consecutive hydrodynamic days and are the result of running the model using a fixed sandwave bed.

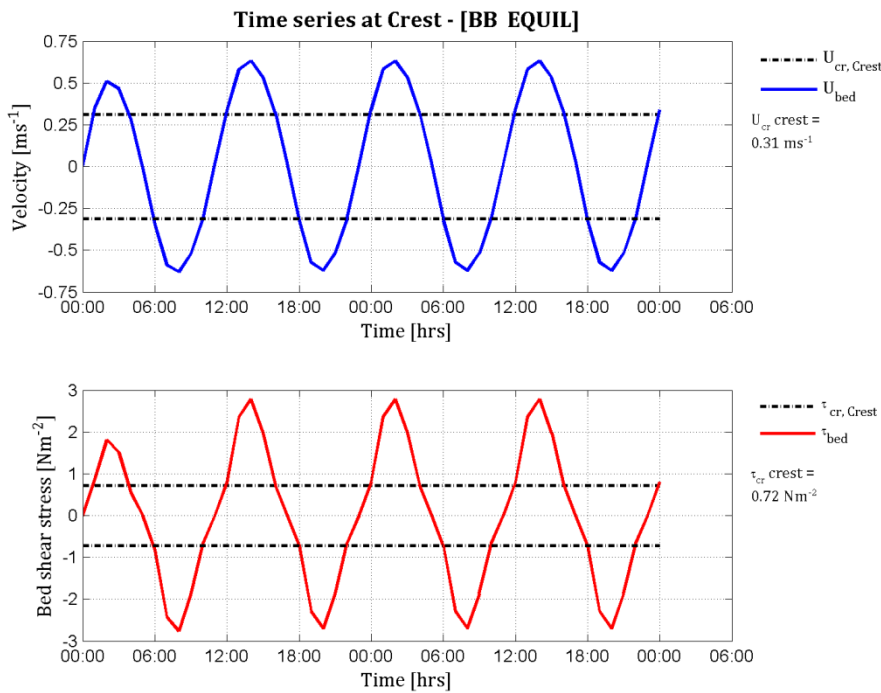


Figure 7-15: Baker Beach equilibrium configuration time series for velocities and shear stresses at the Crest monitoring point, using a sandwave height of 9.8 m with a length of 125 m.

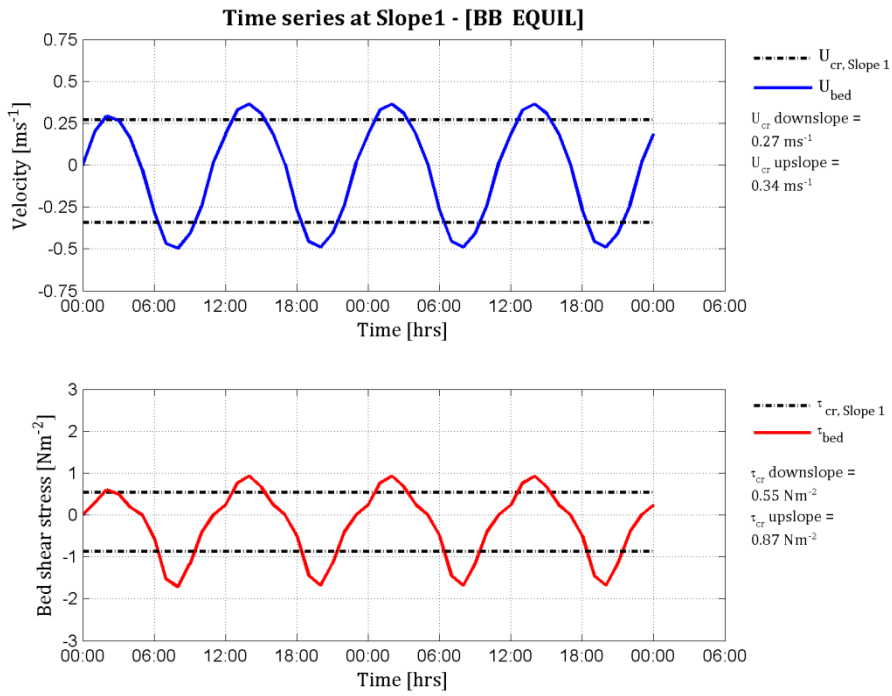


Figure 7-16: Baker Beach equilibrium configuration time series for velocities and shear stresses at the Slope1 monitoring point, using a sandwave height of 9.8 m with a length of 125 m.

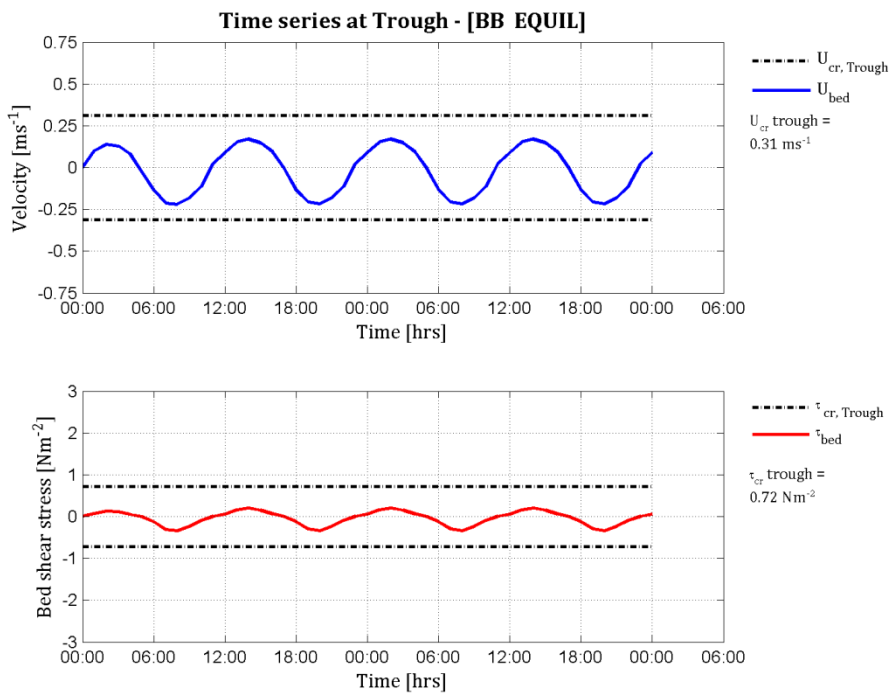


Figure 7-17: Baker Beach equilibrium configuration time series for velocities and shear stresses at the Trough monitoring point, using a sandwave height of 9.8 m with a length of 125 m.

Figure 7-15 illustrates that at the *Crest* of the center sandwave peak flood and peak ebb near-bed flow velocities are both 0.63 ms^{-1} , exceeding the *Crest* critical flow velocity of 0.31 ms^{-1} . Bed shear stress time series show that the maximum bed shear stress of 2.78 Nm^{-2} exceeds the critical bed shear stress of 0.72 Nm^{-2} . The duration of exceedence time Δ is approximately 80% of the time which means that 70% of the time, near bed flow velocities and bed shear stresses exceed the critical flow velocity and critical bed shear stress. Time series show that the near-bed flow velocities at the start and end of the morphodynamic simulation¹⁷ (i.e. after 24:00 and 48:00 hours, respectively) are equal to the critical flow velocity of 0.31 ms^{-1} . This is observed for the bed shear stress as well.

The time series in Figure 7-16 illustrate that at *Slope1* of the center sandwave peak flood and peak ebb near-bed velocities of 0.36 and 0.50 ms^{-1} , exceed the down- and upslope critical flow velocity of 0.27 and 0.34 ms^{-1} respectively. Bed shear stress time series show that peak flood and peak ebb bed shear stresses of 0.93 and 1.72 Nm^{-2} , exceed the down- and upslope critical bed shear stresses of 0.55 and 0.87 Nm^{-2} respectively. The duration of exceedence time Δ is approximately 50% of the time.

Figure 7-17 illustrates that at the *Trough* right of the center sandwave peak flood and peak ebb near-bed velocities of 0.17 and 0.22 ms^{-1} , do not exceed the *Trough* critical flow velocity of 0.31 ms^{-1} . Bed shear stress time series show that peak flood and peak ebb bed shear stresses of 0.20 and 0.34 Nm^{-2} do not exceed the critical bed shear stress of 0.72 Nm^{-2} .

Mouth Center equilibrium H 13.5m L 150m – time series

Figures 7-18 through 7-20 display the equilibrium time series at Mouth Center for both near-bed flow velocities (blue lines) versus the critical near-bed flow velocity (dotted lines) and the time series for bed shear stress (red lines) versus the critical bed shear stress (dotted lines). Time series are shown for two consecutive hydrodynamic days and are the result of running the model using a fixed sandwave bed.

Figure 7-18 illustrates that at the *Crest* of the center sandwave peak flood and peak ebb near-bed flow velocities are 0.60 and 0.66 ms^{-1} respectively, exceeding the *Crest* critical flow velocity of 0.31 ms^{-1} . Peak flood and peak ebb bed shear stresses of 2.55 and 3.06 Nm^{-2} both exceed the critical bed shear stress of 0.72 Nm^{-2} . The duration of exceedence time Δ is approximately 70% of the time. Near-bed flow velocities at the start and end of the morphodynamic simulation (i.e. after 24:00 and 48:00 hours, respectively) are close to the critical flow velocity of 0.31 ms^{-1} . This is observed for the bed shear stress as well.

¹⁷ The non-fixed bed runs were initiated after a spin-up time of 1 hydrodynamic day.

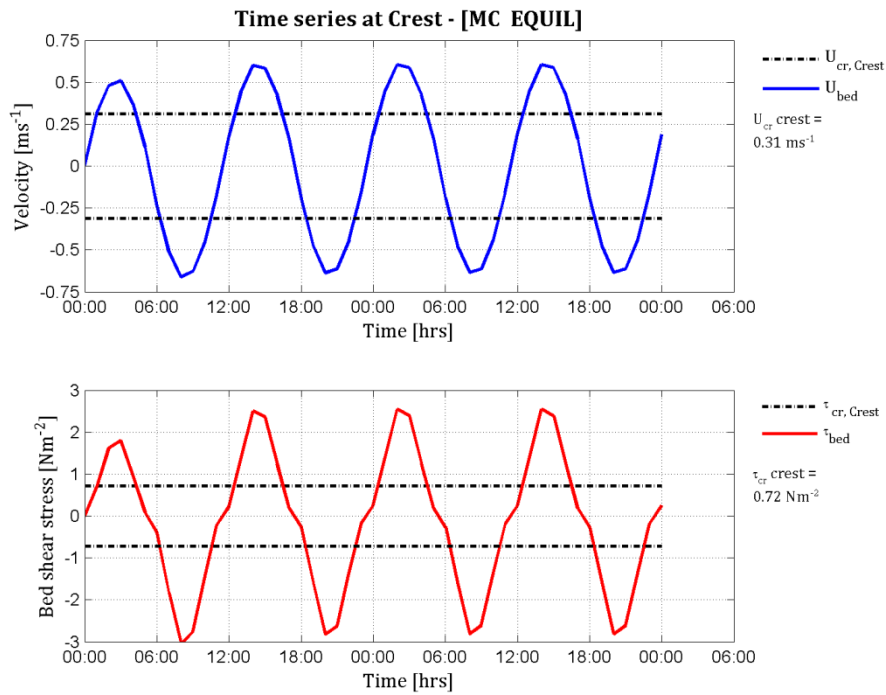


Figure 7-18: Mouth Center equilibrium configuration time series for velocities and shear stresses at the Crest monitoring point, using a sandwave height of 13.5 m with a length of 150 m.

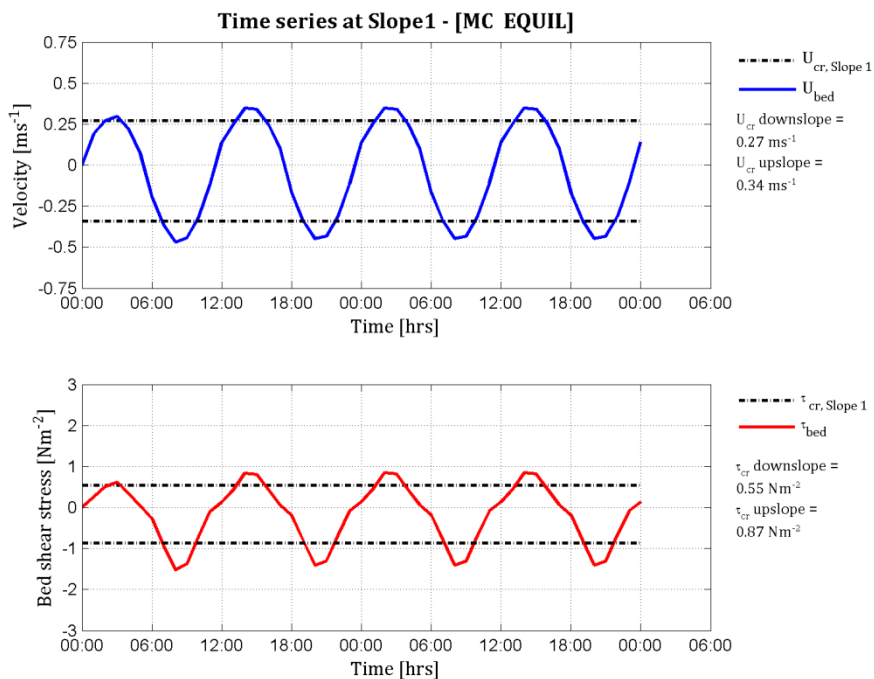


Figure 7-19: Mouth Center equilibrium configuration time series for velocities and shear stresses at the Slope1 monitoring point, using a sandwave height of 13.5 m with a length of 150 m.

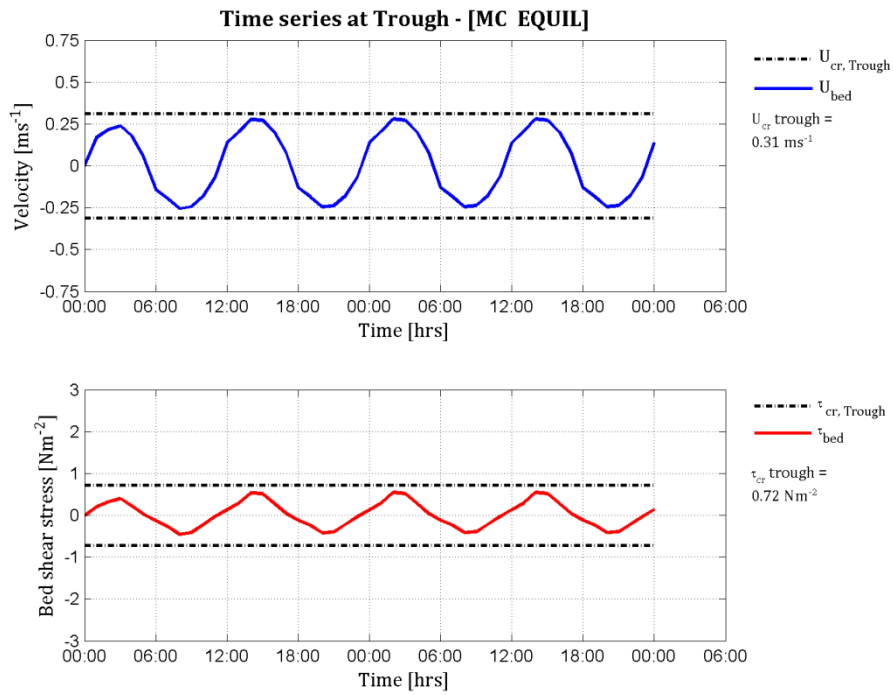


Figure 7-20: Mouth Center equilibrium configuration time series for velocities and shear stresses at the Trough monitoring point, using a sandwave height of 13.5 m with a length of 150 m.

The time series in Figure 7-19 illustrate that at *Slope1* of the center sandwave peak flood and peak ebb near-bed velocities of 0.35 and 0.47 ms^{-1} , exceed the down- and upslope critical flow velocity of 0.27 and 0.34 ms^{-1} respectively. Bed shear stresses at peak flood and peak ebb bed read 0.86 and 1.53 Nm^{-2} and exceed the down- and upslope critical bed shear stresses of 0.55 and 0.87 Nm^{-2} respectively. The duration of exceedence time Δ is approximately 50% of the time.

Figure 7-20 illustrates that at the *Trough* right of the center sandwave peak flood and peak ebb near-bed velocities of 0.28 and 0.26 ms^{-1} , do not exceed the *Trough* critical flow velocity of 0.31 ms^{-1} . Bed shear stress time series show that peak flood and peak ebb bed shear stresses of 0.55 and 0.46 Nm^{-2} do not exceed the critical bed shear stress of 0.72 Nm^{-2} .

7.3 Sensitivity analysis results

7.3.1 Effect of flow separation

This section is largely taken from WL|Delft Hydraulics (2006). The application of the σ -coordinate system in the 2Dv-model allows free surface flow by using boundary layers, meaning that the vertical acceleration component is relatively small. Under these circumstances, the pressure distribution in the vertical may be assumed to be hydrostatic; hence the hydrodynamic pressure may be neglected. The approximation of hydrostatic pressure, or shallow water assumption, simplifies the coupled set of three-dimensional equations¹⁸ to be solved and therefore allows the development of a computationally efficient three-dimensional numerical hydrodynamic model. However, there are situations where the vertical acceleration, and thereby the non-hydrostatic pressure component, cannot be neglected.

This, for example, is the case when flows over abruptly changing bottom topography are considered. As discussed in section 3.2.2, flow separation on large compound bedforms like sandwaves is the result of flow changes from accelerating flow in a very strong adverse pressure gradient to decelerating flow in a slightly favorable pressure gradient along the mildly positive slope of the sandwave. In general, the application of hydrostatic approximation is questionable when vertical scales of flow are of the same order of magnitude as the horizontal scales of the flow. When the requirements for shallow water flow are no longer met, the hydrodynamic component of the pressure has to be resolved in order to get physically realistic flow patterns. Since the display of flow separation requires a description of the vertical acceleration to visualize the turbulent fluid motions and near bed current structures, a non-hydrostatic module of the Z-model in DELFT3D-FLOW is required¹⁹. However the grid used for this study is made using the σ -layer approach, meaning that is not possible to describe the discussed vertical accelerations necessary to describe flow separation.

Recent studies by Winter (2008) on modelling current patterns on large compound bedforms like sandwaves indeed show that instantaneous flow structures as flow separation cannot be reproduced using hydrostatic models. Based on the process based modelling system of DELFT3D-FLOW a 2Dv-model of the Grådyb tidal channel system was setup to calculate the high resolution hydrodynamics of the domain. The finite-differences modelling system was applied both in hydrostatic and non-hydrostatic mode to solve the nonlinear Reynolds averaged Navier-Stokes equations on a rectilinear ($dx = dz = 0.5$ m) grid. The model domain covered a 500 m stretch of the tidal channel and hydrodynamics were driven by a harmonic tidal forcing at the lateral open boundaries.

¹⁸ See section 6.1 for the shallow water equations

¹⁹ For a more extensive elaboration on the non-hydrostatic flow phenomena, see WL|Delft Hydraulics (2006)

One of the conclusions by Winter (2008) was that a correct reproduction of near bed current structures in the lee of steep slope angles required the description of the vertical acceleration, and thereby the non-hydrostatic pressure component. The results showed that instantaneous currents over compound bedforms can only be reproduced realistically by non-hydrostatic simulations.

To illustrate that the 2Dv-model in this study is not capable of producing the vertical accelerations and eddy circulation induced by flow separation, a test run was performed considering uni-directional current flow U_0 of 1.00 ms^{-1} on top of a very steep bottom profile in a water depth of 20 m. Figure 7-21 displays the result of the run, in which a sawtooth shaped profile with a length of 125 m and a height of 12 m is used.

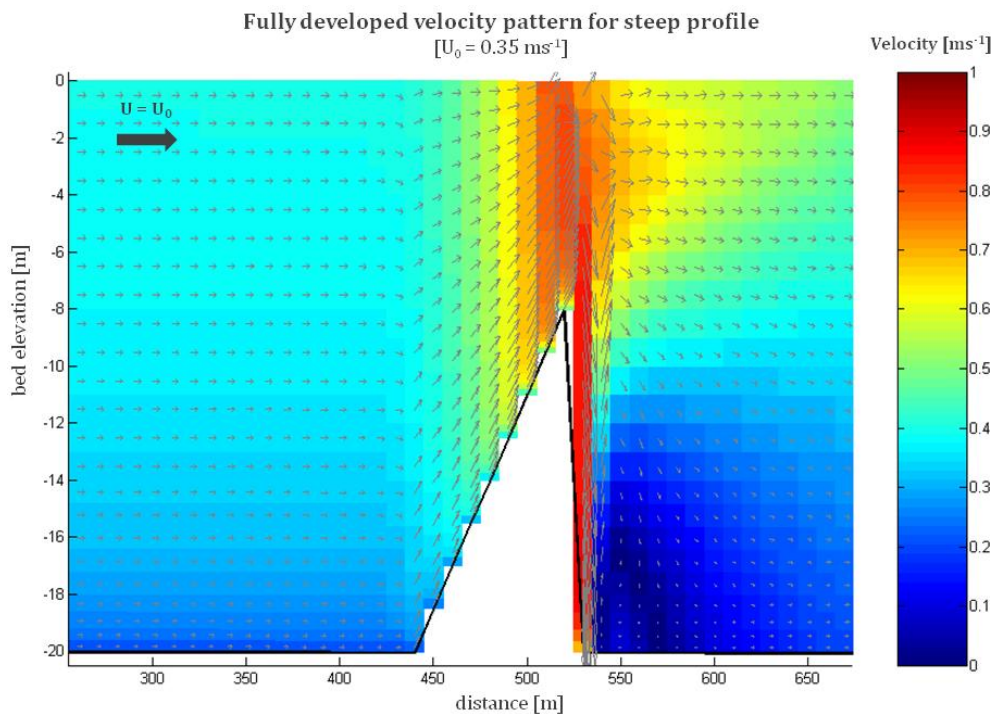


Figure 7-21: Instantaneous velocity pattern over steep profile using the hydrostatic (σ -layer) approach [$U_0 = 0.35 \text{ ms}^{-1}$]. On the right hand side of the crest flow increases to $U = 1.00 \text{ ms}^{-1}$ and velocity vectors are pointed straight down followed by upward pointed vectors.

7.3.2 Effect of bed-slope factor (ALFABS)

Figure 7-22 displays the growth rates that belong to 250 days of sandwave development, based on simulations with five different longitudinal bed-slope correction factors, also known as ALFABS factors, ranging from 0.2 to 5.0 (the default value is 1.0). The parameter adjusts the local bed-load transport on sloping beds by influencing the sediment transport rates, and is based on the Bagnold approach (Bagnold, 1956). Simulations were performed for two sandwave profiles representing equilibrium configurations²⁰ of Baker Beach and Mouth Center median depths, using a tidal velocity of 1.00 ms⁻¹.

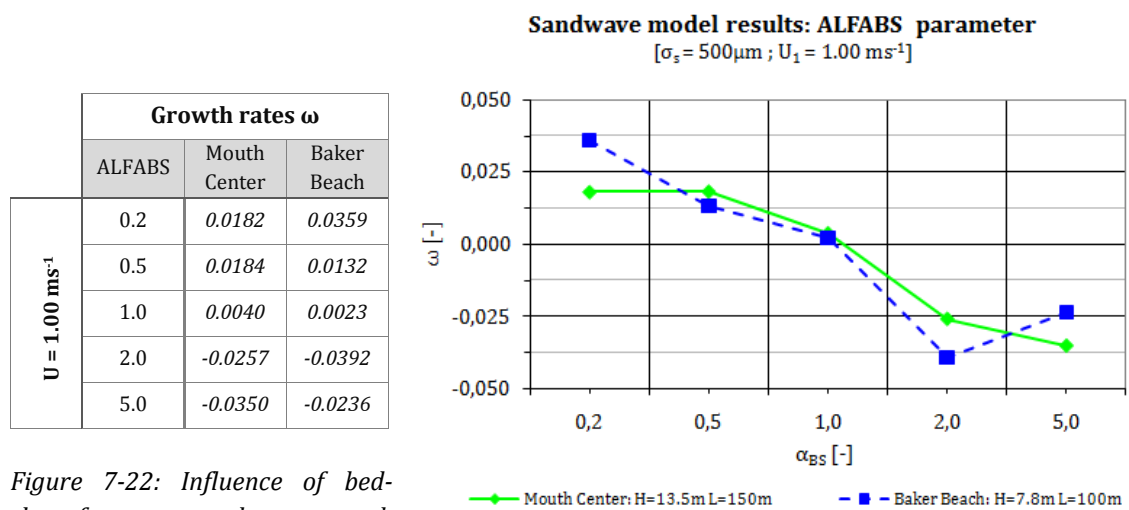


Figure 7-22: Influence of bed-slope factor on sandwave growth rate.

Results show that ALFABS influences growth rates significantly. For ALFABS values smaller than 1, both equilibrium sandwave configurations show growth to larger wave heights to attain a new equilibrium. The opposite is true for ALFABS values larger than 1.0, where both equilibrium sandwave configurations decay to smaller wave heights to attain a new equilibrium.

²⁰ The (default) grain-size of these equilibrium configurations was set on 500 μm

7.3.3 Effect of median grain-size diameter

Figure 7-23 displays the growth rates that belong to 250 days of sandwave development, based on simulations with median grain-size diameters (D_{50}) ranging from 200 μm to 1000 μm . This range of sediment diameters is found in the project areas Baker Beach and Mouth Center (see section 5.2.2). The simulations were performed with two equilibrium sandwave configurations for the median depths of Baker Beach and Mouth Center, using a tidal velocity of 1.00 ms^{-1} .

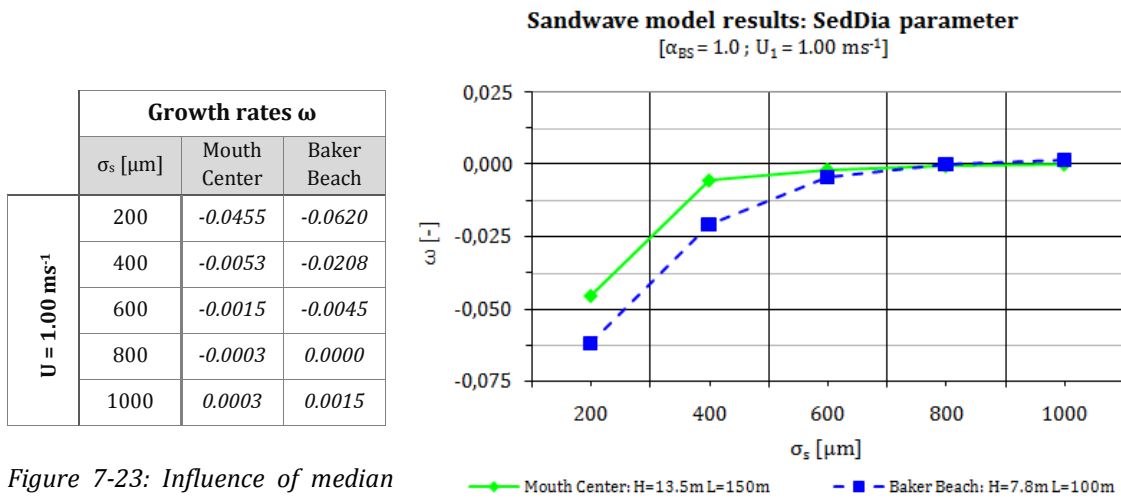


Figure 7-23: Influence of median grain-size on sandwave growth rate.

Results show that the median grain-size influences growth rates significantly. For grain-sizes smaller than approximately 600 μm , both equilibrium configurations result in decay to attain a new (smaller) equilibrium sandwave height. When grain-sizes are larger than 600 μm , both configurations show a higher stability. This is can be explained by the fact that a coarse grain diameter can withstand higher tidal flow velocities under the same circumstances.

8. ANALYSIS AND DISCUSSION

In this chapter the differences between results of the various simulations are analyzed and discussed. The first section elaborates on the sandwave formation mechanism, relating hydrodynamic and bed level configurations to the stability of the modelled sandwaves. The question why sandwaves grow, decay or remain stable using this 2Dv-model will be the main query to be answered in this chapter. Section two compares the sandwave model equilibrium configurations to the actual sandwave dimensions observed in San Francisco Bay. Finally section three deals with the conditions under which the 2Dv-model is able to attain equilibrium and in what respect model parameters can be used for calibration.

8.1 Formation mechanisms

Depending on characteristics such as flow velocity and water depth, results in Chapter 7 demonstrate that the modelled sandwaves show different growth and decay rates for steeper slopes and for higher velocities. Theories on sandwave formation mechanisms discussed in section 3.2.1, contribute stability in sandwave development mainly to a term which hinders the formation of steep slopes and a growing term based on the residual bed shear stress. This section therefore focuses on the analysis of these two terms, exploring the influence of different flow velocities and bed level configurations to the process of sandwave formation using DELFT3D. Note for clarity; the six configurations of sections 7.2.1 and 7.2.2 are referred to when discussing the equilibrium, growing and decaying sandwaves of Baker Beach and Mouth Center.

8.1.1 Contribution of hydrodynamic configuration

On account of the hydrodynamic contribution to the formation process, three different parameters are distinguished; peak tidal currents, (critical) near-bed velocities and (critical) bed-shear stresses. These development contributing factors will be discussed in relation to the formation of sandwaves. The time series in Appendix Q are used for the analysis of the DELFT3D-model results, presenting near-bed flow velocities and bed shear stresses for the different stages of sandwave development.

(Peak) tidal current velocities

The 2Dv-model results listed in Table 7-2 display growth rates for all three tidal current velocities, illustrating that for higher current velocities it is more difficult to find the corresponding equilibrium wave height. For the peak tidal current velocity of 0.50 ms^{-1} all sandwave configurations reach to an equilibrium wave height that increases for larger wave lengths. This can be explained by the fact that for 0.50 ms^{-1} near-bed velocities hardly ever exceed the critical near-bed velocities²¹. Therefore very little sediment transport takes place, resulting in almost no change of initial bed level.

²¹ The overall maximum near-bed current velocity for $U = 0.50 \text{ ms}^{-1}$ equals 0.40 ms^{-1} ; measured on top of the center sandwave crest at 20 m water depth with a sandwave height of 13.7 m.

For the peak tidal current velocity of 1.00 ms^{-1} , the number of sandwave configurations that results in equilibrium is significantly less; 6 of the 10 configurations in Table 7-2 result in equilibrium, obtained only for the larger sandwave lengths. Near-bed velocities belonging to 1.00 ms^{-1} exceed critical near-bed velocities more frequently, resulting in a more diverse set of bed level developments. The highest peak tidal current velocity of 1.50 ms^{-1} results in only one stable sandwave configuration. This relatively high current velocity makes it very difficult for bed level forms to remain stable, due to the rough flow and sediment transport conditions.

Critical near-bed velocity exceedence

The flow velocity time series presented in section 7.2.3 and Appendices O and P, show that instantaneous near-bed velocities exceed the critical near-bed velocities in many cases. When relating the duration of this exceedence to the bed level response this could indicate whether an initial sandwave height will decay, grow or remain stable. Since the formation process involves the transport of sediment from the troughs toward the crests and vice versa, the most interesting monitoring points are *Slope1* and *Slope2*. Because ebb and flood period are equal in these simulations, it should make no difference whether the first or second slope station is analyzed. Below a short analysis of the near-bed velocities measured at *Slope1* is given, based on the results listed in Appendix Q.

- The near-bed ebb velocities on *Slope1* for the equilibrium sandwave configurations in Figures 7-16 and 7-19 are found to be larger than near-bed flood velocities. This explains why the residual near-bed velocities in Figures 7-9 and 7-12 are pointed upslope. The critical near-bed velocities are exceeded 50% of the time for both water depths, with peak near-bed velocities that are about 30 to 45 percent larger than the critical velocity of 0.34 ms^{-1} ;
- The results in Figures O-2 and P-2 for the growing sandwave configurations, show that for both depths critical near-bed velocities on *Slope1* are exceeded 45% of the time using the depth of 20 m and 60% of the time for the depth of 40 m. Similar to the equilibrium case near-bed velocities during ebb are found to be larger than during flood, explaining the direction of residual near-bed velocities in Figures 7-10 and 7-13 pointing upslope. The peak near-bed velocities are about 40 percent larger than the critical velocity of 0.34 ms^{-1} ;
- The near-bed velocity time series on *Slope1* for the decaying sandwaves in Figures O-5 and P-5 show an exceedence of critical near-bed velocities for 65% and 70% of the time, respectively for 20 and 40 m water depth. Again the near-bed ebb velocities are larger than the near-bed flood velocities, explaining the residual current direction in Figures 7-11 and 7-14 pointed towards the crest. The peak near-bed velocities are about 50 percent larger than the critical velocity of 0.34 ms^{-1} .

The three different development scenarios show that the duration of critical near-bed velocity exceedence and maximum near-bed velocities are largest for the decaying sandwave heights. According to the results presented in Appendix Q, the near-bed velocity of the peak tidal current velocity of 1.00 ms^{-1} exceeds the critical near-bed velocities at the crest in all three scenarios (i.e. equilibrium, decay and growth). This means that during most of the time sediments are carried away from the crest region and the increase of sandwave height with respect to the initial height will be relatively small. Results point out that for the decaying sandwaves near-bed velocities at the *Slope* are largest in magnitude and have the longest exceeding time. Residual near-bed velocities at the *Slope* on the other hand, are found to be the smallest for the decaying sandwaves.

For both water depths it appears that the longest exceedence of critical near-bed velocities occurs when sandwave height is decaying. This means that bed level is subjected to crest directed flow for a longer period of time, consequently allowing more transport of sediment towards the crest of the sandwave. If near-bed flow on top of the crest outweighs this formation mechanism by a current velocity that exceeds the near-bed flow for an equal or larger amount of time, than the growing mechanism will be balanced and equilibrium in sandwave development can be achieved. In all scenarios presented in Appendix Q, *Crest* flow velocities were found to have the largest exceeding near-bed velocities showing an almost doubled value of the critical velocity and an exceedence time of nearly 70%. All net transport of sediment towards the crest is then counterbalanced by relatively high velocities on top of the crest.

Critical bed-shear stress exceedence

The bed shear stress time series depicted in section 7.2.3 and Appendices O and P, demonstrate the important effect of exceeding critical near-bed shear stresses in relation to bed level response. Since critical bed shear stress is directly related to the critical near-bed velocity by the relation in Equation 6.10, the similar found exceedence of critical bed-shear stress is consistent to the near-bed velocity time series. Since bed-shear stress depends on the water depth, it will be larger during ebb flow with shallower water depth at the same depth-averaged velocity. When sandwaves grow and (residual) near-bed velocities are directed towards the crest it means that the bed-load transport is dominant; particles remain in the crest region of the sandwave and are transported towards the crest of the sandwave. Decay in sandwave height occurs when bed-shear stress becomes relatively large at the crest.

Figure 8-1 displays the instantaneous sediment transport rates and the bed shear stress for both equilibrium configurations. Both figures clearly show that the moments of maximum and minimum transport rates coincide with peak flood and peak ebb flow velocities. The amount of sediment transported using a velocity of 1.50 ms^{-1} is almost 250 times as large as it is when using a velocity of 0.50 ms^{-1} . Assuming that the Engelund-Hansen transport equation found in section 6.4.2 couples the instantaneous flow velocity and sediment transport directly with $s \sim u^5$, this upslope pointed net direction of flow indicates that there is indeed a net transport of sediment towards the crest of the sandwave for both depths.

The fifth order of relation between flow velocity and sediment transport is a good indicator for the sensitivity of bed level response, enlarging the transport rate of sediment for 1.50 ms^{-1} compared to 0.50 ms^{-1} by a factor 243 $\{(1.50/0.50)^5\}$. The difficulty to attain equilibrium using a peak tidal current velocity of 1.50 ms^{-1} instead of 1.00 ms^{-1} , is well illustrated in Table 7-2 where growth rates are about an order 10 larger for 1.50 ms^{-1} .

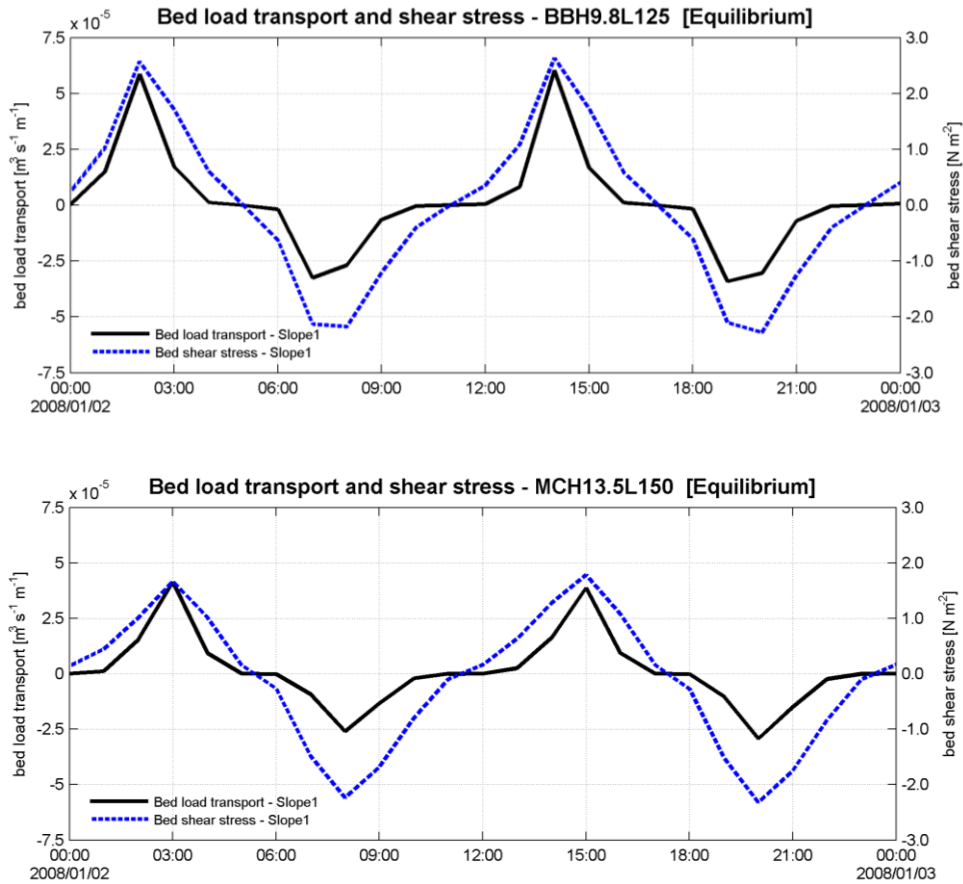


Figure 8-1: Instantaneous sediment transport rates and bed shear stress time series, for the equilibrium sandwave configurations at 20 m and 40 m water depth, respectively.

8.1.2 Contribution of bed level configuration

On account of the bed level contribution to the formation process, three different parameters are distinguished. These development contributing factors will be discussed in relation to the sandwave formation mechanisms.

Water depth

When comparing both decay and growth results for two different depths, it becomes clear that almost identical equilibrium wave heights arise for all lengths. This suggests there is no direct relation between the local water depth and the equilibrium sandwave height. The first indication for this is Figure 8-2 which displays trend lines, marked green and blue for Mouth Center and Baker Beach depth respectively, through all obtained equilibrium wave heights. These lines demonstrate that the equilibrium height is hardly influenced by depth, since the difference between both depth related heights only differs 2 m at most for the largest wave lengths. Another indication is the fact that for the largest lengths (i.e. 150 m and 175 m) height turns out to become significantly high in relation to the local water depth. Considering the maximum obtained height for both depths, it shows that wave heights grow up to a crest level that saturates the water depth for 34% in a depth of 20 m and up to 20% in a depth of 40 m. Despite that this coincides with the theory of McCave (1971) in section 3.1, this strongly supports the idea that water depth does not play a distinctive role in the formation of sandwaves.

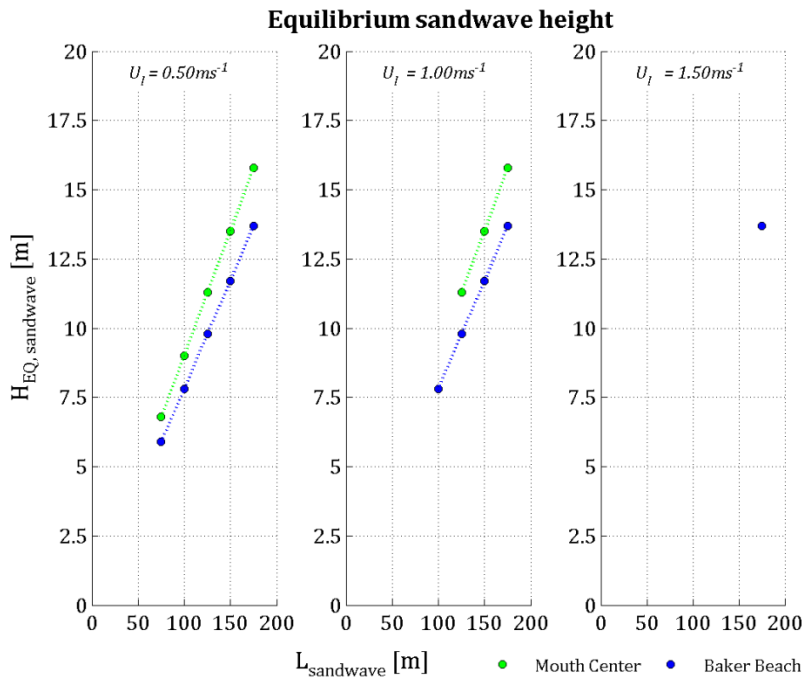


Figure 8-2: Equilibrium sandwave heights for different lengths using the median water depths of Baker Beach and Mouth Center for the flow velocities $U_1 = 0.50, 1.00$ and $1.50 ms^{-1}$. Blue markers correspond to equilibrium heights of Baker Beach median depth, green markers correspond to Mouth Center.

Sandwave length

The 2Dv-model results concerning sandwave lengths have shown that all lengths from 75 m to 175 m remain stable in length development. In other words, all studied sandwave lengths were found to have a rate of change in length that is much smaller than the rate of change in height. Results show that sandwave height changes during a tidal cycle, whereas sandwave length remains stable. This is observed for almost all of the performed simulations. An explanation for this is that the amount of sediment that needs to be transported to change sandwave height is much smaller than the amount needed to change the sandwave length. Figure 8-2 demonstrates that for larger lengths the equilibrium wave height becomes higher, indicating there is a relation between sandwave length and height. This relation is best visible in the trend lines through all equilibrium heights. Both trend lines appear to be following a linear relationship, increasing height for increasing lengths. This relation shows great resemblance for both water depths as trend lines run almost parallel. The smallest sandwave lengths show a more sensitive bed level response than that of the larger lengths, illustrated by the excessive growth rates for smaller lengths in Table 7-2. Since the study only involves sandwave lengths larger than 75 m, a point of discussion is the inability of the 2Dv-model of creating equilibrium in height for the relatively small wave lengths. As explained in Chapter 6 this is most likely the result of the grid size limitation for the smaller lengths. Correctly representing the entire range of sandwave lengths found in San Francisco Bay would result in a very small time step (i.e. long computation times) for the smaller grid sized lengths because of the Courant number limitation. This was not desired for due to the limit amount of time, which is why only sandwave lengths larger than 75 m were considered.

Bed-slope angle

The contribution of a term which limits the bed-slope angle to a certain value is clearly demonstrated in the results obtained in section 7.1.3. Almost all of the sandwave configurations listed in Table 7-2 show the tendency to attain the same length over height ratio, suggesting that there might be an equilibrium bed-slope angle given specific conditions. Slope angles vary from 9 to 10 degrees²² for Mouth Center and Baker Beach depths respectively, based on the length over height ratios listed in Table 7-1. The so called equilibrium bed-slope angles are observed for the 100 m to 175 m wave length range at 20 m depth and for the 150 m and 175 m wave lengths at a depth of 40 m. When applying the equilibrium slope angle to the smallest wave length of 75 m, results in both cases in decay of height. The fact that the inability of reaching bed-slope equilibrium with the smallest wave length does not harmonize with other equilibrium results and because of the consistently unstable behavior in most of the run schemes, emphasizes that more runs are necessary to reveal the reason why this DELFT3D model is unable to attain equilibrium for relatively small sandwave lengths.

²² The equilibrium bed-slope angle is approximated by taking $\tan^{-1} \{H/(\frac{1}{2}L)\}$

8.1.3 Development conditions

To assess the conditions of sandwave development using the 2Dv-model, a comparison is made between the conditions under which the three different outcomes; equilibrium, growth and decay, are obtained. As presented in Tables 8-1 to 8-3 below, all outcomes are bounded by certain restrictions concerning the variables length L , height H , tidal current velocity U and water depth d . The critical velocities are determined using the formulae presented in section 6.4.2. The exceedence period Δ can be described as the duration of time when the calculated near-bed velocity is larger than the critical near-bed velocity, illustrating the amount of time that the bed level is liable to shear velocities and consequently bed-shear stresses which result in the transport of sediment. The period of exceedence is measured by adding up the intervals between the critical value crossings. The three possible outcomes of the 2Dv-model are compared with the theory presented in section 3.2. The focus will be on the development in wave height because this factor appears to be responding more forcefully than wave length. Regarding the velocities only the results for 1.00 ms^{-1} serve as reference.

Theoretically equilibrium in sandwave height will occur when the amount of net sediment transport towards the crest is sufficient, while instantaneous near-bed velocities on top of the crest prevent the formation of (infinitely) large wave heights. Growth in height will occur when the net transport of sediment towards the crest is larger than the erosion due to near-bed crest velocities. Decay in height would take place when the net transport of sediment towards the crest is not large enough to withstand the strong crest velocities, resulting in erosion of the crest and subsequently decay of sandwave height. The DELFT3D results in Appendix Q are compared to these theoretical scenarios to help understand the formation processes.

Equilibrium

| Depth [m] | $U_{\text{peak, max}}$ [ms^{-1}] | Length [m] | Length / Height [-] | $\frac{U_{\text{bed, mx, slope}}}{U_{\text{bed, cr, slope}}}$ [-] | Exceedence period Δ [%] |
|-----------|---|------------|---------------------|---|--------------------------------|
| 20 | 0.50 | > 75 | 12.0 | 0 | 0 |
| | 1.00 | ≥ 100 | 12.7 | ± 1.50 | ± 50 |
| | 1.50 | ≥ 150 | 12.0 | ± 2.50 | ± 75 |
| 40 | 0.50 | > 75 | 10.3 | 0 | 0 |
| | 1.00 | ≥ 125 | 11.1 | ± 1.50 | ± 50 |
| | 1.50 | ≥ 175 | 10.2 | ± 2.50 | ± 75 |

Table 8-1: DELFT3D 2Dv-model restrictions upon achieving equilibrium in sandwave height and length development.

The first scenario of equilibrium shows run results where sandwaves remain stable in their development. No notable change in sandwave length or height is observed after a runtime of one hydrodynamic day, with most of the equilibrium configurations found for the smallest tidal current velocity of 0.50 ms^{-1} . Apparently when initial sandwave profiles are forced with near-bed velocities and bed-shear stresses that do not exceed the critical

values, the initial bed configuration remains stable. Results for 1.00 and 1.50 ms⁻¹ also show equilibrium results, however a trend is visible for both depth that higher velocities require larger wave lengths (and thus heights) to remain stable. As the near-bed slope velocities become larger using higher depth averaged velocities, the critical values are exceeded for a longer duration and with higher magnitudes. Comparing both water depths, it appears that when depth is doubled sandwaves tend to grow steeper (smaller length over height ratio), while the ratio between maximum and critical near-bed velocities remains the same. Studying the residual current velocities for both depths in section 7.2.1 and 7.2.2 it shows that for 20 m depth growing and decaying sandwave configurations there is a small net flow towards the eastern boundary, while for the 40 m depth there is a small net flow towards the western boundary. Water depth appears to affect the direction of a small net current present for the non-equilibrium configurations.

An important point is that all equilibrium configurations tend to grow to wave heights that are relatively large compared to flow depth. The highest achieved height for 20 m equals 13.7 m, while for 40 m this equals 15.8 m. Apart from the fact that larger depths seem to relate with larger heights, this suggests that water depth is not limiting the formation of equilibrium heights since larger lengths keep growing to larger heights until water depth is completely satisfied. Furthermore, given that the amount of equilibrium configurations found for 1.00 ms⁻¹ and 1.50 ms⁻¹ are less than the number found using 0.50 ms⁻¹, does not mean that these velocities do not have the potential in developing equilibrium configurations. It only shows that more runs are necessary to find the equilibrium. Therefore the conclusion that larger velocities do not allow sandwaves to develop cannot be proven until more runs are performed for a larger scale of possible configurations.

Growth

| Depth [m] | U _{peak, max} [ms ⁻¹] | Length [m] | Length / Height [-] | U _{bed, mx, slope} / U _{bed, cr, slope} [-] | Exceedence period Δ [%] |
|-----------|--|------------|---------------------|---|-------------------------|
| 20 | 0.50 | ≥ 75 m | ≤ 12.0 | 0 | 0 |
| | 1.00 | ≥ 100 m | ≤ 12.7 | ± 1.50 | 45 |
| | 1.50 | ≥ 175 m | ≤ 12.0 | ± 2.50 | 75 |
| 40 | 0.50 | ≥ 75 m | ≤ 10.3 | 0 | 0 |
| | 1.00 | ≥ 150 m | ≤ 11.1 | ± 1.50 | 60 |
| | 1.50 | ≥ 200 m | ≤ 10.2 | ± 2.50 | 75 |

Table 8-2: DELFT3D 2Dv-model restrictions upon achieving growth in sandwave height and length development.

The second scenario involves sandwaves starting to grow indefinitely or start growing within acceptable limits. Only the second case is considered, where positive growth rates are about two orders larger than the equilibrium restriction. Initial wave heights are apparently not to high enough to fulfill the balance between bed slope angle and the point of critical flow. Two of the growing sandwaves are presented in Figures N-1 and N-2 of Appendix N. Large disproportional shapes are shown for the run at 20 m depth, while the

40 m depth run shows growing sandwaves that are more within acceptable limits. Results in Appendix Q show that for growing profiles maximum near-bed current velocities are smallest of all three scenarios on top of the crests and at the slopes. However in the troughs of the waves, maximum near-bed velocities are largest of all. This is striking considering that the wave heights used in the growing scenarios are half the height of equilibrium in 20 m depth (5.0 m instead of 9.8 m) and a third of the equilibrium height in 40 m depth (5.0 m instead of 13.5 m). Smaller wave heights mean larger flow depths, hence smaller near-bed velocities due to smaller depth averaged velocities. Especially since these large velocities are observed in the troughs, this shows there is large activity in the troughs of the sandwaves with high bed-shear stresses that exceed the critical values with 20% for 20 m depth and 80% for 40 m depth. And with crest velocities being the smallest for growing sandwaves, the hindering crest velocities term in the formation process is not large enough to compensate for the instantaneous upslope velocities, all the way from the trough of the sandwave where near-bed activity is highest.

Decay

| Depth [m] | $U_{\text{peak, max}}$ [ms^{-1}] | Length [m] | Length / Height [-] | $U_{\text{bed, mx, slope}} / U_{\text{bed, cr, slope}}$ [-] | Exceedence period Δ [%] |
|-----------|---|--------------|---------------------|---|--------------------------------|
| 20 | 0.50 | ≤ 75 m | ≥ 12.0 | 0 | 0 |
| | 1.00 | ≤ 100 m | ≥ 12.7 | ± 1.50 | ± 65 |
| | 1.50 | ≤ 175 m | ≥ 12.0 | ± 2.40 | ± 80 |
| 40 | 0.50 | ≤ 75 m | ≥ 10.3 | 0 | 0 |
| | 1.00 | ≤ 150 m | ≥ 11.1 | ± 1.50 | ± 70 |
| | 1.50 | ≤ 200 m | ≥ 10.2 | ± 2.40 | ± 80 |

Table 8-3: DELFT3D 2Dv-model restrictions upon achieving decay in sandwave height and length development.

The third scenario involves sandwaves that decay either to a flat bed, showing erroneous irregularities, or decay within acceptable limits. Only the second case is considered, where negative growth rates are about two orders larger than the equilibrium restriction. When sandwave profiles decay normally, it means that either flow conditions are too extreme for given sandwave characteristics (e.g. grain-size) or the initial profile is too steep/gentle, resulting in a large surplus of sandwave height that has to change rapidly within moments after the start of simulation. The decay in wave height goes much faster than decay in length profile due to the significantly smaller volume of sediment to be transported for a change in height. The effect of this is that the 2Dv-model morphodynamics are focused on change in height, with more or less fixed nodes of length. If the initially chosen wave height is too large the model shows decay in height, or negative growth rates, until the height fulfills the equilibrium condition. Decaying sandwaves have therefore exceeded the balance between critical near-bed velocities and the compensation of gravity as the result of the length over height steepness ratio.

Results in Appendix Q show that for decaying sandwave profiles maximum near-bed current velocities are largest of all three scenarios on the slopes. Since high crest velocities are expected with decaying sandwaves this must be seen in the results as well. Compared to the maximum near-bed crest velocities for growing sandwaves they are indeed higher. However more importantly, the bed level exposure to critical value exceeding velocities is largest of all three scenarios on the slopes. Knowing that a decay of sandwave height is coupled with a net transport of sediment downhill of the slopes (i.e. sediment is transported away from the crest) this should be seen in the results as well. This however does not appear to be the case. The residual flow patterns for the decaying sandwaves presented in sections 7.2.1 and 7.2.2 (see Figures 8-3a and 8-3b), illustrate a residual current that is directed towards the crest of the sandwave however with a clear asymmetry in flow pattern observed on both sides of the crest. Asymmetry can cause the decay in wave height. To explain this, a reference must be made to the theoretically proven presence of (symmetrical) vertical residual circulation cells in section 3.2.1. If there is a disturbance in the flow pattern making it asymmetric, this results in a larger transport of sediment on one side of the slope than on the other side. This causes the initially symmetrical sandwave profile to distort, as seen in Figures N-3 and N-4 of Appendix N. When bed levels become distorted the flow pattern will follow accordingly, thus inducing a chain reaction that results in an ever decaying mechanism.

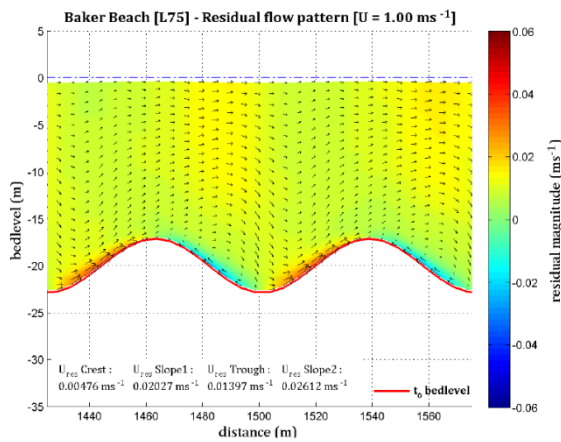


Figure 8-3a: Residual flow pattern of Baker Beach decaying sandwave configuration. Showing a net current directed towards the eastern boundary. Note the scale on y-axis.

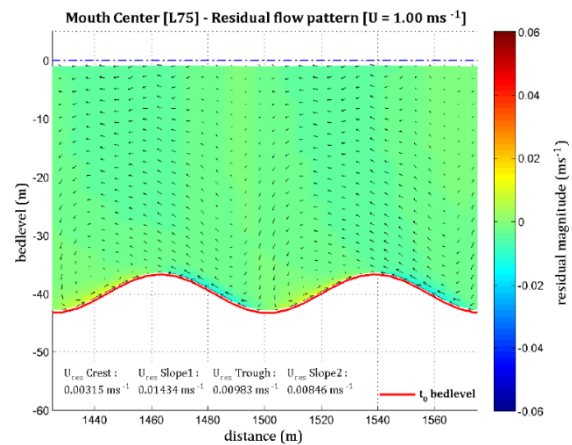


Figure 8-3b: Residual flow pattern of Mouth Center decaying sandwave configuration. Showing a net current directed towards the western boundary. Note the scale on y-axis.

8.2 2Dv-model results vs field data results

8.2.1 Comparing data

In this section the capability of DELFT3D to model the San Francisco sandwaves using the 2Dv-model is discussed. A comparison is made between the 2Dv-model results and the collected field data. Field data includes two distinguishable areas, described in section 4.2.1 as Baker Beach in the south of the inlet mouth and Mouth Center in the center of the inlet mouth. Both areas were chosen because of their wide collection of sandwaves that differ in dimension and because of the diversity in tidal flow velocities and difference in depth and median grain-size. The performed model runs have resulted in a large set of useful data, with simulations carried out for several different circumstances. However, only a select amount of results is needed to evaluate the capability of DELFT3D in modelling sandwaves. Table 8-4 presents the final results of field and 2Dv-model data, showing bed level and hydrodynamic features for both project areas. The following points will be discussed for both project areas; water depth, sandwave height and length, median grain-size, peak tidal velocities and finally the shape of the sandwave.

| Features | FIELD DATA | | 2DV-MODEL DATA | |
|-----------------------------|-----------------------|-----------------------|-----------------------|-----------------------|
| | <i>Baker Beach</i> | <i>Mouth Center</i> | <i>Baker Beach</i> | <i>Mouth Center</i> |
| Median water depth | 20.3 m | 40.8 m | 20 m | 40 m |
| Sandwave height | 1.2 m | 2.9 m | 5.9 – 13.7 m | 6.8 – 15.8 m |
| Sandwave length | 30.0 m | 57.7 m | 75 – 175 m | 75 – 175 m |
| Median grain size | 232 μm | 768 μm | 500 μm | 500 μm |
| Peak ebb current velocity | 1.31 ms^{-1} | 1.82 ms^{-1} | 1.83 ms^{-1} | 1.70 ms^{-1} |
| Peak flood current velocity | 1.38 ms^{-1} | 1.46 ms^{-1} | 1.87 ms^{-1} | 1.74 ms^{-1} |

Table 8-4: Field data results versus DELFT3D model results. Median values of sandwave field data are compared with the range of values found using the 2Dv-model. Peak current velocities calculated with the 2Dv-model are the largest velocities of all performed runs, using the velocity magnitude of 1.50 ms^{-1} . These peak velocities are found on top of the (largest) center sandwave.

8.2.2 Baker Beach comparison

Water depth

According to field data the area of Baker Beach has a median depth of 20.3 m; the 2Dv-model was therefore set on a water depth of 20 m. This way the project area depth is correctly simulated in this way displaying a 2 km long field of varying sandwave heights in the bed of the 3 km long domain (see Figure 6-2). 2Dv-model results for the Baker Beach depth show that water depth does not appear to affect the development of sandwave height or length. Figure 8-2 clearly shows the increase of height for increasing lengths, apparently uninfluenced by the local water depth. Therefore, since no relation between sandwave height and depth was found in the field data analysis ($R^2 = 0.20$) and no relation between sandwave length and depth at all ($R^2 = 0.01$), the depth of 20 m is stated not to affect the development of sandwaves.

Sandwave height

The range of sandwave heights present in Baker Beach varies mildly. The histogram in Figure 5-2 shows that the largest heights found in the area are little over 3 m high. With a median wave height of approximately 1 m this illustrates a rather small set of wave heights. The 2Dv-model wave heights found are relatively large varying from 6 m to almost 14 m high. However, the linear trend line between height and length for the 20 m depth in Figure 8-4 suggests that sandwave heights can indeed match the (smaller) wave lengths found in Baker Beach if extrapolated to the smallest lengths (i.e. order of 10 m). Since this has not worked out so far, more research has to be done in for instance the use of smaller grid-sizes for the benefit of stable smaller wave length development. In short, there is no sound match between the 2Dv-model heights and the field data points of Baker Beach.

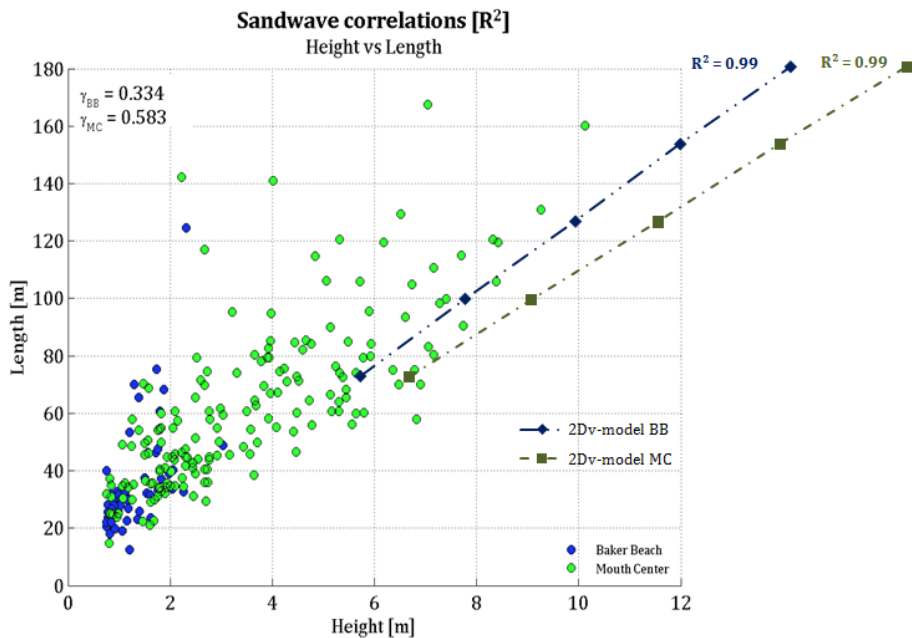


Figure 8-4: 2Dv-model data overlay on top of the collection of field data points. Baker Beach markers are colored blue, Mouth Center markers are green. The 2Dv-model data points drawn are the equilibrium heights applying $U = 1.00 \text{ ms}^{-1}$, with a linear trend line showing an R^2 value of 0.99 for both project areas.

Sandwave length

Sandwave lengths found in Baker Beach vary greatly. The range of lengths has a median value of 30 m, while the maximum found length equals almost 125 m. This broad set of wave lengths has partly been applied in the 2Dv-model setup, using a minimum length of 75 m. Unable to compare the smallest (median) sandwave length only the trend line can suggest that in theory the 2Dv-model should be able to produce matching length and height configurations.

Median grain-size

Results in section 7.3.3 illustrate the relevance of median grain-size in the development of sandwaves in the 2Dv-model. The median grain-size found in the area of Baker Beach has a value of 232 μm . Except for the sensitivity analysis runs, all simulations were carried out using a compromising median grain-size of 500 μm . When using 232 μm instead of 500 μm , configurations are expected to show lower stability since finer grain-sizes are less able to withstand similar flow velocities.

Peak tidal current velocity

The peak tidal current velocity present in the vicinity of Baker Beach measures 1.38 ms^{-1} , the 2Dv-model was set on a maximum forcing current velocity of 1.50 ms^{-1} . The graphs in Figure 8-2 show less equilibrium configurations using the highest current velocity of 1.50 ms^{-1} . It also illustrates that only the largest set of sandwaves can withstand higher forced flow velocities and that the smallest set of sandwaves are more suited for lower flow velocities. The last part is in agreement with the velocities found near Baker Beach. Figure 2-5 and 2-6 show that during minimum and maximum Golden Gate flow discharges, ebb and flood velocities are relatively low just offshore of Baker Beach. The fact that DELFT3D is able to simulate relatively small sandwave configurations using 0.50 ms^{-1} is therefore promising.

8.2.3 Mouth Center comparison

Water depth

According to field data the area of Mouth Center has a median depth of 40.8 m; the 2Dv-model was therefore set on a water depth of 40 m. This way the project area depth is correctly simulated in this way displaying a 2 km long field of varying sandwave heights in the bed of the 3 km long domain. 2Dv-model results for the Mouth Center depth show that water depth does not appear to affect the development of sandwave height or length. Figure 8-2 clearly shows the increase of height for increasing lengths, apparently uninfluenced by the local water depth. Therefore, since no relation between sandwave height and depth was found in the field data analysis ($R^2 = 0.05$) and no relation between sandwave length and depth at all ($R^2 = 0.05$), the depth of 40 m is stated not to affect the development of sandwaves.

Sandwave height

The range of sandwave heights present in Mouth Center varies greatly. The histogram in Figure 5-2 shows that the largest heights found in the area are over 10 m high. With a median wave height of almost 3 m this illustrates a rather large and diverse set of wave heights. The 2Dv-model computed wave heights are relatively large varying from 7 m to almost 16 m high. Considering that field and 2Dv-model data in Figure 8-4 appear to correlate well mutually, the outcome of the 2Dv-model for the 40 m depth sandwaves is promising. For the lengths of 75 m and 100 m equilibrium heights of 6.8 m and 9.0 m were found. These configurations are also found in Mouth Center according to Figure 8-4, proving that the 2Dv-model is able to generate the San Francisco sandwave dimensions.

Sandwave length

Sandwave lengths found in Mouth Center vary greatly. The range of lengths has a median value of 58 m, while the maximum found length equals almost 168 m. This broad set of wave lengths is well fitted to the 2Dv-model setup, using a minimum length of 75 m and a maximum of 175 m. When comparing the range of 2Dv-model lengths with the median and maximum field data wave lengths, the 2Dv-model shows great resemblance. The 2Dv-model is therefore well able to produce the great length scales found in the area of Mouth Center.

Median grain-size

Results in section 7.3.3 illustrate the relevance of median grain-size in the development of sandwaves in the 2Dv-model. The median grain-size found in the area of Mouth Center has a value of 768 μm . Except for the sensitivity analysis runs, all simulations were carried out using a compromising median grain-size of 500 μm . When using 768 μm instead of 500 μm , configurations are expected to show more stability since coarser grain-sizes are more able to withstand similar flow velocities. Given that the largest set of flow velocities is found in the region of Mouth Center, matches well with the relatively large median grain-size.

Peak tidal current velocity

The peak tidal current velocity present in the vicinity of Mouth Center equals 1.82 ms^{-1} , the 2Dv-model was set on a maximum forcing current velocity of 1.50 ms^{-1} . The graphs in Figure 8-2 show less equilibrium configurations using the highest current velocity of 1.50 ms^{-1} . As a matter of fact, no configuration was found in 40 m depth to remain stable forcing 1.50 ms^{-1} flow velocities. The same figure also illustrates that only the largest set of sandwaves can withstand higher forced flow velocities and that the smallest set of sandwaves are more suited for lower flow velocities. The first part is in agreement with the velocities found near Mouth Center. Figure 2-5 and 2-6 show that during minimum and maximum Golden Gate flow discharges, ebb and flood velocities are highest in Mouth Center. The fact that DELFT3D is still able to simulate large sandwave configurations using 1.50 ms^{-1} is therefore promising; however more research is needed in sandwave formation using higher flow rates.

8.3 Sensitivity of model parameters

In this section the 2Dv-model parameters and settings are discussed. Calibration of these setting can help to benefit the accuracy of the model.

Bed-slope factor (ALFABS)

The sensitivity analysis carried out for the range of bed-slope-factors in section 7.3.2 revealed that the stability of sandwaves can be influenced significantly by this parameter. Apparently, a larger bed-slope correction factor results in smaller transport rates for upsloping flow and larger transport rates for downsloping flow. Vice versa is the case for a smaller bed-slope factor. Eventually this would result in longitudinal spreading of the sandwave shape. This can be interpreted as an overall trend in steepening sandwaves for lower longitudinal bed-slope factors (i.e. smaller than 1.0) and a trend of flattening the sandwaves for higher longitudinal bed-slope factors (i.e. larger than 1.0). This confirms the ability of the parameter to adjust transport rates by means of slope effects.

Thus far the outcome of the 2Dv-model results has proven the ability of simulating the San Francisco sandwave dimensions rather well, with the exception of stable small scale sandwaves (i.e. ≤ 75 m) and stable sandwave development for higher current velocities. Given that a bed-slope factor larger than 1.0 can reduce growth and enhance growth when smaller than 1.0, this could help making the smallest set of wave lengths develop more gradually towards an equilibrium. In other words, when preventing large transport rates for downsloping flow this could prove stability for length smaller than 75 m. More research on this is needed to prove this hypothesis.

Grain-size diameter

Results in the sensitivity analysis for several grain-size diameters, show that sediment transport rates decrease for increasing grain-sizes and increase for decreasing grain-size. According to Tonnon *et al.* (2007) sandwaves tend to increase in height using grain-sizes larger than $300 \mu\text{m}$, assuming the dominant transport load is bed-load. If an increase in grain-size does indeed affect the height of the sandwave, than heights can be reduced when applying smaller grain-size diameters. This might explain the relation between the grain-size diameter and sandwaves dimensions found in the tidal inlet mouth, showing a significant correlation with sandwave height given the R^2 value of 0.62. The 2Dv-model runs with different grain-sizes demonstrate the influence of grain-size on the growth rate of sandwave height, resulting in growth for coarser grain-sizes and decay for finer bed material. Using $\sigma_s \geq 600 \mu\text{m}$, results in highly stable sandwave configurations. However, more research on this is needed to prove this.

In addition on the effect of sandwave growth, Tonnon *et al.* (2007) states that sandwaves grow when bed-load transport is dominant (weak tidal currents and relatively coarse sediment); and decay for dominant suspended transport (strong currents and relatively fine sediment). Given that the default sediment diameter in the 2Dv-model runs was set on $500 \mu\text{m}$, which is relatively coarse material, the expectation is that all sandwaves will grow when lengths are sufficiently large (i.e. when $L \gg 75$ m).

9. CONCLUSIONS AND RECOMMENDATIONS

In this chapter final conclusions are drawn and recommendations made. The first part contains the conclusions and recommendations regarding the 2Dv sandwave model. The second part answers the research questions formulated in the first chapter.

9.1 DELFT3D sandwave model

In general, the model gives reasonable results for obtaining stable sandwave configurations under various circumstances. Although length scales smaller than 75 m or larger than 175 m have not been described using the 2Dv-model, the results give a valuable indicative idea of how sandwaves develop in the inlet mouth of San Francisco Bay. Some aspects of the model however, deserve specific attention.

9.1.1 The 2Dv-model

Boundary conditions

The setup of the 2Dv-model is based on generating a progressive tidal wave through a one-cell-wide profile model, by applying a small phase difference between both water level boundary conditions. This set of boundary conditions however appears to generate a (small) net residual current, resulting in a net migration of the sandwaves in the same direction.

Morphological factor

An important point of focus is the correct use of morphological factors (MORFAC) in the 2Dv-model. When studying the development of sandwaves and subsequently residual flow velocities, morphodynamic response (i.e. sediment transport) is directly related to this factor. If this is not modelled correctly, incorrect conclusions can be made. When applying a larger forced flow velocity in the model this is an important thing to bear in mind.

9.1.2 Representing San Francisco Bay sandwaves

Sandwave dimensions

A description of the full range of length scales found in the inlet mouth of San Francisco Bay is incomplete due to grid-size limitation of the 2Dv-model. This grid-size limitation is simply because of limited available run time. The Baker Beach and Mouth Center sandwave dimensions were found to vary greatly length, ranging from approximately 30 m in 20 m water depth to a maximum of 175 m in 40 m water depth. Since the model is limited to describe only the largest set of lengths accurately using the computational grid-size of 5 m, the smallest set of length scales could not be modelled correctly. If the goal of further research is to make sounds predictions, a new series of simulations should be performed with a smaller grid.

Tidal flow conditions

The access channel to San Francisco Bay is dominated by high velocity flows generated by jet currents that are formed by peak ebb and flood tides as they flow through the Golden Gate. These powerful and spatially variable currents result in an incredibly diverse array of sandwaves both inside and outside the Golden Gate. One of the challenges of the 2Dv-model was to correctly represent the flow velocities that range an average of 0.50 ms^{-1} near Baker Beach to peak velocities at over 2.00 ms^{-1} in the Mouth Center. The choice of boundary conditions resulted in a model that allowed sandwaves to form using flow velocities ranging from 0.50 to 1.50 ms^{-1} . Results showed that for the largest flow magnitudes the 2Dv-model shows difficulty in producing stable sandwave configurations. The complexity of and uncertainties regarding the correct representation of morphodynamic development, makes it difficult to ensure that the model output for a larger set of flow velocities is correct (i.e. larger than 1.50 ms^{-1}). To further improve the model, it is desirable to study the effect of higher flow velocities on morphodynamic change carefully.

Median grain-size diameters

Sediment at the mouth of San Francisco Bay is highly variable, ranging from very fine sand on the outer reaches of the ebb tidal delta, to coarse sand and gravel in the inlet throat, in the center of the sandwave field. The distribution of sediment grain-size is linked to tidal current strength, with the coarsest sediment associated with the strongest currents. For reasons of comparison, the mean of both median grain-size diameters served as the representative median grain-size for both project areas. This resulted in a value of $500 \text{ }\mu\text{m}$, which was set as the default grain-size in the 2Dv-model. The fact that between both project areas the median diameters differ by a factor 3, and that the sensitivity analysis results show that a difference in median grain-size influences sandwave growth significantly, implies that more studies are necessary to study the resemblance in sandwave development by using the actual grain-size to diameters.

9.1.3 Recommendations for further improvement

Before the 2Dv sandwave model is used to describe the San Francisco sandwaves more accurately than it does now, several improvements are suggested:

Analysis of boundary conditions

By changing the set of boundary conditions, exactly determining the velocity generated by the water level exertion or by applying a counteracting bed slope angle, the relatively small induced horizontal residual current can be reduced.

Study the effect of horizontal grid refinement

By refining the grid for accurate representation of relatively small sandwave lengths or by using different grids for different lengths, the development of smaller scale sandwaves can be studied properly.

Study the influence of applying larger sandwave lengths

Since no simulations were performed using lengths larger than 175 m, any conclusions regarding the influence of water depth to the development of sandwave height cannot be proven. Applying larger sandwave lengths should result in a flattening curve for the ever increasing sandwave height. If there is a limit, than water depth does play a significant role.

Study the effect of sediment transport formulations

Different types of sediment transport formulations should be investigated to distinguish for example bed-load and suspended load transport. The relatively straightforward Engelund-Hansen sediment transport equation only allows for the calculation of total sediment transport.

Study the effect of turbulence model

The turbulence model in the 2Dv-model was set on default, meaning that the k-epsilon model is used. In this second order turbulence closure model both the turbulent energy k and dissipation rate of turbulent kinetic energy ϵ are calculated by means of a transport equation. Turbulence affects the distribution of sediment over the water column and therefore the proportion of bed-load and suspended transport, ultimately resulting in growth or damping of the sandwave. Since the morphological development of the sandwave is affected by the choice of the turbulence model, the choice of turbulence model is important and should therefore be investigated to further improve the model.

Validation with measurements

With more extensive field data, e.g. near bed flow velocity measurements, the model can be validated with measurements and residual velocities. The same holds for grain-size collection on top of the crest, the slope and in the troughs of the sandwaves. This way the distribution of sediment grain-size in the development of sandwaves can be studied.

9.2 Research objective

The primary objective of this study is to study the capability of DELFT3D to model the San Francisco sandwaves using a 2Dv-model, with emphasis on assessing the formation mechanisms. To achieve the objective, the research questions posed in chapter 1 are answered:

9.2.1 Main questions

I. What are the main mechanisms that control the development of sandwaves?

A wide range of sandwave configurations investigated under various flow circumstances, reveal the necessity of equilibrium between the bed slope angle and the exceedence of critical near-bed current velocities and bed shear stresses. The relation between equilibrium sandwave height and water depth as observed in previous studies is not observed using the 2Dv-model, even when depths are doubled. In the case of Baker Beach and Mouth Center almost similar equilibrium heights arise, differing only 2 m for the largest wave lengths. This is most likely due to close to identical bed slope angles found for both depths with similar comparable near-bed current velocities and bed shear stresses. These similar values cause sandwaves to grow to an almost identical height. The difference in residual circulation patterns between both depths is then possibly the reason why heights do not grow to an exact same value. In 40 m depth equilibrium residual circulation cells show a far more symmetrical pattern than that in 20 m depth.

II. Which requirements are necessary for the 2Dv-model to reach a state of sandwave equilibrium?

When applying the largest set of sandwave configurations ranging from 75m to 175 m, equilibrium in wave height for all three tidal current velocities and both water depths is found. For this range of lengths results show that sandwave height development is hardly influenced by the local water depth. This is observed for an increase in velocity, however the highest flow magnitude only allows for one equilibrium configuration to develop. This implies that other bed slope configurations are required in order to obtain equilibrium, consequently enhancing or decreasing the final equilibrium wave height. Table 8-1 in section 8.1.3, shows the conditions for all variable parameters in order to develop an equilibrium sandwave profile.

9.2.2 Sub questions

III. *Under what conditions is DELFT3D capable of describing the hypothesized sandwave formation mechanisms?*

In order to describe the vertical residual circulation cells relatively low peak tidal velocities must be applied, ranging from 0.50 ms^{-1} to 1.00 ms^{-1} . Dimensions of sandwave length must be larger than 75 m, in other words the length scale cannot be smaller than fifteen times the computational grid-size using a cell width of 5 m. A similarity with the theory of McCave is (1971) that sandwave crests grow up to approximately one third of the water depth, is indeed the case for the set of sandwave lengths used in this study. This strongly hints that the 2Dv-model is presenting *real* physically sandwaves with sound hydrodynamic processes instead of deriving an artificial solution.

IV. *What is the influence of the residual current on the morphologic behavior of the sandwaves?*

The equilibrium sandwave configurations are obtained with use of a relatively small net residual current (displayed order of 10^{-3}), negating the necessity of obtaining realistic length scales by means of a significant net residual flow (i.e. order 10^{-1}). As for flow separation, this phenomenon has not been studied since the 2Dv-model is not able to generate this kind of flow characteristic when assuming the pressure distribution in the vertical to be hydrostatic.

REFERENCES

- Aliotta, S., and G.M.E. Perillo (1987), A sandwave field in the entrance to Bahía Blanca Estuary, Argentina, *Marine Geology* 76, 1-14
- Allen, J.R.L. (1968), Current Ripples: Their Relation to Patterns of Water and Sediment Motion, *Elsevier*, Amsterdam, 433 pp
- Ashley, G.M. (1990), Classification of large-subaqueous bedforms: A new look at an old problem, *Journal of Sedimentary Petrology* 60(1), 160-172
- Bagnold, R.A. (1956), The flow of cohesionless grains in fluids. Proc. Royal Soc. Philos. Trans., London, vol. 249, pp. 71-81
- Barnard, P.L. and Hanes, D.M. (2006), Coastal monitoring of the May 2005 dredge disposal offshore of Ocean Beach, San Francisco, California. *U.S. Geological Survey Open-File Report*, Report Series 2006-1140, pp. 27
- Barnard, P.L., J. Eshleman, L. Erikson, and D.M. Hanes (2006), Coastal Processes Study at Ocean Beach, San Francisco, CA: Summary of Data Collection 2004-2006, *U.S. Geological Survey Open-File Report*, Report Series 2007-1217
- Barnard, P.L., D.M. Hanes, R.G. Kvitek, and P.J. Iampietro (2006a), Sand Waves at the mouth of San Francisco Bay, California: U.S. Geological Survey Scientific Investigations Map, no. 2006-2944, 5 map sheets
- Barnard, P.L., D.M. Hanes, D.M. Rubin, R.G. Kvitek (2006c), Giant sand waves at the mouth of San Francisco Bay: *Eos*, Transactions of the American Geophysical Union, v. 87, no. 29, p. 285 - 289.
- The Bay Institute (1998), From Sierra to the sea—The ecological history of the San Francisco Bay-Delta watershed: San Rafael, California, *The Bay Institute of San Francisco*, 248p
- Belderson, R.H. (1986), Offshore tidal and non-tidal sand ridges and sheets: differences in morphology and hydrodynamic setting, In: Knight R.J., and J.R. McLean (eds), Shelf sands and sandstones, *Can. Soc. Petrol Geol. Mem. 11*, 293-301
- Bouma, A.H., et al. (1980), Identifications of bedforms in Lower Cook Inlet, Alaska, *Sedimentary Geology*, 26 (1980) 157-177
- Bijker, R., J. Wilkens, and S.J.M.H. Hulscher (1998), Sandwaves, where and why? *In Proceedings of the 8th international offshore and polar engineering conference 2*, Montreal, Canada, 153-158
- Bridge, J.S. (2003), Rivers and floodplains: forms, processes, and sedimentary record, ISBN 0-632-06489-7
- Buijsman, M.C. (2007), Ferry-observed variability of currents and bedforms in the Marsdiep inlet, *Doctoral thesis*, Utrecht University
- Chin, J.L., F.L. Wong and P.R. Carlson (2004), Shifting Shoals and Shattered Rocks - How Man Has Transformed the Floor of West-Central San Francisco Bay, U.S. Geological Survey
- Dalrymple, R.W. et al. (1978), Bedforms and their hydraulic stability relationships in a tidal environment, Bay of Fundy, Canada, *Nature*, 275: 100-104
- Engelund, F., and J. Fredsøe (1982), Sediment ripples and dunes, *Annual Review of Fluid Mechanics*, 14: 13-37

- Engelund, F., and Hansen, E. (1967), A monograph on sediment transport in alluvial streams, Teknisk Forlag, Copenhagen, Denmark
- Gilbert, G.K., (1917), Hydraulic mining debris in the Sierra Nevada: U.S. Geological Survey Professional Paper 105, 154 p
- Hoekstra, P., et al. (2004), Bedform migration and bedload transport on an intertidal shoal, *Continental Shelf Research* 24, 1249-1269
- Hulscher, S.J.M.H. (1996a,b), Tidal induced large-scale regular bedform patterns in a three-dimensional shallow water model, *Journal of Geophysical Research* 101(C9), 20 727-20 744
- Hulscher, S.J.M.H., and G.M. v. d. Brink (2001), Comparison between predicted and observed sandwaves and sand banks in the North Sea, *Journal of Geophysical Research* 106 (C5), 9327-9338
- Hulscher, S.J.M.H., and C.M. Dohmen-Janssen (2005), Introduction to special section on Marine Sandwave and River Dune Dynamics, *Journal of Geophysical Research* 110, F04S01, doi: 10.1029/2005JF000404
- Huthnance, J. (1982), On one mechanism forming linear sand banks, *Estuarine, Coastal and Shelf Science* 4, 79-99
- Knaapen, M.A.F. and Hulscher, S.J.M.H. (2002), Regeneration of sand waves after dredging, *Coast. Eng.* 46, 277-289
- Knaapen, M.A.F. (2005), Sandwave migration predictor based on shape information, *Journal of Geophysical Research* 110, F04S11
- Konigsmark, T. (1998), Geological trips, San Francisco and the Bay Area: Gualala, California, *GeoPress*, 174 p
- Kvitek, R.G. (2007), California State University Monterey Bay Sea Floor Mapping Lab. <http://seafloor.csumb.edu/SFMLwebDATA.htm>
- Langhorne, D.N. (1982), A study of the dynamics of a marine sandwave, *Sedimentology* 29, 571-594
- Lesser, G., J. van Kester, and J.A. Roelvink (2000), On-line sediment transport within DELFT3D-FLOW, Report Z2899, WL | Delft Hydraulics.
- Miller, R.L., and R.J. Byrne (1966), The angle of repose for a single grain on a fixed rough bed, *Sedimentology* 6, 303-314
- Németh A.A., et al. (2002), Modelling sandwave migration in shallow shelf seas, *Cont. Shelf Research* 22, 2795-2806
- Nichols, F.H., et al. (1986), The modification of an estuary: Science, *version* 231, 567-573
- National Oceanic and Atmospheric Administration (NOAA, 2006a), National Data Buoy Center: Silver Spring, Maryland
- Pawlocicz, R., B. Bearsley, and S. Lentz (2002), Classical tidal harmonic analysis including error estimates in MATLAB using T_TIDE, *Computers and Geosciences*, v. 28, p. 929-937
- Rubin, D.M. and D.S. McCulloch (1979), The Movement and Equilibrium of Bedforms in Central San Francisco Bay, *Pacific Division of the American Association for the Advancement of Science*, ISBN 0-934394-01-6
- Rubin, D.M., and D.S. McCulloch (1980), Single and superimposed bedforms; a synthesis of San Francisco Bay and flume observations, *Sedimentary Geology*, 26 (1980) 207-231
- Santoro et al. (2002), Sand Waves in the Messina Strait, Italy, *Journal of Coastal Research*, Special Issue 36

- SCRIPPS Institution of Oceanography (2007), The Coastal Data Information Program. San Diego, Integrative Oceanography Division, Scripps Institution of Oceanography
- Terwindt, J.H.J. (1971), Sandwaves in the southern bight of the North Sea, *Marine Geology* 10, 51-67
- Tonnon, P.K., et al. (2006), The morphodynamic modelling of tidal sandwaves on the shoreface, *Coastal Engineering* 54, 279–296
- Van der Meer, F.M. (2005), Research proposal: Modelling of spatial and temporal variations in offshore sand waves: process-oriented approach
- Van Rijn, L.C., (1993), Principles of sediment transport in rivers, estuaries and coastal seas. AQUA Publications, the Netherlands
- Van der Veen, H.H., S.J.M.H. Hulscher, and M.A.F. Knaapen (2006), Grain-size dependency in the occurrence of sandwaves, *Ocean Dynamics*, 56(3-4), 228–234
- Whitmeyer, S.J., and D. FitzGerald (2006), Sandwaves that impede navigation of inlet navigation channels, *ERDC/CHL CHETN IV-68*, Vicksburg, MS: U.S. Army Engineer Research and Development Center
- Winter, C. and Ernstsens, V. (2007) Spectral Analysis of bedforms, in: C. Dohmen-Janssen and S.J.H.M. Hulscher (Ed) River, Coastal and Estuarine Morphodynamics. 90-912
- WL|Delft Hydraulics (2006), DELFT3D-FLOW user manual; Simulation of multidimensional hydrodynamic flows and transport phenomena, including sediments, *User manual*, Deltares, The Netherlands

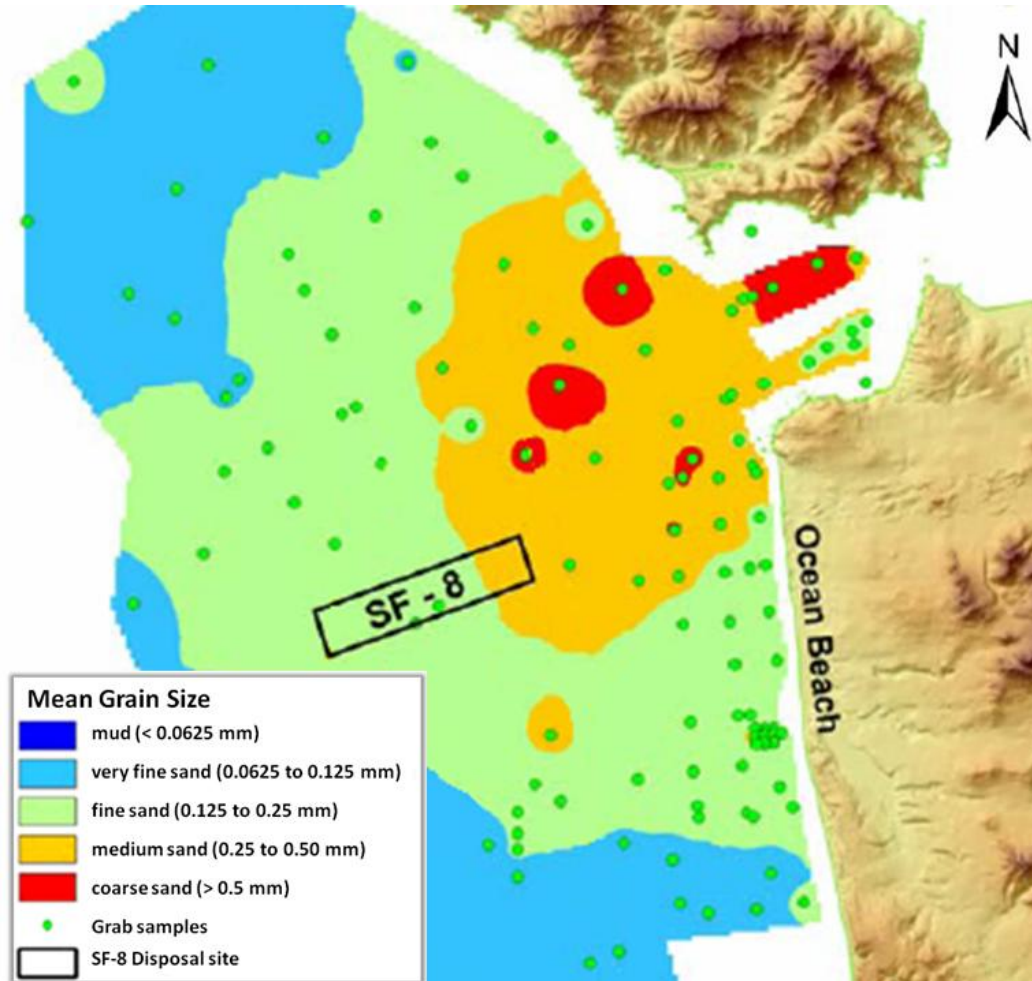
APPENDICES

A. SAN FRANCISCO BAY



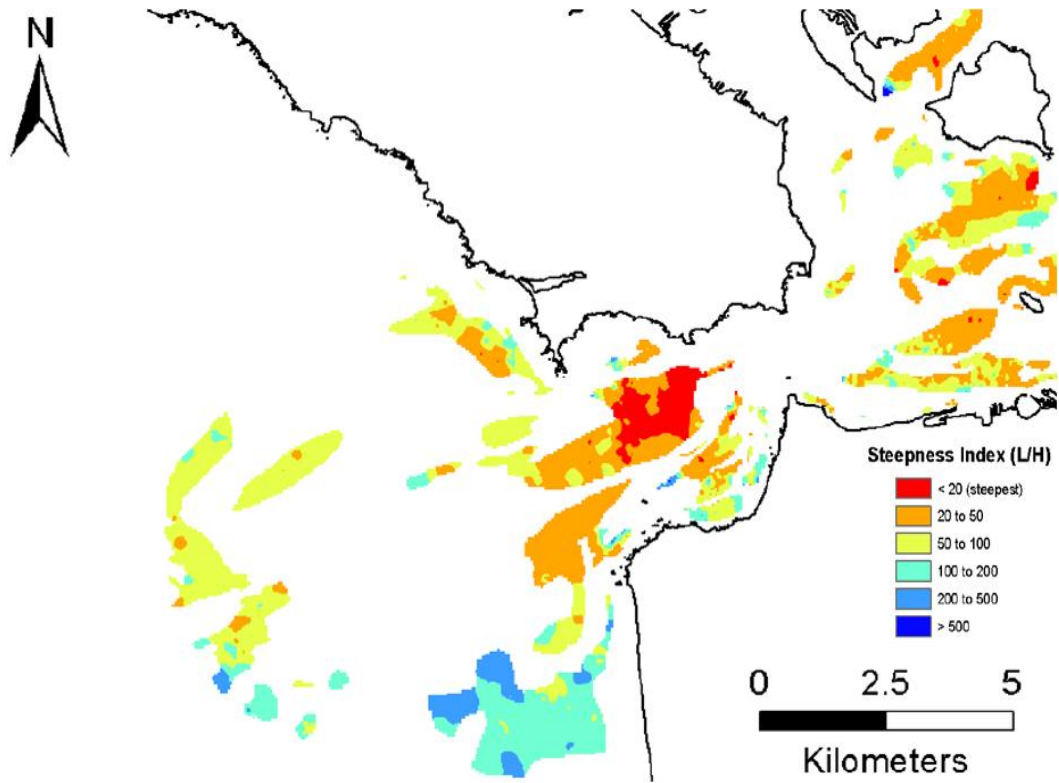
San Francisco Bay, consisting of three subembayments—north bay (San Pablo and Suisun Bays), central bay, and south bay—each characterized by a central area of open water surrounded by intertidal mudflats and marshes. This map shows the bay region as it was in the mid-1850's, before development (by Chin et al., 2004)

B. GRAIN SIZE CLASS



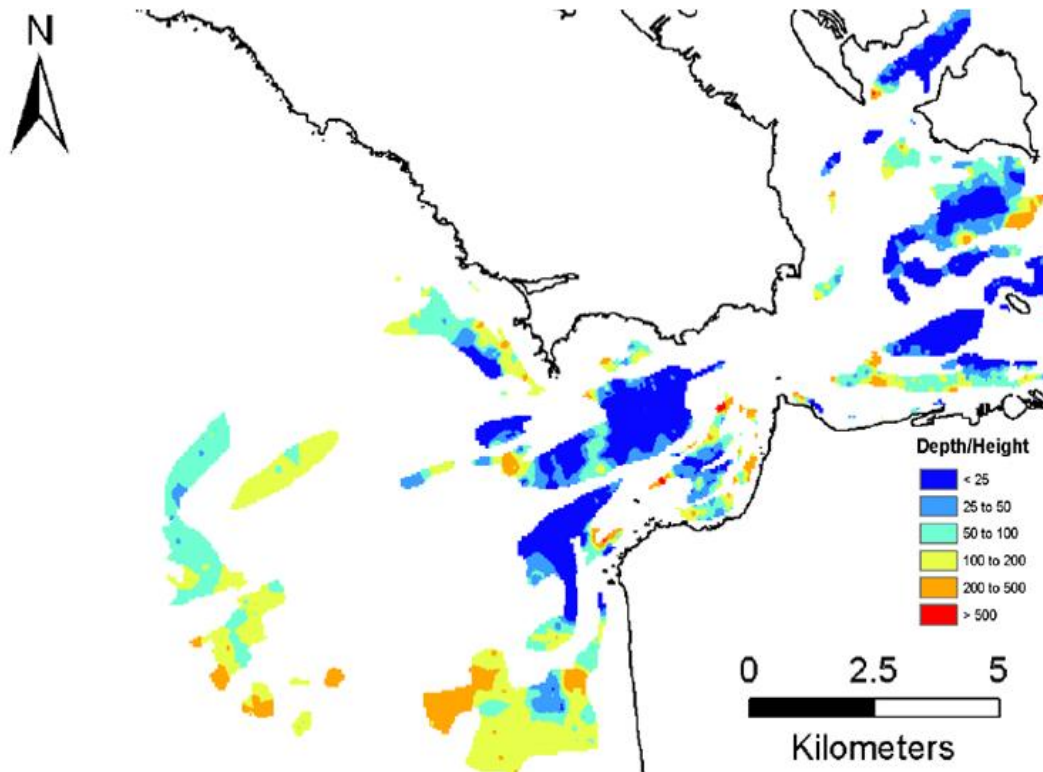
Grid of grain size class at the inlet mouth of San Francisco Bay, using the both Oceanside Biology Laboratory and USGS samples.

C. STEEPNESS INDEX



Distribution of steepness index in the inlet mouth of San Francisco Bay, gridded to 50 m (by Barnard et al., 2006, courtesy of USGS)

D. DEPTH OVER HEIGHT RATIO



Distribution of the depth over height ratios in the inlet mouth of San Francisco Bay, gridded to 50 m (by Barnard et al., 2006, courtesy of USGS)

E. LINEAR THREE-DIMENSIONAL STABILITY MODEL

The three-dimensional shallow water equations that describe the horizontal structure of tidal flow, illustrate the evolution of an incompressible fluid in response to gravitational and rotational accelerations. For calculations, the vertical accelerations are assumed to be small compared to the gravitational acceleration and are not taken into account.

$$\frac{\partial u}{\partial t} + u \frac{\partial u}{\partial x} + v \frac{\partial u}{\partial y} + w \frac{\partial u}{\partial z} - fv = -g \frac{\partial \zeta}{\partial x} + \frac{\partial}{\partial z} \left(A_v \frac{\partial u}{\partial z} \right) \quad [\text{E.1}]$$

$$\frac{\partial v}{\partial t} + u \frac{\partial v}{\partial x} + v \frac{\partial v}{\partial y} + w \frac{\partial v}{\partial z} - fu = -g \frac{\partial \zeta}{\partial y} + \frac{\partial}{\partial z} \left(A_v \frac{\partial v}{\partial z} \right) \quad [\text{E.2}]$$

$$\frac{\partial u}{\partial x} + \frac{\partial v}{\partial y} + \frac{\partial w}{\partial z} = 0 \quad [\text{E.3}]$$

In which u , v and w are the velocity components in x , y and z directions; and $z = \zeta$ is the free surface elevation. Furthermore, f and g are the Coriolis parameter and the acceleration of gravity, respectively. The vertical viscosity A_v indicates how fluid resists to changes in horizontal velocity in vertical direction, and is kept constant to study the horizontal momentum in vertical direction. The boundaries in vertical direction are as follows:

$$\frac{\partial u}{\partial z} = \frac{\partial v}{\partial z} = 0, \quad w = \frac{\partial \zeta}{\partial t} + u \frac{\partial \zeta}{\partial x} + v \frac{\partial \zeta}{\partial y} \quad [\text{E.4}]$$

With the partial slip condition:

$$A_v \frac{\partial u}{\partial z} = Su, \quad A_v \frac{\partial v}{\partial z} = Sv, \quad w = \frac{\partial h}{\partial t} + u \frac{\partial h}{\partial x} + v \frac{\partial h}{\partial y} \quad [\text{E.5}]$$

And the function of the bottom shear stress (τ):

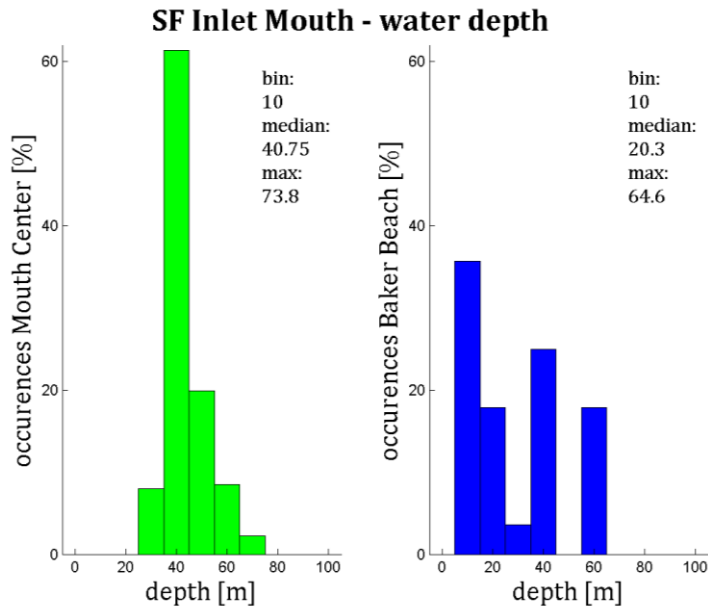
$$S_b = \alpha |\tau|^b \left\{ \frac{\tau}{|\tau|} - \lambda \nabla h \right\} \quad [\text{E.6}]$$

$$\tau = A_v \left(\frac{\partial u}{\partial z}, \frac{\partial v}{\partial z} \right) \Bigg|_{z=\text{bottom}} \quad [\text{E.7}]$$

In which S_b denotes the volumetric sediment transport vector and α represents the bed load proportionality parameter. The exponent b expresses the nonlinearity of transport in relation to the bed shear stress. The sediment transport vector contains a bed-slope correction term which is weighted by λ . Finally, the flow and sediment-transport models are coupled using the sediment balance:

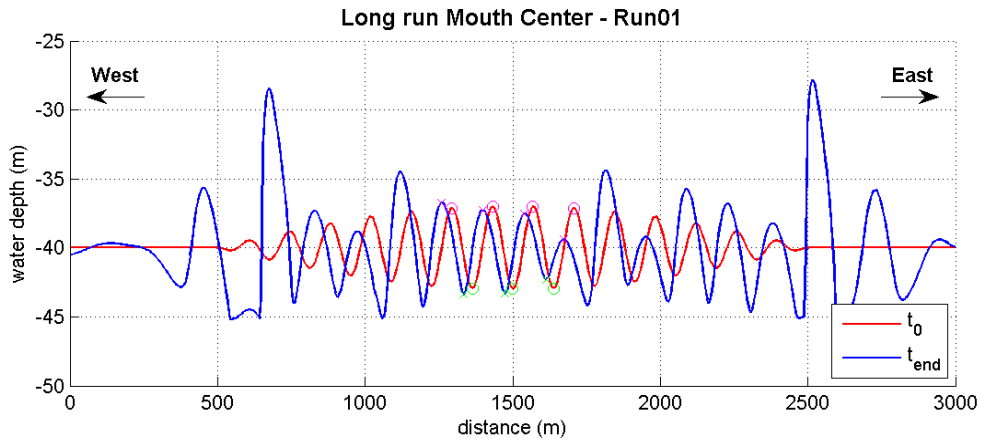
$$\frac{\partial h}{\partial t} + \nabla \cdot S_b = 0 \quad [\text{E.8}]$$

F. WATER DEPTH DISTRIBUTION PROJECT SITES



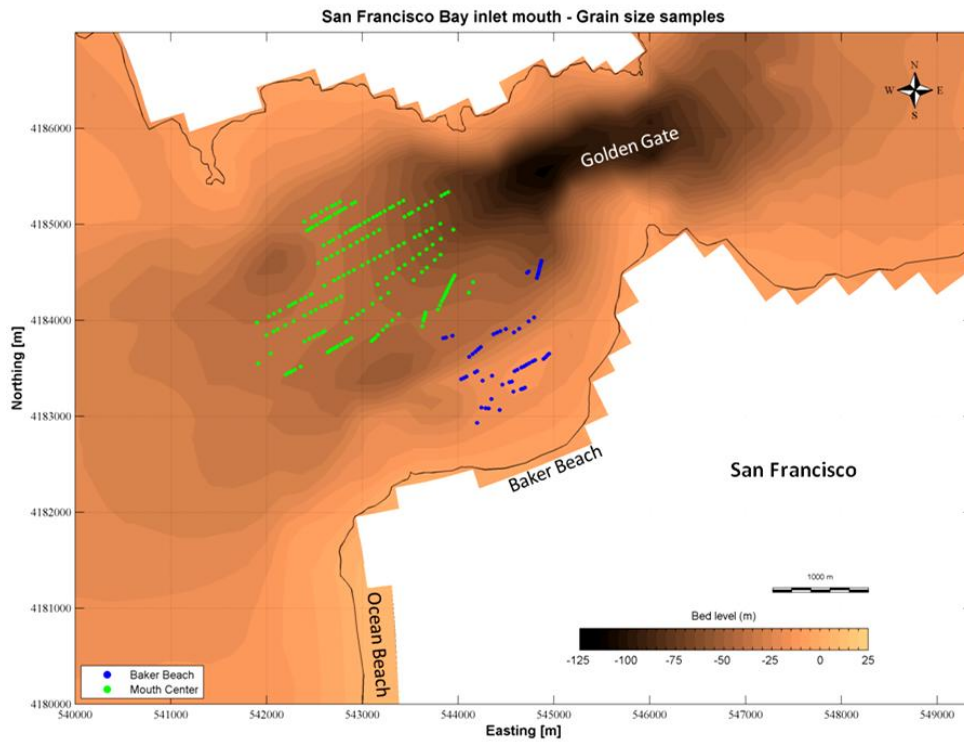
Histograms displaying the distribution of water depths on the project sites entitled as Mouth Center and Baker Beach. The median depth difference is used as the distinctive depth difference for all simulations.

G. LONG TERM BOUNDARY DISTURBANCES



Erroneous result due to boundary limits; affecting the development of sandwave heights and length (after a simulation time of 1250 morphological days)

H. SANDWAVE GRAIN-SIZE SAMPLE LOCATIONS



Sandwave grain-size sample locations in the inlet mouth, divided into two regions; Mouth Center and Baker Beach

I. PROJECT AREA FIELD AND 2DH-MODEL DATA

| Easting (m) | Northing (m) | Water depth (m) | Length (m) | Height (m) | Asymmetry (°) | 0.5σ (mm) | Rms dir (deg) | Gr distance (m) | Mix Spring (m/s) | Mix Neap (m/s) | Mix Flood (m/s) | Mix Ebbs (m/s) | Rms Mag (m/s) |
|-------------|--------------|-----------------|------------|------------|---------------|-----------|---------------|-----------------|------------------|----------------|-----------------|----------------|---------------|
| 542449.5 | 4184937.2 | 37.4 | 34.7 | 1.06 | 0.087 | 0.705 | 207 | 3581 | 1.66 | 0.61 | 1.21 | 1.67 | 0.0908 |
| 542449.5 | 4184954.7 | 37.3 | 36.6 | 1.52 | -0.138 | 0.705 | 207 | 3548 | 1.66 | 0.61 | 1.21 | 1.67 | 0.0908 |
| 542481.1 | 4184973.2 | 37.6 | 48.6 | 1.24 | 0.036 | 0.705 | 207 | 3513 | 1.66 | 0.61 | 1.21 | 1.67 | 0.0908 |
| 542523.1 | 4184997.7 | 36.4 | 54.9 | 2.92 | -0.057 | 0.759 | 206 | 3467 | 1.75 | 0.64 | 1.31 | 1.75 | 0.0788 |
| 542570.5 | 4185025.4 | 36.2 | 45.5 | 3.16 | -0.111 | 0.759 | 206 | 3414 | 1.75 | 0.64 | 1.31 | 1.75 | 0.0788 |
| 542609.7 | 4185048.4 | 36.8 | 34.7 | 2.00 | -0.200 | 0.805 | 206 | 3371 | 1.75 | 0.64 | 1.31 | 1.75 | 0.0788 |
| 542659.7 | 4185065.9 | 37.8 | 25.2 | 0.98 | 0.258 | 0.805 | 206 | 3328 | 1.75 | 0.64 | 1.31 | 1.75 | 0.0788 |
| 542691.6 | 4185078.6 | 36.9 | 60.6 | 2.76 | -0.223 | 0.805 | 206 | 3314 | 1.75 | 0.64 | 1.31 | 1.75 | 0.0788 |
| 542713.8 | 4185109.1 | 37.6 | 44.8 | 2.76 | -0.296 | 0.792 | 206 | 3257 | 1.75 | 0.64 | 1.31 | 1.75 | 0.0788 |
| 542752.5 | 4185121.7 | 38.9 | 39.8 | 2.02 | -0.458 | 0.792 | 201 | 3177 | 1.77 | 0.64 | 1.32 | 1.75 | 0.0742 |
| 542796.8 | 4185151.8 | 39.2 | 39.7 | 1.80 | -0.270 | 0.792 | 201 | 3177 | 1.77 | 0.64 | 1.32 | 1.75 | 0.0742 |
| 542821.1 | 4185171.8 | 38.9 | 79.5 | 3.90 | -0.620 | 0.800 | 201 | 3139 | 1.77 | 0.64 | 1.32 | 1.75 | 0.0742 |
| 542889.8 | 4185211.9 | 40.1 | 40.4 | 2.68 | -0.500 | NaN | 201 | 3065 | 1.77 | 0.64 | 1.32 | 1.75 | 0.0742 |
| 542924.6 | 4185232.3 | 42.1 | 40.4 | 1.80 | -0.500 | 0.770 | 227 | 3027 | 1.85 | 0.61 | 1.26 | 1.65 | 0.0959 |
| 542932.6 | 4185029.0 | 36.6 | 54.9 | 2.06 | -0.446 | NaN | 207 | 3088 | 1.86 | 0.61 | 1.21 | 1.67 | 0.0908 |
| 542471.2 | 4185072.6 | 36.1 | 44.8 | 1.94 | -0.340 | 0.705 | 206 | 3602 | 1.86 | 0.61 | 1.21 | 1.67 | 0.0908 |
| 542510.4 | 4185094.3 | 37.3 | 24.9 | 0.88 | -0.180 | NaN | 206 | 3659 | 1.75 | 0.64 | 1.31 | 1.75 | 0.0788 |
| 542571.7 | 4185128.3 | 36.6 | 65.5 | 2.50 | -0.213 | NaN | 206 | 3393 | 1.75 | 0.64 | 1.31 | 1.75 | 0.0788 |
| 542628.9 | 4185160.1 | 36.7 | 59.5 | 3.04 | -0.488 | 0.770 | 224 | 3274 | 1.64 | 0.61 | 1.23 | 1.63 | 0.0825 |
| 542681.0 | 4185188.9 | 37.1 | 45.2 | 2.92 | -0.531 | NaN | 227 | 3252 | 1.65 | 0.61 | 1.26 | 1.65 | 0.0825 |
| 542720.5 | 4185210.9 | 37.1 | 49.8 | 3.70 | -0.574 | NaN | 227 | 3252 | 1.65 | 0.61 | 1.26 | 1.65 | 0.0825 |
| 542764.0 | 4185235.0 | 38.9 | 44.8 | 2.30 | -0.340 | NaN | 227 | 3185 | 1.86 | 0.65 | 1.40 | 1.81 | 0.0583 |
| 542596.3 | 4184783.4 | 32.9 | 66.6 | 5.14 | -0.430 | 0.779 | 124 | 3449 | 1.86 | 0.65 | 1.40 | 1.81 | 0.0583 |
| 542654.4 | 4184815.9 | 37.2 | 45.6 | 1.90 | -0.127 | 0.884 | 124 | 3384 | 1.86 | 0.65 | 1.40 | 1.81 | 0.0583 |
| 542694.2 | 4184838.2 | 34.5 | 67.8 | 6.78 | -0.340 | 0.884 | 124 | 3340 | 1.86 | 0.65 | 1.40 | 1.81 | 0.0583 |
| 542759.8 | 4184874.9 | 35.9 | 75.1 | 6.36 | -0.417 | 0.929 | 173 | 3267 | 1.84 | 0.65 | 1.43 | 1.80 | 0.0660 |
| 542825.4 | 4184911.5 | 37.5 | 56.1 | 5.56 | -0.288 | 0.888 | 155 | 3194 | 1.83 | 0.64 | 1.43 | 1.80 | 0.0660 |
| 542874.4 | 4184938.9 | 40.1 | 29.5 | 2.70 | -0.288 | 0.888 | 155 | 3139 | 1.83 | 0.64 | 1.43 | 1.80 | 0.0660 |
| 542900.1 | 4184953.3 | 41.7 | 34.2 | 1.78 | -0.057 | 0.868 | 155 | 3111 | 1.83 | 0.64 | 1.43 | 1.80 | 0.0660 |
| 542930.0 | 4184969.9 | 40.8 | 45.7 | 3.56 | -0.291 | 0.868 | 155 | 3078 | 1.83 | 0.64 | 1.43 | 1.80 | 0.0660 |
| 542969.8 | 4184992.2 | 42.2 | 61.8 | 2.98 | -0.475 | 0.831 | 155 | 3033 | 1.83 | 0.64 | 1.43 | 1.80 | 0.0660 |
| 543023.8 | 4185022.4 | 43.6 | 47.5 | 2.30 | -0.562 | 0.811 | 138 | 2974 | 1.77 | 0.61 | 1.38 | 1.74 | 0.0659 |
| 543065.3 | 4185045.6 | 44.3 | 54.2 | 1.76 | -0.298 | 0.811 | 138 | 2928 | 1.77 | 0.61 | 1.38 | 1.74 | 0.0659 |
| 543112.6 | 4185072.0 | 45.8 | 40.9 | 1.90 | -0.257 | 0.791 | 138 | 2876 | 1.77 | 0.61 | 1.38 | 1.74 | 0.0659 |
| 543148.3 | 4185092.0 | 46.3 | 42.8 | 2.44 | -0.425 | 0.778 | 138 | 2826 | 1.77 | 0.61 | 1.38 | 1.74 | 0.0659 |
| 543185.6 | 4185112.9 | 46.4 | 54.2 | 1.38 | -0.087 | 0.778 | 138 | 2795 | 1.77 | 0.61 | 1.38 | 1.74 | 0.0659 |
| 543222.9 | 4185139.3 | 46.3 | 62.8 | 3.68 | -0.666 | 0.775 | 138 | 2795 | 1.77 | 0.61 | 1.38 | 1.74 | 0.0659 |
| 543267.7 | 4185170.0 | 51.2 | 35.2 | 1.28 | -0.511 | 0.775 | 114 | 2683 | 1.68 | 0.38 | 1.21 | 1.69 | 0.0771 |
| 543318.5 | 4185187.1 | 52.4 | 74.2 | 3.30 | -0.639 | 0.785 | 216 | 2649 | 1.88 | 0.38 | 1.21 | 1.69 | 0.0771 |
| 543382.2 | 4185223.3 | 54.4 | 51.3 | 2.50 | -0.569 | 0.787 | 216 | 2578 | 1.88 | 0.38 | 1.21 | 1.69 | 0.0771 |
| 543428.0 | 4185248.4 | 56.5 | 44.7 | 2.04 | -0.103 | 0.821 | 216 | 2529 | 1.88 | 0.38 | 1.21 | 1.69 | 0.0771 |
| 542601.4 | 4184362.7 | 34.0 | 114.7 | 4.84 | -0.435 | 0.652 | 93 | 3586 | 1.71 | 0.39 | 1.38 | 1.62 | 0.0401 |
| 542702.7 | 4184416.5 | 35.5 | 55.2 | 4.08 | -0.222 | 0.768 | 88 | 3471 | 1.79 | 0.62 | 1.44 | 1.68 | 0.0382 |
| 542751.5 | 4184442.4 | 37.7 | 60.7 | 2.10 | -0.333 | 0.768 | 88 | 3416 | 1.79 | 0.62 | 1.44 | 1.68 | 0.0382 |
| 542805.1 | 4184470.9 | 38.5 | 58.0 | 2.78 | -0.303 | 0.792 | 88 | 3416 | 1.79 | 0.62 | 1.44 | 1.68 | 0.0382 |
| 542856.3 | 4184498.1 | 38.3 | 60.7 | 5.30 | -0.020 | 0.871 | 88 | 3356 | 1.79 | 0.62 | 1.44 | 1.68 | 0.0382 |
| 542909.9 | 4184526.6 | 37.4 | 99.8 | 7.40 | -0.379 | 0.849 | 84 | 3238 | 1.80 | 0.62 | 1.44 | 1.68 | 0.0402 |
| 542998.0 | 4184573.5 | 40.3 | 70.1 | 6.48 | -0.424 | 0.811 | 84 | 3139 | 1.80 | 0.62 | 1.44 | 1.68 | 0.0402 |
| 543059.9 | 4184606.3 | 42.1 | 56.4 | 6.60 | -0.601 | 0.847 | 94 | 3069 | 1.84 | 0.64 | 1.43 | 1.74 | 0.0443 |
| 543125.5 | 4184641.2 | 44.8 | 67.4 | 4.10 | -0.259 | 0.798 | 87 | 2995 | 1.78 | 0.61 | 1.39 | 1.68 | 0.0413 |
| 543185.0 | 4184672.8 | 45.6 | 78.2 | 3.78 | -0.690 | 0.798 | 87 | 2928 | 1.78 | 0.61 | 1.39 | 1.68 | 0.0413 |
| 543254.0 | 4184709.5 | 48.5 | 68.8 | 1.58 | -0.608 | 0.771 | 87 | 2850 | 1.78 | 0.61 | 1.39 | 1.68 | 0.0413 |
| 543314.8 | 4184741.8 | 49.9 | 71.5 | 2.60 | -0.596 | 0.738 | 78 | 2782 | 1.73 | 0.59 | 1.33 | 1.62 | 0.0342 |
| 543377.9 | 4184775.3 | 51.5 | 60.7 | 3.50 | -0.288 | 0.738 | 78 | 2711 | 1.73 | 0.59 | 1.33 | 1.62 | 0.0342 |
| 543431.5 | 4184803.8 | 52.6 | 129.4 | 6.52 | -0.542 | 0.740 | 78 | 2651 | 1.73 | 0.59 | 1.33 | 1.62 | 0.0342 |

| Easting (m) | Northing (m) | Water depth (m) | Length (m) | Height (m) | Asymmetry (-) | D-50 (mm) | Res dir (degr) | CG distance (m) | Mx Spring (m/s) | Mx Neap (m/s) | Mx Flood (m/s) | Mx Ebb (m/s) | Res Mag (m/s) |
|-------------|--------------|-----------------|------------|------------|---------------|-----------|----------------|-----------------|-----------------|---------------|----------------|--------------|---------------|
| 543454.8 | 4184064.5 | 53.7 | 58.0 | 6.82 | -0.333 | 0.732 | 70 | 2572 | 1.68 | 0.37 | 1.33 | 1.37 | 0.0383 |
| 543459.0 | 4184091.7 | 58.4 | 82.3 | 4.60 | -0.413 | 0.776 | 70 | 2465 | 1.68 | 0.37 | 1.33 | 1.37 | 0.0383 |
| 543460.7 | 4184093.0 | 58.9 | 69.7 | 5.16 | -0.598 | 0.783 | 70 | 2383 | 1.68 | 0.37 | 1.33 | 1.37 | 0.0383 |
| 543472.3 | 4184093.8 | 62.2 | 99.4 | 7.39 | -0.296 | 0.776 | 75 | 2223 | 1.68 | 0.37 | 1.34 | 1.51 | 0.0415 |
| 543810.2 | 4185005.0 | 63.4 | 130.8 | 9.26 | -0.691 | 0.808 | 62 | 2236 | 1.50 | 0.36 | 1.30 | 1.35 | 0.0415 |
| 541994.5 | 4183846.8 | 36.3 | 85.4 | 4.66 | -0.149 | 0.859 | 101 | 4350 | 1.50 | 0.32 | 1.30 | 1.43 | 0.0425 |
| 543075.5 | 4183895.8 | 36.9 | 49.0 | 3.45 | -0.149 | 0.859 | 101 | 4350 | 1.50 | 0.32 | 1.30 | 1.43 | 0.0425 |
| 543116.1 | 4183895.8 | 36.7 | 71.1 | 4.28 | -0.259 | 0.782 | 92 | 4265 | 1.51 | 0.32 | 1.32 | 1.41 | 0.0443 |
| 542196.9 | 4183949.1 | 37.1 | 94.7 | 3.98 | -0.160 | 0.862 | 92 | 4126 | 1.51 | 0.32 | 1.32 | 1.41 | 0.0443 |
| 542280.1 | 4183952.4 | 37.3 | 21.1 | 1.60 | -0.317 | 0.815 | 85 | 4031 | 1.56 | 0.34 | 1.37 | 1.44 | 0.0430 |
| 542306.0 | 4183952.4 | 37.3 | 21.1 | 1.60 | -0.167 | 0.814 | 85 | 3971 | 1.56 | 0.34 | 1.37 | 1.44 | 0.0430 |
| 542349.9 | 4184043.3 | 36.3 | 54.9 | 3.82 | -0.169 | 0.859 | 85 | 3971 | 1.56 | 0.34 | 1.37 | 1.44 | 0.0430 |
| 542511.8 | 4184111.4 | 33.9 | 74.5 | 4.14 | 0.183 | 0.842 | 81 | 3771 | 1.54 | 0.35 | 1.34 | 1.41 | 0.0456 |
| 542576.0 | 4184145.4 | 32.4 | 44.5 | 4.46 | -0.087 | 0.842 | 81 | 3696 | 1.54 | 0.35 | 1.34 | 1.41 | 0.0456 |
| 542619.4 | 4184166.6 | 34.6 | 58.3 | 3.92 | -0.015 | 0.875 | 86 | 3600 | 1.62 | 0.36 | 1.34 | 1.45 | 0.0446 |
| 542671.3 | 4184193.3 | 34.9 | 60.1 | 4.48 | 0.099 | 0.869 | 86 | 3592 | 1.62 | 0.36 | 1.34 | 1.45 | 0.0446 |
| 542786.7 | 4184280.7 | 34.8 | 60.0 | 5.64 | -0.209 | 0.860 | 81 | 3532 | 1.62 | 0.36 | 1.34 | 1.45 | 0.0446 |
| 542778.1 | 4184288.1 | 36.3 | 55.8 | 4.78 | -0.273 | 0.860 | 81 | 3472 | 1.62 | 0.36 | 1.34 | 1.45 | 0.0446 |
| 542831.6 | 4183979.1 | 39.1 | 74.7 | 2.72 | 0.036 | 0.860 | 71 | 3550 | 1.62 | 0.36 | 1.34 | 1.45 | 0.0446 |
| 542892.7 | 4184021.9 | 37.4 | 74.2 | 5.32 | -0.034 | 0.860 | 71 | 3476 | 1.62 | 0.36 | 1.34 | 1.45 | 0.0446 |
| 542953.5 | 4184064.5 | 36.3 | 65.4 | 5.44 | -0.130 | 0.860 | 76 | 3402 | 1.62 | 0.36 | 1.34 | 1.45 | 0.0446 |
| 543007.0 | 4184102.1 | 40.3 | 120.3 | 5.32 | -0.663 | 0.860 | 72 | 3357 | 1.62 | 0.36 | 1.34 | 1.45 | 0.0446 |
| 543105.7 | 4184171.3 | 40.7 | 104.8 | 6.74 | -0.538 | 0.860 | 72 | 3217 | 1.62 | 0.36 | 1.34 | 1.45 | 0.0446 |
| 543191.5 | 4184231.4 | 43.1 | 95.6 | 5.90 | -0.248 | 0.860 | 68 | 3112 | 1.62 | 0.36 | 1.34 | 1.45 | 0.0446 |
| 543209.8 | 4184286.3 | 43.3 | 79.9 | 5.92 | -0.103 | 0.860 | 68 | 3017 | 1.62 | 0.36 | 1.34 | 1.45 | 0.0446 |
| 543096.6 | 4183763.5 | 43.8 | 25.1 | 0.82 | -0.107 | 0.860 | 66 | 3402 | 1.57 | 0.34 | 1.32 | 1.35 | 0.0688 |
| 543114.4 | 4183801.2 | 43.6 | 25.2 | 0.84 | -0.184 | 0.860 | 66 | 3402 | 1.57 | 0.34 | 1.32 | 1.35 | 0.0688 |
| 543132.3 | 4183819.0 | 43.0 | 44.5 | 2.34 | -0.107 | 0.860 | 66 | 3382 | 1.57 | 0.34 | 1.32 | 1.35 | 0.0688 |
| 543163.8 | 4183850.4 | 43.6 | 70.3 | 1.48 | 0.005 | 0.860 | 66 | 3358 | 1.57 | 0.34 | 1.32 | 1.35 | 0.0688 |
| 543215.6 | 4183900.0 | 42.9 | 59.9 | 1.62 | -0.469 | 0.860 | 66 | 3269 | 1.57 | 0.34 | 1.32 | 1.35 | 0.0688 |
| 543256.1 | 4183942.2 | 42.7 | 79.5 | 2.52 | 0.235 | 0.860 | 64 | 3210 | 1.60 | 0.34 | 1.37 | 1.36 | 0.0787 |
| 543312.5 | 4183998.3 | 43.7 | 95.3 | 3.22 | -0.160 | 0.860 | 65 | 3152 | 1.66 | 0.36 | 1.39 | 1.44 | 0.0672 |
| 543380.0 | 4184063.5 | 44.3 | 85.1 | 3.96 | -0.134 | 0.860 | 65 | 3058 | 1.66 | 0.36 | 1.39 | 1.44 | 0.0672 |
| 543786.8 | 4184115.4 | 44.8 | 49.8 | 1.82 | 0.235 | 0.860 | 66 | 2679 | 1.63 | 0.35 | 1.40 | 1.39 | 0.0832 |
| 543808.7 | 4184160.1 | 44.9 | 44.0 | 2.54 | 0.156 | 0.860 | 66 | 2634 | 1.63 | 0.35 | 1.40 | 1.39 | 0.0832 |
| 543828.0 | 4184199.7 | 46.1 | 40.9 | 2.44 | -0.344 | 0.860 | 66 | 2595 | 1.63 | 0.35 | 1.40 | 1.39 | 0.0832 |
| 543846.0 | 4184236.4 | 47.0 | 34.7 | 2.10 | 0.299 | 0.860 | 66 | 2559 | 1.63 | 0.35 | 1.40 | 1.39 | 0.0832 |
| 543861.2 | 4184267.6 | 48.0 | 22.3 | 1.46 | 0.235 | 0.860 | 66 | 2538 | 1.63 | 0.35 | 1.40 | 1.39 | 0.0832 |
| 543871.0 | 4184287.6 | 48.0 | 22.6 | 1.68 | 0.070 | 0.860 | 63 | 2508 | 1.64 | 0.35 | 1.37 | 1.43 | 0.0890 |
| 543881.0 | 4184307.9 | 48.8 | 37.6 | 2.24 | -0.034 | 0.860 | 63 | 2488 | 1.64 | 0.35 | 1.37 | 1.43 | 0.0890 |
| 543897.5 | 4184341.7 | 49.4 | 36.0 | 2.68 | 0.124 | 0.860 | 63 | 2455 | 1.64 | 0.35 | 1.37 | 1.43 | 0.0890 |
| 543913.3 | 4184374.0 | 49.9 | 34.4 | 2.68 | -0.385 | 0.860 | 63 | 2424 | 1.64 | 0.35 | 1.37 | 1.43 | 0.0890 |
| 543944.2 | 4184406.4 | 50.9 | 34.4 | 1.62 | -0.115 | 0.860 | 62 | 2393 | 1.61 | 0.34 | 1.36 | 1.39 | 0.0723 |
| 543959.8 | 4184437.3 | 52.7 | 53.7 | 4.42 | -0.602 | 0.792 | 114 | 2357 | 1.72 | 0.29 | 1.34 | 1.39 | 0.0723 |
| 543438.9 | 4185080.4 | 54.1 | 38.4 | 3.64 | -0.369 | 0.860 | 62 | 2363 | 1.61 | 0.34 | 1.36 | 1.39 | 0.0723 |
| 543485.7 | 4185106.7 | 57.8 | 34.3 | 1.18 | -0.138 | 0.813 | 81 | 2505 | 1.67 | 0.38 | 1.36 | 1.66 | 0.0516 |
| 543515.6 | 4185123.6 | 57.5 | 88.5 | 3.66 | -0.367 | 0.854 | 81 | 2472 | 1.67 | 0.38 | 1.36 | 1.66 | 0.0516 |
| 543586.8 | 4185163.0 | 60.1 | 82.6 | 5.38 | -0.561 | 0.854 | 81 | 2394 | 1.67 | 0.38 | 1.36 | 1.66 | 0.0516 |
| 543657.8 | 4185203.5 | 62.5 | 72.6 | 3.92 | -0.554 | 0.903 | 81 | 2316 | 1.67 | 0.38 | 1.36 | 1.66 | 0.0516 |
| 543721.1 | 4185239.1 | 64.5 | 119.5 | 6.18 | -0.707 | 0.903 | 81 | 2245 | 1.67 | 0.38 | 1.36 | 1.66 | 0.0516 |
| 543825.2 | 4185297.6 | 69.3 | 38.9 | 2.50 | -0.346 | 0.848 | 36 | 2130 | 1.63 | 0.36 | 1.19 | 1.63 | 0.0763 |
| 543859.1 | 4185316.7 | 69.3 | 38.9 | 2.50 | -0.346 | 0.848 | 36 | 2093 | 1.63 | 0.36 | 1.19 | 1.63 | 0.0763 |
| 543896.5 | 4185337.2 | 73.8 | 84.6 | 4.44 | -0.429 | 0.848 | 36 | 2053 | 1.63 | 0.36 | 1.19 | 1.63 | 0.0763 |
| 541897.7 | 4183978.1 | 39.0 | 141.0 | 4.02 | 0.418 | 0.343 | 101 | 4284 | 1.30 | 0.32 | 1.20 | 1.43 | 0.0495 |
| 542023.1 | 4184042.5 | 36.4 | 60.1 | 5.80 | -0.536 | 0.330 | 101 | 4243 | 1.30 | 0.32 | 1.20 | 1.43 | 0.0495 |
| 542076.6 | 4184069.9 | 69.8 | 69.8 | 2.68 | 0.000 | 0.330 | 101 | 4183 | 1.30 | 0.32 | 1.20 | 1.43 | 0.0495 |

| Easting (m) | Northing (m) | Water depth (m) | Length (m) | Height (m) | Asymmetry (-) | D-50 (mm) | Res dir (degr) | CG distance (m) | Mx Spring (m/s) | Mx Neap (m/s) | Mx Flood (m/s) | Mx Ebb (m/s) | Res Mag (m/s) |
|-------------|--------------|-----------------|------------|------------|---------------|-----------|----------------|-----------------|-----------------|---------------|----------------|--------------|---------------|
| 542198.7 | 4184101.8 | 38.3 | 106.1 | 5.06 | -0.624 | 0.252 | 101 | 4114 | 1.30 | 0.32 | 1.18 | 1.43 | 0.4273 |
| 542200.1 | 4184103.2 | 39.9 | 43.8 | 2.76 | -0.387 | 0.409 | 101 | 4068 | 1.30 | 0.32 | 1.18 | 1.43 | 0.4273 |
| 542210.0 | 4184170.3 | 40.7 | 34.9 | 0.64 | 0.498 | 0.409 | 90 | 3964 | 1.37 | 0.34 | 1.26 | 1.48 | 0.4380 |
| 542303.1 | 4184186.2 | 39.9 | 35.6 | 1.66 | 0.170 | 0.457 | 90 | 3929 | 1.37 | 0.34 | 1.26 | 1.48 | 0.4380 |
| 542361.2 | 4184216.0 | 38.5 | 49.7 | 1.50 | -0.197 | 0.462 | 90 | 3864 | 1.37 | 0.34 | 1.26 | 1.48 | 0.4380 |
| 542405.4 | 4184238.7 | 38.5 | 35.7 | 1.12 | 0.163 | 0.514 | 90 | 3815 | 1.37 | 0.34 | 1.26 | 1.48 | 0.4380 |
| 542458.9 | 4184266.2 | 37.2 | 14.8 | 0.80 | 0.408 | 0.514 | 90 | 3754 | 1.37 | 0.34 | 1.26 | 1.48 | 0.4380 |
| 542472.1 | 4184273.0 | 36.7 | 30.4 | 1.08 | -0.024 | 0.514 | 86 | 3740 | 1.37 | 0.32 | 1.26 | 1.48 | 0.4380 |
| 542535.3 | 4184418.8 | 46.6 | 120.5 | 8.32 | -0.741 | 0.564 | 67 | 2723 | 1.37 | 0.32 | 1.37 | 1.33 | 0.4040 |
| 542620.9 | 4184501.6 | 52.6 | 69.6 | 3.84 | -0.134 | 0.573 | 67 | 2606 | 1.37 | 0.32 | 1.37 | 1.33 | 0.4040 |
| 542671.4 | 4184549.5 | 52.2 | 114.9 | 7.70 | -0.465 | 0.573 | 63 | 2539 | 1.37 | 0.32 | 1.37 | 1.33 | 0.4040 |
| 542734.9 | 4184628.5 | 55.1 | 86.5 | 7.16 | -0.485 | 0.591 | 66 | 2428 | 1.37 | 0.32 | 1.34 | 1.33 | 0.3972 |
| 542815.3 | 4184683.8 | 57.4 | 119.5 | 8.62 | -0.699 | 0.564 | 66 | 2350 | 1.67 | 0.37 | 1.34 | 1.33 | 0.3972 |
| 544109.9 | 4184288.4 | 45.9 | 117.1 | 2.68 | -0.322 | 0.664 | 68 | 2318 | 1.38 | 0.34 | 1.37 | 1.32 | 0.3940 |
| 544154.6 | 4184396.6 | 47.3 | 142.3 | 2.22 | 0.010 | 0.664 | 68 | 2216 | 1.38 | 0.34 | 1.37 | 1.32 | 0.3940 |
| 544263.3 | 4183686.6 | 42.6 | 23.9 | 0.96 | 0.493 | 0.664 | 68 | 2116 | 1.38 | 0.34 | 1.37 | 1.32 | 0.3940 |
| 544265.8 | 4183680.8 | 41.4 | 30.0 | 1.26 | 0.274 | 0.664 | 72 | 3878 | 1.38 | 0.33 | 1.29 | 1.36 | 0.3976 |
| 544268.7 | 4183690.0 | 40.7 | 34.0 | 1.80 | 0.290 | 0.664 | 72 | 3854 | 1.38 | 0.33 | 1.29 | 1.36 | 0.3976 |
| 544273.7 | 4183713.3 | 40.2 | 32.2 | 1.90 | -0.024 | 0.664 | 72 | 3824 | 1.38 | 0.33 | 1.29 | 1.36 | 0.3976 |
| 544279.7 | 4183725.6 | 40.1 | 45.7 | 2.10 | -0.130 | 0.664 | 72 | 3790 | 1.38 | 0.33 | 1.29 | 1.36 | 0.3976 |
| 544282.0 | 4183728.8 | 39.6 | 48.3 | 3.44 | -0.070 | 0.664 | 72 | 3758 | 1.38 | 0.33 | 1.29 | 1.36 | 0.3976 |
| 544282.7 | 4183777.4 | 41.6 | 29.9 | 1.70 | -0.052 | 0.664 | 68 | 3664 | 1.38 | 0.33 | 1.29 | 1.36 | 0.3976 |
| 542846.4 | 4183792.5 | 41.2 | 46.0 | 1.58 | -0.203 | 0.664 | 68 | 3654 | 1.38 | 0.33 | 1.30 | 1.36 | 0.3950 |
| 542886.1 | 4183815.9 | 40.0 | 50.2 | 2.96 | -0.342 | 0.664 | 68 | 3588 | 1.38 | 0.33 | 1.30 | 1.36 | 0.3950 |
| 542199.5 | 4183437.5 | 39.1 | 35.8 | 1.94 | -0.441 | 0.384 | 72 | 4371 | 1.33 | 0.33 | 1.30 | 1.34 | 0.4485 |
| 542231.2 | 4183454.1 | 40.2 | 31.9 | 0.76 | -0.190 | 0.384 | 72 | 4335 | 1.33 | 0.33 | 1.30 | 1.34 | 0.4485 |
| 542259.4 | 4183468.9 | 40.1 | 37.3 | 0.82 | 0.031 | 0.384 | 72 | 4303 | 1.33 | 0.33 | 1.30 | 1.34 | 0.4485 |
| 542292.5 | 4183486.2 | 36.8 | 40.5 | 2.72 | -0.615 | 0.384 | 72 | 4266 | 1.33 | 0.33 | 1.30 | 1.34 | 0.4485 |
| 542357.0 | 4183520.0 | 39.1 | 31.3 | 2.46 | -0.655 | 0.392 | 72 | 4194 | 1.33 | 0.33 | 1.30 | 1.34 | 0.4485 |
| 542395.9 | 4183781.1 | 37.5 | 57.4 | 2.14 | 0.299 | 0.392 | 79 | 4027 | 1.34 | 0.33 | 1.27 | 1.40 | 0.4474 |
| 542446.9 | 4183807.5 | 37.2 | 54.5 | 1.80 | 0.015 | 0.392 | 79 | 3969 | 1.34 | 0.33 | 1.27 | 1.40 | 0.4474 |
| 542495.3 | 4183852.5 | 37.1 | 46.2 | 2.22 | -0.048 | 0.392 | 79 | 3915 | 1.34 | 0.33 | 1.27 | 1.40 | 0.4474 |
| 542536.3 | 4183853.8 | 37.3 | 43.8 | 2.08 | -0.052 | 0.392 | 79 | 3869 | 1.34 | 0.33 | 1.27 | 1.40 | 0.4474 |
| 542575.2 | 4183873.9 | 36.7 | 34.1 | 1.92 | 0.111 | 0.392 | 76 | 3825 | 1.35 | 0.33 | 1.31 | 1.43 | 0.4524 |
| 542605.5 | 4183889.6 | 36.1 | 54.3 | 3.58 | -0.288 | 0.392 | 76 | 3791 | 1.35 | 0.33 | 1.31 | 1.43 | 0.4524 |
| 542622.8 | 4183939.0 | 43.3 | 58.0 | 1.26 | 0.290 | 0.392 | 65 | 2917 | 1.35 | 0.33 | 1.41 | 1.37 | 0.4524 |
| 542636.9 | 4183995.2 | 43.5 | 29.2 | 1.62 | -0.170 | 0.392 | 65 | 2871 | 1.35 | 0.33 | 1.41 | 1.37 | 0.4524 |
| 542643.9 | 4184023.6 | 44.6 | 30.9 | 0.84 | 0.176 | 0.392 | 65 | 2848 | 1.35 | 0.33 | 1.41 | 1.37 | 0.4524 |
| 542651.4 | 4184053.5 | 44.6 | 31.2 | 1.76 | 0.053 | 0.392 | 63 | 2824 | 1.35 | 0.33 | 1.41 | 1.37 | 0.4524 |
| 542659.0 | 4184083.8 | 45.0 | 33.0 | 1.82 | 0.053 | 0.392 | 63 | 2800 | 1.35 | 0.33 | 1.41 | 1.37 | 0.4524 |
| 541910.7 | 4183552.5 | 32.8 | 167.4 | 7.04 | 0.143 | 0.388 | 85 | 4562 | 1.30 | 0.32 | 1.21 | 1.42 | 0.4731 |
| 542042.6 | 4183552.5 | 34.5 | 75.6 | 4.24 | -0.474 | 0.386 | 85 | 4397 | 1.30 | 0.32 | 1.21 | 1.42 | 0.4731 |
| 542326.7 | 4184594.0 | 30.7 | 93.5 | 6.60 | -0.394 | 0.721 | 105 | 3562 | 1.30 | 0.32 | 1.21 | 1.42 | 0.4731 |
| 542620.7 | 4184638.8 | 33.3 | 67.1 | 3.96 | -0.083 | 0.863 | 98 | 3469 | 1.30 | 0.32 | 1.21 | 1.42 | 0.4731 |
| 542679.7 | 4184670.9 | 33.6 | 68.3 | 5.44 | -0.115 | 0.863 | 98 | 3403 | 1.30 | 0.32 | 1.21 | 1.42 | 0.4731 |
| 542739.6 | 4184705.6 | 33.9 | 70.1 | 6.90 | -0.298 | 0.916 | 124 | 3356 | 1.28 | 0.32 | 1.21 | 1.42 | 0.4731 |
| 542801.2 | 4184737.2 | 36.3 | 84.9 | 5.48 | -0.581 | 0.968 | 124 | 3267 | 1.28 | 0.32 | 1.21 | 1.42 | 0.4731 |
| 542875.7 | 4184777.8 | 36.5 | 76.3 | 5.24 | -0.420 | 0.968 | 113 | 3189 | 1.28 | 0.32 | 1.21 | 1.42 | 0.4731 |
| 542942.7 | 4184814.3 | 39.7 | 64.0 | 5.30 | -0.425 | 0.902 | 113 | 3109 | 1.28 | 0.32 | 1.21 | 1.42 | 0.4731 |
| 542998.9 | 4184845.0 | 42.0 | 64.6 | 3.66 | -0.526 | 0.857 | 113 | 3046 | 1.28 | 0.32 | 1.21 | 1.42 | 0.4731 |
| 543055.6 | 4184875.9 | 42.4 | 71.4 | 4.52 | -0.415 | 0.857 | 101 | 2983 | 1.28 | 0.32 | 1.21 | 1.42 | 0.4731 |
| 543118.3 | 4184910.1 | 44.1 | 64.6 | 4.72 | -0.505 | 0.804 | 101 | 2913 | 1.28 | 0.32 | 1.21 | 1.42 | 0.4731 |
| 543175.0 | 4184941.0 | 46.0 | 84.3 | 4.76 | -0.533 | 0.804 | 101 | 2849 | 1.28 | 0.32 | 1.21 | 1.42 | 0.4731 |
| 543159.3 | 4184376.8 | 41.7 | 110.8 | 7.16 | -0.546 | 0.668 | 73 | 3073 | 1.28 | 0.32 | 1.21 | 1.42 | 0.4731 |
| 543246.3 | 4184441.5 | 44.0 | 84.2 | 5.94 | 0.020 | 0.675 | 73 | 2963 | 1.28 | 0.32 | 1.21 | 1.42 | 0.4731 |
| 543317.6 | 4184490.7 | 47.2 | 79.3 | 5.78 | -0.346 | 0.635 | 73 | 2880 | 1.28 | 0.32 | 1.21 | 1.42 | 0.4731 |
| 543382.0 | 4184537.0 | 48.9 | 72.9 | 4.48 | 0.198 | 0.670 | 72 | 2802 | 1.28 | 0.32 | 1.21 | 1.42 | 0.4731 |

| Easting (m) | Northing (m) | Water depth (m) | Length (m) | Height (m) | Asymmetry (-) | D-50 (mm) | Res dir (degr) | CG distance (m) | Mx Spring (m/s) | Mx Neap (m/s) | Mx Flood (m/s) | Mx Ebb (m/s) | Res Mag (m/s) |
|-------------|--------------|-----------------|------------|------------|---------------|-----------|----------------|-----------------|-----------------|---------------|----------------|--------------|---------------|
| 543441.2 | 4184579.5 | 49.8 | 106.0 | 3.72 | -0.433 | 0.634 | 72 | 2730 | 1.72 | 0.58 | 1.37 | 1.38 | 0.9855 |
| 543527.2 | 4184641.4 | 50.5 | 83.3 | 7.06 | 0.031 | 0.640 | 72 | 2626 | 1.72 | 0.58 | 1.37 | 1.38 | 0.9855 |
| 543598.9 | 4184690.0 | 54.5 | 89.9 | 5.14 | -0.640 | 0.640 | 66 | 2544 | 1.67 | 0.57 | 1.34 | 1.35 | 0.9872 |
| 543667.9 | 4184742.5 | 57.1 | 79.3 | 3.94 | 0.143 | 0.676 | 66 | 2456 | 1.67 | 0.57 | 1.34 | 1.35 | 0.9872 |
| 543732.2 | 4184788.8 | 57.4 | 106.0 | 6.38 | -0.420 | 0.656 | 70 | 2378 | 1.88 | 0.56 | 1.33 | 1.37 | 0.9299 |
| 543818.3 | 4184850.7 | 60.2 | 160.3 | 10.12 | -0.707 | 0.685 | 63 | 2275 | 1.85 | 0.56 | 1.33 | 1.35 | 0.9194 |
| 543948.4 | 4184944.3 | 66.8 | 90.6 | 7.74 | -0.322 | 0.699 | 63 | 2118 | 1.85 | 0.56 | 1.33 | 1.35 | 0.9194 |
| 544091.5 | 4185098.4 | 13.7 | 28.1 | 0.78 | 0.212 | NaN | 180 | 2308 | 0.81 | 0.35 | 0.82 | 0.89 | 0.1347 |
| 544197.5 | 4185065.4 | 13.9 | 23.0 | 1.36 | 0.058 | NaN | 180 | 2308 | 0.81 | 0.35 | 0.82 | 0.89 | 0.1347 |
| 544298.3 | 4185041.1 | 13.1 | 32.8 | 0.96 | 0.325 | 0.200 | 188 | 2636 | 0.95 | 0.41 | 0.94 | 1.13 | 0.1315 |
| 544361.1 | 4185062.2 | 13.1 | 23.9 | 0.86 | 0.227 | 0.234 | 188 | 2608 | 0.95 | 0.41 | 0.94 | 1.13 | 0.1315 |
| 544465.9 | 4185089.9 | 13.3 | 29.6 | 0.94 | 0.471 | 0.212 | 188 | 2568 | 0.95 | 0.41 | 0.94 | 1.13 | 0.1315 |
| 544565.9 | 4185250.0 | 13.0 | 31.8 | 1.00 | 0.361 | 0.212 | 188 | 2543 | 0.95 | 0.41 | 0.94 | 1.13 | 0.1315 |
| 544713.8 | 4185338.2 | 13.0 | 32.2 | 1.12 | 0.370 | 0.247 | 188 | 2516 | 0.95 | 0.41 | 0.94 | 1.13 | 0.1315 |
| 544742.1 | 4185355.5 | 13.1 | 23.6 | 0.78 | 0.325 | 0.247 | 188 | 2489 | 0.95 | 0.41 | 0.94 | 1.13 | 0.1315 |
| 544777.5 | 4185372.7 | 12.9 | 28.0 | 0.90 | 0.389 | 0.247 | 188 | 2456 | 0.81 | 0.35 | 0.82 | 0.89 | 0.1347 |
| 544802.1 | 4185366.0 | 13.0 | 27.7 | 0.92 | 0.418 | NaN | 180 | 2453 | 0.81 | 0.35 | 0.82 | 0.89 | 0.1347 |
| 544197.5 | 4182934.2 | 16.5 | 53.5 | 1.20 | 0.242 | NaN | 231 | 3297 | 0.79 | 0.34 | 0.72 | 0.84 | 0.0935 |
| 544241.0 | 4183092.3 | 16.6 | 46.3 | 1.56 | 0.389 | 0.337 | 231 | 3139 | 0.79 | 0.34 | 0.72 | 0.84 | 0.0935 |
| 544286.8 | 4183066.6 | 16.2 | 31.9 | 0.84 | 0.325 | NaN | 231 | 3120 | 0.79 | 0.34 | 0.72 | 0.84 | 0.0935 |
| 544318.4 | 4183082.0 | 15.6 | 40.0 | 0.76 | 0.408 | NaN | 220 | 3108 | 0.78 | 0.34 | 0.74 | 0.79 | 0.0818 |
| 544335.2 | 4183065.6 | 14.4 | 29.9 | 1.04 | 0.266 | NaN | 220 | 3066 | 0.78 | 0.34 | 0.74 | 0.79 | 0.0818 |
| 544345.7 | 4183181.0 | 16.1 | 25.7 | 0.98 | 0.205 | 0.365 | 209 | 3009 | 0.92 | 0.40 | 0.80 | 1.05 | 0.0923 |
| 544254.0 | 4183372.5 | 14.5 | 20.0 | 0.88 | 0.220 | 0.254 | 193 | 2998 | 1.08 | 0.45 | 1.04 | 1.27 | 0.1347 |
| 544353.2 | 4183422.8 | 13.9 | 21.0 | 0.78 | 0.235 | 0.210 | 193 | 2900 | 0.82 | 0.40 | 0.80 | 1.05 | 0.0923 |
| 544355.1 | 4183331.1 | 13.3 | 22.8 | 0.84 | 0.290 | 0.242 | 209 | 2822 | 0.92 | 0.40 | 0.80 | 1.05 | 0.0923 |
| 544355.1 | 4183364.4 | 12.9 | 20.6 | 0.78 | 0.351 | 0.254 | 198 | 2743 | 0.82 | 0.36 | 0.82 | 0.86 | 0.1010 |
| 544559.5 | 4183364.6 | 12.7 | 27.9 | 1.02 | 0.370 | 0.335 | 198 | 2630 | 0.82 | 0.36 | 0.82 | 0.86 | 0.1010 |
| 544574.4 | 4183266.5 | 14.2 | 27.9 | 1.02 | 0.370 | 0.335 | 198 | 2630 | 0.82 | 0.36 | 0.82 | 0.86 | 0.1010 |
| 544653.9 | 4183283.7 | 14.1 | 23.8 | 0.84 | 0.342 | 0.369 | 198 | 2770 | 0.82 | 0.36 | 0.82 | 0.86 | 0.1010 |
| 544676.4 | 4183291.4 | 14.1 | 22.1 | 0.76 | 0.282 | 0.285 | 198 | 2753 | 0.82 | 0.36 | 0.82 | 0.86 | 0.1010 |
| 544697.3 | 4183298.6 | 14.0 | 18.0 | 0.82 | 0.124 | 0.285 | 198 | 2737 | 0.82 | 0.36 | 0.82 | 0.86 | 0.1010 |
| 544036.9 | 4183387.4 | 26.4 | 32.1 | 1.54 | 0.130 | 0.232 | 192 | 3019 | 1.11 | 0.44 | 1.04 | 1.21 | 0.1177 |
| 544059.6 | 4183401.8 | 26.6 | 27.9 | 0.90 | 0.282 | 0.214 | 192 | 2990 | 1.11 | 0.44 | 1.04 | 1.21 | 0.1177 |
| 544086.5 | 4183414.3 | 26.2 | 30.1 | 1.18 | 0.274 | 0.214 | 192 | 2965 | 1.11 | 0.44 | 1.04 | 1.21 | 0.1177 |
| 544173.2 | 4183458.7 | 19.4 | 26.7 | 0.86 | 0.342 | 0.233 | 154 | 2876 | 1.29 | 0.48 | 1.22 | 1.31 | 0.1412 |
| 544197.1 | 4183470.7 | 19.4 | 33.1 | 1.76 | 0.399 | 0.233 | 173 | 2852 | 1.20 | 0.47 | 1.13 | 1.31 | 0.1425 |
| 544115.2 | 4183620.1 | 36.1 | 46.4 | 2.72 | 0.653 | 0.227 | 102 | 2786 | 1.40 | 0.49 | 1.32 | 1.28 | 0.1470 |
| 544156.5 | 4183650.2 | 35.8 | 40.2 | 2.06 | 0.631 | 0.227 | 131 | 2740 | 1.29 | 0.47 | 1.24 | 1.28 | 0.1326 |
| 544181.1 | 4183676.3 | 36.4 | 37.6 | 1.50 | 0.290 | 0.227 | 131 | 2700 | 1.29 | 0.47 | 1.24 | 1.28 | 0.1326 |
| 544209.7 | 4183700.7 | 36.2 | 32.6 | 2.26 | 0.163 | 0.209 | 131 | 2663 | 1.29 | 0.47 | 1.24 | 1.28 | 0.1326 |
| 544234.5 | 4183721.9 | 37.1 | 48.8 | 3.04 | 0.299 | 0.209 | 131 | 2631 | 1.29 | 0.47 | 1.24 | 1.28 | 0.1326 |
| 544369.5 | 4183856.9 | 39.0 | 37.2 | 1.82 | 0.205 | 0.182 | 154 | 2441 | 1.16 | 0.44 | 1.11 | 1.27 | 0.1254 |
| 544403.7 | 4183871.5 | 39.4 | 60.7 | 1.80 | 0.282 | 0.173 | 154 | 2409 | 1.16 | 0.44 | 1.11 | 1.27 | 0.1254 |
| 544439.7 | 4183886.8 | 39.4 | 60.7 | 1.80 | 0.282 | 0.173 | 154 | 2374 | 1.16 | 0.44 | 1.11 | 1.27 | 0.1254 |
| 544495.6 | 4183910.5 | 39.2 | 47.6 | 1.76 | 0.563 | 0.194 | 154 | 2321 | 1.16 | 0.44 | 1.11 | 1.27 | 0.1254 |
| 543842.4 | 4183815.0 | 42.4 | 30.0 | 1.16 | 0.136 | 0.284 | 80 | 2832 | 1.21 | 0.52 | 1.38 | 1.37 | 0.1325 |
| 543871.4 | 4183822.5 | 42.9 | 68.4 | 1.88 | 0.481 | 0.284 | 80 | 2805 | 1.21 | 0.52 | 1.38 | 1.37 | 0.1325 |
| 543937.6 | 4183839.7 | 42.7 | 54.6 | 1.80 | -0.275 | 0.269 | 80 | 2746 | 1.21 | 0.52 | 1.38 | 1.37 | 0.1325 |
| 544821.5 | 4184442.6 | 57.5 | 31.6 | 1.60 | 0.026 | NaN | 137 | 1702 | 1.29 | 0.46 | 1.13 | 1.10 | 0.0933 |
| 544829.9 | 4184473.1 | 59.0 | 19.7 | 0.92 | 0.087 | NaN | 137 | 1673 | 1.29 | 0.46 | 1.13 | 1.10 | 0.0933 |
| 544835.1 | 4184492.1 | 59.6 | 25.9 | 1.40 | -0.219 | NaN | 137 | 1655 | 1.29 | 0.46 | 1.13 | 1.10 | 0.0933 |
| 544841.9 | 4184517.1 | 60.7 | 33.7 | 2.04 | 0.105 | NaN | 137 | 1632 | 1.29 | 0.46 | 1.13 | 1.10 | 0.0933 |
| 544850.8 | 4184549.6 | 62.1 | 23.5 | 1.62 | 0.399 | NaN | 137 | 1601 | 1.29 | 0.46 | 1.13 | 1.10 | 0.0933 |
| 544857.0 | 4184572.3 | 63.0 | 22.7 | 1.16 | -0.153 | NaN | 137 | 1580 | 1.29 | 0.46 | 1.13 | 1.10 | 0.0933 |
| 544862.9 | 4184594.2 | 63.9 | 26.9 | 1.18 | -0.061 | NaN | 213 | 1560 | 1.13 | 0.43 | 1.02 | 1.09 | 0.0935 |
| 544870.0 | 4184620.1 | 64.6 | 12.6 | 1.20 | 0.047 | NaN | 213 | 1536 | 1.13 | 0.43 | 1.02 | 1.09 | 0.0935 |

| Easting (m) | Northing (m) | Water depth (m) | Length (m) | Height (m) | Asymmetry (-) | D-50 (mm) | Res dir (degr) | CG distance (m) | Mx Spring (m/s) | Mx Neap (m/s) | Mx Flood (m/s) | Mx Ebb (m/s) | Res Mag (m/s) |
|-------------|--------------|-----------------|------------|------------|---------------|-----------|----------------|-----------------|-----------------|---------------|----------------|--------------|---------------|
| 544719.9 | 4184497.2 | 56.4 | 19.1 | 1.06 | 0.143 | NaN | 137 | 1728 | 1.29 | 0.46 | 1.13 | 1.10 | 0.0833 |
| 544734.5 | 4184505.5 | 57.1 | 22.1 | 0.84 | -0.394 | NaN | 137 | 1709 | 1.29 | 0.46 | 1.13 | 1.10 | 0.0833 |
| 544585.2 | 4183874.7 | 36.5 | 66.6 | 1.38 | -0.057 | 0.194 | 154 | 2298 | 1.16 | 0.44 | 1.11 | 1.17 | 0.1284 |
| 544635.6 | 4183914.2 | 35.0 | 124.6 | 2.32 | -0.443 | 0.219 | 160 | 2256 | 1.02 | 0.41 | 1.00 | 1.20 | 0.1655 |
| 544735.2 | 4183989.1 | 36.0 | 70.1 | 1.30 | -0.020 | 0.218 | 160 | 2118 | 1.02 | 0.41 | 1.00 | 1.20 | 0.1655 |
| 544791.2 | 4184031.2 | 36.3 | 75.3 | 1.74 | 0.660 | 0.216 | 144 | 2052 | 1.16 | 0.43 | 1.09 | 1.12 | 0.1324 |
| | max | 73.8 | 167.4 | 10.1 | 0.96 | 0.986 | 231 | 4562 | 1.86 | 0.63 | 1.46 | 1.82 | 0.1659 |
| | min | 12.7 | 11.6 | 0.8 | -0.74 | 0.173 | -78 | 1336 | 0.78 | 0.34 | 0.72 | 0.79 | 0.0194 |
| | median | 39.7 | 48.7 | 2.3 | -0.13 | 0.632 | 92 | 3002 | 1.63 | 0.35 | 1.31 | 1.44 | 0.0960 |
| | stdv | 12.8 | 28.9 | 2.0 | 0.32 | 0.246 | 37 | 640 | 0.29 | 0.08 | 0.17 | 0.23 | 0.0338 |

J. FIELD AND 2DH-MODEL DATA SCATTERPLOTS

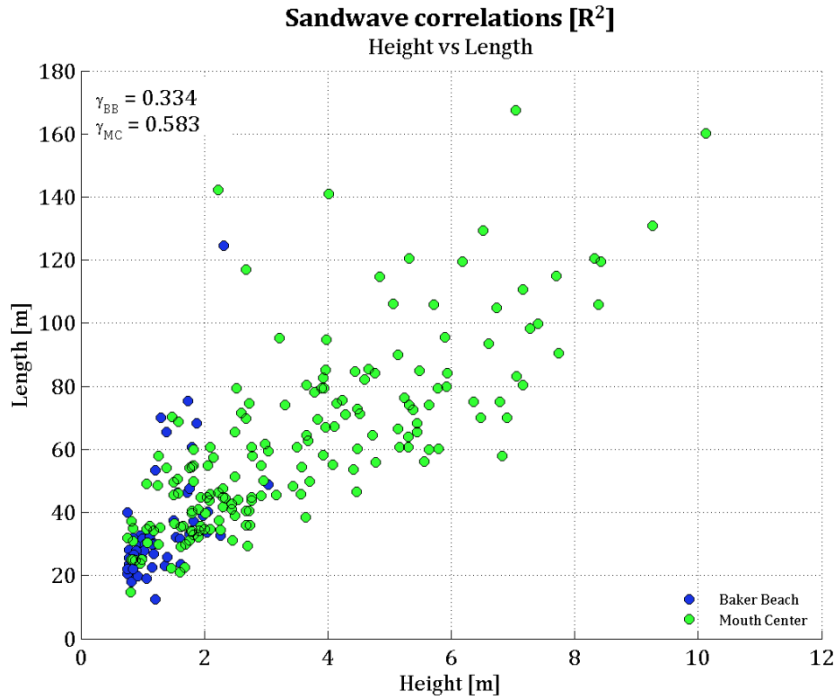


Figure G-1: Scatterplot of sandwave height vs length

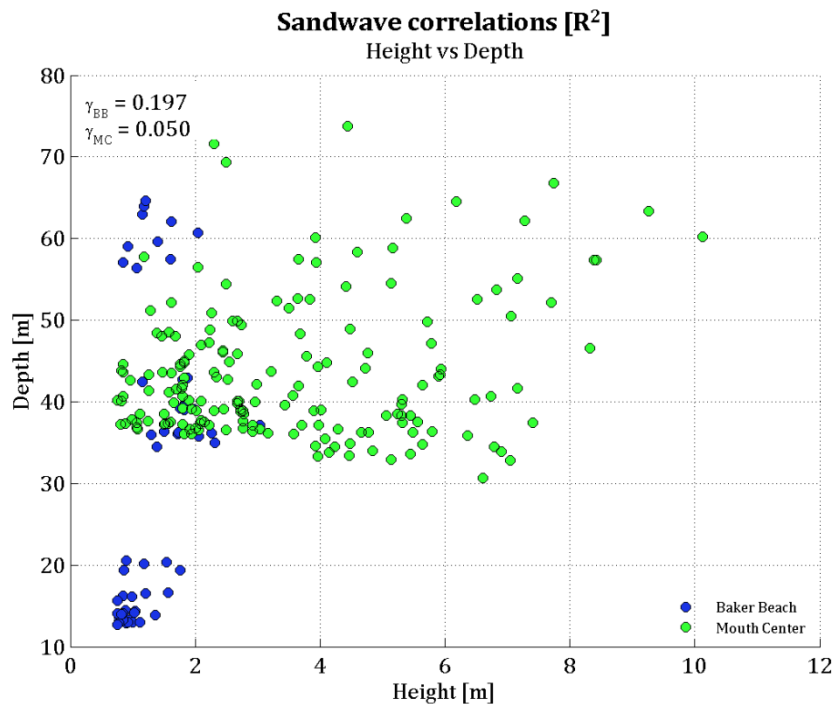


Figure G-2: Scatterplot of sandwave height vs water depth

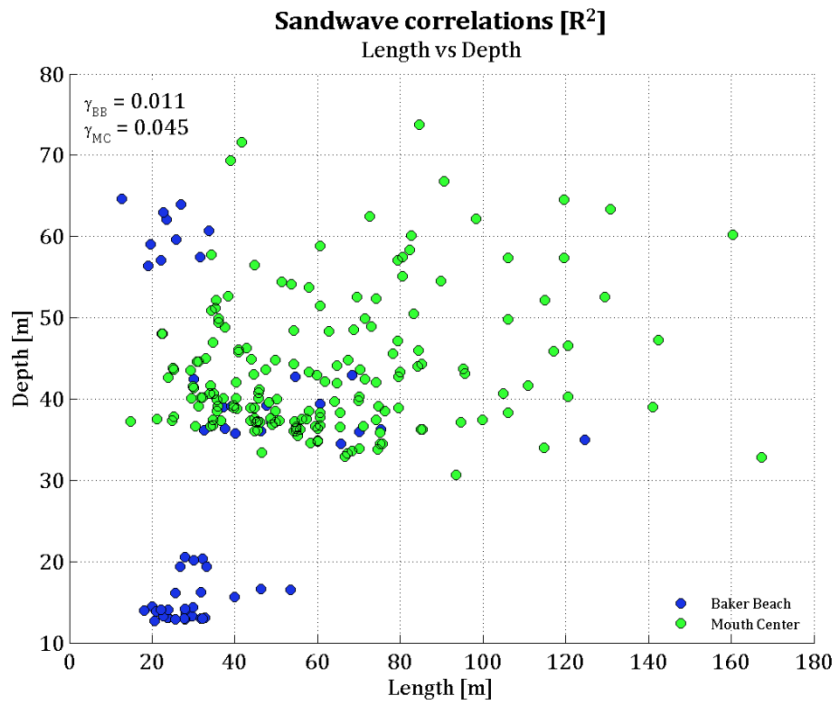


Figure G-3: Scatterplot of sandwave length vs water depth

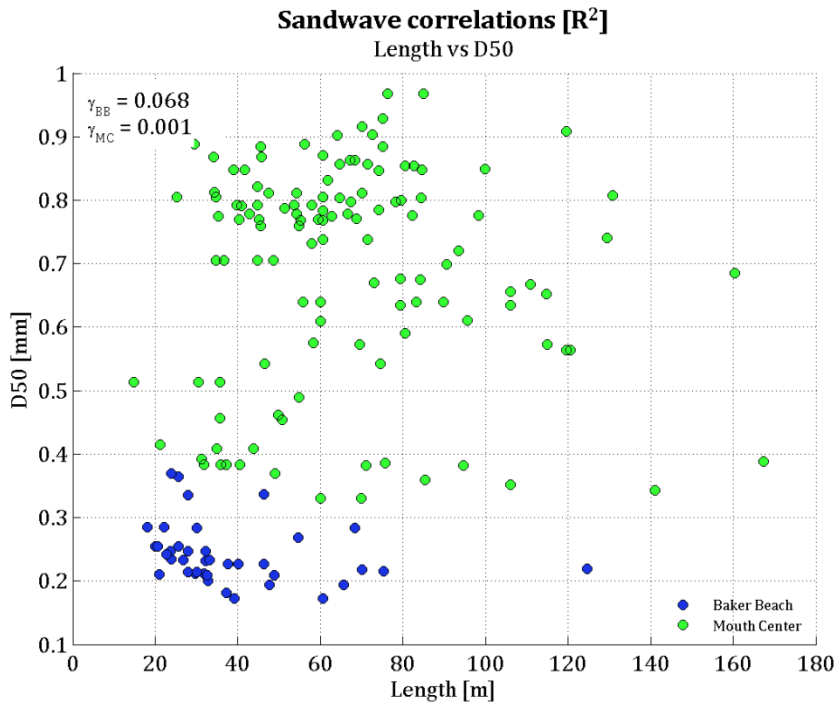


Figure G-4: Scatterplot of sandwave length vs D50

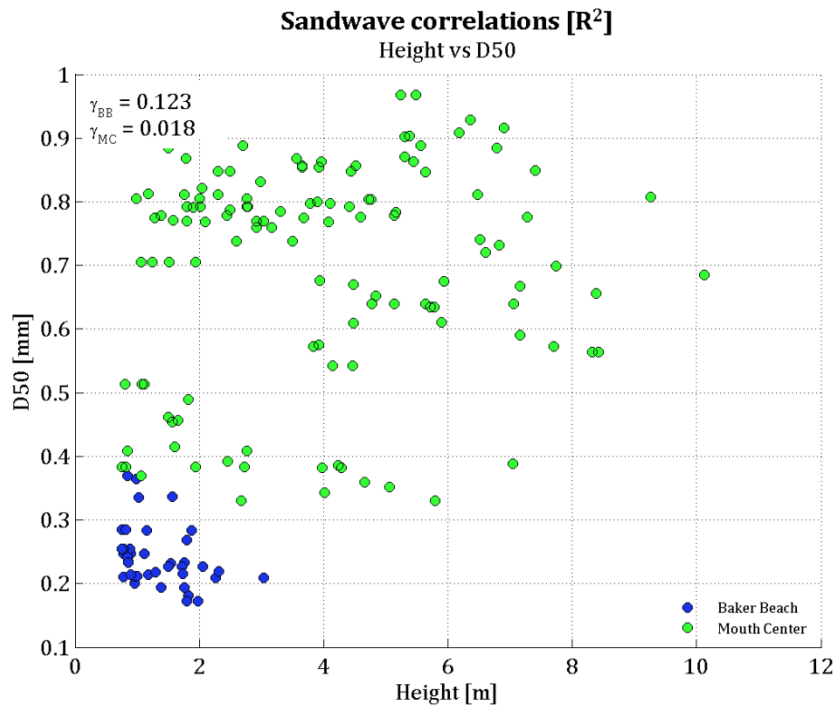


Figure G-5: Scatterplot of sandwave height vs D50

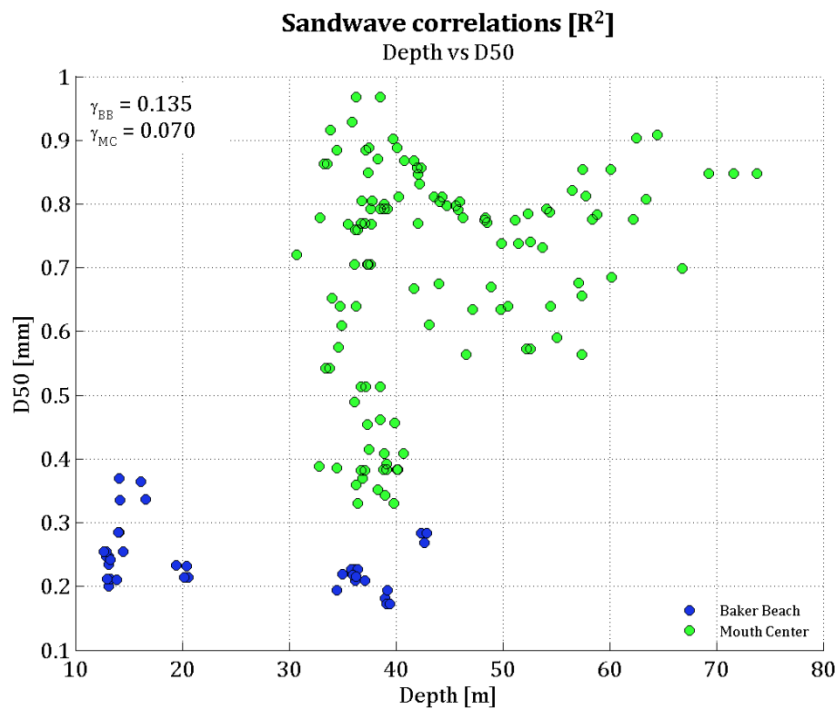


Figure G-6: Scatterplot of water depth vs D50

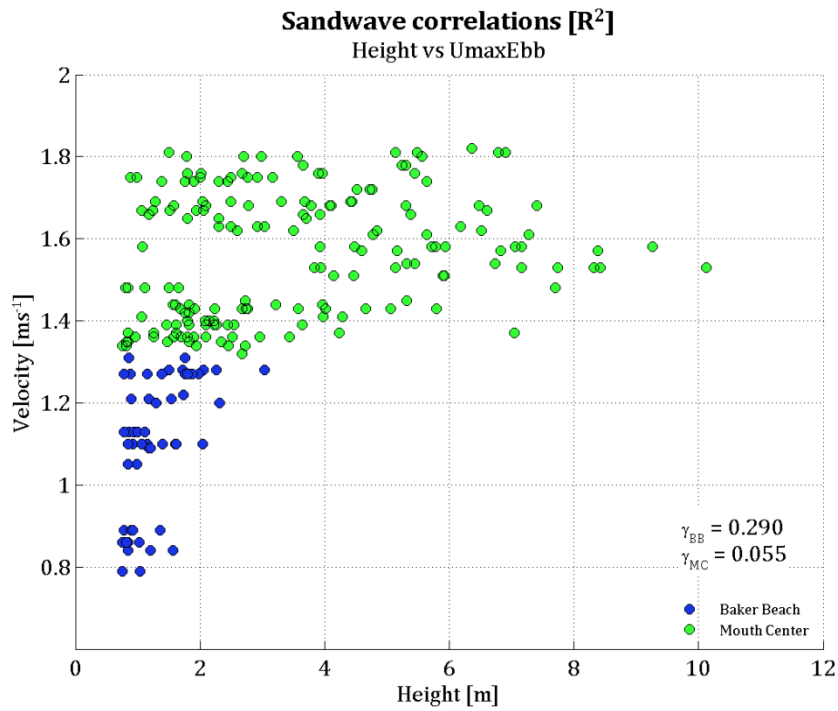


Figure G-7: Scatterplot of sandwave height vs maximum ebb velocity

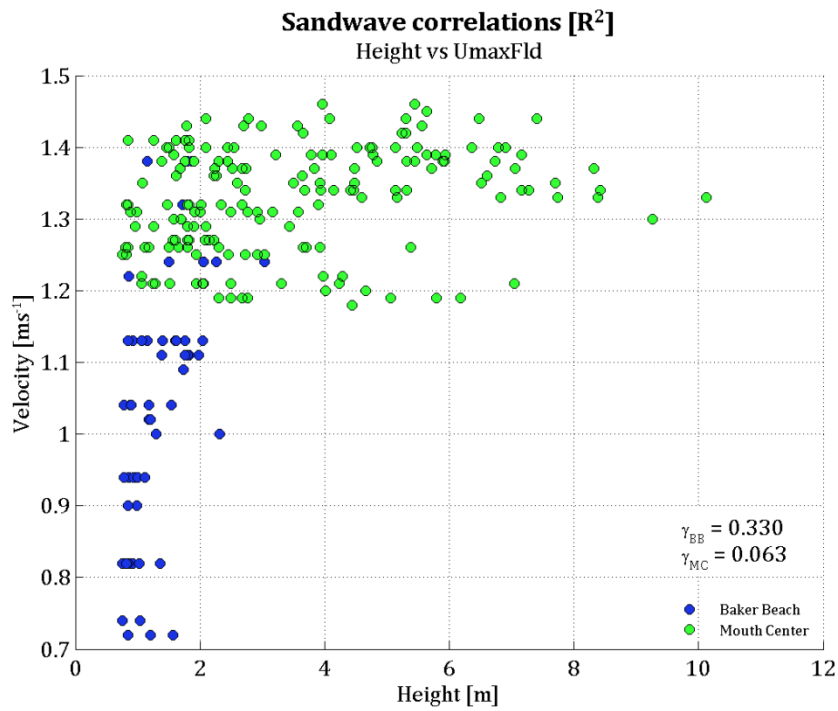


Figure G-8: Scatterplot of sandwave height vs maximum flood velocity

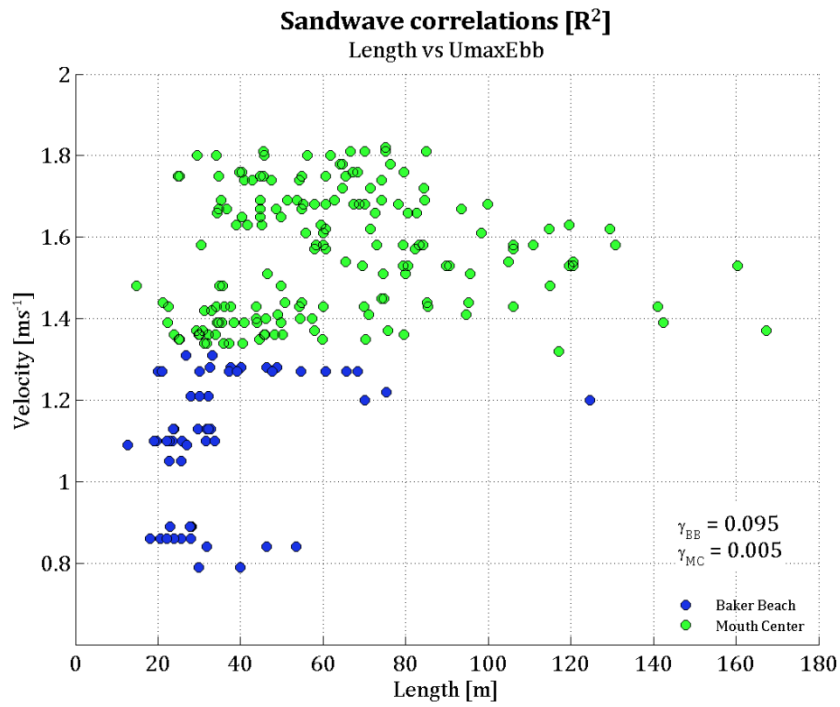


Figure G-9: Scatterplot of sandwave length vs maximum ebb velocity

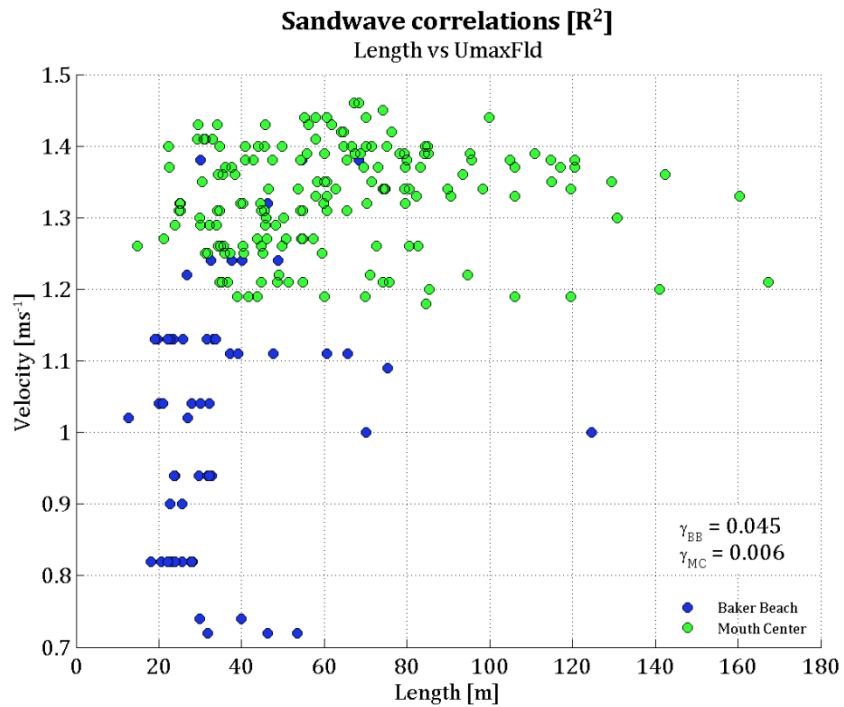


Figure G-10: Scatterplot of sandwave length vs maximum flood velocity

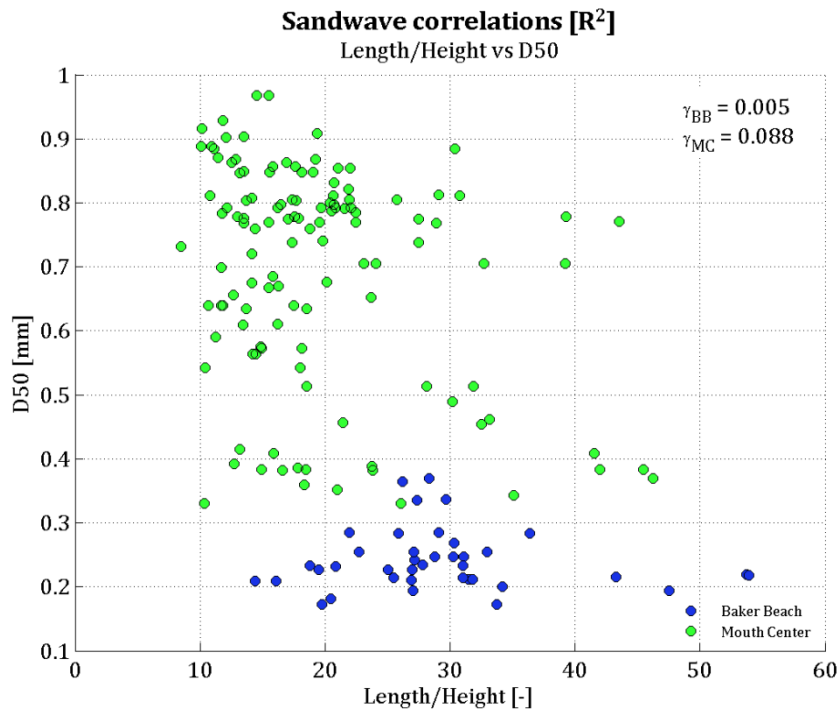


Figure G-11: Scatterplot of sandwave length over height vs D50

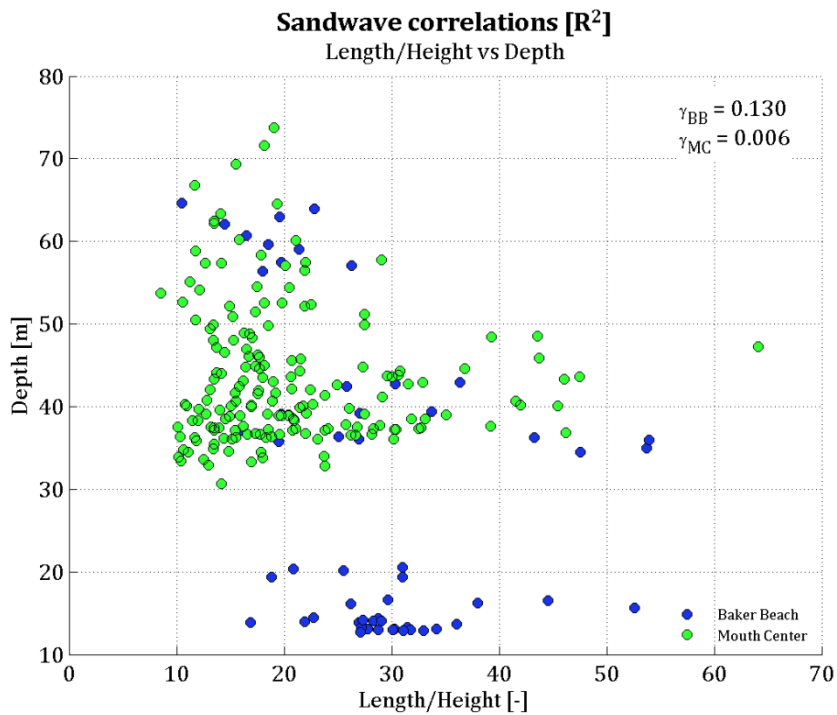


Figure G-12: Scatterplot of sandwave length over height vs depth

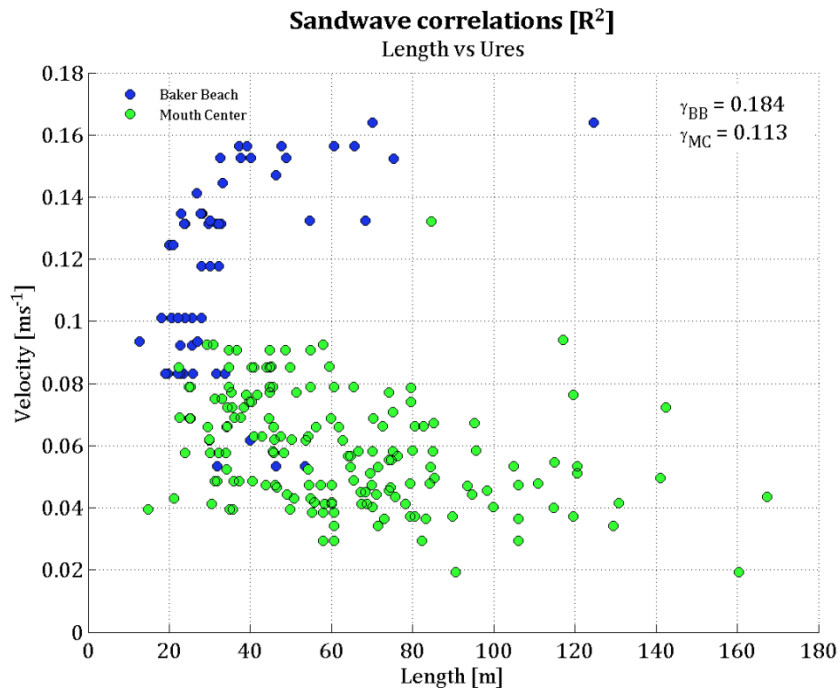


Figure G-13: Scatterplot of residual velocity vs sandwave length

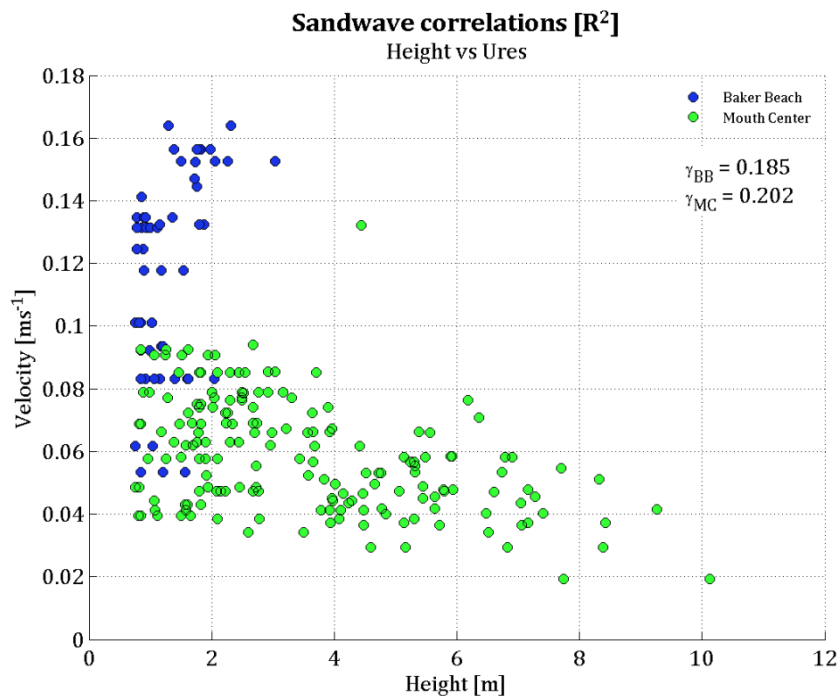


Figure G-14: Scatterplot of residual velocity vs sandwave height

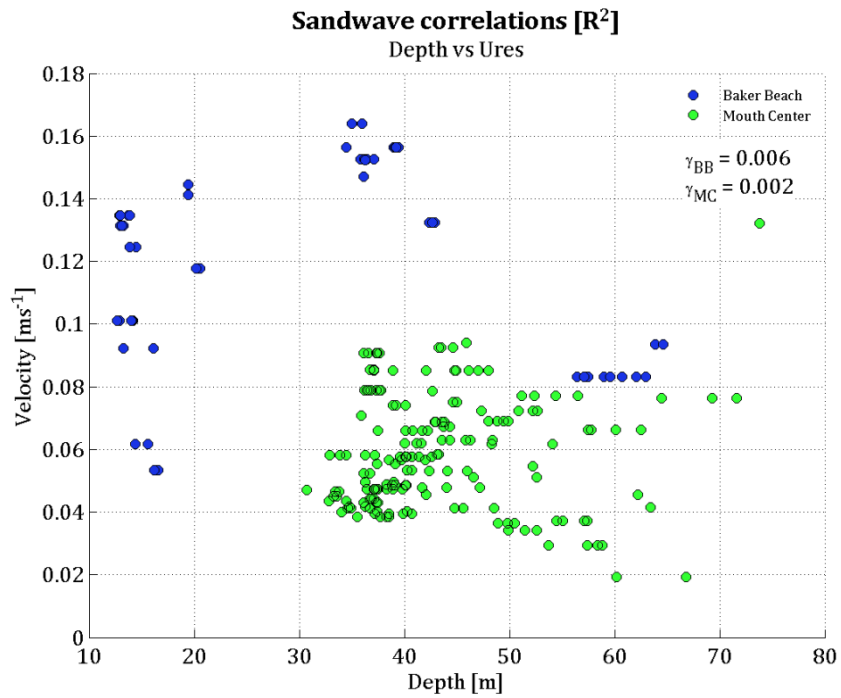


Figure G-15: Scatterplot of residual velocity vs water depth

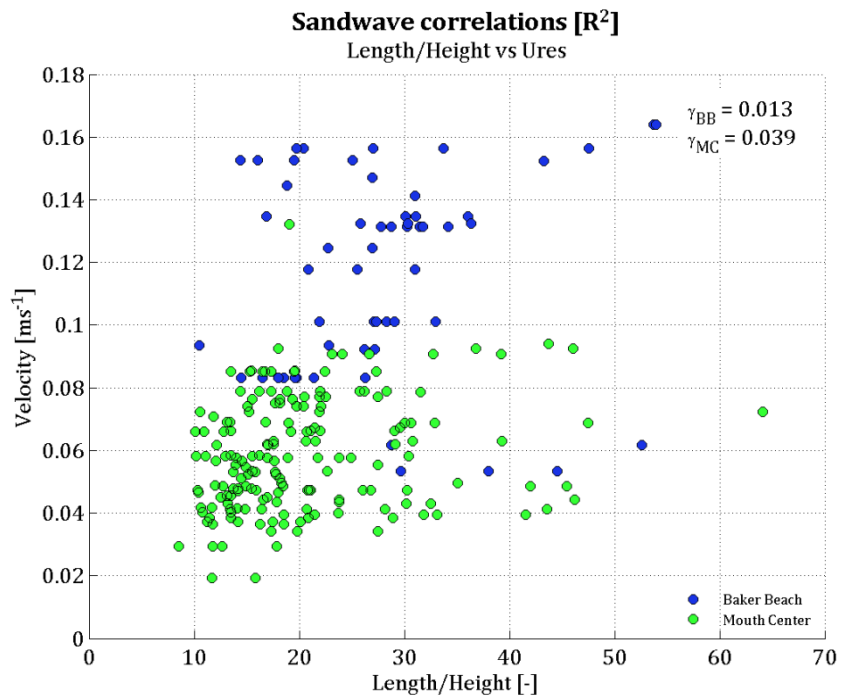


Figure G-16: Scatterplot of residual velocity vs sandwave length over height

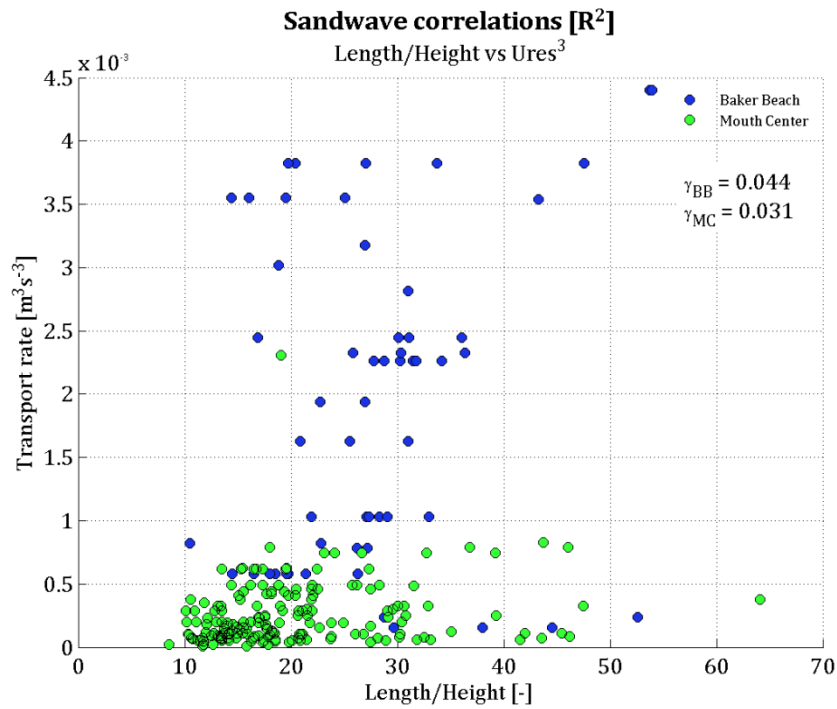


Figure G-17: Scatterplot of transport rate vs sandwave length over height

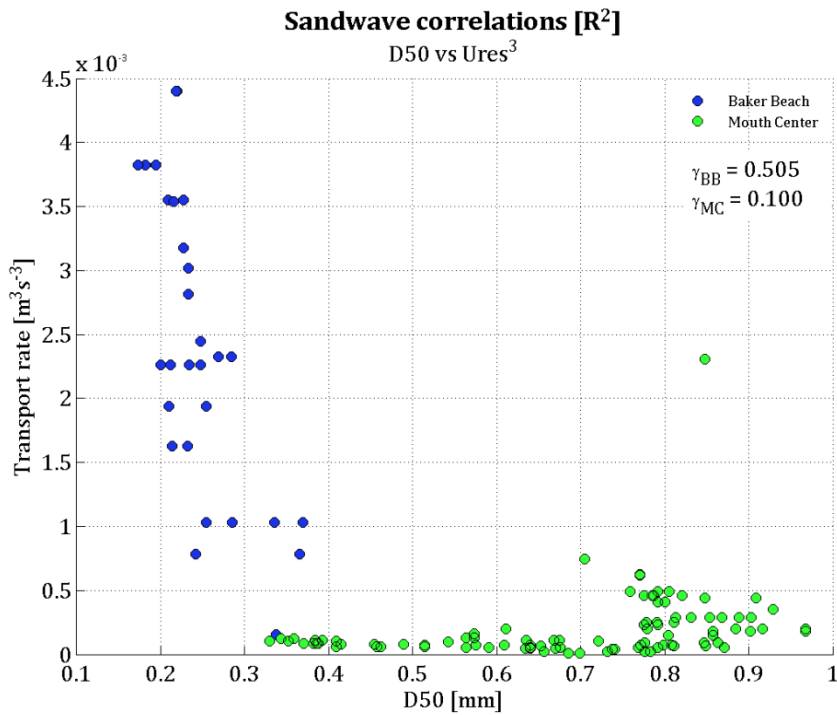
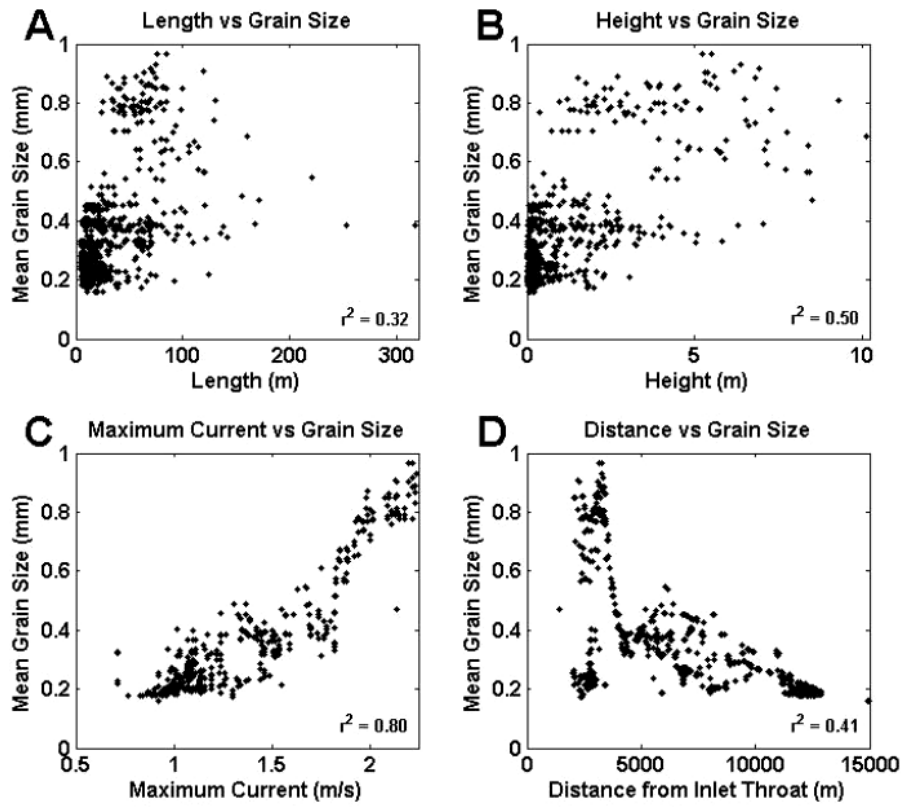


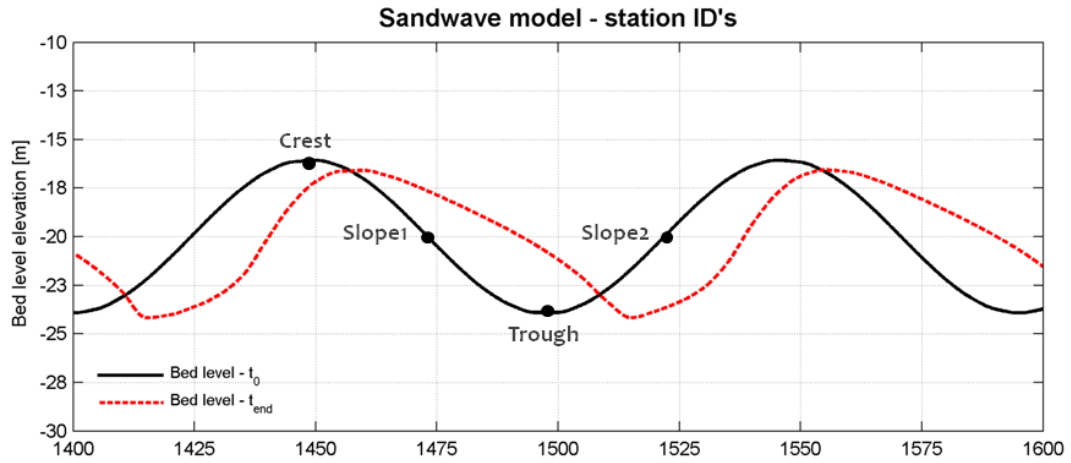
Figure G-18: Scatterplot of transport rate vs D50

K. GRAIN-SIZE RELATIONSHIP WITH SANDWAVES



Scatterplots by Barnard et al., 2006 showing the grain-size relationships with sandwave characteristics and flow in the inlet mouth

L. 2DV-MODEL MONITORING POINTS



Sandwave monitoring points allocated on the crest, lee and stoss slope and trough, to allow studying of the morphodynamic development

M.SIMULATION SETTINGS

An overview of the complete set of model settings is listed in the tables below. These settings are applied for all simulations unless mentioned otherwise.

| General parameters | Value | Details |
|--------------------|-------|---|
| Latitude | 0 ° | Coriolis influence is disregarded |
| Flow time step | 6 s | Optimal time step according to sensitivity analysis ²³ |

Table J-1: Overview of general parameter settings

| Boundary parameters | Value | Details |
|---------------------|-------------|---|
| Open boundary type | Water level | Optimal boundary type according to analysis |
| Forcing | Harmonic | Frequency component of S2-tide (30° per hour) |

Table J-2: Overview of boundary parameters settings

| Physical parameters | Value | Details |
|-----------------------------|-----------------------------------|--|
| Water density | 1000 kg m ⁻³ | Default value |
| Roughness coefficient | 65 √m s ⁻¹ | Chezy roughness formula |
| Wall roughness | Free slip | Neglect shear stress along closed boundaries |
| Horizontal eddy viscosity | 1 m ² s ⁻¹ | Default value |
| Horizontal eddy diffusivity | 10 m ² s ⁻¹ | Default value |
| Turbulence model | k-epsilon | Default |

Table J-3: Overview of physical parameters settings

| Numerical parameters | Value | Details |
|------------------------------|-------|---------|
| Depth at grid cell centers | Mean | Default |
| Forester filter (horizontal) | On | Default |

Table J-4: Overview of numerical parameters settings

²³ See section 6.4.1 for the flow time step evaluation

| Parameter | Name | Initial value |
|---|--------|---------------|
| Update bathymetry during FLOW simulation | MORUPD | True |
| Equilibrium sediment concentration profile at boundary | EQMBC | True |
| Include effect of sediment on water | DENSIN | False |
| Morphological scale factor | MORFAC | 250 / 50 [-] |
| Spin-up time from Tstart to start of morphological change | MORSTT | 1440 [min] |
| Threshold sediment thickness for transport and erosion | THRESH | 0.05 [m] |
| Van Rijn's reference height factor | AKSFAC | 1.0 [-] |
| Longitudinal bed gradient factor for bed load transport | ALFABS | 1.0 [-] |
| Transverse bed gradient factor for bed load transport | ALFABN | 1.5 [-] |
| Current-related reference concentration factor | SUS | 1.0 [-] |
| Current-related transport vector magnitude factor | BED | 1.0 [-] |
| Minimum depth for sediment calculation | SEDTHR | 0.1 [m] |

Table J-5: Morphology input file in DELFT3D-FLOW

| Parameter | Name | Initial value |
|---|--------|----------------------------|
| Reference density for hindered settling | CSOIL | 1600 [kg m ⁻³] |
| Specific density | RHOSOL | 2650 [kg m ⁻³] |
| Dry bed density | CDRYB | 1600 [kg m ⁻³] |
| Mean sediment diameter [D ₅₀] | SEDDIA | 500 [μm] |
| Initial sediment layer thickness at bed | DPSED | 50 [m] |

Table J-6: Sediment parameter settings in DELFT3D-FLOW

N. BED LEVEL RESPONSE FOR GROWTH AND DECAY

Figures N-1 and N-2 display two of the growth configurations of the Baker Beach (BB) and Mouth Center (MC) median water depths, for the velocity amplitude of 1.00 ms^{-1} . The blue dotted line represents the bed level after 125 days. The red dotted line displays the bed level after 250 days.

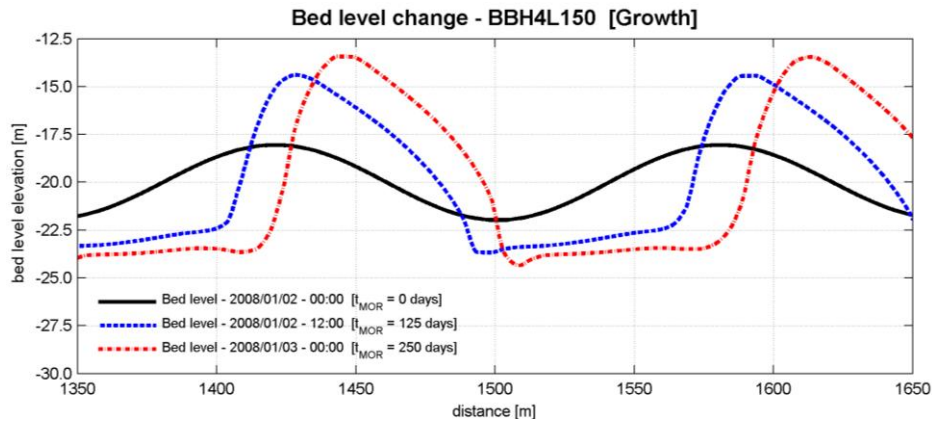


Figure N-1: Bed level change of the sandwave growth configuration in 20 m water depth, for a current velocity of 1.00 ms^{-1} .

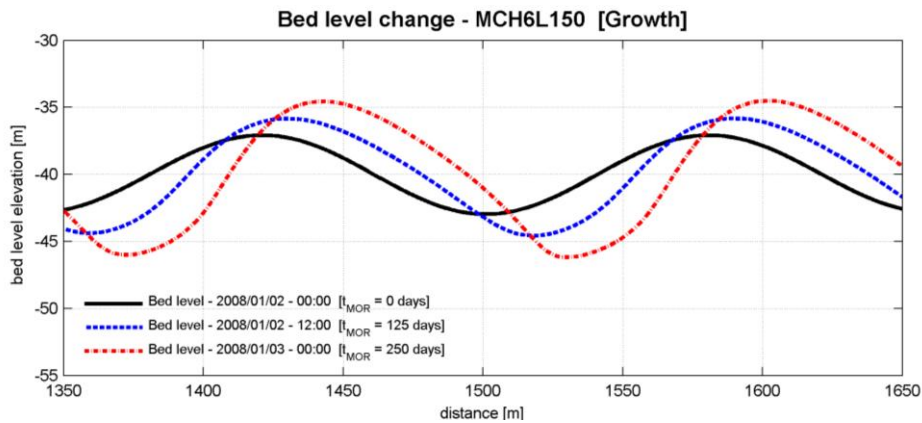


Figure N-2: Bed level change of the sandwave growth configuration in 40 m water depth, for a current velocity of 1.00 ms^{-1} .

Figures N-3 and N-4 display two of the decay configurations of the Baker Beach (BB) and Mouth Center (MC) median water depths, for the velocity amplitude of 1.00 ms^{-1} . The blue dotted line represents the bed level after 125 days. The red dotted line displays the bed level after 250 days.

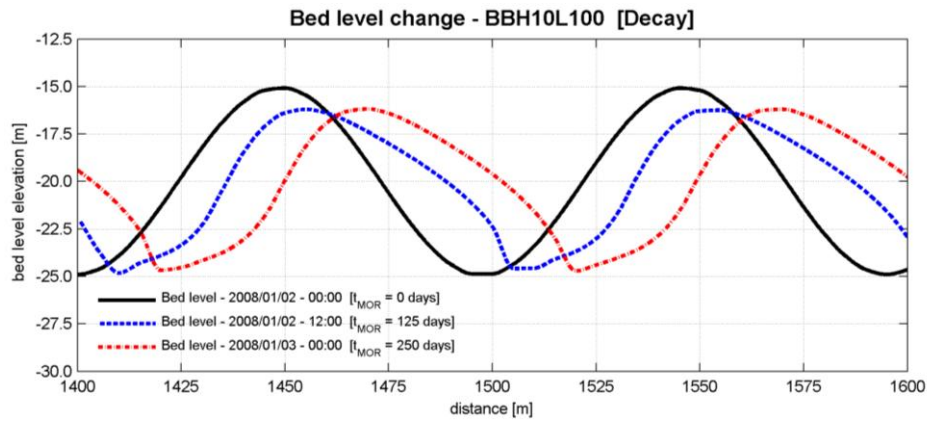


Figure N-3: Bed level change of the sandwave decay configuration in 20 m water depth, for a current velocity of 1.00 ms^{-1} .

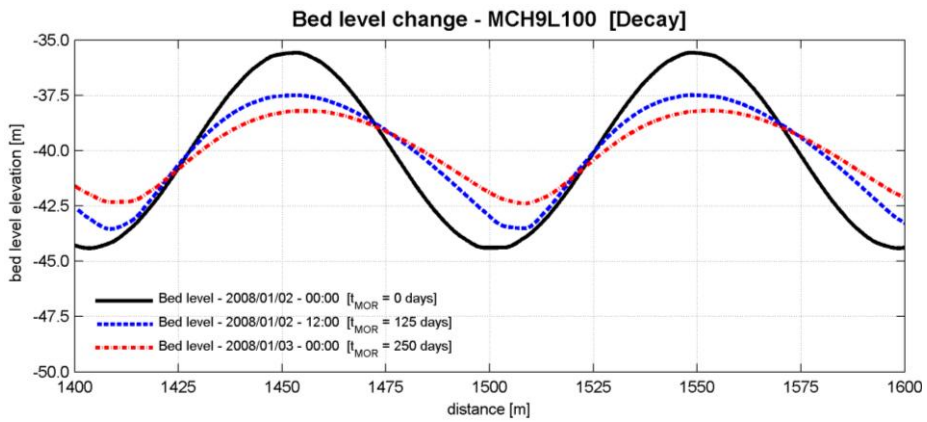


Figure N-4: Bed level change of the sandwave decay configuration in 40 m water depth, for a current velocity of 1.00 ms^{-1} .

O. BAKER BEACH – HYDRODYNAMIC TIME SERIES

Figures O-1 through O-6 display time series at Baker Beach for both near-bed flow velocities (blue lines) versus the critical near-bed flow velocity (dotted lines) and the time series for bed shear stress (red lines) versus the critical bed shear stress (dotted lines), that result in growth and decay respectively. Time series are shown for two consecutive hydrodynamic days and are the result of running the model using a fixed sandwave bed.

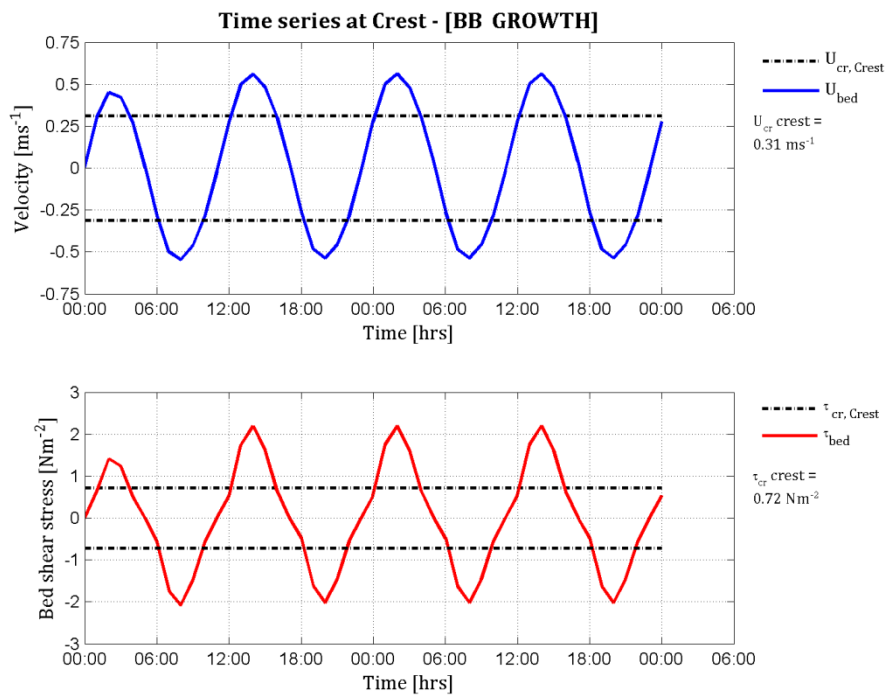


Figure O-1: Baker Beach growth configuration time series for velocities and shear stresses at the Crest monitoring point, using a sandwave height of 5.0 m with a length of 125 m.

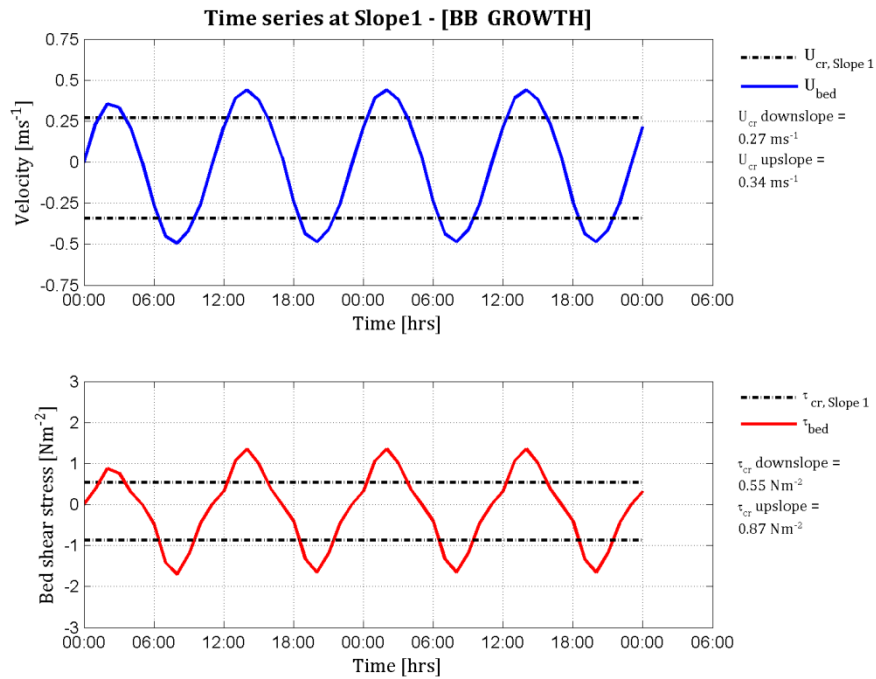


Figure 0-2: Baker Beach growth configuration time series for velocities and shear stresses at the Slope1 monitoring point, using a sandwave height of 5.0 m with a length of 125 m.

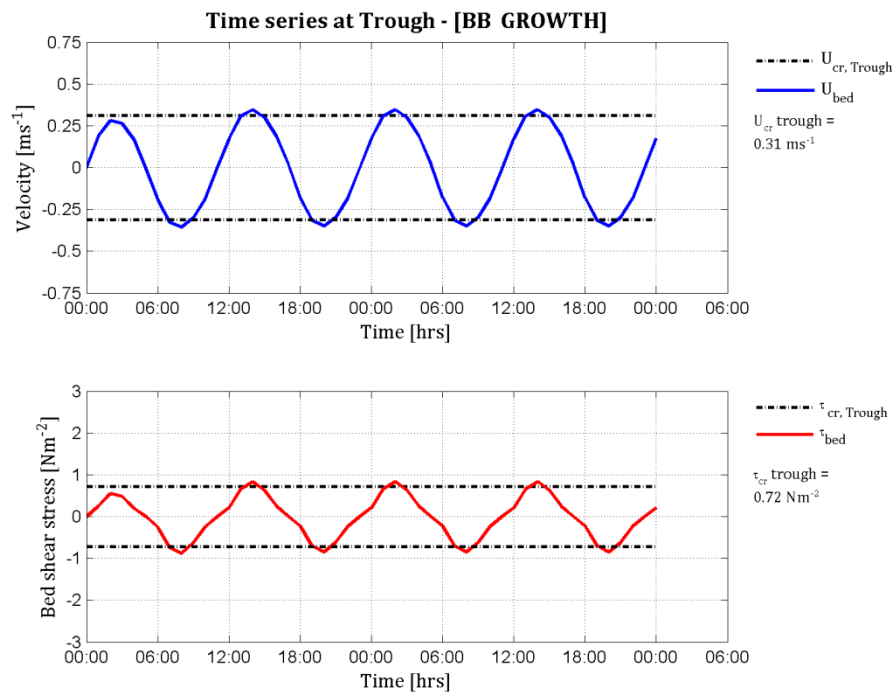


Figure 0-3: Baker Beach growth configuration time series for velocities and shear stresses at the Trough monitoring point, using a sandwave height of 5.0 m with a length of 125 m.

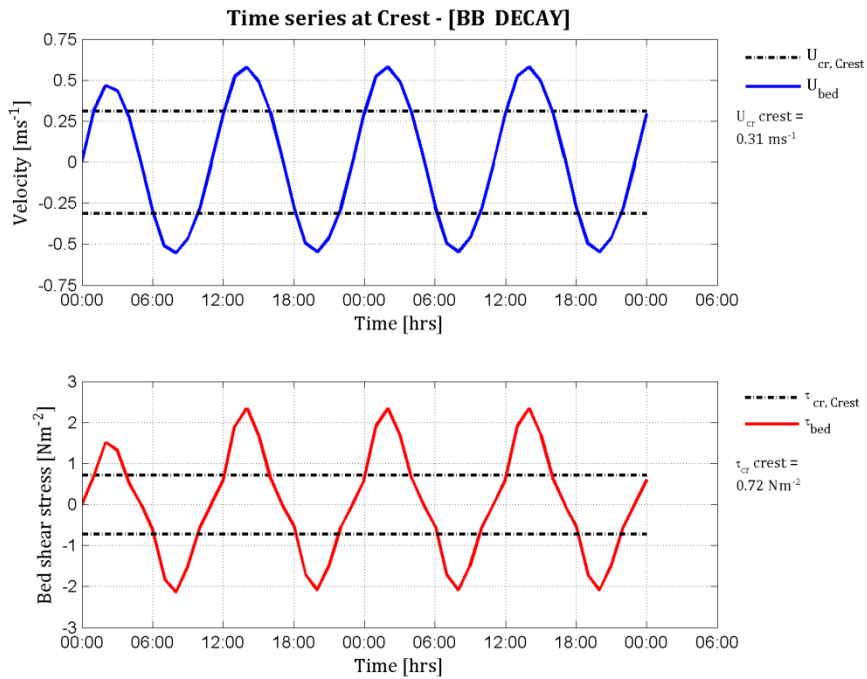


Figure O-4: Baker Beach equilibrium configuration time series for velocities and shear stresses at the Crest monitoring point, using a sandwave height of 5.9 m with a length of 75 m.

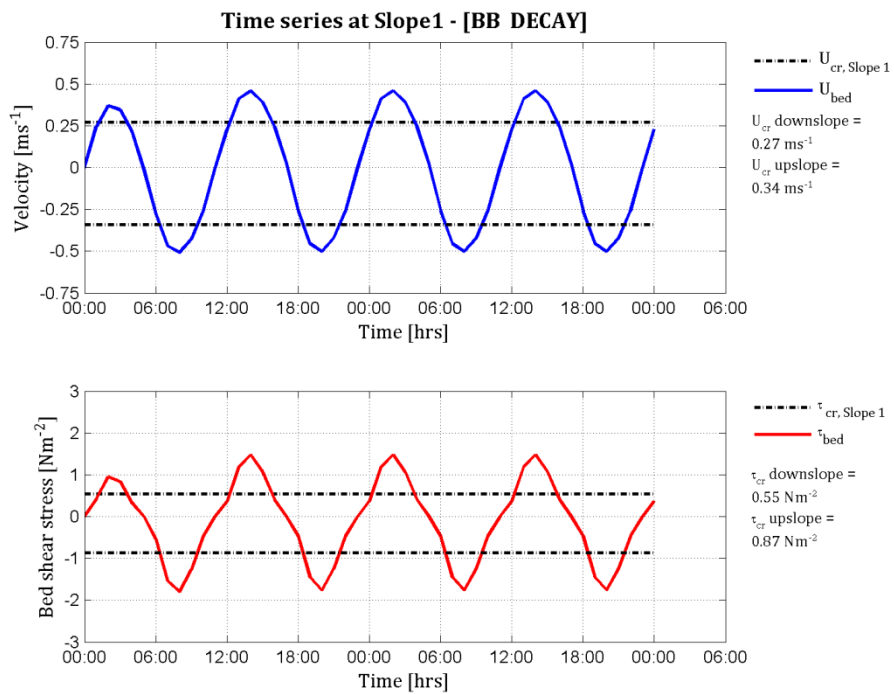


Figure O-5: Baker Beach equilibrium configuration time series for velocities and shear stresses at the Slope1 monitoring point, using a sandwave height of 5.9 m with a length of 125 m.

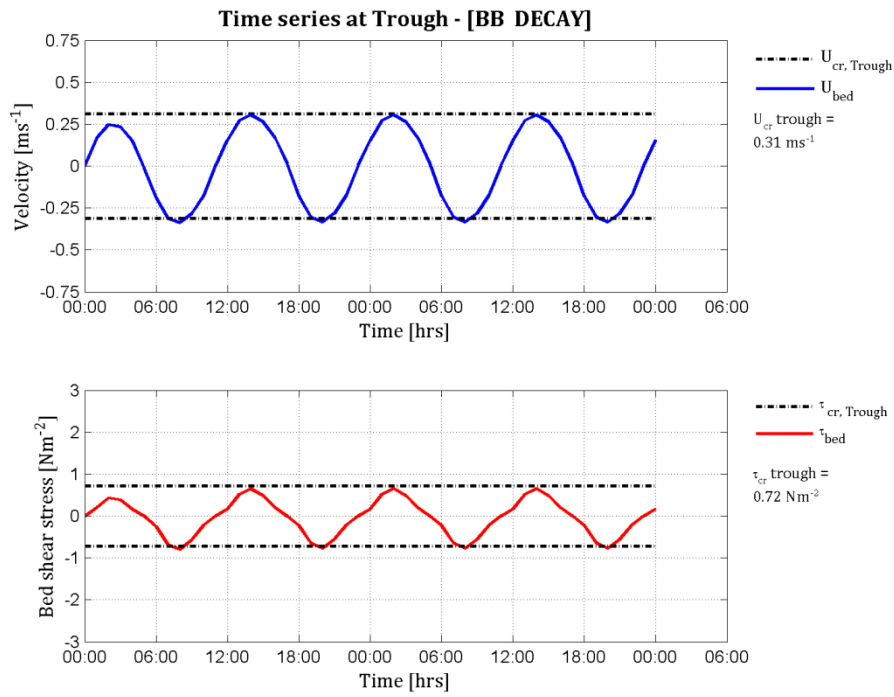


Figure O-6: Baker Beach growth configuration time series for velocities and shear stresses at the Trough monitoring point, using a sandwave height of 5.9 m with a length of 125 m.

P. MOUTH CENTER – HYDRODYNAMIC TIME SERIES

Figures P-1 through P-6 display time series at Mouth Center for both near-bed flow velocities (blue lines) versus the critical near-bed flow velocity (dotted lines) and the time series for bed shear stress (red lines) versus the critical bed shear stress (dotted lines), that result in growth and decay respectively. Time series are shown for two consecutive hydrodynamic days and are the result of running the model using a fixed sandwave bed.

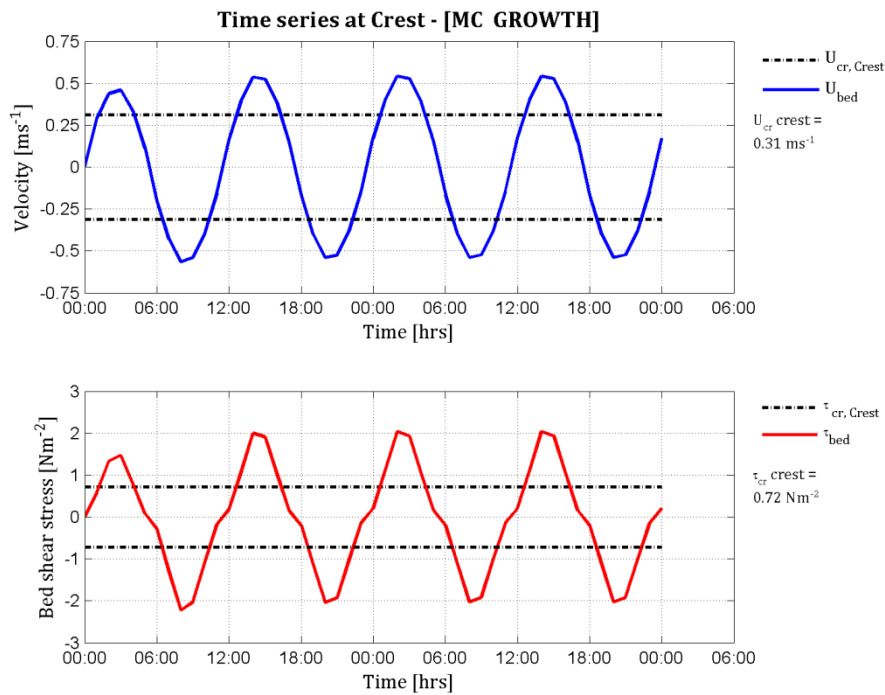


Figure P-1: Mouth Center growth configuration time series for velocities and shear stresses at the Crest monitoring point, using a sandwave height of 5.0 m with a length of 150 m.

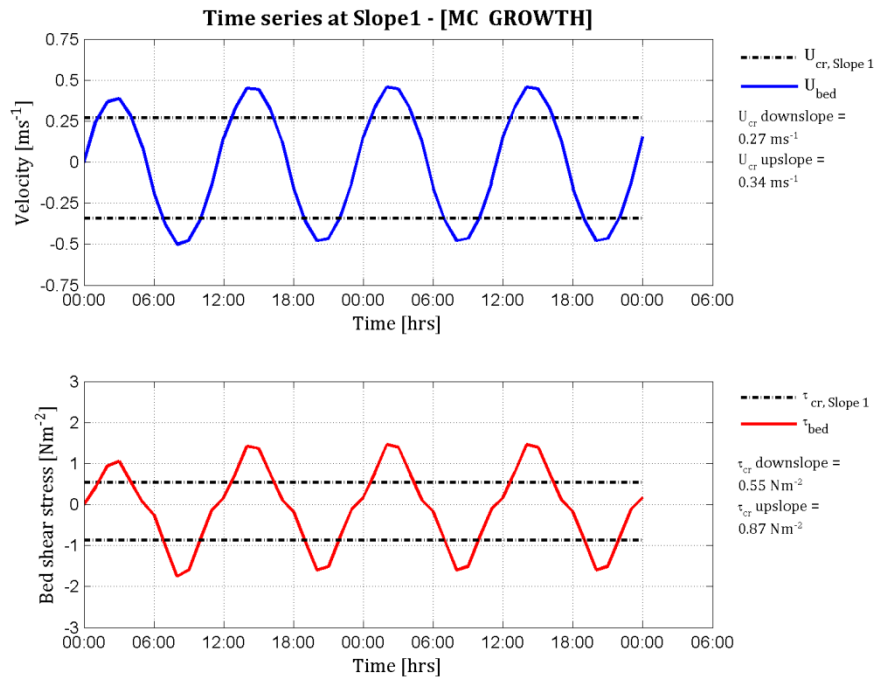


Figure P-2: Mouth Center growth configuration time series for velocities and shear stresses at the Slope1 monitoring point, using a sandwave height of 5.0 m with a length of 150 m.

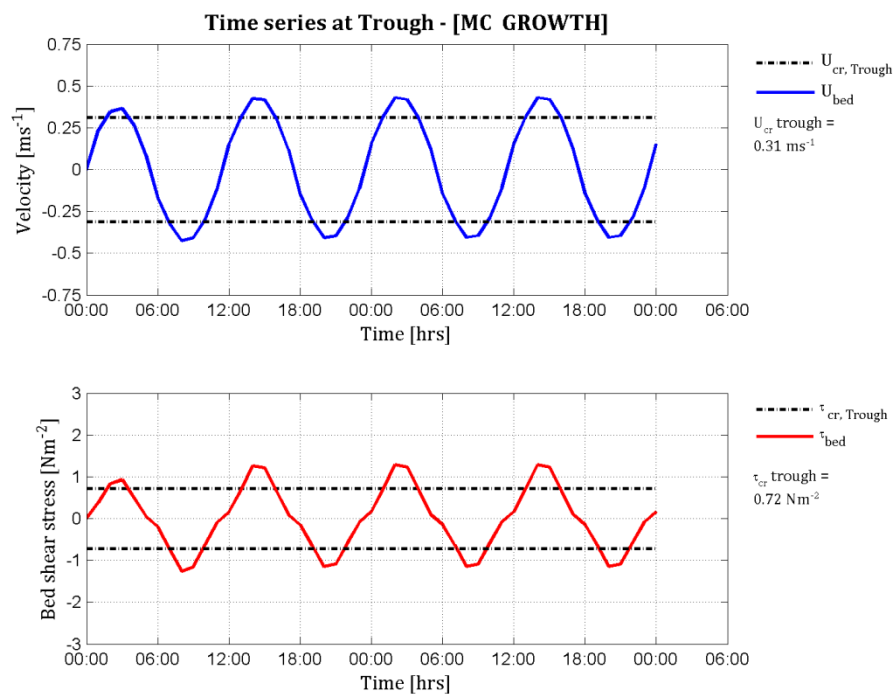


Figure P-3: Mouth Center growth configuration time series for velocities and shear stresses at the Trough monitoring point, using a sandwave height of 5.0 m with a length of 150 m.

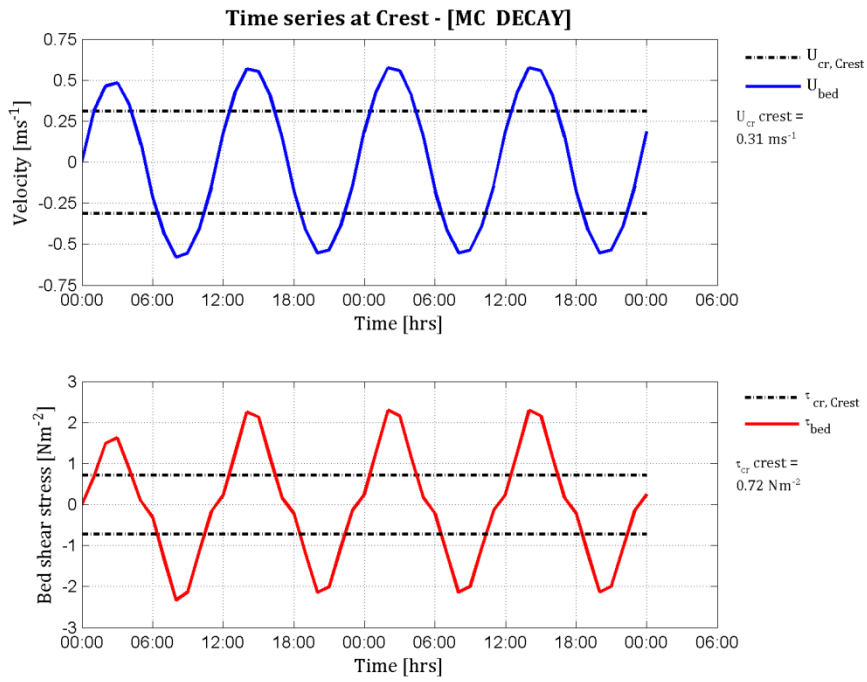


Figure P-4: Mouth Center decay configuration time series for velocities and shear stresses at the Crest monitoring point, using a sandwave height of 6.8 m with a length of 75 m.

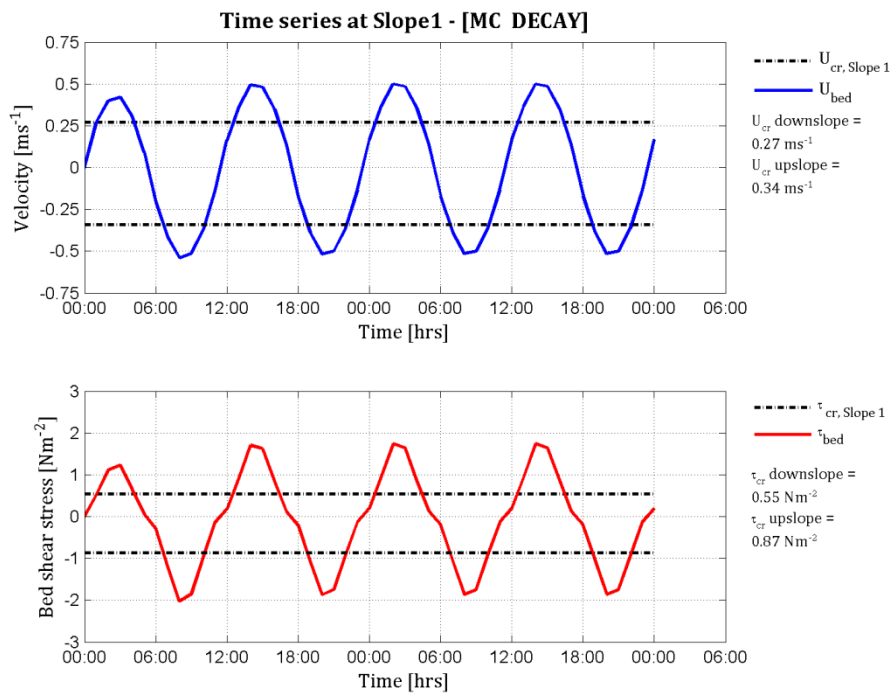


Figure P-5: Mouth Center decay configuration time series for velocities and shear stresses at the Slope1 monitoring point, using a sandwave height of 6.8 m with a length of 75 m.

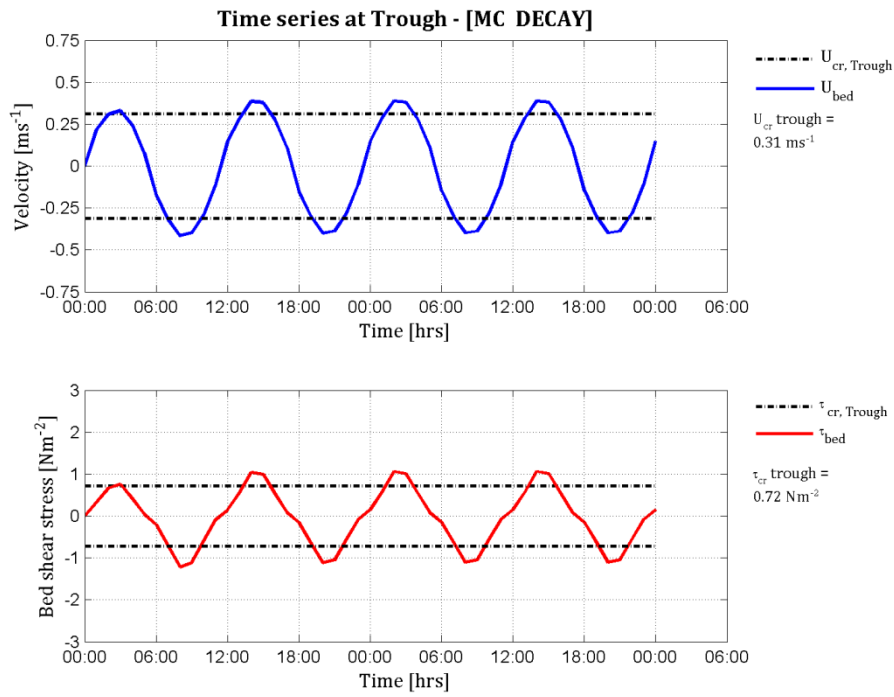


Figure P-6: Mouth Center decay configuration time series for velocities and shear stresses at the Trough monitoring point, using a sandwave height of 6.8 m with a length of 75 m.

Q. TIME SERIES DATA OVERVIEW

| DETERMINING THE FORMATION MECHANISM: | | | | | | | | | | | | |
|--------------------------------------|-------|------------------|-------|--------------------|-------|-------------------------|-------|------------------|-------|--------------------|-------|------|
| MOUTH CENTER = 40 m | | | | | | BAKER BEACH = 20 m | | | | | | |
| EQUILIBRIUM [H13.5 I150] | | DECAY [H6.8 I75] | | GROWTH [H5.0 I150] | | EQUILIBRIUM [H9.8 I125] | | DECAY [H5.9 I75] | | GROWTH [H5.0 I125] | | |
| Ubed_mx | 0.64 | ms-1 | 0.57 | ms-1 | 0.54 | ms-1 | 0.63 | ms-1 | 0.58 | ms-1 | 0.56 | ms-1 |
| Ubed_cr_station | 0.31 | ms-1 | 0.31 | ms-1 | 0.31 | ms-1 | 0.31 | ms-1 | 0.31 | ms-1 | 0.31 | ms-1 |
| Exceedence time [Δ] | 70 | % | 70 | % | 60 | % | 65 | % | 65 | % | 60 | % |
| Ures_station | 0.020 | ms-1 | 0.003 | ms-1 | 0.008 | ms-1 | 0.002 | ms-1 | 0.005 | ms-1 | 0.001 | ms-1 |
| tbed_start | 0.24 | Nm-2 | 0.24 | Nm-2 | 0.21 | Nm-2 | 0.79 | Nm-2 | 0.60 | Nm-2 | 0.53 | Nm-2 |
| tbed_mx | 2.82 | Nm-2 | 2.30 | Nm-2 | 2.04 | Nm-2 | 2.79 | Nm-2 | 2.34 | Nm-2 | 2.20 | Nm-2 |
| tbed_cr_station | 0.72 | Nm-2 | 0.72 | Nm-2 | 0.72 | Nm-2 | 0.72 | Nm-2 | 0.72 | Nm-2 | 0.72 | Nm-2 |
| Ubed_mx | 0.45 | ms-1 | 0.52 | ms-1 | 0.48 | ms-1 | 0.49 | ms-1 | 0.50 | ms-1 | 0.49 | ms-1 |
| Ubed_cr_station | 0.34 | ms-1 | 0.34 | ms-1 | 0.34 | ms-1 | 0.34 | ms-1 | 0.34 | ms-1 | 0.34 | ms-1 |
| Exceedence time [Δ] | 50 | % | 70 | % | 60 | % | 50 | % | 65 | % | 45 | % |
| Ures_station | 0.038 | ms-1 | 0.014 | ms-1 | 0.015 | ms-1 | 0.049 | ms-1 | 0.020 | ms-1 | 0.021 | ms-1 |
| tbed_start | 0.14 | Nm-2 | 0.20 | Nm-2 | 0.17 | Nm-2 | 0.24 | Nm-2 | 0.36 | Nm-2 | 0.32 | Nm-2 |
| tbed_mx | 1.41 | Nm-2 | 1.86 | Nm-2 | 1.60 | Nm-2 | 1.69 | Nm-2 | 1.76 | Nm-2 | 1.65 | Nm-2 |
| tbed_cr_station | 0.87 | Nm-2 | 0.87 | Nm-2 | 0.87 | Nm-2 | 0.87 | Nm-2 | 0.87 | Nm-2 | 0.87 | Nm-2 |
| Ubed_mx | 0.28 | ms-1 | 0.40 | ms-1 | 0.43 | ms-1 | 0.22 | ms-1 | 0.33 | ms-1 | 0.35 | ms-1 |
| Ubed_cr_station | 0.31 | ms-1 | 0.31 | ms-1 | 0.31 | ms-1 | 0.31 | ms-1 | 0.31 | ms-1 | 0.31 | ms-1 |
| Exceedence time [Δ] | 0 | % | 40 | % | 40 | % | 0 | % | 5 | % | 25 | % |
| Ures_station | 0.006 | ms-1 | 0.010 | ms-1 | 0.000 | ms-1 | 0.020 | ms-1 | 0.014 | ms-1 | 0.006 | ms-1 |
| tbed_start | 0.13 | Nm-2 | 0.15 | Nm-2 | 0.16 | Nm-2 | 0.06 | Nm-2 | 0.17 | Nm-2 | 0.21 | Nm-2 |
| tbed_mx | 0.55 | Nm-2 | 1.11 | Nm-2 | 1.29 | Nm-2 | 0.33 | Nm-2 | 0.78 | Nm-2 | 0.86 | Nm-2 |
| tbed_cr_station | 0.72 | Nm-2 | 0.72 | Nm-2 | 0.72 | Nm-2 | 0.72 | Nm-2 | 0.72 | Nm-2 | 0.72 | Nm-2 |